THE DEVELOPMENT OF TARGETED RADIOTHERAPY FOR CENTRAL NERVOUS SYSTEM LEUKAEMIA

Barry Leonard Pizer

A Thesis Submitted for the Degree of
Doctor of Philosophy

The Imperial Cancer Research Fund
Paediatric and Neuro-Oncology Group
Frenchay Hospital
Bristol

March 1992

THE DEVELOPMENT OF TARGETED RADIOTHERAPY FOR CENTRAL NERVOUS SYSTEM LEUKAEMIA.

ABSTRACT.

The use of antibodies to specifically deliver cytotoxic agents to tumour cells has been widely investigated as a means of increasing the therapeutic index of cancer therapy. Nowhere is this more likely to be of benefit than in the treatment of central nervous system (CNS) tumours, in which damage to vital structures by conventional therapies often results in significant sequelae.

Many factors have, however, been identified which limit the clinical success of such targeted therapies. Some of these obstacles may be avoided by the administration of therapeutic agents into a tumour-bearing body compartment. This thesis examines the potential of antibody-targeted radionuclide therapy in the treatment of meningeal leukaemia.

Three monoclonal antibodies (MoAbs) binding to leukaemic cells were fully characterised, and conditions established for antibody labelling with the beta-emitting radionuclide, iodine-131. The specificity of antibody-mediated ^{131}I therapy against a single cell suspension of leukaemic cell lines was demonstrated using an *in-vitro* cell survival assay. Additional experiments have suggested a relationship between the degree of cell kill and the amount of radioisotope bound to the cell surface. These results were supported by a mathematical model.

In recognition of the limitations of *in-vitro* models, a small animal model of CNS leukaemia was established. Prolonged survival of animals treated with intrathecally administered ^{131}I-MoAbs was observed, as compared to untreated controls.

A multicentre phase I/II clinical study was initiated, in which a transient response to a single intrathecal injection of ^{131}I-MoAbs was noted in six of seven children with CNS relapse of acute lymphoblastic leukaemia. Toxicity was

acceptable. The biodistribution of radioconjugates was examined and models developed for the estimation of radiation dose to both cerebrospinal fluid and normal tissues. The results of these investigations, together with those from the *in-vitro* model, have suggested strategies by which the efficacy of therapy may be improved.

DEDICATION.

To my wife Jenni, and children Joseph, Oliver, Matthew and Elliot, without whom this thesis would have been completed nine months earlier.

ACKNOWLEDGEMENTS.

I would foremost like to acknowledge Dr John Kemshead whose constant academic and moral support has been invaluable throughout the period of this work. Scientific support was also gratefully received from Professor J Chessells, Mr V Papanastassiou, Mr H Coakham, Dr T Wheldon, Dr J O'Donoghue, Dr W Millar, Dr T Moss, Professor K Trott and Dr A Renwick.

Technical input was provided by a large number of individuals. I particularly wish to thank Mr J Hancock for his tireless assistance with the *in-vitro* studies. I am also grateful to Dr K Urch and Dr M Glennie, who provided the impetus for the animal studies, which were strongly supported by the staff of the Animal Units at the University of Bristol and the Institute of Child Health, London. Thanks are due to Dr B De Stavola and Dr D Altman who provided the statistical input to this work, and to Mr F Zananiri for collaboration with the development of the dosimetric models. Antibodies were kindly supplied by Dr W Tax, Dr E Vitetta and Dr W Cassano.

I wish to express my gratitude to my medical colleagues and all members of staff involved in the clinical program and, most importantly, to the participating children and their relatives.

In preparation of this manuscript, I would like to acknowledge the secretarial skills of Miss S Murphy and the photographic expertise of Mr G Freke. This work has been generously funded by the Imperial Cancer Research Fund.

CONTENTS.

FIGURES.

TABLES.

CHAPTER 1.

GENERAL INTRODUCTION.

Successful treatment of cancer necessitates the eradication of all malignant cells capable of indefinite proliferation. A few types of cancer are amenable to surgery, but many have infiltrated regionally or are widely disseminated at the time of presentation. These require additional therapeutic modalities, principally chemotherapy and/or radiotherapy.

All forms of regional or systemic therapy are not tumour-specific, and whilst many regimens are successful in destroying tumour cells, they may also cause widespread damage to normal body tissues. For most cancers, this toxicity prohibits the administration of potentially curative therapy. Thus, the search for new therapeutic agents must attempt to improve the balance between therapeutic efficacy and toxicity.

1. Site Specific Delivery of Cytotoxic Agents.

A method of increasing this "therapeutic index" is to selectively localise tumoricidal agents to cancer cells. One strategy available involves the exploitation of physiological mechanisms preferentially associated with tumour cells. An example of this is the use of radioactive ^{131}I in the treatment of thyroid tumours. Iodine is a normal constituent of thyroid hormones and the mechanisms for uptake and metabolism of iodine are preserved in the majority of thyroid carcinomas [1].

A similar philosophy underlines the interest in the use of *meta*-iodobenzylguanidine (*m*IBG) as both a diagnostic and therapeutic agent. This compound is an iodinated aromatic analogue of adrenaline/noradrenaline. It is taken up by an active transport mechanism and stored in the cytoplasm/chromaffin granules of a variety of tumours derived from the

sympathetic nervous system, particularly phaeochromocytoma and neuroblastoma [2].

Several studies have demonstrated *m*BG, radiolabelled with either ^{123}I or ^{131}I, to be both a specific and sensitive agent in the radiolocalisation of these tumours [3] [4]. Recent studies have also revealed encouraging tumour responses when high activities of ^{131}I-labelled *m*BG are administered to children with relapsed or unresponsive neuroblastoma [5] [6] or as part of initial induction therapy for this condition [7].

Unfortunately, few tumours have physiological characteristics that can be exploited in this way. Thus, additional strategies are necessary to change the biodistribution of the cytotoxic agent.

(a) Colloidal delivery systems.

These systems include the use of phospholipid vesicles (liposomes) [8], emulsions (lipid microspheres) [9], polymeric microspheres and natural carriers such as low density lipoproteins. Their success appears to be limited by their *in-vivo* bio-availability. Particles of greater than 7 μm are rapidly filtered out by the capillaries of the lung and reticuloendothelial system, although improvements to the biodistribution of these agents have been made by altering the surface charge of the particle [9].

Fidler *et al.*, have concentrated on exploiting the natural fate of liposomes in the body by using them to target tissue macrophages with specific immunomodulators. Using liposomally-entrapped lymphokines or macrophage activators, they have demonstrated the *in-vitro* activation of peripheral blood monocytes which are able to selectively lyse neoplastic cells [10]. The *in-situ* activation of mouse alveolar macrophages was also examined in a mouse model, in which syngeneic melanoma was allowed to metastasize to the lung. Both therapeutic efficacy and specificity was demonstrated. These

and other studies suggest a potentially useful, but limited role in cancer therapy for colloidal delivery systems.

Colloidal suspensions of radioisotopes have also been investigated as a means of delivering high doses of radiation to tumour-bearing body compartments and to tumour cavities. This approach is based upon the concept of reducing the clearance of isotope relative to that of the non-colloidal agent and thus maintaining a high local concentration of radionuclide (see below).

(b) Polyclonal antibody conjugates.

(i) Background and non-therapeutic studies

The most widely investigated approach to site specific delivery is to link cytotoxics to a passive delivery system. As early as 1906, Ehrlich postulated that anti-tumour antibodies might have therapeutic potential as carriers of toxic substances that could be selectively targeted to tumour cells [11]. This hypothesis was initially investigated using polyclonal antisera, and later, polyclonal and monoclonal antibody (MoAb) preparations. A variety of carrier-conjugated toxic substances have been investigated. These include conjugates of radioisotopes (beta-emitters, alpha-emitters and emitters of Auger electrons) [12] [13] [14]; drugs (eg. vindesine, chlorambucil and methotrexate) [15] and plant (eg. ricin A chain), bacterial (eg. pseudomonas exotoxin) and fungal toxins [16].

In 1948, Pressman and Keighley observed that antibodies could be radiolabelled with ^{131}I, and that immunoreactivity was preserved after labelling [17]. They showed that iodinated rabbit antibodies to rat kidney were localised in the kidney after intravenous (IV) injection, and that no such localisation was seen with a control, anti-ovalbumin antibody. Pressman later prepared a radio-iodinated antiserum against the Wagner osteosarcoma which he was able to localise to this tumour in rats [18]. Using a paired-labelling approach in

which tumour-bearing (Murphy lymphosarcoma) animals were simultaneously injected with ^{131}I-labelled immune and ^{133}I-labelled non-immune antisera, he was able to demonstrate specific localisation of the ^{131}I-labelled antiserum following tumour resection. It became clear to these and other workers, that antibodies to either fibrin or fibrinogen were responsible for the localisation of these antisera in rapidly growing tumours such as the Murphy lymphosarcoma. In a series of 141 patients given diagnostic activities of ^{131}I-anti-fibrin antibody, tumour localisation was achieved in 65% of cases [19].

Improvements in radiolocalisation studies subsequently focused on the generation of more specific antisera. This followed the characterisation of a number of tumour associated antigens such as carcinoembryonic antigen (CEA), human chorionic gonadotrophin (HCG), alphafetoprotein (AFP), prostatic acid phosphatase (PAP), and colon-specific antigen-p (CSAp) [20]. In 1973, Primus *et al.,* described the preparation of a goat anti-CEA antisera, purified by Sephadex G-200™ and DEAE-cellulose column chromatography [21]. Again using a paired-labelling technique, they demonstrated specific localisation of ^{131}I-anti-CEA in the human colon carcinoma, GW-39, xenografted in the cheek pouch of Syrian hamsters.

The next important development was the improvement in antibody purity by means of affinity chromatography. One problem with this method is the preferential selection of low affinity antibodies, which are more readily eluted from the chromatography column. Nevertheless, Primus and colleagues demonstrated a three to four-fold improvement in tumour uptake employing the same model system as that used previously [22].

Clinical trials using affinity-purified antisera, pioneered by Goldenberg and colleagues, commenced in 1977 [20]. By 1983, this group had conducted radioimmunodetection (RAID) studies in over 450 patients with a variety of tumours, predominantly carcinomas [20]. In a review of 173 patients in whom ^{131}I-anti-CEA was used as the imaging agent, the sensitivity of the technique

ranged between 50% (pancreatic cancer) and 91% (colorectal carcinoma). In the largest series, of 51 patients with colorectal cancer, only two putative false-positive results were obtained, together with a false-negative rate of 14%. This group has also reported encouraging results of RAID for tumours expressing AFP, HCG, PAP and CSAp [20].

(ii) Therapeutic studies.

This and similar work formed the basis for the first therapeutic studies using radiolabelled polyclonal antibodies. Initial trials were undertaken by Dr Order and colleagues at the John Hopkins Medical School using affinity-purified polyclonal antisera, raised in rabbits against either purified ferritin or CEA, and radiolabelled with ^{131}I. Eight adult patients were enroled into a pilot study; four with primary hepatic carcinoma, two with colonic carcinoma and one each with lung carcinoma and a primary carcinoma of the floor of the mouth [12]. Patients were treated using a combined therapeutic strategy, namely; two cycles of chemotherapy (5-fluorouracil and adriamycin) together with 21 Gy external beam radiotherapy, followed after one month by the administration of between 58 and 117 mCi of ^{131}I conjugated with either anti-CEA or anti-ferritin antibodies. Whereas no extra-hepatic tumours responded to therapy, a response was noted in three patients with primary hepatic carcinoma. All three responders had, however, demonstrated a degree of tumour regression prior to administration of isotopic immunoglobulin.

The same multi-agent regimen was employed in a larger phase I/II study in the treatment of patients with primary liver tumours. Of 27 eligible patients, 18 had received between 37 and 157 mCi of ^{131}I-IgG at the time of reporting [23]. Of these, only nine were evaluable for response, six of whom demonstrated a partial response to the treatment regimen. As expected, the major toxicity in this trial was myelosuppression, with 21% of patients developing a severe leucopaenia and/or thrombocytopaenia.

A major criticism of these studies was the combined nature of the therapeutic regimen, making it impossible to obtain a true evaluation of both the efficacy and toxicity associated with radiolabelled immunoglobulin. In 1985, the same group reported on the use of single modality isotopic immunoglobulin therapy in 38 patients with advanced, progressive Hodgkin's disease [24]. All patients received an initial course of treatment of ^{131}I-anti-ferritin, consisting of 30 mCi on day 0 and 20 mCi on day five. Patients demonstrating either a tumour response or static disease by day 56 received two additional cycles of therapy. To reduce the immunogenicity of the immunoglobulin, antibodies used in the second and third cycles of therapy were obtained from different species. Fifteen of 37 evaluable patients demonstrated an objective tumour response, of which one achieved a complete remission. Responses were predominantly associated with the first treatment cycle, with only two patients benefiting from a second cycle. Again, toxicity was primarily manifest by myelosuppression, but leucocyte counts of less than 1 x 10^9/litre and platelet counts of less than 20 x 10^9/litre were only observed in two and four patients respectively.

The John Hopkins Group has further developed their therapeutic strategy by investigating the use of the long-range β-emitting radionuclide, ^{90}Yttrium. In a pilot study, six patients with refractory Hodgkin's disease were treated with between one and three cycles of IV ^{90}Y-labelled polyclonal anti-ferritin antisera [25]. They received between 10 and 30 mCi per treatment, followed 18 days later by infusion of cryopreserved autologous bone marrow. Three patients obtained a complete response and one, a partial response to therapy, whilst two had tumour progression on treatment. Acute toxicity was limited to bone marrow aplasia, without a clear benefit for transplantation after 20 mCi ^{90}Y, but the suggestion of a positive effect after 30 mCi, in terms of the rate of bone marrow re-engraftment. No toxic deaths were observed.

(c) Monoclonal antibodies.

Interest in the use of antibodies as passive carriers of cytotoxic substances was increased following the description of hybridoma technology by Kohler and Milstein in 1975 [26]. MoAbs can be chosen with well defined specificity, relatively high affinity and of selected isotype. Following production of the hybridoma, antibodies may be produced and purified at relatively low cost and in essentially unlimited quantities. However, whilst the role of MoAbs in tumour diagnosis *in-vivo* is firmly established, their place as agents for tumour therapy and to a lesser extent RAID, remains essentially experimental.

Three sources of MoAb are available; mouse, rat and human, although most studies have employed mouse monoclonals. Selection of MoAbs is initially based upon their *in-vitro* and *in-vivo* specificity. With the possible exception of those recognising the idiotype of immunoglobulin expressed on the surface of B-cells, no reagent has been discovered that is truly tumour-specific. Instead, antibodies have been developed that recognise antigens which are expressed at high concentration on tumours, with restricted expression on normal tissues. Additional factors influencing selection of antibodies for therapy include the ease of production and purification, isotype, antibody affinity, the number of antigenic binding sites on the targeted tumour and the degree of heterogeneity of antigenic expression.

The cytotoxic effect of the unconjugated antibody must also be considered. This is partly related to the antibody isotype. Cytotoxicity due to either antibody dependent cellular cytotoxicity (ADCC) or complement dependent cytotoxicity (CDC) has been predominantly investigated. In a number of *in-vitro* systems, the relative strength of ADCC reactions for murine monoclonals has been assessed as $IgG_{2a} > IgG_{2b} > IgG_1$ [27] [28] [29]. CDC appears particularly associated with IgM murine antibodies, although this has been noted for antibodies of the IgG_3 subclass [30].

The *in-vivo* inhibition of tumour growth by unconjugated MoAbs has been widely reported. Using a nude mouse model inoculated with human colorectal carcinoma, Herlyn demonstrated suppression of tumour growth by IgG_{2a} antibodies capable of inducing ADCC *in-vitro* [31]. Similar effects have been reproduced in a variety of other animal models [32] [33].

The ability of unconjugated antibodies to act as biological response modifiers in destroying cancer cells was examined in a large number of clinical studies in the early 1980's. These concentrated on the treatment of haematological malignancies, including B-cell lymphoma [34], chronic lymphatic leukaemia [35], cutaneous T-cell lymphoma [36], acute lymphoblastic leukaemia (ALL) [37] and acute myeloid leukaemia (AML) [38]. Antibodies were generally of the IgG_{2a} subclass and recognised either a well characterised tumour associated antigen (eg. Leu-1 and T65) or were raised against the idiotype of the patient's B-cell lymphoma. In general, for patients with circulating blasts, there was an immediate 50 - 75% reduction in the circulating tumour cell count. However, responses were very transient, with counts returning to baseline levels within 24 - 48 hours, producing a typical "sawtooth" pattern in circulating cell numbers. For patients with malignant T-cell infiltration of skin or lymph nodes, reduction in tumour cell mass was demonstrated in about a half of patients, the response not persisting, however, for more than a few weeks after cessation of therapy [39].

The most encouraging results were noted in patients with B-cell lymphoma treated with infusions of anti-idiotype antibody. Miller described such a patient treated in a dose escalation fashion with eight doses of antibody, who entered a complete remission sustained for over six years [35] [40]. Of seven additional patients treated in a similar way, four had a partial remission lasting between one and six months [41].

Several of these studies identified factors limiting the therapeutic efficacy of antibody therapy. Toxicity was mainly manifest by allergic

phenomena related to the antibody infusion, eg. fever, chills, dyspnoea, rash and hypotension. Whilst these symptoms were not generally severe, anaphylaxis was reported [42] In these studies, patients were treated with large doses of antibody, with cumulative amounts of up to 1.75 g. Similar toxicity in trials of antibody conjugate therapy has been much less frequently reported.

Two studies demonstrated that the presence of circulating antigen from both B- and T-cells effectively blocked MoAb from binding to tumour cells *in-vivo* [34] [36]. It was also shown that leukaemic cells can undergo antigenic modulation as a direct consequence of MoAb binding to the cell surface *in-vivo* [36] [37]. The loss of antigen appeared specific and did not appear to involve other cell surface proteins. Furthermore, antigenic modulation appeared to be a specific response to certain antigen/antibody interactions such as those involving the common ALL antigen (CALLA), surface immunoglobulin and the L17 F12 antigen. It has also been shown that the mechanism of modulation may be different for various antigens. Boyse *et al.*, demonstrated that in the presence of specific antibody and other serum factors, TL antigen-positive leukaemia cells rapidly became antigen-negative *in-vivo* as a result of the rearrangement of the TL antigen, which could still be detected on the cell surface [43]. This is in contrast to modulation of CALLA, which has been shown to be lost from the membrane after binding by antibodies such as J5 [44]. Furthermore, CALLA appears to be internalised within leukaemic cells during modulation. Whereas this appears disadvantageous for serotherapy, modulation of antibody is crucial for the effectiveness of antibody conjugated to agents such as toxins, which require cell internalisation to exert their cytotoxic effect.

(d) Radiolabelled monoclonal antibodies.

(i) Background and non-therapeutic studies.

Several animal models examining the specificity of MoAb accumulation have been developed. Moshakis *et al.*, used an immunosuppressed CBA/lac mouse bearing a human malignant teratoma xenograft to demonstrate the specific localisation of a MoAb, LICR-LON/HT13 [45]. As in other studies, the "localisation index" of specific to non-specific antibody increased with time, from approximately 2:1 at 24 hours to 10:1 at 96 hours. Excess non-labelled specific immunoglobulin was shown to inhibit tumour uptake of specific radioconjugate, providing further evidence for the specific nature of tumour accumulation of antibody.

In our institution, Jones *et al.*, established a nude mouse model xenografted with the human neuroblastoma cell line, TR14 [46]. The dual-label method with tumour resection was undertaken with the "specific" MoAb, ^{131}I-UJ13A, and a control MoAb, ^{125}I-FD44. Whilst there was marked variation in the accumulation of the antibodies between tumours, the median ratio of UJ13A to FD44 was 7:1. This was equivalent to a median of 6% (range 1.9 - 20.1%) of the injected dose per gram of tumour at 24 hours after injection. Using increased quantities of ^{131}I-UJ13A (150 μCi per mouse), tumours of approximately 1 cm^3 regressed to 10% or less of their original volume over a 21 day period. Repeat injections of conjugate caused tumours to apparently disappear, but regrowth at the original site always occurred.

Results of similar work using animal models generally suggest a high, but variable, specific uptake of isotope, of between 1 and 10% of the injected dose per gram of tumour [47] [48]. These studies have been extended to explore the effect of a number of variables affecting tumour accumulation of radionuclide. These include the accumulation of antibody fragments ($F(ab')_2$ and Fab) [49], new radionuclides [13] [50], tumour size [51], protein dose [52], different ^{131}I-labelling methods [53] and differences in antigen expression [54].

The degree of optimism resulting from pre-clinical work has not been sustained with regard to therapeutic studies in humans. Localisation studies in patients have demonstrated that whilst it is possible to approach the specificity ratios observed in animal models, it has not been possible to obtain the same order of absolute isotope accumulation [55] [56]. Epenetos *et al.*, administered pairs of tumour-associated MoAbs radiolabelled with either ^{131}I or ^{125}I, to 19 patients prior to surgical excision of primary and metastatic breast, ovarian and gastrointestinal tumours [57]. Based on estimates of antibody uptake in resected normal and neoplastic tissues, good tumour:non-tumour ratios were obtained with specific antibodies (maximum tumour:non-tumour ratio of 26:1). However, the absolute amount of radiolabel detected in tumours was small, with a mean value of 0.015% of total injected activity per gram of tumour at 24 hours post-administration.

Several other studies of a variety of MoAbs in humans have revealed similarly disappointing results in terms of the percentage of injected dose accumulating in the tumour. Tumour uptake has generally been in the range of 0.1 to 0.001% per gram of tumour [58] [59] [60]. Explanations for the differences between the isotope uptake observed in animal models and patient studies include a "dilution factor" in the relative amounts of antibody administered between animals and humans, increased catabolism of murine antibodies in humans and differences in tumour structure and microvasculature affecting antibody extravasation and tumour penetration.

(ii) Therapeutic studies.

The results of early clinical trials of systemically injected radioimmunotherapy, especially in patients with solid malignant deposits, were generally disappointing. Encouraged by data from a nude mouse model (see above), our own group undertook a phase I trial of high dose ^{131}I-UJ13A, administered as a single IV injection, in children with relapsed neuroblastoma,

unresponsive to conventional chemotherapy [61]. Six children each received between 35 and 50 mCi of ^{131}I-UJ13A. No patient with large solid deposits of neuroblastoma received benefit from this procedure. Only one response was seen; in a three year old boy whose bone marrow cleared of tumour for a period of eight months and whose small bony lesions showed radiological improvement.

Rosen *et al.*, investigated administration of ^{131}I-labelled MoAb, T101, to patients with cutaneous T-cell lymphoma [62]. Of five patients receiving a single injection of between 100 and 150 mCi of ^{131}I-T101, two demonstrated a partial response and three, a minor response to therapy, lasting from a few weeks to three months. Carrasquillo *et al.*, explored the use of radiolabelled Fab fragments as diagnostic and therapeutic agents in disseminated malignant melanoma [63]. Localisation studies were undertaken in 40 patients, ten of whom were selected for therapy. These received between one and four doses of ^{131}I labelled Fab fragments of either MoAb, anti-p97 or 48.7. Individual activities ranged between 30 and 342 mCi, and cumulative doses of between 132 and 861 mCi. Only two patients demonstrated a tumour response, with only one achieving a true partial response.

With regard to B-cell lymphoproliferative disease, De Nardo *et al.*, reported five patients (three with lymphoma, one with CLL and one with lymphomatous transformation of CLL) who received between one and 10 doses of ^{131}I-Lym-1, with cumulative activities of between 37 and 324 mCi [64]. Three patients demonstrated evidence of a variable tumour response in terms of either a reduction in tumour volume or number of circulating blast cells.

(iii) Limitations to therapy.

Several obstacles to successful therapy have been identified. As observed in localisation studies, foremost amongst these is the inability to deliver a sufficient amount of radionuclide, and hence radiation dose, to all

tumour deposits before activity-limiting toxicity, predominantly myelosuppression, supervenes [65].

The ability of the radiolabel to reach tumour sites is hindered by the widespread volume of distribution and rapid reticuloendothelial uptake following IV injection. Attempts to overcome this problem include administration of agents into the arterial supply of the tumour-bearing region in an attempt to offer a so-called "first pass" advantage. Using a paired-label approach in a D-54 malignant glioma xenograft rat model, Lee *et al.*, demonstrated a 20% advantage of intra-carotid (IC) over IV administration of ^{131}I-labelled MoAb, 81C6, in terms of isotope accumulation [66]. However, as with other studies of the intra-arterial route of administration, no similar advantage was observed for the IC route to localise this antibody within gliomas of patients [67].

An additional factor limiting the availability of antibody to bind to tumour, is the complexing of antibody with tumour shed antigens, eg. oncofoetal antigens such as CEA [68] and the melanoma antigen P-97. Attempts to overcome this may include the administration of a large amount of non-radiolabelled antibody to complex free antigen prior to radioimmunotherapy [69].

The delivery of macromolecules to solid tumour is also limited by the complex and highly heterogenous nature of its vascular supply. In part, this results from variations in the derivation of tumour vessels, i.e. vessels either recruited from the pre-existing network of the host vasculature, or those from the angiogenic response of host vessels to cancer cells [70] [71] [72]. In addition, as a tumour enlarges, the vascular surface area decreases, and necrotic and semi-necrotic areas develop with low blood flow rates. The spatial distribution of macromolecules within tumour is thus heterogenous and their average uptake decreases with increasing tumour size.

Transport of macromolecules across the microvascular wall is another major factor in determining the degree of delivery of radionuclide associated with an antibody carrier. Ultrastructural studies of human and animal tumours have shown that tumour vessels are, in general, more "leaky" to fluid and macromolecules compared to those of several normal tissues [73]. However, the apparent advantage conferred by increased vessel "leakiness" appears more than offset by the disadvantageous transvascular pressure gradients within tumours. Several investigators have demonstrated that the interstitial pressure in tumours is significantly higher than in normal tissues [73] [74]. As the tumour grows, this pressure rises up to 30 mm Hg, presumably due to the proliferation of tumour cells in a confined space and the absence of functioning lymphatic vessels. The increase in interstitial pressure has been shown to be higher in the centre of a tumour and correlates with a reduction in tumour blood flow and the development of necrosis. Interstitial osmotic pressure is also probably higher in tumours than in normal tissues, leading to reduced transvascular osmotic flow of macromolecules [73].

Once a macromolecule such as IgG has extravasated, its movement occurs by diffusion and convection through the interstitial space. In a tumour with high interstitial pressure, convective transport is slowed and transport by diffusion is further hindered by the relatively large distances between tumour vessels. Jain has suggested that where tumour vessels are 200 μm apart, it takes "days" for macromolecules to reach uniform concentration by diffusion for a tumour of radius 1 mm, and "months" where the tumour radius is 1 cm [73]. In addition, as a result of the high interstitial pressure, there may be a significant loss of interstitial fluid from the periphery of the tumour. Butler *et al.*, measured this fluid loss to be 0.14 to 0.22 ml/hour/g of tissue in four different rat mammary carcinomas [75].

The affinity of the antibody for antigen may also affect the overall diffusion rate. Whilst higher antibody affinity significantly increases the

antibodies concentration proximal to tumour vessels, it may retard their movement to distal locations in the tumour interstitium [50].

In-vivo de-halogenation is also considered an important factor in determining the efficiency of targeting with iodinated antibodies. In animal models this predominantly occurs following tumour binding and may be caused by enzymes such as iodotyrosinases, responsible for the extensive de-halogenation of thyroid hormones, which bear a close structural similarity to the iodotyrosines created in conventional protein iodinations [76]. Alternative binding technologies are being developed in an attempt to circumvent this phenomenon [76].

A number of strategies have been proposed to overcome some of the problems with antibody delivery to solid tumours. Several physical (eg. heat, radiation) and chemical (eg. vasoactive drugs) factors may lead to an increase in tumour blood flow [72]. A problem with this approach is that the increase in blood flow is short-lived and usually confined to well vascularised regions, such that the maldistribution of macromolecules may not be improved. Another approach may be based on lowering the tumour interstitial pressure, for example, by the use of lytic enzymes such as hyaluronidase [77]. An alternative strategy would be to lower the tumour cell density without destroying the vasculature, eg. by pre-irradiation [78].

A further approach, and that most keenly investigated, is based on increasing the interstitial transport rate of molecules by means of lower molecular weight agents, eg. either monomeric (Fab) or dimeric ($F(ab')_2$) antibody fragments. Fragments have the theoretical advantage of both increased vascular and interstitial permeability, with the potential for enhanced penetration into tumours as compared with whole immunoglobulin. This advantage has indeed been demonstrated in both *in-vitro* tumour spheroid model systems [79] and in animal models [49]. Evidence for similar advantage in terms of isotope accumulation in patients is, however, lacking [80].

Additional characteristics of lower molecular weight species must be considered. Their lack of Fc domains reduces uptake and metabolism by the reticuloendothelial system and cells catabolising carbohydrate residues, which are predominantly located on the Fc portion of the molecule. This, combined with a smaller molecular size, results in a faster rate of whole body clearance, by a factor of at least two-fold [81]. This tends to improve the quality and specificity of RAID [49]. For therapy, enhanced clearance results in a reduced whole body and possible critical organ exposure to the toxic agent, thereby increasing the therapeutic index. However, the tumour exposure to isotope may also be reduced, with possibly more reliance on repeated conjugate administration to obtain an equivalent radiation dose to the tumour. An alternative approach to improve the therapeutic ratio is to enhance the clearance of the cytotoxic agent by means of a second antibody directed against the anti-tumour antibody, and administered at the time of maximal tumour uptake [82] [83].

An additional problem with the preparation of univalent (eg. Fab) antibody fragments is a consequent reduction in association constant. For radioimmunotherapy with fragments, more attention to antibody radiolabelling is also required to ensure that the procedure does not result in a loss of immunoreactivity. This has lead to further interest in site-specific labelling technology, eg. making a fragment incorporating its own radionuclide binding site.

Another potential advantage for the use of antibodies lacking the Fc region is a reduction in immunogenicity of rodent antibodies. The sensitization of humans to xenogenic protein, i.e. the human anti-mouse antibody (HAMA) response is considered a major obstacle to the success of antibody-mediated targeted therapy. This prevents, in many cases, successful repeated delivery of therapy due to due to the rapid clearance of resulting immune complexes.

Schroff *et al.*, reported the emergence of the HAMA response in phase I clinical trials of MoAbs, T101, in patients with CLL and CTCL, and 9.2.27 in patients with malignant melanoma [84]. This report documented pre-existing antiglobulin levels in the serum of a proportion of patients and a similar proportion of healthy controls. Following MoAb administration, all patients with CTCL, and three of nine patients with melanoma developed elevated titres of anti-mouse Ig. The response occurred rapidly (within two weeks) and was principally directed against the Fc component of the antibody. In a further analysis of the HAMA response in patients receiving T101, Shawler *et al.*, suggested that the anti-idiotypic component of the HAMA response rose steadily with the number of antibody administrations [85]. This has also been observed with radiolabelled murine MoAbs [86].

Several approaches have been developed in an attempt to overcome this problem. One method is to reduce the intensity of the HAMA response by the use of immunosuppressive agents such as cyclosporin A, cyclophosphamide and steroids [87]. A second approach is to either produce specific unresponsive MoAbs or to alter immunogenicity by the coupling of substances such as polyethylene glycol. This may convert xenogenic MoAbs into specific tolerogens. A third way is to use human MoAbs produced from Epstein-Barr virus transformed lymphocytes or from human or human-mouse hybridomas. Finally, using recombinant DNA technology, it is now possible to engineer MoAbs to where only either the variable regions or the antigen binding sites alone are defined by rodent gene sequences, while the rest of the molecule is "human" [88]. In the latter case, the contribution of rodent protein is less than 5%. This technology may also be used to construct antibody fragments eg. single-domain antibodies (dAbs) or those which consist solely of antigen-binding protein sequences (minimal recognition units). A non-radiolabelled humanised antibody directed against the CDw52 antigen has recently been used to treat two patients with relapsed non-

Hodgkin's lymphoma. Good remissions were induced in both, and no anti-globulin response arose, despite antibody administration of up to six weeks [89]. Nevertheless, there remains the potential for developing an anti-idiotypic or anti-allotypic response to these reagents. On the other hand, the use of humanised MoAbs is likely to result in very prolonged vascular carriage. Whilst this may be beneficial for the use of MoAbs as biological response modifiers, this may result in an unacceptable exposure of normal tissues to a conjugated toxic agent, which may not be compensated for by a similar increase in tumour exposure.

The activity-limiting toxicity associated with systemically administered targeted radiotherapy is generally myelosuppression due to the sterilisation of haemopoetic stem cells within the red bone marrow. Attempts to overcome this have included the harvesting and re-infusion post-therapy of the patients marrow. Press *et al.*, reported a study of patients with unresponsive B-cell lymphoma, who received between 250 and 482 mCi ^{131}I-labelled MoAb, MB-1 (CD 20), followed by autologous bone marrow infusion [90]. All four patients sustained a complete remission of between four and 12 months (see also Chapter 13).

(iv) The choice of radionuclide.

Therapeutic studies of antibody-mediated therapy have mainly employed ^{131}I as the radiation source. This isotope decays to ^{131}Xe with a half-life of 8.04 days. It predominantly exerts its cytotoxic effect by the emission of β-electrons, with an average energy of 0.183 MeV and a mean pathlength in water (R_{50}) of 0.285 mm [91]. The choice of this agent is based upon a number of factors, including relative ease and low cost of production methods, and the well established methodology for protein labelling. A proportion (~ 15%) of the emitted energy is in the form of gamma emissions

(80% with energy 0.36 MeV) which has enabled gamma scintigraphy to be used as a means of examining the *in-vivo* fate of the radiolabel.

Several mathematical models have been developed which examine the relative merits of candidate radionuclides for tumour targeting [92] [93] [94]. These point for the need to tailor the choice of radionuclide to morphology, particularly size, of the tumour to be targeted. For larger tumours, especially those in which antibody penetration into the tumour is significantly restricted, or where there is marked heterogeneity of antibody penetration or antigen expression, long range β-emitters are most appropriate, for which the crossfire effect (the irradiation of non-targeted cells by radionuclide bound to neighbouring targeted cells) will make a significant contribution to tumour dose. As tumour size decreases, the gain from crossfire decreases, making the choice of shorter-range emitters more appropriate [92] [93]. As a result of such considerations, it is clear that ^{131}I is not an ideal isotope for targeting the majority of tumours, and the use of alternative radionuclides has been the focus of much research.

Humm has classified suitable radionuclides for consideration into: (1) alpha-emitters such as ^{211}At and ^{212}Bi; (2) low-range β-sources (mean range <200 μm) eg. ^{33}P, ^{191}Os and ^{199}Au; (3) medium-range β-sources (mean range >200 μm, <1 mm) eg. ^{131}I, ^{111}Ag, ^{67}Cu, ^{77}As and ^{186}Re; (4) long-range β-sources (mean range >1 mm) eg. ^{90}Y, ^{32}P and ^{188}Re and (5) electron captive and internal conversion decaying radionuclides eg. ^{125}I, ^{77}Br and ^{197}Hg [92].

Of these, only ^{131}I and ^{90}Y have been widely used in clinical trials, although a trial is being undertaken of a ^{125}I-labelled MoAb in the treatment of glioma [95], and pre-clinical investigations of a number of other agents, notably the alpha-emitters, have been conducted [13] [96] [97].

(v) Dosimetry and radiobiology.

The development of targeted radiotherapy has necessitated new approaches to tumour dosimetry, as well as consideration of the radiobiology of this form of radiotherapy. To date, dosimetry has relied upon the quantification of isotope accumulation using planar gamma camera imaging and estimates of tumour and organ doses using the MIRD (Medical Internal Radiation Dose) formalism [91]. By these means, absorbed doses in the order of 10 - 45 Gy with ^{131}I and 10 - 30 Gy with ^{90}Y have been reported [83] [90] [98]. Radioimmunotherapy has also been shown to result in very low dose rates of between 5 and 30 cGy/hour [99]. One particular problem with these methods is the lack of definition of the heterogeneity of radionuclide distribution, which is clearly present in the majority of solid tumours.

Attempts to provide quantification of source heterogeneity include imaging with single photon emission computed tomography (SPECT) and positron emission tomography (PET) [99]. Calculations of cumulative absorbed dose may also be performed directly using dosimeter probes inserted into accessible regions of tumour. Examples of such probes include thermoluminescent dosimeters (TLDs) and dosimeters based upon the metal oxide semiconductor field effect transistor (MOSFET) [100].

A third approach is that based upon autoradiographic procedures. Either frozen or processed tissue sections may be analysed using conventional film autoradiography or by a much faster technique employing phosphor imaging plates [99]. These methods have the advantage of particularly high spatial resolution and are appropriate for use with very short range emitters, eg. emitters of alpha-particles or Auger electrons.

A number of radiobiological problems are posed by the differences between targeted and conventional radiotherapy. These include: dose-rate effects on both tumour and normal tissues, the relative biological effectiveness of radionuclide therapy and the role of tumour and targeting heterogeneity in

dose deposition [93]. Dale has extended the linear-quadratic model to derive equations for the "relative effectiveness" of continuous radiation exposures [101]. O'Donoghue and Wheldon used these equations to demonstrate that large dose-rate effects are possible, especially for late-responding normal tissues [102]. Other mathematical models have also been developed to explore these issues [103].

There is very little experimental data on the comparison between radioimmunotherapy and external beam irradiation in terms of biological effect for an equivalent total dose. Wessels *et al.*, measured the growth delay of TK-82 renal cell carcinoma xenografts implanted into nude mice receiving single fraction external beam irradiation, multifraction external beam irradiation, or ^{131}I-MoAb therapy [104]. TLDs were used to quantify the average absorbed dose for radioimmunotherapy. They concluded that over a range of similar absorbed doses, an equivalent to superior tumour growth delay was obtained for radioimmunotherapy as compared with acute dose rate external beam radiotherapy.

(vi) Compartmentalisation of therapy.

One approach to avoiding obstacles posed by the vascular delivery of radioimmunoconjugates was pioneered by the Hammersmith Hospital Oncology Group. The authors argued that administration of antibody into a restricted space would result in a higher tumour to normal tissue ratio. The specificity and intrinsic affinity of the antibody carrier should make them superior to previously used agents such as colloidal radioactive gold [105] and phosphorus [106].

The first three patients treated in this way had a carcinomatous effusion in each of three different body cavities [107]. Each patient was given 20 mCi ^{131}I conjugated to MoAb, HMFG2, into the relevant tumour-bearing cavity. No toxicity was observed and a tumour response was documented in each patient.

The estimated radiation dose delivered to malignant sites was between 50 and 70 Gy.

This group subsequently concentrated on developing this therapy for patients with ovarian carcinoma extending within the peritoneal cavity. A series of 24 patients with persistent epithelial ovarian carcinoma after surgery and chemotherapy were reported in 1987 [108]. Patients were classified as either having "minimal residual disease" or "macroscopic disease", defined as tumour deposits of either less than 2 cm or greater than 2 cm in diameter respectively. The dose of ^{131}I administered intraperitoneally (IP) was escalated from 20 mCi to 205 mCi per patient and this was conjugated to a variety of tumour-binding MoAbs. Toxicity was reported as acceptable and was chiefly manifest by nausea and vomiting (9/24), fever (7/24) and mild abdominal pain (4/24). Bone marrow toxicity was not reported.

All eight patients with macroscopic disease failed to respond to therapy and died within nine months of treatment. Assessment of response in 16 patients with "minimal residual disease" was complicated by a "second-look" laparoscopy only being performed in three. However, of this group, nine continued in complete remission after antibody-guided therapy. Of these, five relapsed after three to 20 months, but four remained clinically free from disease at the time of reporting, at between six and 36 months from treatment.

This group also investigated further the role ^{131}I radioimmuno-conjugates when delivered into other body compartments. Pectasides *et al.*, reported the results of therapy in patients with malignant effusions of the pericardium and pleural cavity [109]. All three patients with pericardial effusions responded to the therapy, with no fluid re-accumulation after three, 12 and 18 months respectively. Seven patients with pleural effusions had a similar response, maintained for the follow-up period of between three and 18 months. No clinical or other toxicity was observed.

More recently, the Hammersmith group have extended their studies to investigate the role of ^{90}Y-labelled MoAbs [110]. Disease extent prior to targeted therapy varied widely, from patients with bulky disease and ascites, to 13 patients with no evidence of disease, who received therapy as an adjuvant measure. Patients were given an IP injection of between 5 and 30 mCi ^{90}Y conjugated to MoAb HMFG1 using the chelating agent, diethylene-triamine-penta-acetic acid (DTPA).

Of the first 14 patients treated, one developed severe myelo-suppression following an injection of 16.3 mCi ^{90}Y. To protect the bone marrow from this bone-seeking radionuclide, subsequent patients received an IV infusion of sodium calcium ethylene-diamine-tetra-acetic acid (EDTA) to chelate free circulating ^{90}Y. Only minimal toxicity was subsequently observed in 16 patients given a dose of up to 30 mCi ^{90}Y-DTPA-HMFG1. Of the 17 patients with demonstrable disease at the time of therapy, responses were observed in only one of eight patients with nodular deposits. In three of five patients with ascites, this had not recurred at the time of death at between seven weeks and three months post-treatment. Twelve of the 13 women administered conjugate as an adjuvant were clinically free of disease with follow-up times of up to 20 months. The authors stressed the instability of DTPA-labelled MoAbs, a phenomenon noted previously by others [111], and pointed to the need for the development of more stable chelators (eg. macrocycles) of radiometals to reduce myelosuppression and allow further dose escalation.

(e) Radionuclide therapy for leptomeningeal malignancy.

Workers at our own institution also recognised the potential of compartmentalised antibody-mediated radiotherapy and that this approach could be applied to the treatment of central nervous system (CNS) tumours.

The subarachnoid space lying between the two leptomeninges, the pia and arachnoid mater, and containing the cerebrospinal fluid (CSF), was considered a unique body cavity in which to investigate this mode of therapy. Its volume is relatively small, 100 - 160 ml in adults [112], and a high activity concentration of radioimmunoconjugate would be expected following injection. Furthermore, unlike the serous cavities, the production and composition of CSF is well regulated, with the potential for radioconjugate to be adequately distributed to tumour deposits throughout the CSF pathways. Leptomeningeal involvement is a well recognised complication of a number of tumour types, resulting from either systemic dissemination, eg. carcinoma and leukaemia, or as a result of extension from primary sites elsewhere within the CNS, eg. medulloblastoma and other so-called primitive neuroectodermal tumours (PNETs).

Although many of these tumours are radiosensitive, conventional therapy, particularly with high dose external beam radiotherapy, is associated with a high risk of significant neurological sequelae (see below), a factor limiting the intensity of therapy. This, and the highly malignant nature of this group of tumours, is responsible for their generally very poor prognosis.

(i) Radiocolloids.

Based on the rationale describe above, intrathecally-administered radioactive gold (^{198}Au) colloid has been widely investigated for the treatment of meningeal tumours. ^{198}Au is predominantly an emitter of β-electrons with an average energy of 0.32 MeV and a mean path length (R_{50}) in water of 0.99 mm (R_{95} = 1.88 mm) [91].

In 1968, D'Angio *et al.*, described the results of therapy in eight patients with medulloblastoma and two with leukaemia [113]. Each received, by lumbar puncture (LP), either one or two doses of between 9 and 15 mCi of ^{198}Au colloid. This was given following craniospinal external beam irradiation

with a further course of irradiation to residual sites of disease. Acute toxicity occurred following ten of 15 injections, and was manifest by transient signs of aseptic meningitis of variable severity. The combined treatment approach resulted in control of spinal disease in five of eight patients with medulloblastoma, but the efficacy of radioactive gold itself could not be determined. In contrast, neither patient with acute leukaemia showed any response to treatment.

Four years later, Gold *et al.*, described this group's further experience in 14 patients with disseminated medulloblastoma [114]. An unexpected and severe toxicity reported in this series was the occurrence of the cauda equina syndrome in five patients. This was characterised by leg and back pain (5/5), weakness (5/5) and paraesthesia (3/5) of the lower extremities and a varying degree of loss of bowel and bladder control (3/5). The cauda equina syndrome was thought to have resulted from lumbo-sacral pooling of radiocolloid with a consequently high radiation dose to the nerve roots. The authors attempted to prevent the development of this complication by tilting the patient in a 60° to 90° head-down position at the time of administration of radiogold. Nine further patients with medulloblastoma, managed in this way, were reported in 1974, none of whom had developed the cauda equina syndrome at follow-up times of between 12 and 42 months [115]. Nevertheless, this complication has probably hindered the widespread development of this technique.

In Jena, Germany, the use of intrathecal (IT) ^{198}Au-colloid has, however, been intensively investigated as a means of replacing external beam radiotherapy in the prevention of overt CNS acute lymphoblastic leukaemia (ALL) (see below). Metz *et al.*, reported the application of this technique incorporated into five therapeutic protocols used in 73 children with ALL, and administered following remission induction chemotherapy [116]. A single lumbar injection of between 46 and 181 MBq was followed by tilting of the child head-down for 15 - 30 minutes. Acute toxicity was acceptable, with a

9.6% incidence of both headache and vomiting. No delayed toxicity attributable to therapy was observed in any child.

The true therapeutic efficacy of IT gold is difficult to assess in this uncontrolled study. The follow-up period varied between 0 and eight years. In addition, each protocol included the use of IT methotrexate (MTX) during both the remission induction phase and the continuation chemotherapy phase. Five patients (6.8%) developed overt CNS ALL during continuation chemotherapy, with a further patient developing this complication after discontinuation of the treatment protocol.

Colloidal radioisotopes have also been used in the treatment of overt CNS ALL. In a study by Sackmann *et al.*, 32 patients who achieved meningeal remission with IT MTX were randomised to receive, at six week intervals, either IT MTX and dexamethasone or IT injections of colloidal radioactive chromium phosphate (Cr $^{32}P0_4$) [117]. No significant difference was observed in terms of the duration of meningeal remission between each group. Injection of the ^{32}P colloid was tolerated well, but three of 16 patients receiving this agent subsequently developed severe cauda equina syndrome. As with ^{198}Au-colloid, this probably occurred as a result of sacral nerve route irradiation by a long-range β-emitter pooling in the lower spine.

(ii) Radiolabelled monoclonal antibodies.

In 1990, our group reported the results of a pilot study of IT radioimmunotherapy in I5 patients with neoplastic meningitis [118]. All patients had failed an "adequate" trial of conventional therapy and had evidence of leptomeningeal dissemination of tumour that was shown to bind the MoAb chosen as the targeting agent. The patients presented with a heterogenous group of malignancies, namely; five with PNETs, four with carcinomatous meningitis, two with glioma, two with melanoma, one with B-cell lymphoma and one with spinal teratoma. They each received a single

injection of between 11 and 60 mCi ^{131}I-MoAb, administered into the CSF by LP (3/15), via an intraventricular Ommaya reservoir (10/15) or by both routes (2/15). Pharmacokinetics were determined by immuno-scintigraphy, undertaken from five days following therapy, and sequential sampling of blood and CSF.

Acute toxicity was most frequently manifest as aseptic meningitis. This occurred in 7/15 patients, and was characterised by a triad of headache, nuchal rigidity and nausea and vomiting. Symptoms typically began at four to six hours after injection and persisted for between eight and 48 hours. Of more concern was the development of seizures in two patients, which in one case possibly contributed to a toxic death, 72 hours from conjugate administration. The second patient developed status epilepticus ten days after therapy, but subsequently made a full recovery. Reversible bone marrow suppression of WHO grade 3/4 occurred in three of eight evaluable patients, following an injected activity of between 55 and 60 mCi.

Of nine patients evaluable for tumour response, eight had significant clinical signs at the time of treatment. Five demonstrated a marked improvement in clinical condition, which continued for at least seven months from therapy. The improvement in neurological status was accompanied by a complete objective response in these, and a sixth asymptomatic patient, which was assessed on the basis of either CSF cytology and/or myelographic changes. Of this group, one had pineoblastoma, one B-cell lymphoma, two melanoma, one medulloblastoma and one breast carcinoma. The event free survival of responders ranged from seven to 26 months (mean 12 months; median 9.5 months).

Pharmacokinetic studies revealed clearance of ^{131}I from the CSF by biexponential kinetics. The distribution of radionuclide within the neuraxis, as determined by scintigraphy, correlated well with the anticipated distribution of tumour, but unexpected areas of isotope accumulation were noted.

The results from this study were considered sufficiently encouraging to continue with full phase I/II studies. Two groups of diseases were particularly selected in which to evaluate further this approach to treatment; lymphoproliferative disease and PNETs. This thesis is concerned with the development of targeted radiation therapy for the former group of malignancies, particularly CNS leukaemia.

2. Central Nervous System Leukaemia.

(a) Historical perspectives.

In 1948, Sidney Farber demonstrated that antifolate therapy could result in temporary remission in some children with ALL [119]. Since that time, exceptional progress has been made. In more recent series, at least 60% of children with ALL can be expected to be alive and free of disease five years from diagnosis [120]. Improved survival can be attributed to many advances, perhaps none more important than the provision of effective therapy for the prevention of CNS leukaemia.

In the 1960's, prior to the introduction of CNS preventive therapy, the CNS became the most frequent site of initial relapse in children with ALL [121]. In some studies, the incidence of this complication was as high as 75% [122] [123]. Although morbidity from CNS leukaemia was serious, the main problem of this complication was its apparent influence on shortening haematological remission. It was also apparent that established CNS ALL was extremely difficult to eradicate [124].

Once CNS leukaemia was identified as the major factor limiting disease control in childhood ALL, interest developed in attempts to prevent this complication. It was postulated that at the time of diagnosis, leukaemic cells already existed in the meninges and remained there after clinical remission was

achieved, and further that a pharmacological barrier, the so-called "blood-brain barrier", protected the meninges from the effects of drugs in the systemic circulation. The CNS thus represents a "sanctuary site" for leukaemic cells. Other such sites include the testes and the eye [125].

Pinkel suggested that radiotherapy of the CNS early in remission could eradicate the residual cells and prevent CNS relapse. From 1962 to 1965, children with ALL at the St Jude Children's Research Hospital (SJCRH) received either 5 or 12 Gy of craniospinal irradiation early in remission. This had little impact on the frequency of CNS relapse, which still occurred as an initial event in 40% of cases.

Pinkel and colleagues subsequently increased the dose of craniospinal irradiation to 24 Gy. This was found to be remarkably effective, with the risk of initial CNS relapse falling to 4% of a group of 45 patients. The efficacy of this regimen was confirmed in a controlled study (SJCRH Study VI) [126]. Subsequent studies demonstrated that spinal irradiation could be replaced by a course of IT MTX early in remission, with a consequent reduction in toxicity [127]. From this work came substantial evidence that presymptomatic CNS therapy prevented haematological relapse. In the SJCRH Total Therapy VI study, 58% of patients who received early craniospinal radiotherapy, were in continuous haematological remission eight to 11 years after diagnosis [128]. Thus, with presymptomatic CNS therapies, childhood ALL became curable in more than half of the children afflicted with this disease.

(b) Pathogenesis.

It is widely accepted that leukaemic cells enter the CNS at the time of active haematological disease. The other possibility is that non-detectable cells in the marrow enter the CNS at any time during systemic remission [129].

The mechanism by which leukaemic cells enter the CNS is not fully understood. The two major hypotheses are either the direct spread of cells

from the cranial bone marrow into the CNS and/or the entry of cells by the haematogenous route. Evidence for the former mechanism has come from observations in both animals and patients, which suggest that leukaemic cells in the cranial bone marrow migrate into the meninges by way of the adventitia of bridging veins and the perinuerium of nerves traversing the subdural space [130]. Azzarelli and Roessman demonstrated that the incidence and density of leukaemic infiltration in patients followed a gradient from the dura mater (93% of cases) to the brain parenchyma (16% of cases) [131]. Evidence for the haematogenous route comes from other post mortem studies, in which leukaemic cells were noted to first appear in the walls of superficial arachnoid veins, indicating that circulating leukaemic cells enter the CNS by migrating through the venous endothelium [132]. The method of ingress has important therapeutic implications. If the direct route predominates, craniospinal radiotherapy, which eradicates cells from cranial and vertebral bone marrow, may have greater efficacy in preventing CNS infiltration. If the haematogenous route is foremost, then systemic chemotherapy may be more effective.

Most workers agree that once leukaemic cells have entered the CNS, the disease begins in the superficial leptomeninges. It then invades the CSF, the deep arachnoid and eventually the Virchow-Robin spaces. Finally, and only in advanced disease, do cells penetrate into the brain parenchyma [131] [132]. The pia-glial membrane thus represents a relative barrier in this process.

Leukaemic cells appear to proliferate very slowly within the CNS, relative to those within the bone marrow. Patients have sustained isolated CNS relapses after as many as ten years of continuous initial haematological remission [133]. Studies of CSF samples from patients with overt CNS leukaemia, and observations of post mortem histological material, have revealed that CSF blasts have ^{3}H-thymidine labelling indices of less than 2% and mitotic indices below 0.02% [134] [135]. These proliferation kinetics may be a

further obstacle to the effectiveness of chemotherapy, especially with cell cycle specific agents.

With regard to the egress of CNS cells into the systemic circulation, intracerebral or IT injection of leukaemic cells in animal models consistently results in systemic leukaemia [130] [136]. Both direct infiltration and haematogenous spread (reverse diapedesis) have been demonstrated [130] [137]. Circumstantial evidence for this process in man is provided by the high rate of bone marrow relapse after isolated CNS involvement and the prevention of bone marrow relapse after effective therapy to the CNS.

(c) Clinical manifestations.

Patients who develop symptomatic CNS leukaemia most frequently present with signs and symptoms of raised intracranial pressure, including headache, nausea and vomiting, irritability, neck stiffness, lethargy, and papilloedema [138]. Other manifestations include: visual disturbances, cranial nerve palsies, myelopathy, seizures, hypothalamic syndromes, vertigo, ataxia and auditory disturbances. In addition, many treatment centres perform routine surveillance lumbar punctures, resulting in the majority of diagnoses of CNS relapse being made in asymptomatic individuals.

(d) Diagnosis.

In frank CNS relapse of ALL, the number of leukaemic cells within the CSF varies widely between less than 10 x 10^6/litre to as high as 65 x 10^9/litre, with a median of approximately 0.5 x 10^9/litre [125]. The cell count does not appear to correlate with the immediate treatment response, but with counts in excess of 1 x 10^9/litre, early recurrence is more likely [139]. In symptomatic cases, the opening lumbar thecal pressure is elevated in 90%, CSF protein concentration is elevated above 0.4 g/litre in 20 - 50% and CSF glucose concentration reduced below 0.4 g/litre in 55 - 70% of cases [125].

Cytochemistry, immunocytochemistry and chromosomal analysis may help confirm the diagnosis [140]. Other diagnostic investigations such as the CSF levels of polyamine, beta-2-microglobulin and beta-glucuronidase have been proposed, but are not established as routine procedures [141] [142].

(e) Incidence at diagnosis and prognostic factors for risk of CNS relapse.

CNS leukaemia at diagnosis occurs in between 3 and 5% of children with ALL [143] [144]. The risk for this occurrence is proportional to the initial blood white cell count (WCC) and is dependent on the patients age, being greater in infants and adolescents. In a report by the CCSG, those children with ALL with "low", "average" and "high" risk of marrow relapse had CNS leukaemia rates at diagnosis of 1.3, 2.7 and 7.6% respectively [143].

A number of initial features have been identified as positive risk factors for those children without CNS disease at diagnosis. These include high initial blood WCC [145] [146], T-cell disease [147] [148] [149], young age [146], thrombocytopaenia [123] and lymphadenopathy, hepatomegaly or splenomegaly [145] [146] [123]. However, no single factor has so far been identified which predicts with any degree of certainty whether an individual will not develop overt CNS disease. Even children at "low risk" for marrow relapse have a 50% incidence of CNS relapse when no specific presymptomatic measures are taken [150]. It is clear, therefore, that presymptomatic CNS therapy should be given to all children who present with ALL.

(f) Current methods of presymptomatic CNS therapy.

Regimens used to prevent overt CNS leukaemia consist of CNS radiotherapy, IT chemotherapy, high dose IV chemotherapy, or combinations of these modalities.

(i) Cranial irradiation and intrathecal methotrexate.

The prototypic CNS regimen developed at SJCRH consisted of cranial irradiation, 24 Gy in 14 or 15 fractions, combined with IT MTX, 12 mg/m^2 every three to four days for five doses. Its efficacy was confirmed in the Children's Cancer Study Group (CCSG) Study 101 [151].

Bleyer and colleagues subsequently devised an alternative IT MTX dosage regimen, in which a standard dose of 12 mg was given to all children three or more years of age. Lower doses were proposed for younger children [152]. This was based on pharmacokinetic considerations, and in turn relates to the relatively rapid growth in the CNS (and increase in CSF volume) with age, such that by three years, approximately 80% of CNS growth is complete. Data from the CCSG provided evidence for the superiority of this regimen over one based on body surface area [152]. In addition, the administration of IT MTX on a weekly basis appears equally effective, but less toxic than when given twice weekly.

The CCSG also showed that in patients with an initial WCC of less than 50 x 10^9/litre, a dose of cranial irradiation of 18 Gy is equally as effective as that of 24 Gy [153]. For patients with a higher initial WCC, there was a higher rate of CNS relapse, but the difference was of borderline statistical significance.

In the UK, most children with ALL are treated according to Medical Research Council (MRC) United Kingdom Acute Lymphoblastic Leukaemia (UKALL) study protocols. In the most recent study, UKALL X (1985-1990), CNS-directed therapy consisted of six weekly doses of IT MTX (12 mg for patients aged three years and above) and cranial irradiation (18 or 24 Gy for children with an initial WCC of below or above 50 x 10^9/litre respectively).

Despite the effectiveness of regimens containing CNS irradiation, many groups have investigated ways in which this mode of therapy may be circumvented. Proposed benefits of avoiding external beam CNS radiotherapy include: (1) reducing neuropsychological, neuroendocrine,

growth inhibitory, myelosuppressive and carcinogenic toxicity (see below), (2) the wider availability and lower cost of IT or IV chemotherapy than radiotherapy and (3) the observation that CNS irradiation may be administered with greater efficacy to the child who experiences an isolated meningeal relapse and has previously received CNS directed therapy not containing CNS irradiation (see below).

(ii) Intrathecal and intermediate dose intravenous methotrexate.

Several groups have investigated this strategy [154] [155]. In one study, children were randomised to receive treatment with either 24 Gy cranial radiation plus IT MTX or with moderate-dose (500 mg) IV MTX plus IT MTX [154]. In both standard and increased risk patients, the rate of CNS relapse was significantly higher in the IV MTX group than in the group receiving radiotherapy. However, the testicular relapse rate was much lower in the IV MTX group (one patient) than in the radiotherapy group (ten patients). Whereas there was no difference in the rate of bone marrow relapse in the group at increased risk, this was less common in the standard risk group given IV MTX (9/117) than in the group receiving radiotherapy (24/120) ($p < 0.01$).

(iii) Intrathecal chemotherapy.

Therapeutic schedules have consisted of either MTX alone or MTX combined with IT hydrocortisone with or without IT cytosine arabinoside (triple IT chemotherapy). In the CCGS-161 study, maintenance IT MTX (every eight weeks) was found be to as effective as 18 Gy cranial irradiation for low risk patients [156]. This strategy is being investigated further in the MRC UKALL XI trial.

The Paediatric Oncology Group (POG) studied IT triple chemotherapy during induction/consolidation therapy and every eight weeks thereafter

during continuation chemotherapy. This resulted in a total of ten CNS relapses (4.3%) for 234 patients in all risk groups, as compared to seven CNS relapses out of 105 patients (6.1%) who received doses of IT MTX and 24 Gy cranial irradiation [157]. Triple IT chemotherapy delivered in this way subsequently became the standard method in the POG for the prevention of CNS relapse [127].

(iv) High dose intravenous methotrexate with leucovorin rescue.

This approach is aimed to achieve high concentrations of MTX in the CNS following systemic administration, thereby avoiding or reducing the need for IT chemotherapy and/or CNS radiotherapy. Möe and colleagues have demonstrated the efficacy of a regimen of eight infusions of 6 - 8 g/m^2 IV MTX in high risk patients [158]. In another study, 180 children with intermediate or poor prognosis, were randomised to receive either high-dose IV MTX alone (ten doses) or cranial irradiation (24 Gy) plus five doses of IT MTX [159]. The dose of IV MTX was very high, 34 g/m^2 over 24 hours, in order to simulate the CSF drug concentrations achieved with IT MTX. There appears to be no difference in the isolated CNS relapse rate between these two groups. However, there is data to suggest that the IV MTX regimen is less toxic in terms of deleterious effect on both intellectual and academic function [160].

In summary, it is clear that CNS (and systemic) therapy should be tailored to the prognostic subgrouping. Therapy for the prevention of CNS disease should be also considered in terms of the overall therapeutic management. The best CNS therapy is one that is associated with the highest long-term disease-free and overall survival and at the lowest cost to the patient in terms of toxicity, even if results in a higher incidence of CNS relapse.

(g) Overt CNS leukaemia.

(i) Treatment.

Again, optimum therapy for frank relapse of CNS leukaemia has yet to be determined. Most centres employ a regimen that first clears the CSF of leukaemic cells with IT chemotherapy and then consolidates with either craniospinal irradiation or maintenance IT chemotherapy.

The efficacy of craniospinal irradiation was demonstrated in the SJCRH study VI. Eleven of 33 children who received 24 Gy to the neuraxis for CNS relapse, remained in complete remission for more than ten years [161]. This dose of spinal irradiation is, however, not generally employed owing to its significantly increased toxicity as compared to regimens prescribing a lower doses (eg. 12 Gy) in conjunction with IT chemotherapy.

The first MRC meningeal leukaemia trial showed an improved median remission of greater than two years using IT MTX to clear the CSF followed by 25 Gy cranial and 10 Gy spinal irradiation. This compared to a median CNS remission of only 3.8 months in patients given only cranial irradiation following IT MTX [162]. This was reflected in a significantly prolonged event-free survival in patients receiving neuraxis radiotherapy.

The strong tendency for haematological relapse to follow CNS disease has led the MRC and other groups to adopt systemic re-induction and intensification therapy following diagnosis of CNS relapse and prior to craniospinal irradiation. Wells *et al.*, reported ten patients with isolated CNS relapse during maintenance therapy who were treated with IT MTX and cranial spinal radiotherapy (24 Gy cranial and 12 Gy spinal) [163]. Only one had a second CNS relapse and five were in complete remission for between one and three years. Of six patients also treated with systemic re-induction therapy, five were in long-term remission at the time of reporting. A similar regimen was recommended for first CNS relapse of ALL in the recent MRC UKALL X study protocol.

Other groups have attempted to avoid the significant risk of neurotoxicity associated with a second course of CNS irradiation by the prolonged administration of IT chemotherapy. Studies by Sullivan and others have demonstrated that this approach is able to prolong CNS remission [164]. However, more recent reports of multidrug IT chemotherapy regimens [165] [166] suggest that duration of remission with these approaches is shorter than that obtained with regimens involving craniospinal irradiation.

Interest has also been expressed in the delivery of chemotherapy by the intraventricular route. It has been clearly shown that the distribution of drugs delivered intraventricularly is superior to that for the lumbar route [167]. In addition, it is probable that a greater number of malignant cells exist in the cerebral ventricles at the time of CNS relapse than at the initial diagnosis, which may be exposed to sub-optimal levels of drug when delivered by lumbar puncture [127]. The superiority of the ventricular route of administration was demonstrated in two controlled, but non-randomised, studies [168;169].

Both high-dose IV MTX with leucovorin rescue [170] and high-dose cytarabin [171] have also been shown to consistently induce CNS remissions in patients with overt disease and may prove useful in either replacing or augmenting CNS irradiation.

(ii) Prognosis.

The outcome for a first isolated CNS relapse of ALL appears variable. Patients who initially relapse in the CNS after the completion of all chemotherapy appear to have a relatively good prognosis. Bleyer reported seven of nine such patients, who were retreated with IT MTX and CNS irradiation, and were alive and in complete remission at between one and four years after the CNS relapse [127]. Similarly, several studies have demonstrated a relatively good rate of long-term complete second remission, of between 30

and 50%, in patients who have received CNS prophylaxis without prior CNS irradiation [161] [162].

The prognosis appears worse for children who have received previous CNS irradiation. In a report of study CCG-101, only three of 31 such children were in long-term remission, as compared to 36% of previously unirradiated patients [127]. In contrast, in a review of four studies of re-treatment with IT MTX and craniospinal irradiation for isolated first CNS relapse of leukaemia, 17 of 59 (28.8%) patients overall were in complete remission at the time of reporting [162]. However, follow-up times were relatively short, at between eight months and five years.

There is a paucity of data on the prognosis of patients with second or subsequent CNS relapse of ALL. In a report of the second MRC leukaemic trial, the median duration of CNS remission for this group was approximately 30 weeks [172]. It appears that whilst the CSF can often be cleared of lymphoblasts using IT chemotherapy, the duration of both CNS remission and haematological remission is much shorter than that following first CNS relapse. It is likely that in these circumstances, very few patients are able to be treated such that a sustained remission is achieved.

(h) CNS Involvement in lymphoproliferative disease other than childhood ALL.

(i) Adult ALL.

When assessed as a function of duration at risk, the incidence of overt CNS leukaemia in adult ALL approaches that in childhood ALL [173] [174]. In an autopsy series, 81% of patients with ALL had evidence of CNS infiltration [175]. Controlled trials have clearly demonstrated an advantage of therapies, similar to those employed in children, in the prevention of CNS relapse [174].

However, they appear not to have yet made a significant impact on prolonging haematological remission or survival [127].

(ii) Acute myeloid leukaemia (AML).

CNS disease in AML occurs in between 20 and 50% of children [176] [177], and 9 to 47% of adults [127], if no preventative measures are taken. It appears particularly prone to occur with acute myelomonocytic or acute monocytic leukaemia. Therapy with either cranial irradiation and IT MTX or with IT cytarabine appears to be effective in reducing the incidence of overt CNS disease [127]. As with adult ALL, there is little evidence of an effect on the length of haematological remission, and opinion remains divided on the need for presymptomatic therapies in this condition.

(iii) Non-Hodgkin's lymphoma (NHL).

Leptomeningeal infiltration is also increasingly recognised in patients with both B- and T-cell NHL [178] [179]. In the UK, patients with T-cell NHL are generally treated according to the current MRC UKALL protocol which includes both cranial irradiation and IT MTX. The UKCCSG B-cell NHL protocols include therapy with either IT MTX or IT triple chemotherapy.

(i) Toxicity associated with radiation therapy to the CNS.

(i) Acute and sub-acute reactions.

When administered alone, CNS radiotherapy is occasionally associated with symptoms of headache, vomiting, drowsiness and anorexia [125]. A few patients have been described who, having received one or two doses of IT MTX, developed a severe encephalopathy within three to 30 hours after the first dose of cranial irradiation [180] [181]. In one case, this reaction proved fatal.

A sub-acute reaction, the somnolence syndrome, is frequently seen following whole brain irradiation, even with doses as low as 18 Gy. This syndrome has been noted in up to 78% of irradiated children and usually begins five to seven weeks after the start of cranial irradiation [182]. It is characterised by drowsiness, nausea and malaise, and is associated with diffuse slowing of electrical activity on the electroencephalogram. The pathogenesis is thought to relate to temporary inhibition of myelin synthesis [127]. The syndrome is, however, benign and usually abates within ten to 30 days [182].

(ii) Delayed toxicity.

Whilst both moderate and high dose IV chemotherapy and IT chemotherapy may result in severe delayed toxicity when administered alone, regimens involving CNS irradiation appear to be most neurotoxic [127].

With regard to cranial irradiation alone, its association with brain necrosis is well recognised. Sheline reviewed 83 reported, mostly fatal, cases occurring following treatment for a variety of malignant and benign conditions [183]. Whilst most cases were associated with a radiation dose greater than 50 Gy, fatal necrosis was also noted with doses as low as 36 Gy.

The severe neurotoxicity associated with cranial irradiation for primary brain tumours is being increasingly recognised. Most recent studies report that a significant number of survivors of medulloblastoma (whole brain radiation dose 25 - 35 Gy) suffer from long-term neuropsychological disability including a reduction in intelligence score, learning disorders and sensorimotor and visual disturbances [184] [185] [186]. It is also reported that the majority of survivors develop growth hormone dysfunction [187].

The delayed neurotoxicity associated with combined CNS irradiation and IT MTX range from a mild intellectual deficit to fatal leucoencephalopathy (see below). A number of workers have shown significantly reduced intelligence amongst children treated with 24 Gy cranial irradiation and IT MTX

[188] [189] [190]. In a review of such studies, Bleyer reported that generally the mean overall intelligence score in irradiated children is 10 to 15 points lower than the mean scores in non-irradiated leukaemic children or sibling controls [127]. Performance skills appear to be more affected than verbal skills. It is clear that the younger the child is at the time of cranial irradiation, the greater the risk and severity of deficits [188] [190].

The most severe complication of these therapies is that of white matter necrosis or necrotizing leucoencephalopathy [191]. Whilst this condition may be sub-clinical or result in few symptoms, a typical case begins four to 12 months after irradiation with signs of progressive dementia. This may be fatal, but usually results in permanent neurological damage. Patients who have received a combination of cranial irradiation, IT MTX and high doses of IV MTX are most at risk [127]. With combined 24 Gy irradiation and IT MTX, the reported incidence varies between 2 and 15% [127]. However, Rubinstein reported a 47% risk of this condition in patients having received greater than 35 Gy cranial irradiation and a total dose of IT MTX of greater than 150 mg [192].

The reported incidence of growth hormone deficiency following 24 Gy cranial irradiation is variable. Some centres have been observed no effect on final height [193], whereas others report a substantial height loss [194]. For doses greater than 30 Gy, there appears a definitely substantial risk of growth hormone dysfunction [195] as well as other deleterious effects on the hypothalamic pituitary axis. Precocious puberty, probably due to gonadotrophin deficiency, has also been observed following whole brain irradiation with doses as low as 18 Gy [196].

Only few studies to date have documented the toxicity associated with 18 Gy cranial irradiation. Similarly, due to the relatively low incidence of overt CNS leukaemia and its poor prognosis, there are few detailed reports of the effects of two courses of CNS directed therapy in CNS ALL, i.e. including

radiation doses of 42 - 48 Gy. However, there can be little doubt that these cumulative doses of cranial radiation, allied to therapy with IT and/or IV chemotherapy, are associated with a significant risk of severe neuropsycological and neuroendocrine sequelae [183] [195] [197] . For second or subsequent CNS relapse, the risk of neurotoxicity almost certainly precludes a third course of CNS irradiation.

3. Aims of the Present Study.

The principle objective of this thesis is to develop targeted radiation therapy for leptomeningeal malignancy, particularly CNS leukaemia. This necessitated the selection and characterisation of MoAbs for use in both pre-clinical experimentation and a clinical programme. Optimum conditions for radiolabelling required investigation. A series of experiments were planned to explore the effect of variation in the specific activity of radioconjugates.

Specificity is central to the concept of targeted therapy. An *in-vitro* cell survival assay was developed to explore this issue as well as other radiobiological aspects of targeting ^{131}I against a single cell suspension of tumour cells. These issues were further examined by a mathematical model. The *in-vitro* model is appropriate for the investigation of other potentially useful radionuclides. The Auger-emitting radioisotope ^{125}I was examined in this respect.

In recognition of the limitations of *in-vitro* models, a small animal model of CNS leukaemia was established to investigate the efficacy of targeted therapy, to examine specificity and explore treatment variables.

Following pre-clinical experimentation, a multicentre phase I/II clinical study was initiated. Particular attention was paid to the biodistribution of radioimmunoconjugates injected into the CSF. Models for the estimation of radiation dose to both CSF and normal tissues were developed.

CHAPTER 2.

GENERAL MATERIALS AND METHODS.

MATERIALS.

Chemical Reagents	Supplier
Acetic acid	Fisons PLC
Acrylamide	British Drugs House (BDH)
Agar Noble	Difco
Agarose Noble	Difco
Agarose IEF	Pharmacia
Ammonium persulphate	BDH
Ammonium sulphate	BDH
Bisacrylamide (N'N-Methylene Bisacrylamide)	BDH
Bromophenol blue	Sigma
Bovine Serum Albumin (BSA)	Sigma
Butan-1-ol	Fisons PLC
Chloramine-T	Hopkin and Williams Ltd
Chlorhexidine	Imperial Chemical Industries PLC
Chloroform	Fisons PLC
Citric Acid	FSA Laboratory Supplies
Coomassie Brilliant Blue R250	LKB Bromma
Cyclophosphamide (100 mg dry powder)	Degussa Pharmaceuticals Ltd
Dimethyl sulphoxide (DMSO)	Fisons PLC
Dithiothreitol	Sigma

Donor Calf Serum (aseptically collected)	Gibco Ltd
DPX mountant	BDH
Eosin	BDH
Ethanol	Hayman Ltd
Ether	BDH
Fibrowax™	BDH
Ficoll	Sigma
Foetal Calf Serum (FCS)	Gibco Ltd
Formalin (buffered neutral formalin-BNF)	Sol Media
Glutamine (-L)	Gibco Ltd
Glutaraldehyde	BDH
Glycine	FSA Laboratory Supplies
Glycerol	Fisons PLC
Haematoxylin	BDH
Heparin (Mucous) (5000 IU/ml)	Leo Laboratories
Human Plasma Protein Fraction (HPPF) (Human Albumin Solution 4.5%)	Blood Transfusion Service
Hydrochloric acid (HCl)	Fisons PLC
Hypnorm™	Janssen Pharmaceuticals Ltd.
Hypnovel™ (Midazolam 10 mg/5 ml)	Roche Products Ltd.
India Ink	Staedtler
Iodogen™ (1, 3, 4, 6-tetrachloro 3 α diphenyl glycouracil)	Pierce
Isopaque™ (Metrizoate)	Nycomed
Isoton™	Coulter Electronics Ltd
Methanol	BDH
Methotrexate (5 mg/2 ml; pH 8.5)	Lederle
Methylene Blue Injection	Evans Pharmaceuticals

Penicillin (5000 IU/ml)-Streptomycin (5000 μg/ml)	Gibco Ltd
Pentobarbitone	Roche Products Ltd
Pharmalyte™	Pharmacia
Potassium iodide	Fisons PLC
Pristane oil (2, 3, 10, 14 - Tetramethyl Pentadecane)	Sigma
Propan-1-ol	Fisons PLC
Scott's reagent	BDH
Sodium azide	BDH
Sodium chloride (NaCl)	Fisons
Sodium dodecyl sulphate (SDS)	BDH
Sodium hydroxide (NaOH)	BDH
Sodium iodide (NaI)	Fisons PLC
Sodium metabisulphite	Hopkin and Williams Ltd
Sorbitol (-D)	Sigma
Sulphosalacylic Acid	Hopkin and Williams Ltd
Sulphuric acid (H_2SO_4)	Fisons PLC
Trichloroacetic acid (TCA)	Fisons PLC
TEMED (N, N, N'-Tetramethyl Ethylene Diamine)	Bio Rad
Tris (Tris-(hyroxymethyl)-Methylamine)	Fisons PLC
Trypan Blue	Sigma
Xylene	Sol Media
Zaponin™ lysing reagent	Coulter Electronics Ltd

Chromatography Materials.

Protein-A Sepharose CL-4B™	Pharmacia Fine Chemicals
CNBr-activated Sepharose™	Pharmacia Fine Chemicals
Sephadex G-25™	Pharmacia Fine Chemicals

Sephacryl S-300 HR™	Pharmacia Fine Chemicals

Radionuclides.

Iodine-125 (IMS:30)	Amersham International
Iodine-131 (IBS:30)	Amersham International

Immunological Reagents.

Fluorescein (FITC) conjugated rabbit anti-mouse $F(ab')_2$ fragment	Dakopatts
Goat Ig to mouse $IgG_1/Ig_{2a}/IgG_{2b}/IgG_3/IgM(Fc)$	Nordic Immunological Laboratories Ltd

Monoclonal Antibodies.

Anti-Id-1 (RJD)	Professor G Stevenson Tenovus Research Laboratories Southampton UK
HD37	Professor B Dorken University of Heidelburg Germany
M340	Dr J Kemshead Imperial Cancer Research Fund Bristol UK
RFAL3	Professor G Janossy Royal Free Hospital London UK
UJ13A	Dr J Kemshead Imperial Cancer Research Fund Bristol UK
UJ181.4	Dr J Kemshead Imperial Cancer Research Fund Bristol UK

WCMH	Dr W Cassano University of Florida USA
WT1	Dr W Tax St Radoudziekenhuis Nijmegen The Netherlands

Tumour Cell Lines

Cell Line	Tumour Type	Reference
KM3	pre-B ALL	[198]
Nalm 6	pre-B ALL	[199]
Nalm 16	pre-B ALL	[200]
Reh	pre-B ALL	[201]
Daudi	B-cell lymphoma	[202]
GH1	T-ALL	[200]
JM	T-ALL	[198]
MOLT 4	T-ALL	[203]
L_2C	Guinea pig B-ALL	[204]

Buffers and Solutions.

Acrylamide (30% stock solution)	30 g acrylamide 0.8 g bisacrylamide to 100 ml with distilled water (dH_2O)
Agarose IEF Brilliant Blue stain	1.0 g Coomassie Brilliant Blue 300 ml dH_2O 150 ml methanol 50 ml acetic acid
Agarose IEF destain	300 ml dH2O 150 ml methanol 50 ml acetic acid
0.1 M Citrate Buffer	0.1 M citric acid titrated to required pH with 5 M NaOH

Ficoll-Isopaque	63.53 g Ficoll in 600 ml dH_2O 133.7 ml Isopaque to 1 litre in dH_2O
Ouchterlony Coomassie Brilliant Blue stain	5 g Coomassie Brilliant Blue 450 ml ethanol 100 ml acetic acid 450 ml dH_2O
Ouchterlony destain	250 ml ethanol 100 ml acetic acid 450 ml dH_2O
Phosphate Buffered Saline (PBS) (0.15 M; pH 7.2)	8 g/litre NaCl 0.2 g/litre KCl 0.15 g/litre Na_2HPO_4 0.2 g/litre KH_2PO_4 pH 7.2
Polyacrylamide gel Brilliant Blue stain	1 g Coomassie Blue 500 ml methanol 100 ml acetic acid 400 ml dH_2O
Polyacrylamide gel destain	700 ml dH_2O 200 ml methanol 100 ml acetic acid
SDS PAGE running buffer	3.03 g/litre Tris 14.42 g/litre glycine 1 g/litre SDS pH 8.8
SDS PAGE sample buffer	0.5 ml glycerol 0.5 ml 10% SDS 0.4 ml 0.25 M Tris pH 6.8 3.1 ml dH_2O 0.01% bromophenol blue

Culture Media.

Complete RPMI 1640 (Roswell Park Memorial Institute)	Gibco; supplemented with 10% heat-inactivated (HI) (56°C for 60 minutes) FCS 2 mM L-glutamine 100 IU/ml penicillin 100 µg/ml streptomycin

Complete Dulbecco's modification of Eagles Medium (DMEM)	Flow Laboratories; containing 3.7 g/litre sodium bicarbonate, supplemented with 20% HI FCS 2 mM L-glutamine 100 IU/ml penicillin 100 µg/ml streptomycin
Complete Hams F12	Gibco; supplemented with % HI aseptically collected donor calf serum 2 mM L-glutamine 100 IU/ml penicillin 100 µg/ml streptomycin

GENERAL METHODS.

1. Cell Culture.

(a) Maintenance of hybridomas and human tumour cell lines in tissue culture.

Hybridomas were grown in 60 mm tissue culture dishes containing 5 ml complete DMEM supplemented with mouse macrophages. Human tumour cell lines were grown in 750 ml tissue culture flasks containing 25 - 100 ml complete RPMI medium. Both hybridomas and human cell lines were maintained at 37°C in a 6% CO_2/94% air incubator. Cells were inspected daily and sub-cultured 1:2 - 1:4 when approaching confluency.

(b) Harvesting of mouse macrophages.

Female Balb/c mice were sacrificed and the peritoneum washed with 6 ml of complete DMEM. The exudate containing approximately 2 x 10^5 macrophage cells was withdrawn and centrifuged at 400 x g for five minutes. Cells were resuspended in fresh complete DMEM at a ratio of one washing per 50 ml of medium.

(c) Recloning of hybridomas by limiting dilution.

Cells in exponential growth phase were centrifuged at 400 x g for five minutes and resuspended in 5 ml complete DMEM. The proportion of viable cells was calculated by Trypan Blue exclusion and the cell population diluted to give an estimated 1, 3 and 10 live cells per 200 µl of tissue culture medium. A 96 well plate was seeded with 200 µl of cell suspension at each dilution and incubated at 37°C. Wells were examined daily for cell growth and screened for antibody production by indirect immunofluorescence. Wells containing

antibody producing cells at lowest dilution were chosen for subsequent expansion.

(d) Monoclonal antibody production in ascites.

Hybridomas in exponential growth phase were prepared for injection by repeated washing and centrifugation in PBS. 5×10^6 cells per mouse were resuspended in 500 µl of PBS and injected intraperitoneally (IP) into female Balb/c mice, primed 10 days before injection with 500 µl pristane oil IP. Ascitic fluid was collected 2 - 3 weeks later, centrifuged at 700 x g for 10 minutes and filtered before use with Millipore filters of progressively smaller pore size (0.9 µm, 0.45 µm and 0.22 µm).

(e) Cryopreservation of hybridomas and human tumour cell lines.

Cell lines were harvested, centrifuged at 400 x g for five minutes, and resuspended in complete medium containing 10% DMSO at a concentration of 10^7 cells/ml. 1 ml of cell suspension was transferred to a sterile Nunc freezing vial which was placed on top of tissue paper, lying on a bed of solid carbon dioxide. After 2 - 4 hours, cells were transferred to a liquid nitrogen storage facility. Cells were recovered by rapid thawing at 37°C, washed, and resuspended in tissue culture medium.

(f) Trypan Blue exclusion for quantifying cell viability.

20 µl of a cell suspension was mixed with 20 µl of Trypan Blue vital dye and loaded into the counting chamber of a haemocytometer. All cells excluding blue dye were scored as viable.

2. Protein Purification.

(a) Preparation of an Ig fraction from ascites by ammonium sulphate precipitation [205].

Saturated ammonium sulphate was prepared by adding 500 g of the salt to 500 ml of distilled water and heating to 50°C. The solution was cooled to room temperature, decanted and the pH adjusted to 7.2 with 5 M NaOH.

Ascites was diluted 1:1 with 0.9% NaCl. Ammonium sulphate was added to a concentration of 45% v/v and protein precipitated by stirring at room temperature for 30 minutes. The precipitate was separated by centrifugation at 1000 x g for 15 minutes, washed twice in a 45% v/v solution of saturated ammonium sulphate and redissolved in PBS. This procedure was repeated using a 40% solution of saturated ammonium sulphate and the final solution dialysed against PBS for 24 - 36 hours at 4°C.

(b) Protein-A affinity chromatography for isolation of IgG [206].

Staphylococcal Protein-A, covalently linked to Sepharose CL-4B™, was swollen in PBS for 30 minutes and 5 ml of gel packed into a 10 ml glass column. The column was equilibrated with binding buffer (1.5 M glycine, 3.0 M NaCl, pH 8.9 with NaOH) and 5 ml of ascites or protein solution loaded onto the column. The column was washed with binding buffer until no further unbound protein was detected in the effluent by optical density at 280 nm. Protein-A bound IgG was sequentially eluted with 0.1 M citrate buffer at pH intervals of 6, 5, 4 and 3. The pH of the eluted protein was rapidly adjusted to between 7.0 and 7.4 by the addition of 1 M Tris-HCl pH 8.9 and the final solution dialysed against PBS at 4°C.

(c) Adjustment of the protein concentration of antibody solutions.

The protein concentration was determined by UV absorption at 280 nm, assuming that a 1 mg/ml solution has an absorbance of 1.4 OD units. Purified antibody was concentrated by placing the solution in pre-moistened dialysis tubing (Medicell International - pore size 50 kDa) surrounded by dry Ficoll at 4°C. After sufficient absorption of solvent across the dialysis membrane, the tubing was washed in PBS, the protein solution decanted and the protein concentration recalculated. Volumes of less than 15 ml of protein solution were concentrated with either a ultrafiltration cell (Amicon) or a Minicon™ macrosolute well concentrator (Amicon).

3. Characterisation of the Protein Product.

(a) SDS Polyacrylamide Gel Electrophoresis (SDS PAGE) [207].

A 2 mm separating gel was prepared by polymerisation of a 30% stock solution of acrylamide/bisacrylamide in 1 M Tris-HCl pH 8.8 buffer with 20 µl of TEMED, 0.2% SDS and 100 µl of a 10% w/v solution of ammonium persulphate. The concentration of acrylamide was varied depending on the desired separating conditions. Polymerization was allowed to proceed for 60 minutes with an overlay of 50% isobutanol to exclude air from the gel. This was removed together with unpolymerized gel at the end of the reaction. A stacking gel of 3% acrylamide was prepared in 1 M Tris-HCl pH 6.8, containing 0.1% SDS, 10 µl of TEMED and 50 µl of a 10% w/v solution of ammonium persulphate. This was poured onto the separation gel, encasing a 2 mm well-forming comb, and polymerization allowed to proceed for 30 minutes. Following application of the protein samples, the gel slab was fixed vertically in the electrophoresis tank and running buffer poured into the upper and lower reservoirs. Electrophoresis was run at a constant voltage of 250 V until

the bromophenol blue marker dye approached the bottom of the gel (3 - 4 hours).

(b) Preparation of protein samples for SDS gel electrophoresis.

Non-reduced samples were prepared by adding protein to 50 µl SDS sample buffer and boiling for one minute. Reducing conditions were obtained by the addition of 1 M dithiothreitol to the sample buffer to produce a final concentration of 0.1 M.

(c) Staining of proteins following SDS PAGE.

The gel was stained with Coomassie Brilliant Blue overnight on a platform shaker and destained until the background had cleared. Undried gels were stored in 7% acetic acid to prevent further leaching of the stain.

For more sensitive delineation of protein bands, a silver staining technique was used. Gels were fixed in a solution of 10% ethanol/5% acetic acid for one hour (two changes of solution) and then placed in 10% solution of oxidising reagent (Bio Rad silver staining kit) for 10 minutes. The gels were washed thoroughly in double distilled water and then stained for 30 minutes with a 10% solution of Bio Rad silver stain. Following a further wash in distilled water, the silver stain was developed with three changes of Bio Rad developer. The reaction was rapidly terminated with 5% acetic acid as soon as bands of the desired intensity were seen.

(d) Determination of molecular weights.

To calculate the molecular weight of any protein after electrophoresis, a series of protein standards of appropriate molecular weight range (Bio Rad), were separated on the same gel. A standard curve was produced by a semi-logarithmic plot of molecular weight against the relative mobility of a protein

[208]. For gels subjected to autoradiography, a similar method was employed using 20 nCi ^{14}C-methylated protein standards (Amersham).

(e) Isoelectric focusing of proteins (IEF).

Agarose IEF gels were prepared by boiling 0.3 g of agarose IEF and 3.6 g sorbitol in double distilled water. The solution was cooled to 75°C before adding 1.9 ml of Pharmalyte™ (pH 3 - 10). The mixture was poured onto the hydrophilic surface of Pharmacia Gelbond™, contained within a casting frame (Pharmacia). When the gel was set (30 minutes), it was removed from the frame and allowed to harden overnight in a humidity chamber at room temperature. The gel was placed on a Pharmacia flat-bed apparatus and using 0.05 M H_2SO_4 as the anode solution and 1 M NaOH as the cathode solution, was electrofocused at 1500 V and 15 W for 1.5 hours.

(f) Fixing and staining of IEF gels.

Following electrofocusing, gels were fixed in an aqueous solution of 5% w/v sulphosalacylic acid plus 10% w/v trichloracetic acid for 30 minutes. Gels were destained for one hour and thoroughly dried under filter paper. Gels were stained in 0.2% Coomassie Brilliant Blue for 5 - 10 minutes before further destaining to allow visualisation of protein bands. The gel was again dried for storage.

(g) Determination of the isoelectric point.

The isoelectric point (pI) of a protein was calculated by focusing a series of protein standards of known pI (pI standard kit, Pharmacia) on each gel. A plot of their pI versus distance from the cathode produced a standard curve from which unknown pI's were estimated.

(h) Size exclusion chromatography by Fast Protein Liquid Chromatography (FPLC™, Pharmacia).

The protein sample was diluted 1:1 in PBS and filtered through a 0.22 µm Millex™ filter. By means of a sample loop, 50 - 200 µl of solution was loaded onto a Superose-12™ gel filtration column (Pharmacia). This was run with degassed and filtered PBS as the eluting buffer at a flow rate of 0.5 ml/minute. Sample fractions of 0.5 ml were collected by means of an automated fraction collector. Protein was detected by a 280 nm UV light monitor incorporated into the system.

For gel filtration of high molecular weight species, eg. IgM and IgG aggregates, greater definition was obtained using a 600 x 20 mm column packed with Sephacryl S-300 HR™.

(i) FPLC anion exchange chromatography.

This was performed on a Pharmacia Mono Q™ column. To run the column, a computer-controlled continuous ion gradient was established using two buffers; 20 mM Tris-HCl pH 7.0 and 20 mM Tris-HCl, 1 M NaCl pH 7.0. Both buffers were degassed and filtered on the day of use.

(j) FPLC cation exchange chromatography.

This was performed as for FPLC anion exchange chromatography, but using a Pharmacia Mono S™ column with the ion gradient produced with 0.05 M acetic acid and 0.5 M NaCl, 0.05 M acetic acid.

(k) Estimation of endotoxin contamination of antibody solutions.

The concentration of endotoxin in protein solutions was determined by the Limulus Amebocyte Lysate test (LAL, Lysate and Radiopharmaceutical Consultancy). LAL in single test vials was aseptically reconstituted with 200 µl of the test sample and pre-warmed to 37°C. The tube was gently mixed and

placed vertically at 37°C for one hour. After the incubation period, the tube was slowly inverted 180°. If, after rotation, the gel was firm and did not release itself down the side of the tube, the test was positive. Each test was compared to a series of tubes containing control standard endotoxin, aseptically reconstituted in pyrogen-free solvent and diluted to concentrations of between 0.1 and 0.006 ng/ml.

4. Biological Characterisation.

(a) Determination of antibody isotype by the Ouchterlony diffusion technique [209].

2 ml of a 1% agarose solution was drawn over glass microscope slides on a levelling plate using a large bore pipette, and left to set. Wells were made using an Ouchterlony cutter. 2 µl of antibody under test was placed in the central well and 2 µl of the subclass specific antisera in the peripheral wells. Following overnight incubation at 4°C in a humidity chamber, the slides were dried, rehydrated in 0.9% NaCl for 10 minutes, dried again, washed in distilled water and dried completely. The precipitation lines were visualised by staining for three minutes in Coomassie Brilliant Blue Ouchterlony stain and destaining for three minutes. Drying the slides after destaining provided a permanent record of the antibody isotype.

(b) Indirect immunofluorescence to detect antigen expression on human tumour cell lines.

Cell lines in exponential growth phase were harvested and washed twice in PBS containing 1% HPPF and 0.02% sodium azide. 10^6 cells were centrifuged at 400 x g for five minutes in 3 ml LP3 plastic tubes and resuspended in 50 µl PBS. Cells were incubated with 50 µl of the primary antibody, at a concentration known to saturate antigen binding sites, for 30 minutes at room temperature. After centrifugation and washing twice in PBS/1% HPPF, a

second layer of FITC-conjugated rabbit anti-mouse IgG in excess was applied for 30 minutes for immunofluorescence staining. The cells were washed twice, and 10 µl of cell suspension in PBS mounted on glass microscope slides. The samples were analysed using a Zeiss Photomicroscope III™ with epi-illumination optics. Analysis included an antibody of known biological activity as a positive control and the use of an isotype-matched irrelevant antibody as a negative control to estimate background immunofluorescence.

(c) Indirect immunofluorescence for quantifying antibody biological activity.

To quantify the biological activity of any antibody, the method described in Section 4b was used. The starting concentration was, however, known, as determined by optical density at 280 nm. Serial doubling dilutions of antibody were tested and the biological activity was defined by the dilution at which immunofluorescence fell from saturation. To enable a comparison between different antibodies, the titre was adjusted to reflect a standard starting concentration (1 mg/ml).

(d) Determination of biological activity by fluorescence activated cell sorter (FACS) analysis.

Cells were stained as described in section 4b. The cell pellet was resuspended and fixed in 500 µl PBS containing 1% paraformaldehyde. Cells were analysed in a Becton Dickinson Facscan™, reading fluorescence intensity from 5 x 10^3 recorded events.

(e) Modification of indirect immunofluorescence to detect antigen expression on tissues.

Fresh tissue were snap-frozen in liquid nitrogen and stored at -70°C. Specimens were mounted in OCT embedding medium (Miles Laboratories), and 5 µm sections cut on a Bright's cryostat. These were placed on glass

microscope slides and incubated with primary antibody as described in Section 4b. After incubation, slides were placed in a rack, washed with PBS for 12 minutes, and the second layer of an excess of FITC-rabbit anti-mouse IgG applied. Visualisation of immunofluorescence was as described in Section 4b.

(f) Modification of the immunofluorescence technique to detect antigen expression on cells within the CSF.

CSF cytospin preparations on glass microscope slides were made by centrifugation using a Shandon Cytospin II™ cytocentrifuge. The slides were air dried and fixed for 30 seconds with acetone at -20°C. Slides were then examined as in Section 4e using the antibody of interest.

5. Radiolabelling.

MoAb iodinations with ^{131}I and ^{125}I were performed with either the stationary phase chloramide, Iodogen™ [210] or using a modification of the Chloramine-T technique [211].

(a) The iodogen technique.

Iodogen was dissolved in chloroform to a concentration of 100 µg/ml. 200 µl aliquots of the solution (20 µg iodogen) was then dispensed into borosilicate glass vials (12 x 37 mm) (Wheaton) and evaporated under a gentle stream of nitrogen gas. A fine deposit of iodogen remained at the base of the vials which were sealed and stored at 4°C. Iodogen-coated vials were used within seven days of preparation. For the reaction procedure, MoAb in PBS (maximum volume 125 µl) was dispensed into an iodogen tube with a stochiometrically appropriate quantity of radioiodine. The reaction vessel was

gently agitated for 10 minutes before the reaction was terminated by removal of products.

(b) The modified Chloramine-T technique.

MoAb in 100 µl PBS was dispensed into conical polypropylene tubes and radiolabelled by the addition of iodine and 10 µl of a 0.8 mg/ml solution of Chloramine-T. The reaction was terminated after two minutes by the addition of 20 µl of a 1 mg/ml solution of sodium metabisulphite and an excess (600 µg) of potassium iodide.

Following iodination by either technique, the radiolabelled protein was separated from unreacted iodine by Sephadex G-25™ gel filtration. A 15 ml column (Analytichem) was packed with 12 ml of swollen Sephadex G-25™ and equilibrated in PBS containing 1% HPPF as carrier protein. The radiolabelled antibody was loaded on the column and washed through with PBS/1% HPPF. The effluent was collected in sequential 0.6 ml fractions and assayed for radioactivity using an Isocal™ radionuclide assay calibrator (Vinten). Two or three fractions corresponding to the chromatographic peak were collected and the rest discarded.

(c) Determination of Radioactivity.

Quantitative measurement of gamma radioactivity was performed using a 1282 Compugamma™ automated gamma counter (LKB Wallac), providing automatic deadtime correction, interfaced with an IBM computer using the Ultroterm™ 2 software package. Results are given in counts per minute (cpm). The activity in MBq is given by:

$$\mathbf{MBq} = \frac{\mathbf{cpm \times F}}{\mathbf{60 \times 10^6}}$$

where,

F is the conversion factor for counts to disintigrations. For ^{125}I, F = 1.25 and for ^{131}I, F = 4, given gamma counter efficiencies of 80 and 25% respectively (see below)

and **60×10^6** is the number of disintigrations per minute in 1 MBq.

The gamma counter was calibrated for ^{125}I by means of a standard capsule of ^{129}I (LKB) and for ^{131}I by repeated measurement of a standard source of ^{131}I. This gave counting efficiencies of 80% for ^{125}I and 25% for ^{131}I, which remained unchanged throughout the period of this project. A dual channel facility was also available for determining individual isotopic activities in a mixture of ^{131}I and ^{125}I. In this situation, a computer calculated correction was applied to account for spillover of ^{131}I radiation into the ^{125}I counting chamber.

(d) Determination of free-iodine contamination by trichloracetic acid (TCA) precipitation.

Radiolabelled antibody was diluted 1:100 in PBS and 100 µl mixed by vortexing with 400 µl of cold 10% TCA and 500 µl of PBS containing 1% HPPF. The mixture was incubated on ice for 15 minutes and then centrifuged at 10,000 x g for a further 15 minutes. The supernatant was separated from the precipitate and both assayed for radioactivity. The protein-bound iodine was estimated as the proportion of total activity present in the protein precipitate.

(e) Assessment of structural integrity of radioconjugates by FPLC gel filtration.

Radiolabelled protein was diluted in PBS to give an activity of 10^5 - 10^7 counts per minute in a volume of 200 µl. This was loaded onto a Superose-12™ gel filtration column incorporated into the FPLC apparatus, and run under conditions described in section 3h. Ninety sequential 0.5 ml fractions were

individually assayed for radioactivity, and an elution profile plotted of counts per minute against fraction number.

(f) Determination of the immunoreactive fraction of radiolabelled antibodies.

Direct radiobinding assays were established to determine the immunoreactive fraction of radioimmunoconjugates. For antibodies recognising leukaemia associated cell surface antigens, a modification of the method described by Lindmo was used. For antibodies raised against neural antigens, a conventional direct binding assay was employed, estimating the immunoreactive fraction under conditions of antigen excess.

(i) Modification of the method of Lindmo for determining immunoreactive fraction [212] [213].

Lindmo described a method, based on a modified Lineweaver-Burk plot, by which the fraction of immunoreactive radiolabelled antibody is accurately determined by linear extrapolation to binding at infinite antigen excess. The theoretical background to this approach has been previously described [212]. This method was employed in a liquid phase direct radioimmunoassay for the investigation of iodinated antibodies recognising leukaemia associated antigens. An appropriate human leukaemic cell line (T-ALL or B-ALL) was cultured and harvested in exponential growth phase. Cells were washed in PBS and centrifuged at 400 x g for five minutes. The cell pellet was resuspended in PBS and the proportion of live cells determined by Trypan Blue exclusion. The live cells were concentrated to 25 x 10^6/ml in a volume of 4 ml which was divided into two aliquots. From each aliquot a series of six doubling dilutions were made in LP3 tubes pre-coated for 60 minutes at 37°C with 1% HPPF in PBS. Final concentrations of 25.0, 12.5, 6.25, 3.13, 1.56 and 0.78 x 10^6/ml in 1 ml PBS were prepared. In order to saturate cell binding sites for subsequent measurement of non-specific binding, 50 - 100 µg of

unlabelled antibody was added to each tube of one series of 1 ml dilutions. These were incubated at 4°C for one hour. Radiolabelled antibody was added to both series of cell suspensions at a concentration of 0.5 - 1.0 ng/ml (maximum volume 50 µl). The tubes were incubated for four hours at 4°C on a Roto-Torque™ rotator (Cole Palmer Instruments) at 10 rpm. Following incubation, the total activity in each tube was measured in a gamma counter. The cells were washed four times by centrifugation at 400 x g for five minutes and resuspended in 2 ml of PBS. Cell bound activity was then measured. For each cell concentration, specific cell-bound activity was determined as the difference between bound activities of unblocked and pre-blocked cells. A plot of T/B as a function of I/C was then constructed where, T is the total incubated activity, B is the specific cell-bound activity and C is the cell concentration (x 10^6/ml). By extrapolation, the origin of the abscissa represents infinite antigen excess, and the intercept with the ordinate defines the value $Y_o = 1/r$, the inverse of the immunoreactive fraction (r).

(ii) Determination of the immunoreactive fraction at antigen excess.

For antibodies recognising neural antigens, immunoreactivity was estimated at antigen excess by a conventional binding assay. A homogenate of fresh whole adult brain was prepared in PBS and stored in 1.5 ml aliquots at -70°C. To assay for immunoreactivity, aliquots of brain were thawed, centrifuged at 10,000 x g and washed in PBS. 1 ml samples were placed in LP3 tubes, pre-blocked at 37°C for 1 hour with PBS/1% HPPF. Approximately 1 ng ^{131}I-labelled test antibody was diluted in 100 µl PBS, together with an equivalent quantity of a ^{125}I-labelled irrelevant antibody. The antibody solution was then added in triplicate to the brain homogenate and incubated for four hours at 4°C on a tube rotator. Following incubation, the total activity of each isotope was measured using the dual channel facility of the gamma counter and

the homogenate washed four times in PBS by centrifugation at 10,000 x g. The supernatant was discarded and the activity of each isotope in the brain pellet measured. The immunoreactive fraction was determined by subtracting the mean percentage binding of the irrelevant antibody from that of the specific antibody.

CHAPTER 3.

SELECTION AND CHARACTERISATION OF MONOCLONAL ANTIBODIES.

1. Introduction.

The initial phase of this project necessitated the selection of antibodies recognising leukaemia associated antigens that were suitable for use in both *in-vitro* experimentation and for administration to patients. Candidate antibodies required biological characterisation, including screening against human leukaemic cells and normal tissues, particularly neural structures in view of their potential therapeutic use within the subarachnoid space. It was intended to investigate binding characteristics by Scatchard analysis and the dynamics of binding of radiolabelled antibody in terms of loss of cell-associated radioactivity following antibody-antigen interaction.

2. Antibody Selection.

Three murine MoAbs were selected as candidates for use in both *in-vitro* and clinical studies, namely; WCMH, HD37 and WT1. WCMH was raised in 1987 by Dr W Cassano at the University of Florida, USA [214]. It binds the 95 - 100 kDa common acute lymphoblastic leukaemia antigen (CALLA - CD10). HD37 was raised by Professor B Dorken at the University of Heidelburg, Germany [215]. It binds the 90 - 95 kDa antigen, CD19. WT1 was raised by Dr W Tax at the University Hospital, Nijmegan, The Netherlands [216]. It recognises the 40 kDa CD7 antigen.

All three reagents were raised by somatic cell hybridization of spleen cells from Balb/c mice and myeloma fusion partners; P3 X63 Ag 8.653 in the

case of WCMH and HD37, and Sp 2/0-Ag 14 in the case of WT1. Neither myeloma cell line synthesize endogenous light or heavy chains. For WCMH and HD37, the immunogen was blast cells taken from patients with pre-B ALL. Infant thymocytes, removed during cardiac surgery, were used as the immunogen for WT1.

3. Antibody Purification.

The WCMH hybridoma was initially expanded in complete DMEM medium under conditions described in Chapter 2; 1a. The cell line was subsequently cloned by limiting dilution in 96 well plates (Chapter 2; 1c). Tissue culture supernatants were tested by indirect immunofluorescence on the pre-B ALL cell line, Reh. Using this technique, it was possible to detect antibody-producing hybridomas originally cloned at one cell per 200 µl complete medium. This population was expanded into 24 well plates and finally into 60 mm tissue culture dishes. Both hybridoma cell lines and tissue culture supernatants were screened on three occasions for mycoplasma contamination by the cell enriched PPLO agar assay (Courtesy of Mr I Ray, Imperial Cancer Research Fund, London). No contamination was detected. In addition, the hybridoma was examined under electron microscopy for evidence of viral contamination (Courtesy of Ms R Tilley, Imperial Cancer Research Fund, London). Only intracellular C-type viral particles were observed, in common with the majority of hybridomas.

WCMH produced as mouse ascites was purified by ammonium sulphate precipitation and Protein-A Sepharose affinity chromatography (Chapter 2; 2b). Greater than 95% of the Protein-A bound antibody was eluted from the affinity column by 0.1 citrate buffer titrated to pH 6. Antibody yields were 2.2 - 4.9 mg protein/ml of ascites. WCMH was also produced in bulk culture at the Imperial Cancer Research Fund's Clare Hall laboratories. Following

Protein-A affinity chromatography of 12 litres of tissue culture supernatant, 120 - 180 mg of purified antibody was obtained from each batch.

HD37 was supplied as clinical grade material by Dr E Vitetta, University of Texas, USA, and complies with the Food and Drug Administration (FDA) regulations for human administration.

WT1 was kindly donated by Dr W Tax, and supplied as either mouse ascites or purified antibody. Where appropriate, WT1 ascites was purified by ammonium sulphate precipitation followed by Protein-A affinity chromatography. 0.1 citrate buffer pH 5 eluted greater than 95% of the bound antibody from the column. Antibody yields were 3.8 - 4.8 mg protein/ml of ascites.

4. Quality Control of Antibody Production.

(a) SDS polyacrylamide gel electrophoresis.

Each batch of purified antibody was examined for purity by SDS polyacrylamide gel electrophoresis under reducing and non-reducing conditions, using 12% and 8% acrylamide gels respectively (Chapter 2; 3a). Greater than 95% purity of MoAbs was consistently demonstrated (Figure 3.1).

Silver staining of polyacrylamide gels increases the sensitivity of protein band delineation by a factor of between 10 and 50 [217] (Chapter 2; 3c). Figure 3.2 demonstrates the silver staining pattern of antibodies, WT1, WCMH and HD37 on a non-reduced 8% SDS polyacrylamide gel. A high degree of purity of all three reagents is confirmed. Both WCMH and WT1 appear as doublets which may arise from differential glycosylation. There are fainter, higher molecular weight bands suggestive of protein aggregation. HD37 resolves into one dense band and multiple lighter bands, again suggesting differential antibody glycosylation.

Figure 3.1

SDS polyacryamide gel electrophoresis of antibodies, WCMH, HD37 and WT1.

8% non-reduced and 12% non-reduced polyacryamide gels stained with Coomassie Brilliant Blue.

Lanes: A, HD37; B, WCMH; C, WT1; D, Molecular weight markers.

Molecular weight markers:

Protein	Molecular Weight
Myosin	200,000
E.coli β-galactosidase	116,250
Rabbit muscle phosphorylase b	97,400
Bovine serum albumin	66,200
Hen egg white ovalbumin	42,699
Bovine carbonic anhydrase	31,000
Soybean trypsin inhibitor	21,500
Hen egg white lysozyme	14,400

Figure 3.1

Non-Reduced

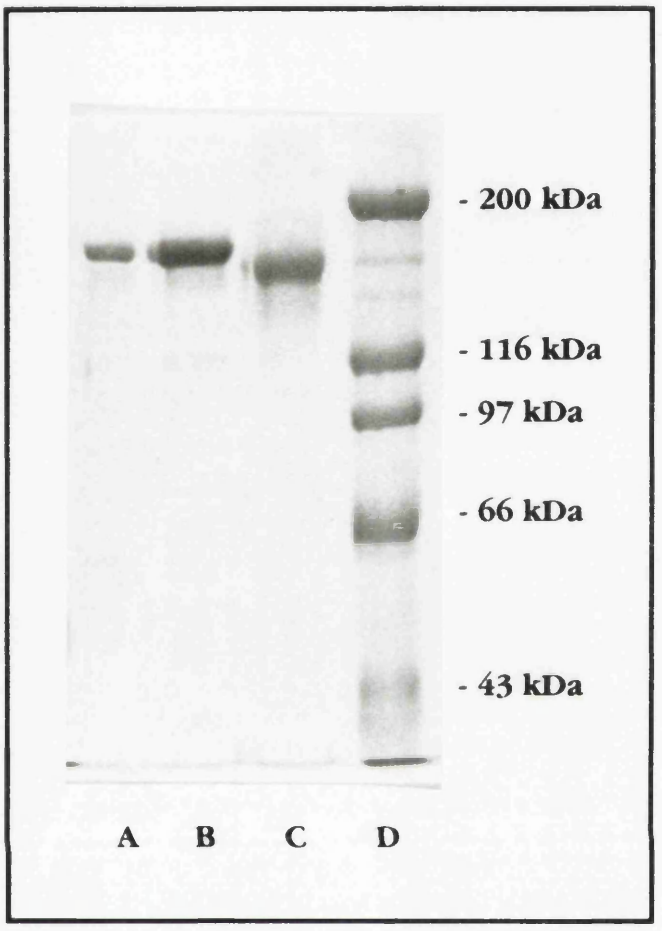

Reduced

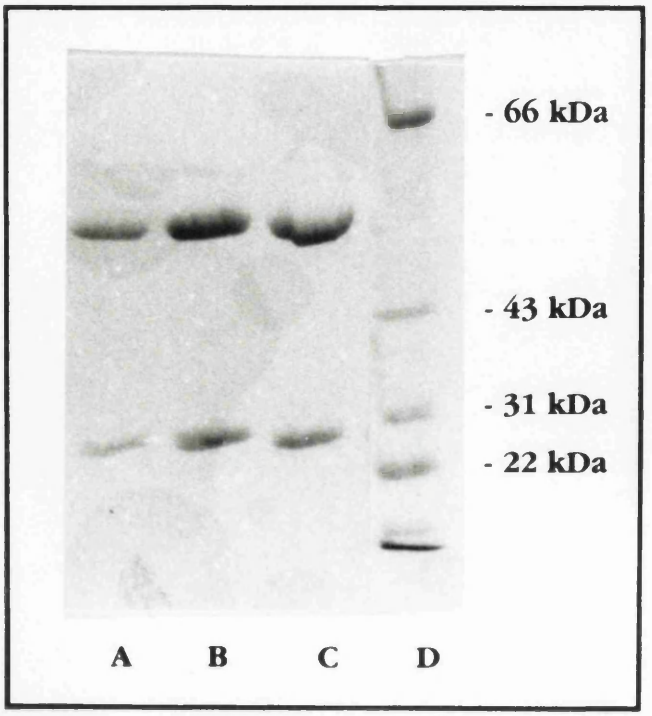

Figure 3.2

Silver staining of SDS polyacrylamide gel.

8% polyacrylamide gel of non-reduced MoAbs delineated with silver stain.

Lanes: A, WT1; B, WCMH; C, HD37; D, molecular weight markers (see Figure 3.1)

Figure 3.2.

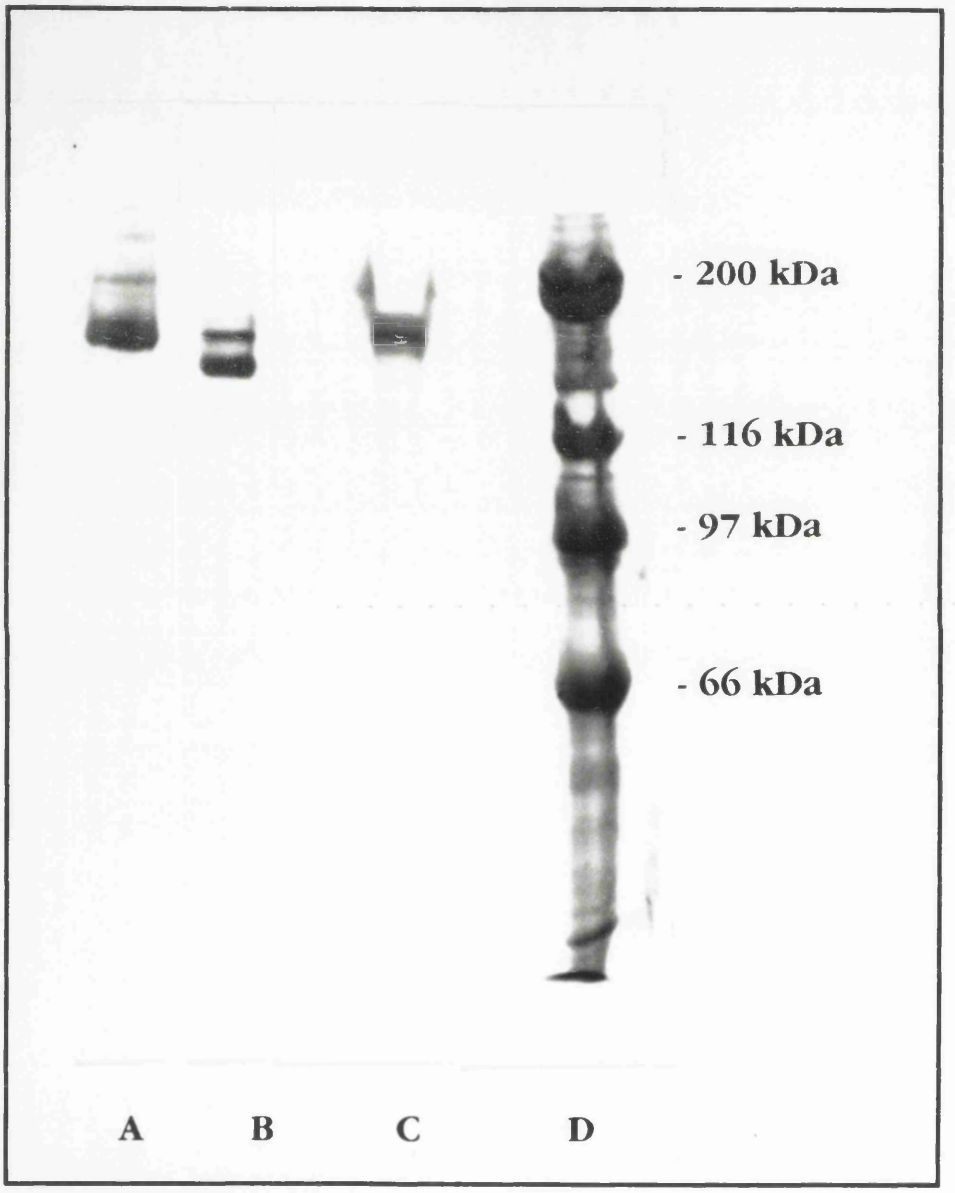

(b) FPLC gel filtration and ion-exchange chromatography.

Further evidence of antibody purity was obtained for antibodies, WCMH, HD37 and WT1 by FPLC gel filtration and both anion- and cation-exchange chromatography (Chapter 2; 5h, 5i, 5j) (Figure 3.3). For all three reagents, each technique consistently demonstrated a monomeric antibody species with no significant antibody aggregation.

(c) Isoelectric focusing.

Purified MoAb was analysed by isoelectric focusing in a pH gradient of 3 - 10 (Chapter 2; 3e) on agarose gels, fixed and stained with Coomassie Brilliant Blue (Figure 3.4). WCMH resolved into four bands with pI's lying between 5.6 and 5.9. Focusing of HD37 revealed seven bands with pI's of between 5.7 and 6.2. Six bands were demonstrated for WT1, with pI's lying between 5.8 and 6.1. The focusing patterns remained constant between different batches of purified antibody, as long as the material was prepared from a standard source.

(d) Endotoxin contamination.

The degree of endotoxin contamination of purified antibody solutions was tested routinely by the Limulus Amebocyte Lysate test (Chapter 2; 3k). The sensitivity of the assay system was established by means of control endotoxin, and was consistently between 0.0125 and 0.025 ng/ml. 200 µl aliquots of antibody, at 1 mg/ml in PBS, were assayed in single test vials. In no instance was the endotoxin concentration of purified WCMH, HD37 or WT1 greater than 0.025 ng/ml. This would be expected to result in an amount of injected endotoxin below the FDA upper limit for intrathecal drugs; 0.02 ng/kg body weight [218]. Distilled water and PBS used in the laboratory were also found to maintain an endotoxin content of no greater than this concentration, whereas tap water was strongly positive for endotoxin.

Figure 3.3

FPLC gel filtration and ion-exchange chromatography of antibodies, WCMH, HD37 and WT1.

A = FPLC gel filtration on a Superose 12™ column equilibrated with PBS.

B = FPLC anion-exchange chromatography on a Pharmacia Mono-Q™ column. Mobile phase 0.05 M Tris-HCl pH 7.0; eluted with a 0 - 100% sodium chloride gradient.

C = FPLC cation-exchange chomatography on a Pharmacia Mono-S™ column. Mobile phase 0.05 M acetic acid; eluted with a 0 - 100% sodium chloride gradient.

Figure 3.3

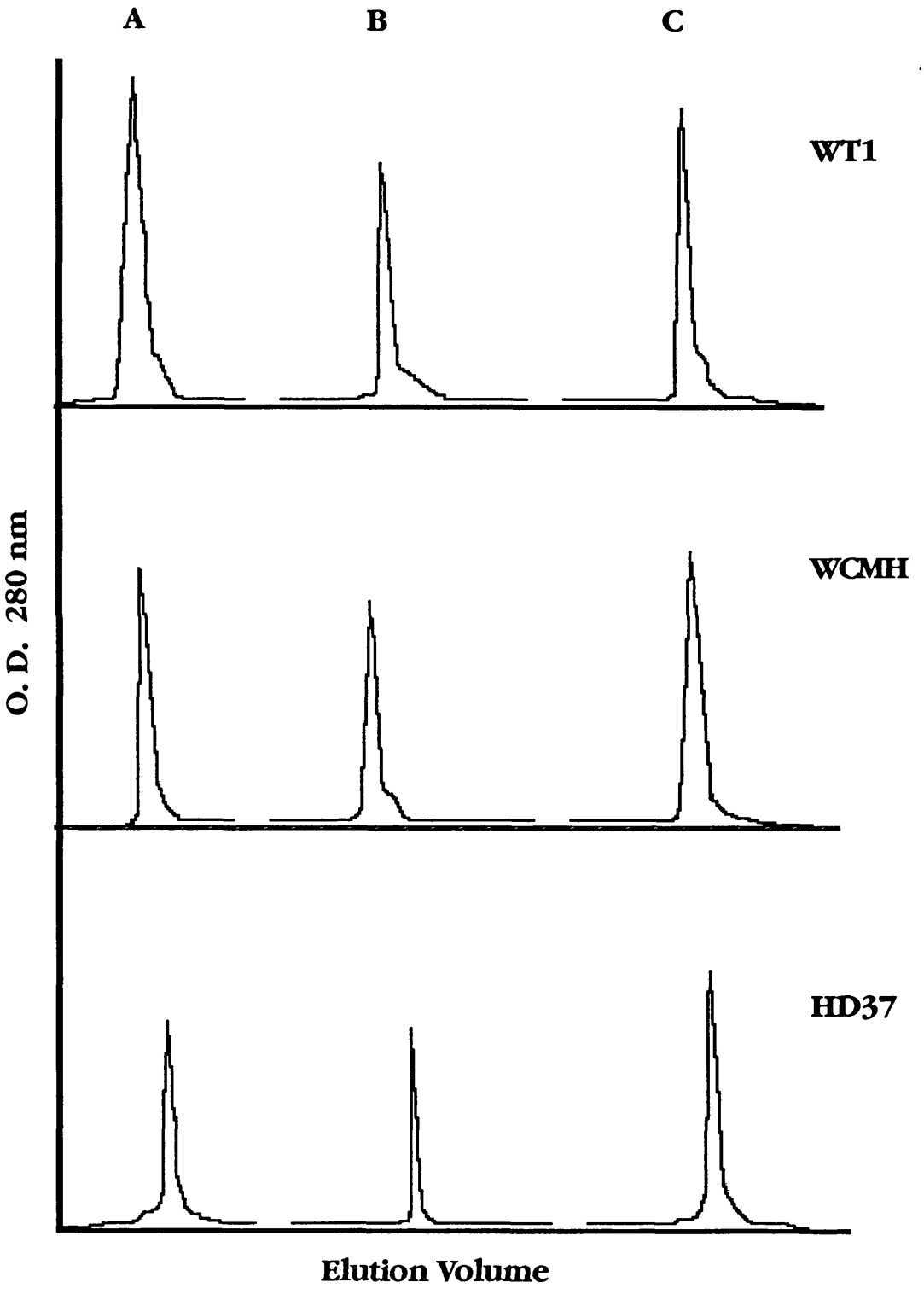

Figure 3.4

Isoelectric focusing of antibodies, WCMH, HD37 and WT1.

Focusing undertaken in agarose, across a pH gradient of 3 - 10. Staining with Coomassie Brilliant Blue.

pI markers:

Protein	pI (24 °C)
Amyloglucosidase	3.50
Soybean trypsin inhibitor	4.55
β-lactoglobin A	5.20
Bovine carbonic anhydrase B	5.85
Human carbonic anhydrase B	6.55
Horse myoglobin	6.85
Horse myoglobin	7.35
Lentil lectin	8.15
Lentil lectin	8.45
Lentil lectin	8.65
Trypsinogen	9.30

Figure 3.4.

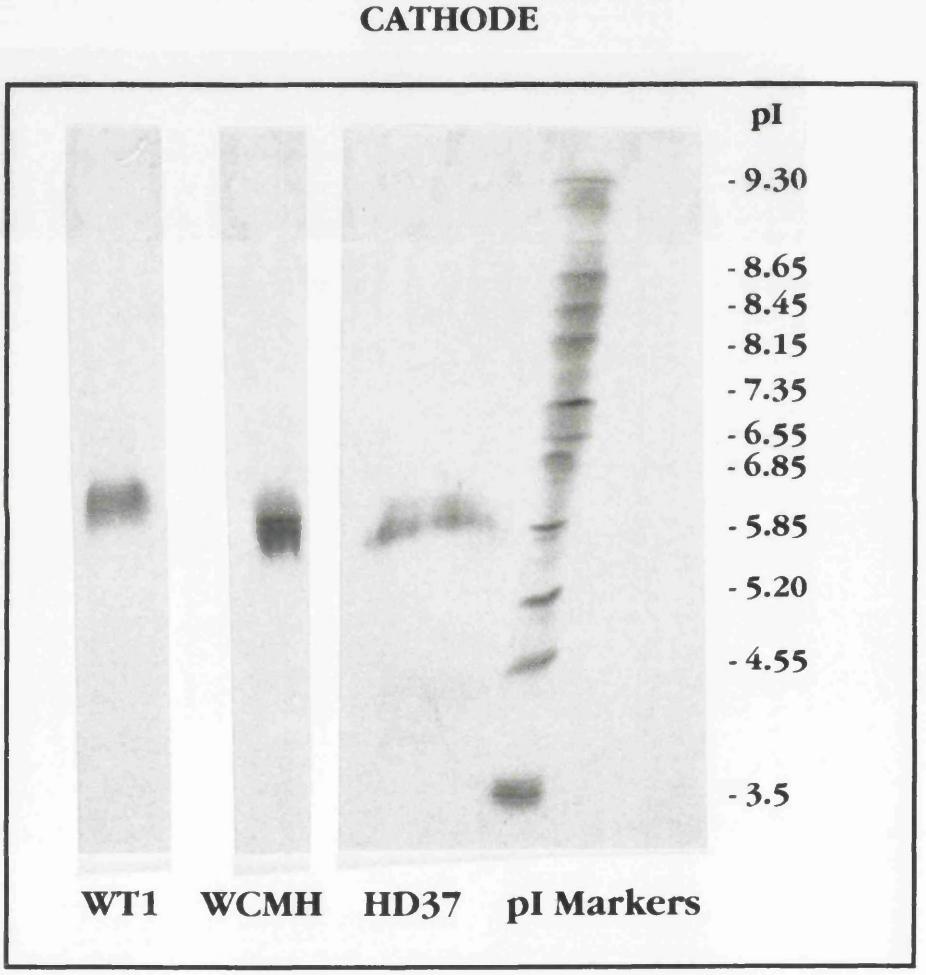
CATHODE
pI
- 9.30
- 8.65
- 8.45
- 8.15
- 7.35
- 6.55
- 6.85
- 5.85
- 5.20
- 4.55
- 3.5
WT1
WCMH
HD37
pI Markers
ANODE

5. Biological Characterisation.

(a) Antibody isotype.

The isotype of purified antibodies, WCMH, HD37 and WT1 was confirmed by the Ouchterlony technique (Chapter 2; 4a) (Figure 3.5). This demonstrated WCMH and HD37 to be of the IgG_1 isotype, and WT1 to be of the IgG_{2a} subclass.

(b) Indirect immunofluorescence on human leukaemic cell lines.

To confirm the binding profiles of MoAbs and to select appropriate cell lines for subsequent experimentation, antibodies were screened by indirect immunofluorescence against both B-lineage ALL/lymphoma and T-ALL cell lines (Chapter 2; 4b). WCMH (CD10) and HD37 (CD19) recognised antigens present on the B-lineage tumours, Nalm 6, Reh, Daudi and KM3. No binding was detected when tested against the T-ALL lines, GH1, JM and MOLT 4. Conversely, WT1 (CD7) reacted strongly with GH1, JM and MOLT 4 but failed to bind to any B-lineage tumour. All three antibodies showed membrane capping on indirect immunofluorescence, in common with many of the reagents reacting with haemopoetic cells.

For each batch of antibody, quantitative biological activity against one or more appropriate cell lines was examined as part of the quality control procedure (Chapter 2; 4c) (Figure 3.6). Table 3.1 shows that minimum biological activity observed for antibodies, WCMH, HD37 and WT1 at a starting concentration of 1 mg/ml. In no instance was the biological activity less than 1/512.

The binding of antibodies, WCMH and HD37 to B-ALL cells lines and WT1 to T-ALL lines was also examined by Facscan™ analysis (Chapter 2; 4d). WCMH and HD37 (50 µl at a concentration of 1 mg/ml) were tested against the B-cell line Nalm 6 and compared with an isotype-matched irrelevant antibody,

Figure 3.5

Isotype of antibodies, WCMH, HD37 and WT1 by radial immunodiffusion (Ouchterlony technique).

Central wells contain 2 µl of purified antibody. Peripheral wells contain 2 µl of isotype-specific antisera. An immunoprecipitate between test antibody and relevent antisera is demonstated by staining with Coomassie Brilliant Blue.

Figure 3.5

WCMH

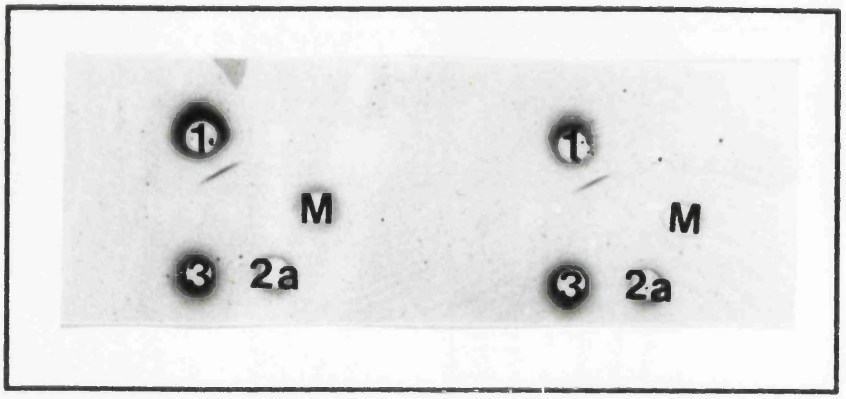

HD37

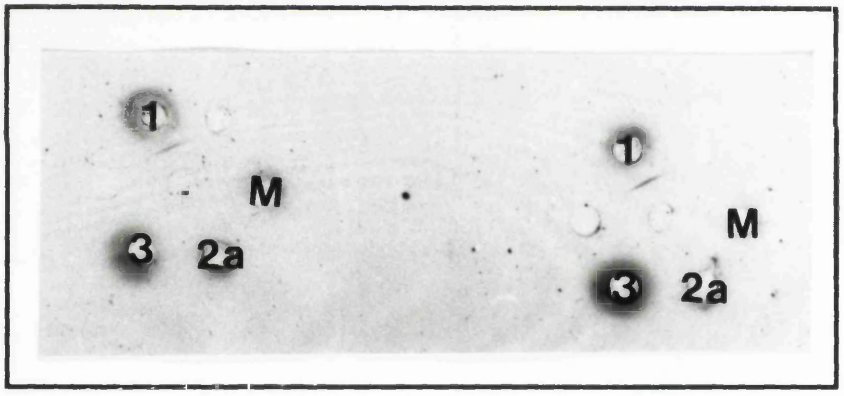

WT1

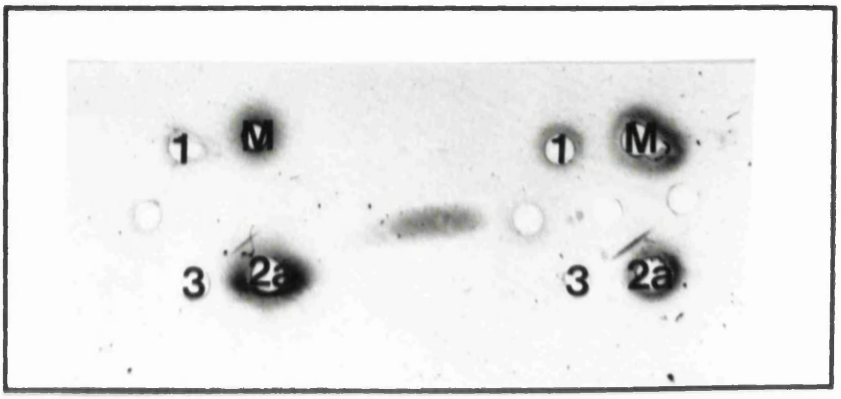

Figure 3.6

Quantitative biological activity of antibodies by indirect immunofluorescence.

Plot of relative intensity of immunofluorescence on cell line, Reh, against dilution of WCMH (50 µl) at a starting concentration of 1 mg/ml.
Biological activity is 1:2000, the dilution at which immunofluorescence fell from saturation.
Relative fluorescence activity graded as: 3, intense; 2, strong; 1, weak; 0, absent.

Figure 3.6

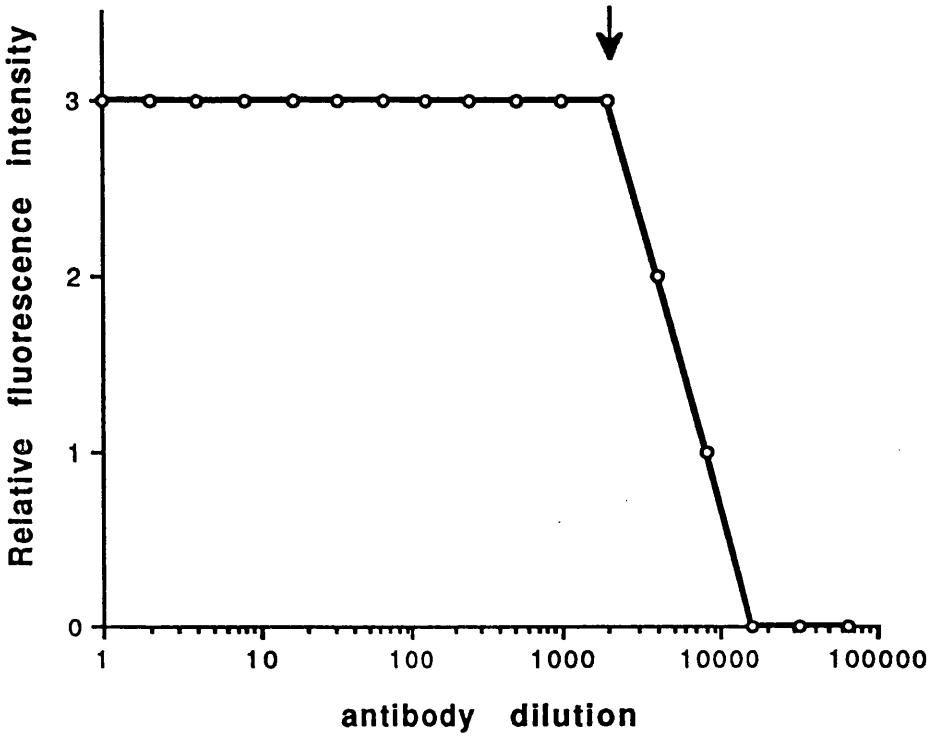

Table 3.1:

Minimum biological activity of purified monoclonal antibodies as determined by indirect immunofluoresence.

Antibody	Cell Line						
	Nalm 6	Reh	KM3	Daudi	GH1	JM	Molt 4
WCMH	1/512	1/512	1/1000	1/2000	-	-	-
HD37	1/512	1/512	1/512	1/2000	-	-	-
WT1	-	-	-	-	1/1000	1/512	1/1000

Reference mass of antibody = 50 µg.

UJ181.4, at the same concentration. WT1 was similarly tested against the T-ALL line, JM and compared with UJ13A ($1gG_{2a}$). Analysis confirmed the binding pattern observed by light microscopy (Figure 3.7).

(c) Reactivity with normal human tissue.

In view of their proposed administration into the CSF of patients, binding of antibodies, WCMH, HD37 and WT1 to normal human neural tissue was examined by indirect immunofluorescence (Chapter 2; 4e). Antibodies (50 µl) were screened at concentrations of 1 mg/ml and 50 µg/ml against cerebrum, cerebellum, meninges and peripheral nerve on five occasions. In no instance was binding detected.

Antibodies were also examined for reactivity with normal human kidney (n=2). As previously reported, the CD10 antigen, as recognised by WCMH, was shown to be expressed on human renal glomeruli and tubules (Figure 3.8). No binding was demonstrated for either HD37 or WT1.

6. Scatchard Analysis for the Calculation of Antibody Equilibrium Constant and Number of Antigen Binding Sites.

The equilibrium (affinity) constant and the number of binding sites per cells were determined for each antibody on human ALL cell lines by the method of Scatchard [219]. MoAb was radiolabelled with ^{125}I using the iodogen technique (Chapter 2; 5a). The specific activity of the radiolabelled protein was estimated by assuming an 80% protein recovery after Sephadex G-25™ column chromatography and by measuring the radioactivity associated with protein in an aliquot of the reagent.

To estimate the level of non-specific binding of radiolabelled antibody to both cells and plates within the assay system, a preliminary experiment was performed to determine the minimum amount of unlabelled antibody required to saturate the binding sites of 2.5×10^5 target cells. Cells were

Figure 3.7

Facscan™ analysis of binding of WCMH, HD37 and WT1 to leukaemic cell lines.

Cells stained with 50 µl antibody at 1 mg/ml were analysed by Facscan™, reading fluorescence intensity from 5000 recorded events.

Ordinate = number of events.
Abcissa = fluorescence intensity

open histograms = test antibody
closed histograms = negative control

A = WCMH staining of Nalm 6 cells.
Negative control, UJ181.4.

B = HD37 staining of Nalm 6 cells.
Negative control, UJ181.4.

C = WT1 staining of JM cells.
Negative control, UJ13A.

Figure 3.7

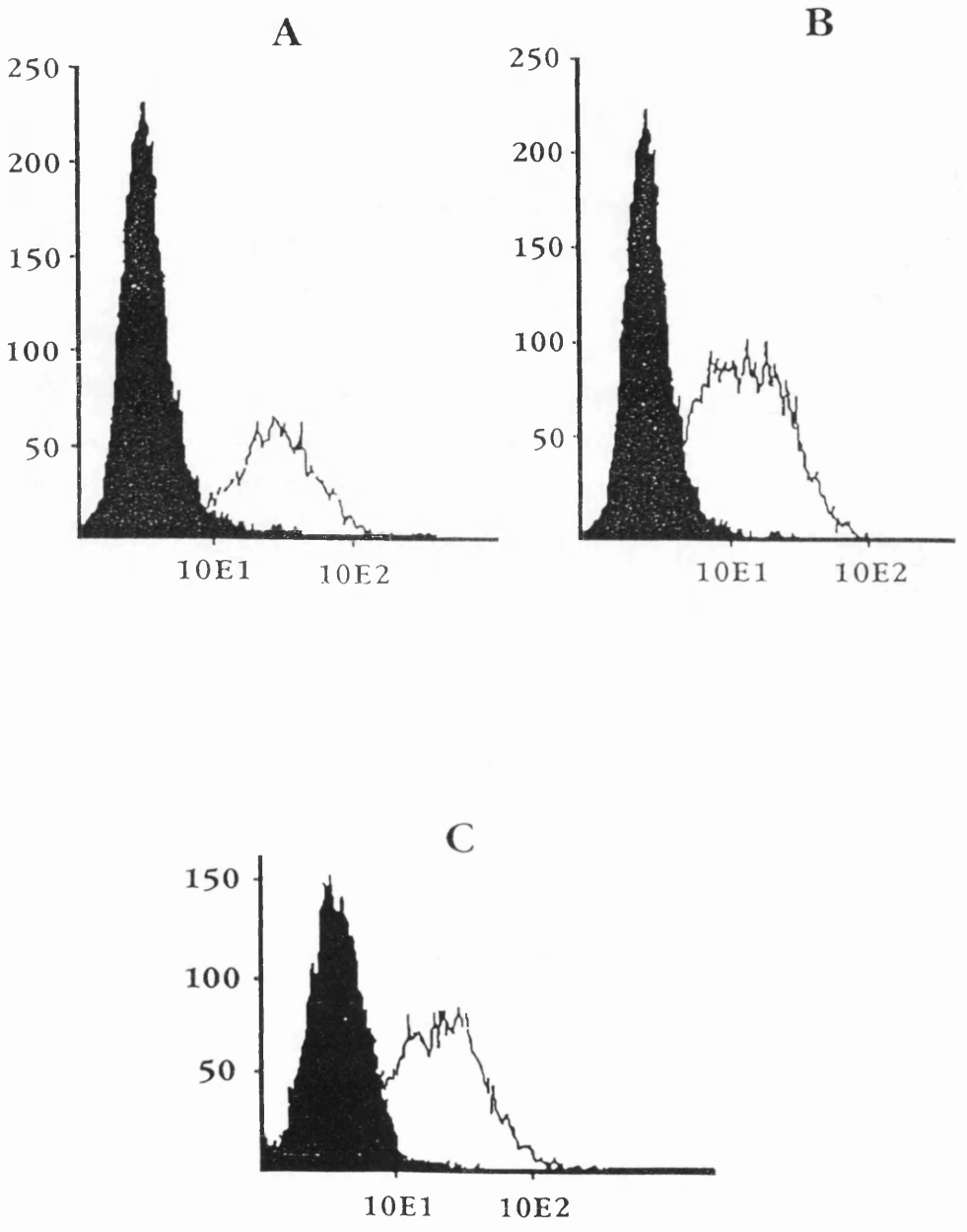
A
250
200
150
100
50
10E1
10E2
B
250
200
150
100
50
10E1
10E2
C
150
100
50
10E1
10E2

Figure 3.8

Immunofluorescence staining of normal human kidney with WCMH.

WCMH (5 μg) was incubated with freshly frozen normal adult kidney and stained by indirect immunofluorescence. Intense staining of renal glomeruli (G) and tubules (T) is demonstrated.

Figure 3.8

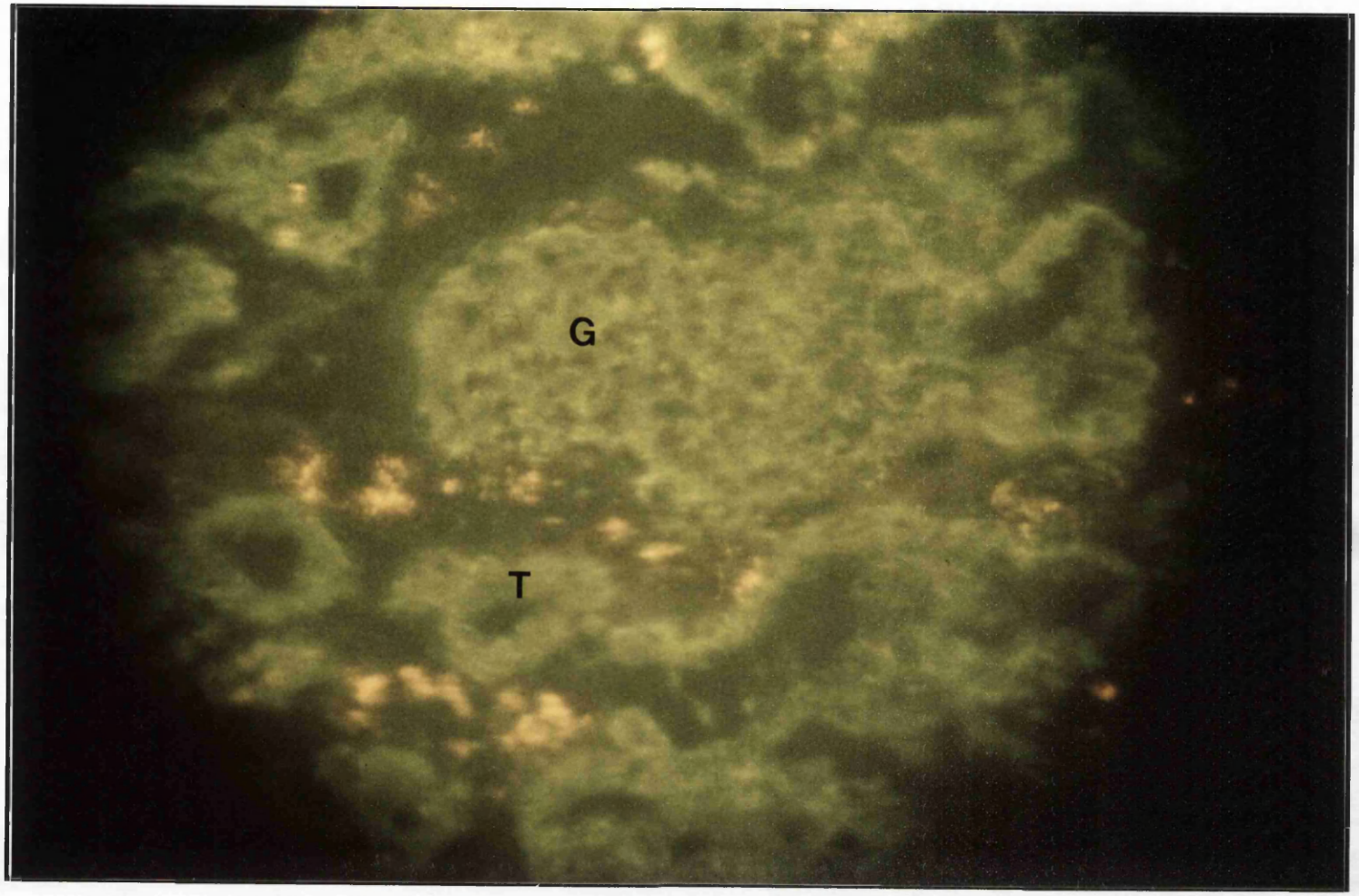

harvested and centrifuged at 400 x g for five minutes. 2.5 x 10^5 viable cells were pipetted into a 96 well microtitre plate, which had been pre-blocked overnight at 4°C with a solution of 5% bovine serum albumin (BSA) in PBS.

Each of nine serial dilutions, amounting to between 1 and 50 μg of unlabelled antibody, was added in triplicate to the wells, with three wells receiving no antibody. Following incubation for 30 minutes at room temperature (RT), 10^5 cpm of ^{125}I- labelled antibody was added to each well and the final volume adjusted to 100 μl with PBS. After a further 30 minutes at RT, the microtitre plate was centrifuged at 400 x g for five minutes in a Jouan plate centrifuge. Cells were resuspended and washed with PBS/1% BSA on two further occasions. Molten wax was used to seal each well and the amount of cell bound radioactivity measured in an LKB Wallac™ gamma counter. The cell-bound activity, expressed as cpm, was plotted against amount of incubated cold antibody as in Figure 3.9. Here, 4 μg cold WT1 was shown to saturate the binding sites of 2.5 x 10^5 JM cells. This amount of antibody was thus used to determine the degree of non-specific binding in the Scatchard analysis. A similar result was obtained for both WCMH and HD37, as tested against the cell lines, Nalm 6 and Reh, for which 2 - 4 μg of antibody was saturating.

To measure total antibody binding, 2.5 x 10^5 viable cells were added in triplicate to each of 10 wells. A second plate was used to set up a second series of identical wells to estimate the degree of non-specific binding. In the first series of wells, serial dilutions of 10^5 cpm, in 10^4 cpm increments, were added to a total volume of 100 μl in PBS. This was repeated in the second series of wells, but with the addition of the pre-determined amount (2 - 4 μg) of unlabelled antibody. Antibody was incubated with cells at room temperature for 30 minutes. Plates were centrifuged, washed twice in PBS/1% BSA and the radioactivity in each well counted as above. To derive both the equilibrium constants and the number of available antibody binding sites per cell, the law

Figure 3.9

Determination of the amount of non-radiolabelled antibody required to saturate binding sites of 2.5 x 10^5 cells.

2.5 x 10^5 JM cells were incubated for 30 minutes with between 0 and 50 µg of unlabelled WT1. The amount of antibody required to block binding of 10^5 cpm ^{125}I-WT1 was determined. 4 µg was demonstrated to be saturating.

Figure 3.10

Scatchard plot of the binding of ^{125}I-WT1 on cell line, JM.

Ordinate: Ratio of specific bound counts to unbound counts of ^{125}I-WT1.

Abcissa: Specific bound counts (cpm) of ^{125}I-WT1.

Slope: 6.04 / 1000 cpm - as generated by least squares analysis.

Intercept of abcissa: 9.6 x 10^3 cpm.

Figure 3.9

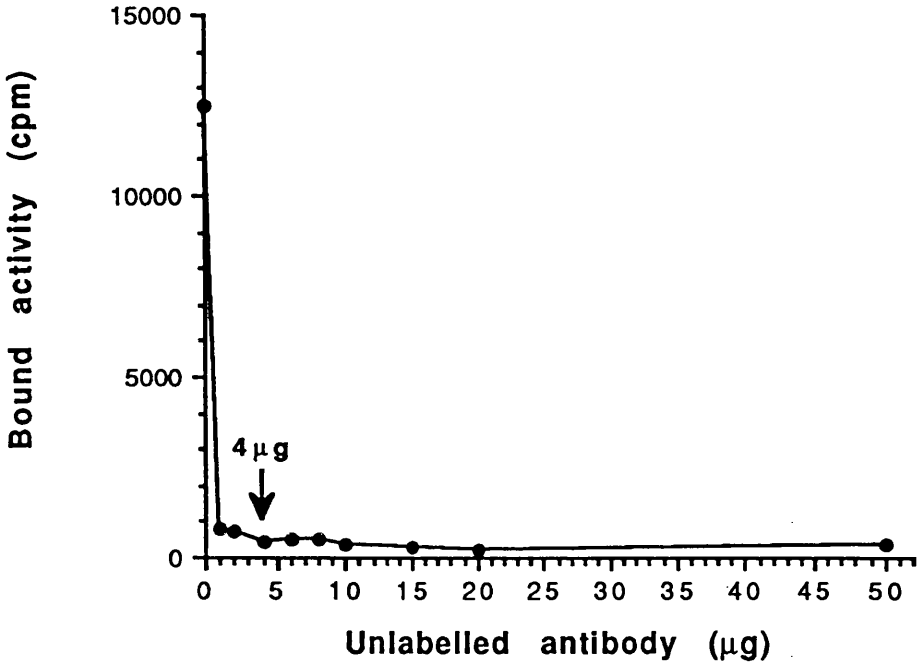

Figure 3.10

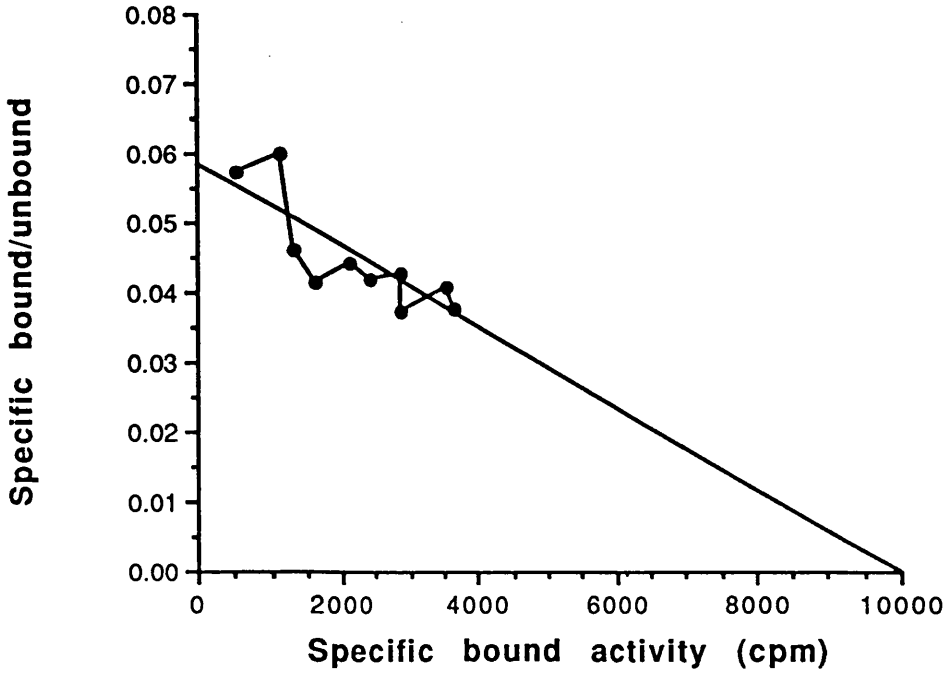

of mass action as used by Scatchard and elaborated for MoAbs by Trucco and Petris [220], was employed. A plot of bound activity against bound/unbound activity describes a linear function, as determined by least squares analysis, the slope of which generates the equilibrium constant. By extrapolation, the intercept with the abscissa defines a value from which the number of binding sites per cell can be calculated.

An example of this assay system for WT1, tested against the T-ALL cell line, JM, is described in Table 3.2, along with the resulting Scatchard plot in Figure 3.10. The gradient of this curve is $6.04 \times 10^{-3}/10^3$ cpm and the specific activity of ^{125}I-WT1 is 0.178 μg of protein per 10^6 cpm.

Converting 10^3 cpm into molar units:

From the antibody specific activity: 10^3 cpm = 1.78×10^{-10} g protein

For a volume of 100 μl: 10^3 cpm = 1.78×10^{-6} g/litre

Dividing by the molecular weight of antibody (1.55×10^5): 10^3 cpm = 1.148×10^{-11} M

The equilibrium constant ($\mathbf{K_a}$) is:

$$\mathbf{K_a} = 6.04 \times 10^{-3}/1.148 \times 10^{-11} = 5.26 \times 10^8 \text{ M}^{-1}$$

The number of binding sites per cell is derived from the intercept of the curves with the abscissa, which in this example is 9.6×10^3 cpm, equivalent to 1.10×10^{-14} Moles bound per 2.5×10^5 cells. Dividing by the number of cells (2.5×10^5) and multiplying by Avogadro's Constant (6×10^{23}) gives a value of 2.65×10^4 particles/cell.

Table 3.2

Scatchard analysis of antibody WT1 against cell line JM.

Counts Added (x 10^3 cpm)	Total Bound (x 10^3 cpm)	Non-Specific Bound (x 10^3 cpm)	Specific Bound (x 10^3 cpm)	Unbound (x 10^3 cpm)	Specific Bound/ Unbound
10	0.617	0.074	0.543	9.46	0.057
20	1.207	0.078	1.129	18.87	0.060
30	1.415	0.092	1.323	28.68	0.046
40	1.713	0.113	1.600	38.40	0.042
50	2.243	0.127	2.116	47.88	0.044
60	2.543	0.125	2.418	57.58	0.042
70	2.943	0.082	2.861	67.14	0.043
80	2.942	0.074	2.868	77.13	0.037
90	3.692	0.171	3.521	86.48	0.041
100	3.771	0.137	3.634	96.37	0.038

Scatchard analyses were performed for antibody WCMH against the B-lineage ALL lines, Nalm 6 (n=3) and Reh (n=2). HD37 was also tested against these lines (Nalm 6, n=3; Reh, n=2). WT1 was assayed on two occasions against the T-ALL line, JM (Table 3.3). For WCMH, the mean equilibrium constant was 4.85 x 10^8 M^{-1} when tested against Nalm 6, and 6.44 x 10^8 M^{-1} against Reh. For HD37, the mean equilibrium constants were 1.19 x 10^9 M^{-1} and 1.15 x 10^9 M^{-1} respectively. The mean equilibrium constant of WT1 was 4.70 x 10^8 M^{-1}. For WCMH the mean number of binding sites per cell varied between 1.39 and 5.51 x 10^5, and for HD37 between 1.04 and 3.84 x 10^4, when tested against Reh and Nalm 6 respectively. A mean epitope density of 2.71 x 10^4 per cell was observed for WT1 on the cell line, JM.

Table 3.3

Binding characteristics of antibodies, HD37, WCMH and WT1 as determined by Scatchard analysis.

Antibody	Cell Line	Affinity Constant - K_a (M^{-1})	Binding Sites per Cell
HD37	Nalm 6	Expt. 1. 1.51×10^9 2. 1.10×10^9 3. 0.97×10^9 Mean: 1.19×10^9	Expt. 1. 2.84×10^4 2. 3.84×10^4 3. 5.08×10^4 Mean: 3.84×10^4
HD37	Reh	Expt. 1. 1.14×10^9 2. 1.15×10^9 Mean: 1.15×10^9	Expt. 1. 1.17×10^4 2. 9.18×10^3 Mean: 1.04×10^4
WCMH	Nalm 6	Expt. 1. 3.33×10^8 2. 5.08×10^8 3. 6.15×10^8 Mean: 4.85×10^8	Expt. 1. 4.70×10^5 2. 6.34×10^5 3. 5.49×10^5 Mean: 5.51×10^5
WCMH	Reh	Expt. 1. 4.65×10^8 2. 8.22×10^8 Mean: 6.44×10^8	Expt. 1. 1.20×10^5 2. 1.58×10^5 Mean: 1.39×10^5
WT1	JM	Expt. 1. $5.26 \times 10^8\ M^{-1}$ 2. $4.14 \times 10^8\ M^{-1}$ Mean: $4.70 \times 10^8\ M^{-1}$	Expt. 1. 2.65×10^4 2. 2.76×10^4 Mean: 2.71×10^4

7. Loss of Surface-Bound Radioactivity from Cells Incubated with Monoclonal Antibodies.

The loss of bound radiolabelled MoAbs, as a function of time and temperature, was determined. Antibodies were radiolabelled with ^{125}I using the iodogen technique to a specific activity of 185 MBq/mg protein (Chapter 2; 5a). Only those reagents containing less than 10% free iodine contamination and of greater than 50% immunoreactivity were used (Chapter 2; 5d, 5f).

1 x 10^6 viable cells were resuspended in 1 ml RPMI 1640 complete medium and dispensed into LP3 tubes. A saturating amount of radiolabelled antibody (10^6 cpm) was added in triplicate and the cells incubated for one hour at 4°C. Following three washes, cells were resuspended in 2 ml complete medium and transferred to fresh LP3 tubes, pre-blocked for 60 minutes at 37°C with PBS containing 1% BSA. The cell-bound radioactivity was then determined. Cells were subsequently incubated at either 37, 21 or 4°C, the tubes being gently rotated on a Luckham Mutimix Major™ tube roller. At time points two, six and 24 hours the cell suspension was centrifuged and the unbound radioactivity estimated by counting a 100 µl aliquot of supernatant. The free iodine content of each aliquot was determined by TCA precipitation (Chapter 2; 5d). Mean total unbound radioactivity was expressed as a percentage of the total activity remaining in the tube and plotted against time of incubation for each temperature level.

Following two hours incubation at 37°C, 32.3% of the activity of ^{125}I-WT1 originally bound to JM was present in the supernatant, as compared with dissociated activities of 31.9% and 12.5% for ^{125}I-HD37 and ^{125}I-WCMH targeted to KM3 respectively (Figure 3.11). For ^{125}I-WT1, a further marked loss of bound activity was observed to a mean of 61.1% at six hours. After this time the rate of cell loss declined, reaching a total of 64.5% at 24 hours. A smaller increase in dissociated material was observed for ^{125}I-HD37, equivalent to 40.8

Figure 3.11

Loss of bound radioactivity from cells incubated with radiolabelled antibodies, WCMH, HD37 and WT1.

10^6 cells were incubated with ^{125}I labelled antibodies (n=1). Following washing, cell-bound activity was measured prior to reincubation in fresh medium. At 2, 6 and 24 hours, the degree of dissociated activity was estimated by counting an aliquot of supernatant. Curves represent per cent of total actvity in the supernatant as a fuction of time, at each of three temperatures.

A: Antibody WT1; cell line, JM.

B: Antibody HD37; cell line KM3.

C: Antibody WCMH; cell line KM3.

——— 37°C

– – – – – – 21°C

– · – · – 4°C

Figure 3.11

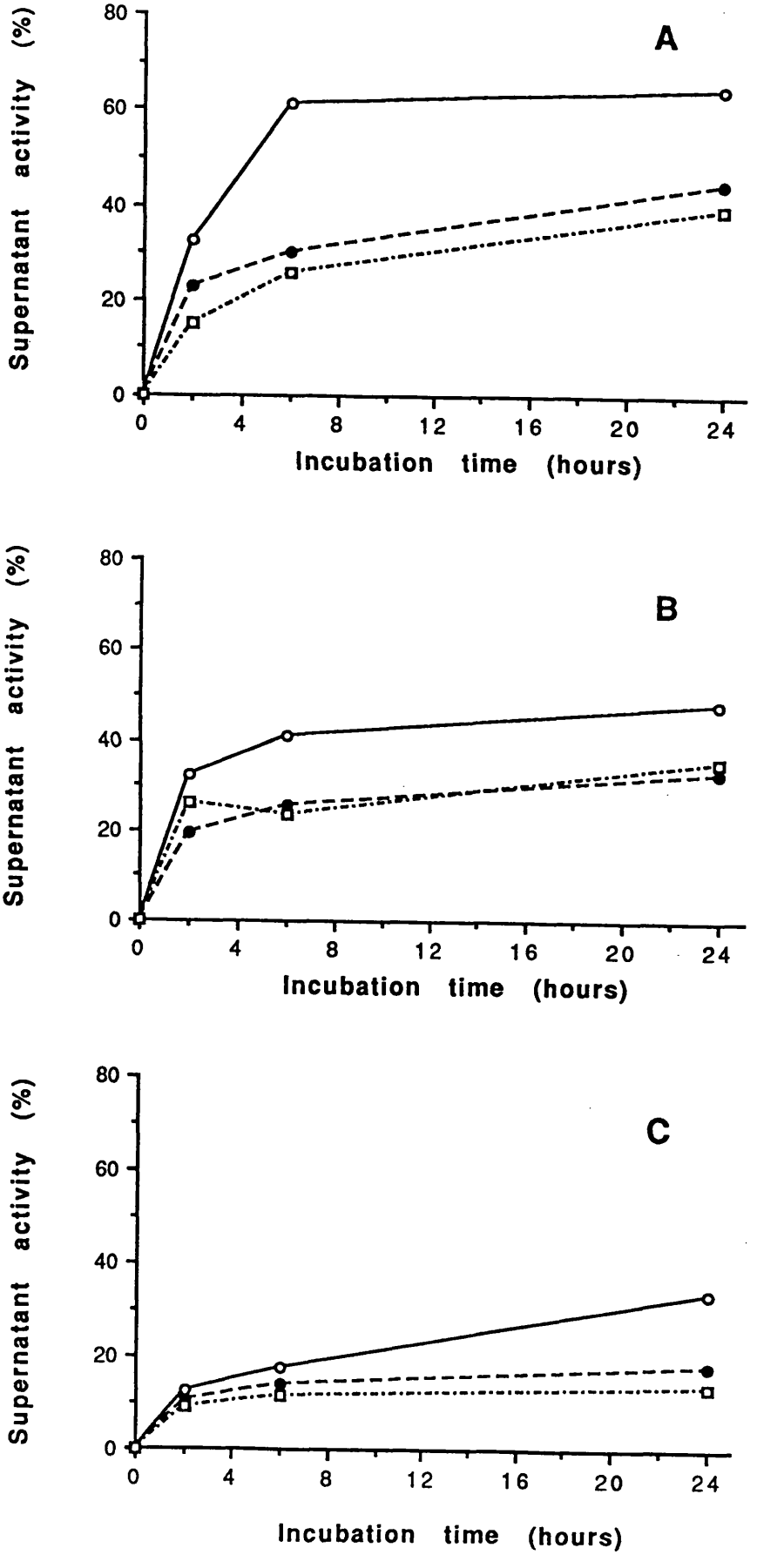
A
B
C
Supernatant activity (%)
Incubation time (hours)
0
20
40
60
80
0
4
8
12
16
20
24

and 48.0% at six and 24 hours respectively. The least loss of bound activity was noted for ^{125}I-WCMH with values of 17.3 and 33.3% at six and 24 hours respectively. For each antibody, dissociated activity showed marked temperature dependency, with a reduction in loss of bound activity from cells incubated at 21 and 4°C. In each instance, at least 80% of the activity remained as TCA precipitable material, implying preservation of the structural integrity of the conjugate.

8. Discussion.

Following the introduction of hybridoma technology, it was hoped that MoAbs could be identified that bind epitopes expressed solely on tumour cells. However, with the possible exception of idiotypes on B-cell tumours, no antigen has been found that is truly tumour-specific. Nevertheless, antibodies selected for therapy should recognise antigens that are widely expressed on tumours and exhibit minimum expression on normal cells. The three candidate antibodies for use in these studies were thus characterised with regard to their biological distribution on leukaemic cell lines and on normal tissues, with particular regard to neural structures.

The CD10 antigen, as recognised by WCMH, first identified by Greaves *et al.*, in 1975 [221], is a commonly used marker, defining a set of early pre-B leukaemias (common acute lymphoblastic leukaemia). The amino acid sequence of this 95 - 100 kDa membrane glycoprotein is identical to that of neutral endopeptidase (enkephalinase), a widely distributed membrane-bound metallo-peptidase [222]. CD10 is present on blasts in 85 - 90% of cases of B-lineage ALL [223]. Whilst it is not found on blood B-cells, CD10 is present at a number of stages during B-cell differentiation. In addition, a similar, but not identical, antigen has been found on neutrophils [224].

The 90 - 95 kDa glycoprotein antigen CD19, as recognised by HD37, is the most broadly distributed B-lineage marker. It is observed from a very early stage of B-cell development, i.e. by the time of V_H rearrangement [224]. It is expressed in more than 98% of cases of B-lineage ALL and in virtually all cases of B-cell derived non-Hodgkin's lymphoma (NHL) [223]. WT1 recognises the pan-T 40 kDa glycoprotein antigen CD7, the most widely expressed marker in T-ALL, found on blast cells in greater than 95% of cases of T-ALL and T-cell lymphoma [223]. Tax found no evidence of binding of WT1 to B-lymphocytes, B-lineage lymphoblasts, myeloid or erythroid cells [216]. Thus, in terms of antigen distribution on human lymphoproliferative malignancy, these three candidate antibodies are applicable to the great majority of cases of ALL and NHL.

In this study, the predicted binding of WCMH and HD37 to all four B-cell lines, and of WT1 to three T-ALL lines, was confirmed by immunofluorescence using both light microscopy and Facscan™ analysis. These cell lines were thus considered suitable for use in further experiments.

The expression of CD19 and CD10 on a subset of cells during normal B-lineage differentiation is of importance when considering the use of antibodies binding these antigens as carriers of radioisotope within the sub-arachnoid space. If such antibodies are cleared from the CSF into the systemic circulation and retain immunoreactivity, there is a potential for increased myelosuppression as a result of selective targeting of radionuclide within the bone marrow. However, data from immunofluoresence studies suggest that CD19 and CD10 is present on fewer than 5% of marrow mononuclear cells [225]. These and other investigations into normal lymphopoesis suggest that expression of these antigens on the pleuripotent stem cell is most unlikely [226]. In support of this, our clinical studies with WCMH and HD37 have not revealed increased myelosuppression as compared with other MoAbs not binding to bone marrow elements (Chapters 10, 12).

It is essential that antibodies injected intrathecally should not react with components of the central nervous system, an area not normally investigated for the expression of leukaemia-associated antigens. Repeated examination by immunofluorescence failed to detect any such binding.

WT1 has been screened extensively for reactivity with normal tissues [216] [227]. No evidence of binding of WT1 to cells or tissues of non-T lymphoid origin has been detected. A WT1 immunotoxin has also been subject to toxicity tests in Rhesus monkeys as part of an evaluation for the treatment of meningeal T-cell leukaemia. All animals developed a CSF pleocytosis, which generally resolved by four weeks after injection [228]. However, apart from some animals which exhibited a moderate loss of appetite, no gross evidence of behavioural change or neurotoxicity was observed.

Ghetie *et al.*, found no positive binding when HD37 was screened against a wide range of normal tissues by a modified immunoperoxidase technique [229]. Apart from one antibody, AB-1 (IgM), binding to vascular endothelium, no CD19 antibody has been shown to react with normal human tissue outside the haemopoetic system [224].

CD10 expression is, however, found on a number of normal tissues such as fibroblasts, myo-epithelial cells of the breast, epithelial cells of the small intestine and in the kidney, being present on the luminal surface of the proximal tubules and the visceral epithelium of the renal glomerulus [224] [230]. This staining pattern on kidney was confirmed for WCMH, and thus renal toxicity was closely monitored in patients receiving this antibody (Chapter 10; 2i).

WCMH and HD37 are of the IgG_1 isotype, whereas WT1 is confirmed as an IgG_{2a} antibody. This is of clinical relevance as although all antibody isotypes have been shown to mediate antibody dependant cellular cytotoxicity (ADCC), the relative strength of ADCC reactions has been assessed as $IgG_{2a} > IgG_{2b} >$

IgG_1 (Chapter 1; 1c). Tax demonstrated an immunosuppressive effect of WT1 in an *in-vivo* model system, to which ADCC was said to contribute [216].

Scatchard analysis demonstrated equilibrium constants comparable with other antibodies used in clinical studies [229] [231]. A moderately high epitope density was observed for all cell lines tested, notably for the CD10 antigen on Nalm 6 and Reh cell lines, for which greater than 10^5 binding sites for WCMH were demonstrated. This factor has been shown to be of possible relevance to studies of *in-vitro* cytotoxicity with radioconjugates of these reagents (Chapter 6; 4).

In this study, radiation dose to cells has been shown to increase when beta-emitting radionuclides are bound as a result of antibody targeting (Chapter 6). Dissociation of bound radiolabelled antibodies will clearly abolish this effect. This study has shown significant, temperature-dependent losses of ^{125}I, most marked for conjugates of the CD7 antibody, WT1. This may result from a simple dissociation of antibody from antigen, which may be exaggerated in this experimental system as, at time 0, all antibody was bound to cells. With no antibody in the surrounding medium, the binding equilibrium will be shifted towards a state of dissociation. However, the marked effect of temperature on the loss of radionuclide implies a more energy-dependent process such as antigen modulation resulting in loss of conjugate by either shedding of the antibody-antigen complex or by exocytosis following antibody internalization. Modulation is well recognized for leukaemia-associated antigens and has been noted together with antibody internalization for CD10 [232], CD19 [233] and CD7 [234]. Shedding of CD10 has been observed both *in-vitro* and in clinical studies of serotherapy for patients with common ALL [235].

Further work is underway to define mechanisms which may result in the marked loss of cell-bound radiolabelled antibody. This will include studies of antigenic modulation and internalization which almost certainly contribute

to the specific cytotoxic effect of WT1, HD37 and WCMH when conjugated to the Auger emitting radionuclide, ^{125}I (Chapter 8; 4), and are of probable relevance to the advantage in targeting cells with ^{131}I-labelled MoAbs (Chapter 6).

CHAPTER 4.

CHARACTERISATION OF RADIOIMMUNOCONJUGATES.

A series of experiments were undertaken to investigate the immunoreactivity and structural integrity of WCMH, HD37 and WT1 following labelling to varying specific activities with both ^{125}I and ^{131}I.

1. A Comparison of Chloramine-T and Iodogen Methods of Antibody Labelling with Isotopes of Iodine.

100 µl of either HD37 or WCMH, at a concentration of 1 mg/ml, was iodinated with 37 MBq ^{125}I by either the Chloramine-T or iodogen methods. Following Sephadex G-25™ column chromatography, the activity of the chromatographic peak was measured in a Vinten Isocal™ radionuclide calibrator. The labelling efficiency (LE) of each reaction was calculated as:

$$LE = \frac{\text{Radioactivity of labelled product}}{\text{Total radioactivity used}} \times 100\%$$

The specific activity of the labelled product was subsequently determined. The degree of free iodine contamination of the final product was estimated by precipitation with 10% TCA (Chapter 2; 5d) and the immunoreactive fraction (IRF) by a modified Lindmo radiobinding assay (Chapter 2; 5f), using the pre-B ALL cell line, Reh.

An example of the data generated from a binding assay of ^{125}I-WCMH against the Reh cell line is shown in Table 4.1, along with the the resulting double-inverse plot in Figure 4.1. The intercept of the curve with the ordinate ($\mathbf{Y_O}$) equals 1.2144. The immunoreactive fraction (**r**) is thus calculated as:

$$\mathbf{r} = \frac{\mathbf{1}}{\mathbf{Y_O}} \mathbf{\times 100\%} = 82.3\%$$

Table 4.1

Data from a binding assay to determine the immunoreactive fraction of ^{125}I-WCMH.

Cell Concentration (10^6/ml)	Inverse Cell Concentration (ml/10^6)	No Pre-treatment		Pre-saturated Cells		Calculated Data		
		Total Applied (T) (cpm)	Total Bound (cpm)	Total Applied (cpm)	Non-specific Binding (cpm)	Specific Binding (B)	B/T	T/B
25	0.04	56677	41028	53179	307	40728	0.719	1.39
12.5	0.08	54587	37453	52222	206	37247	0.682	1.47
6.25	0.16	54606	31685	55186	215	31470	0.576	1.74
3.125	0.32	52060	21601	54007	197	21404	0.411	2.43
1.563	0.64	58867	15433	53916	226	15207	0.258	3.88
0.781	1.28	53969	9237	55515	255	8982	0.166	6.02

Figure 4.1

Modified Lindmo binding assay of ^{125}I-WCMH against Reh.

0.78 to 25 x 10^6 Reh cells, in 1 ml PBS, were incubated at 4°C with 0.5 ng ^{125}I-WCMH. Specific bound activity was calculated as the difference between total and non-specific bound activity (obtained from cells presaturated with unlabelled WCMH).
T/B is plotted against 1/C where:

T = Total applied activity (cpm)
B = Specific bound activity (cpm)
C = Cell concentration (x 10^6/ml)

The curve was generated by least squares analysis.

Figure 4.1

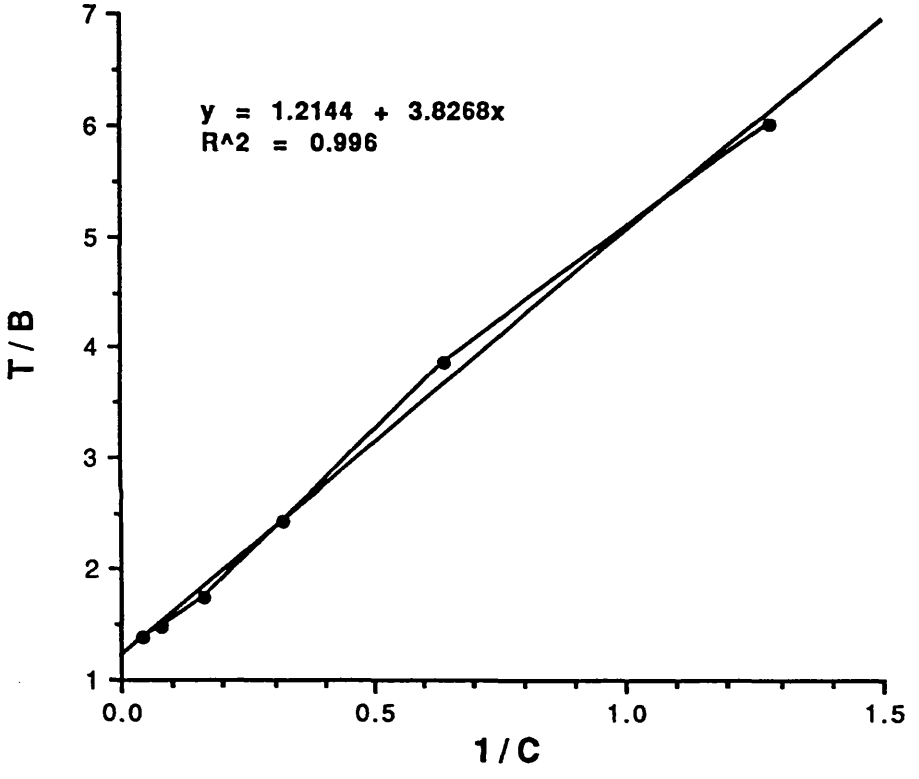

Each experiment was repeated on two occasions. Results are expressed in terms of the means of labelling efficiency, calculated specific activity, IRF and free iodine content (Table 4.2).

Table 4.2

Comparison of Chloramine-T and iodogen techniques for radiolabelling antibodies.

Antibody	Iodination Technique	Labelling Efficiency (%)	Specific Activity (MBq/mg)	Immuno-reactive Fraction (%)	Free Iodine (%)
WCMH	Chloramine-T	37.1	137	37.0	5
WCMH	Iodogen	79.3	293	82.3	1
HD37	Chloramine-T	48.8	181	36.0	5
HD37	Iodogen	87.7	324	73.5	6

This data demonstrates an advantage for the iodogen technique in terms of both the efficiency of ^{125}I labelling and resultant immunoreactivity. On the basis of this data, and that from others [236] [237], subsequent radiolabellings were performed using the iodogen method.

2. Variables Associated with Antibody Labelling.

(a) Methods

A series of experiments were undertaken to investigate whether the specific activity to which antibodies are radiolabelled influences the efficiency of iodination and/or the immunoreactivity and structural integrity of the resulting conjugates. Iodination with ^{125}I and ^{131}I was also compared, along with comparison of the stability of the labelled product with respect to time following the radiolabelling procedure.

MoAbs, WCMH, HD37 and WT1 were radiolabelled with 37 MBq of either ^{125}I or ^{131}I using the iodogen technique (Chapter 2; 5a). The intended specific activity was varied by adjusting the concentration of antibody solution, whilst maintaining a constant volume of 100 µl in the iodogen tube. Antibodies were radiolabelled with ^{125}I to a specific activity of between 185 and 1110 MBq/mg protein, and with ^{131}I to a specific activity of between 37 and 1110 MBq/mg protein. Following iodination, the Sephadex G-25™ gel filtration peak was collected and the labelling efficiency calculated as described above. The free iodine content and IRF were determined for each product within four hours of radiolabelling.

To follow changes in the immunoreactive fraction with time, labelled antibodies were diluted in 6 ml PBS at a concentration of 0.15 MBq/ml and incubated at 37°C. At 24 hours, further radiobinding assays were performed and the free iodine content measured. This was repeated for ^{131}I conjugates following a further six days incubation at 37°C.

Structural preservation of antibody conjugates with respect to time was examined by SDS polyacrylamide gel electrophoresis and autoradiography. Each ^{125}I and ^{131}I conjugate was diluted to 0.15 MBq/ml in 2 ml of PBS, normal human serum or normal human CSF. Serum was obtained from donors within the laboratory and CSF from patients with ALL in CNS remission. Immediately following mixing, a 200 µl aliquot was removed from each solution and frozen at -20°C. The remaining solution was incubated at 37°C for seven days. Day 0 and day 7 samples containing 2 x 10^4 cpm were size separated on a 5% non-reducing polyacrylamide gel (Chapter 2; 3a), along with ^{14}C-methylated protein markers. Following staining with Coomassie Blue, the gel was dried under vacuum and heat onto Whatman 3M chromatography paper using a Bio Rad 383 gel drier and subjected to autoradiography at -80°C using Fuji RX™ X-ray film.

(b) Results.

(i) Effect of varying specific activity on labelling efficiency and immunoreactive fraction.

The mean labelling efficiency and IRF following antibody labelling to different specific activities with either ^{125}I or ^{131}I is shown in Figures 4.2 and 4.3 respectively. Data for IRFs on day 0 is presented in Table 4.3.

For ^{125}I-HD37, mean labelling efficiency varied between 88% at a specific activity of 185 MBq/mg protein and 56% at a specific activity of 740 MBq/mg protein. Labelling efficiency at the highest specific activity of 1110 MBq/mg protein was 59%. For ^{131}I conjugates of HD37, efficiencies of 65 to 46% were observed. For antibody WCMH, labelling efficiencies of 79 to 52% and 75 to 65% were demonstrated for ^{125}I and ^{131}I respectively. The lowest range of labelling efficiencies, of 57 to 45%, were observed for ^{125}I radiolabellings of WT1. However, due to failure of the radionuclide calibrator, the efficiency of these iodinations was calculated by a different method, using a gamma counter. For ^{131}I-WT1, efficiency of labelling varied between 79 and 55%. In no instance was the free iodine content of radioconjugates greater than 15%, with 85% of values less than 10%.

For all conjugates, a clear trend towards decreasing IRF with increasing specific activity was demonstrated (Figure 4.3). For ^{131}I conjugates of WCMH, a maximum IRF of 91.2% was observed at a specific activity of 37 MBq/mg protein, decreasing to 48.2% at 1110 MBq/mg. Respective IRFs of between 89.2% and 37.5% were calculated for ^{131}I-HD37 and between 87.5% and 43.1% for ^{131}I-WT1. For WT1 and WCMH, no difference in the slopes of the curves was observed when ^{125}I and ^{131}I conjugates were compared. The IRFs for ^{125}I-HD37 at specific activities of 370 and 1110 MBq/mg protein are slightly higher than the respective values for ^{131}I-HD37.

Table 4.3

Change in immunoreactive fraction of antibodies following radiolabelling.

Conjugate	Specific Activity (MBq/mg)	Immunoreactive Fraction (IRF) (%) (Change in IRF from day 0)		
		Time Following Radiolabelling (days)		
		0	1	7
^{125}I-WCMH	185	78.9	78.6 (-0.3)	-
	370	71.0	-	-
	555	68.9	69.8 (+ 0.9)	-
	740	61.5	53.0 (-8.5)	-
	1110	45.5	41.7 (-3.8)	-
^{131}I-WCMH	37	91.2	88.3 (- 2.9)	68.5 (-22.7)
	370	72.3	68.5 (-3.8)	47.1 (-25.5)
	1110	48.2	46.5 (-1.7)	27.9 (-20.3)
^{125}I-HD37	185	73.4	69.7 (-3.7)	-
	370	79.2	76.3 (-2.9)	-
	555	69.5	56.4 (-13.1)	-
	740	55.2	55.4 (+0.2)	-
	1110	54.6	46.5 (-8.1)	-
^{131}I-HD37	37	89.2	82.2 (-7.0)	81.7 (-7.5)
	370	65.6	69.6 (-4.0)	61.8 (-3.8)
	1110	37.5	38.2 (+0.7)	27.9 (-9.6)
^{125}I-WT1	185	86.0	58.5 (-27.5)	-
	370	83.0	72.3 (-10.7)	-
	555	70.5	75.5 (-5.0)	-
	740	64.1	60.6 (-3.5)	-
	1110	44.4	50.8 (-6.4)	-
^{125}I-WT1	37	87.5	75.8 (-11.7)	82.6 (-4.9)
	370	75.5	61.3 (-14.2)	49.8 (-25.7)
	1110	43.1	47.2 (+4.1)	22.3 (-20.8)

Figure 4.2

Efficiency of antibody radiolabelling with increasing specific activity.

WCMH, HD37 and WT1 were radiolabelled with 37 MBq ^{125}I and ^{131}I using the iodogen technique, to a specific activity of between 37 and 1110 MBq/mg protein. Labelling efficiency was calculated from the total activity in the labelled product.

A = WCMH

B = HD37

C = WT1

---- Iodine-125

——— Iodine-131

Figure 4.2

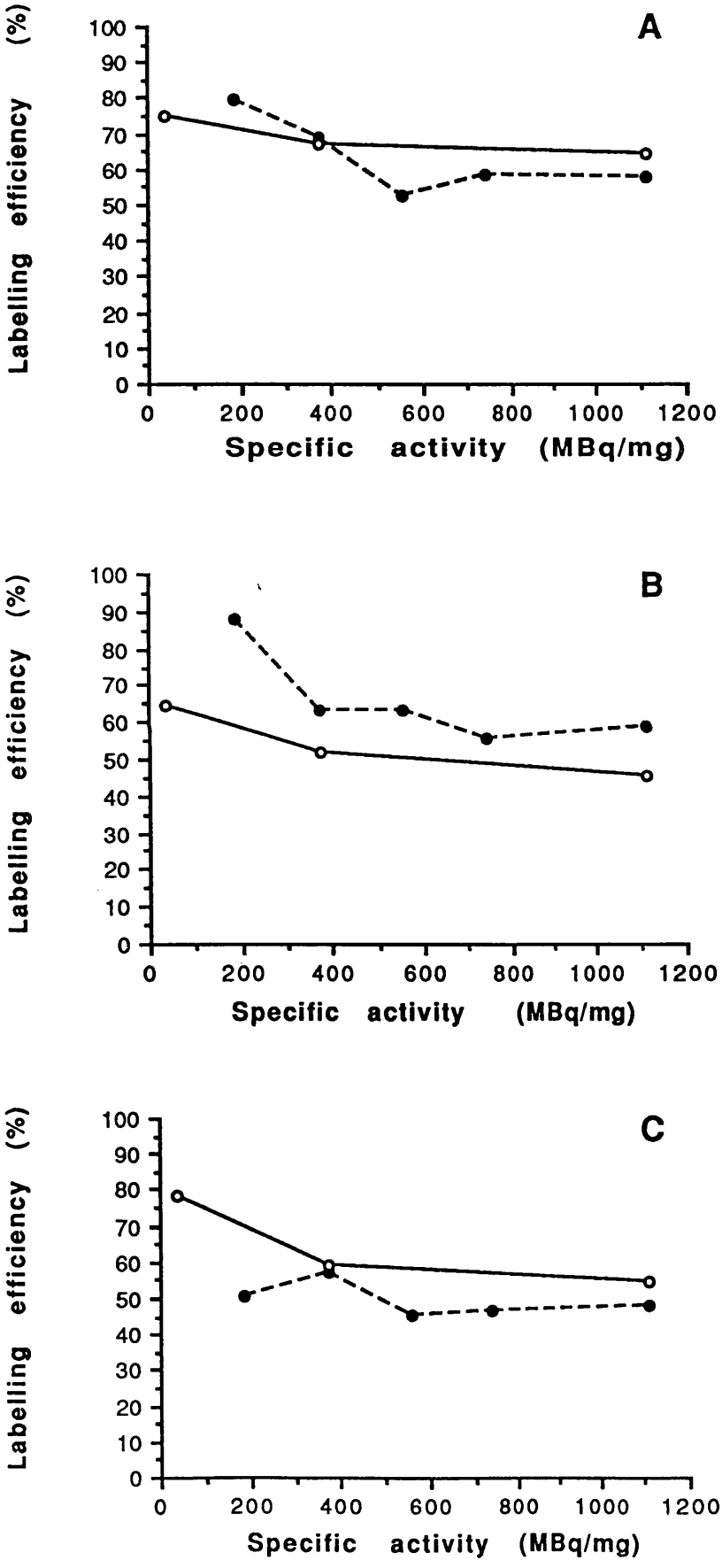
A
B
C
Labelling efficiency (%)
Specific activity (MBq/mg)
0
10
20
30
40
50
60
70
80
90
100
0
200
400
600
800
1000
1200

Figure 4.3

Variation in immunoreactive fraction with increasing specific activity.

WCMH, HD37 and WT1 were radiolabelled with 37 MBq ^{125}I and ^{131}I using the iodogen technique, to a specific activity of between 37 and 1110 MBq/mg protein. Immunoreactive fraction was determined using a modified Lindmo binding assay.

A = WCMH

B = HD37

C = WT1

---- Iodine-125

——— Iodine-131

Figure 4.3

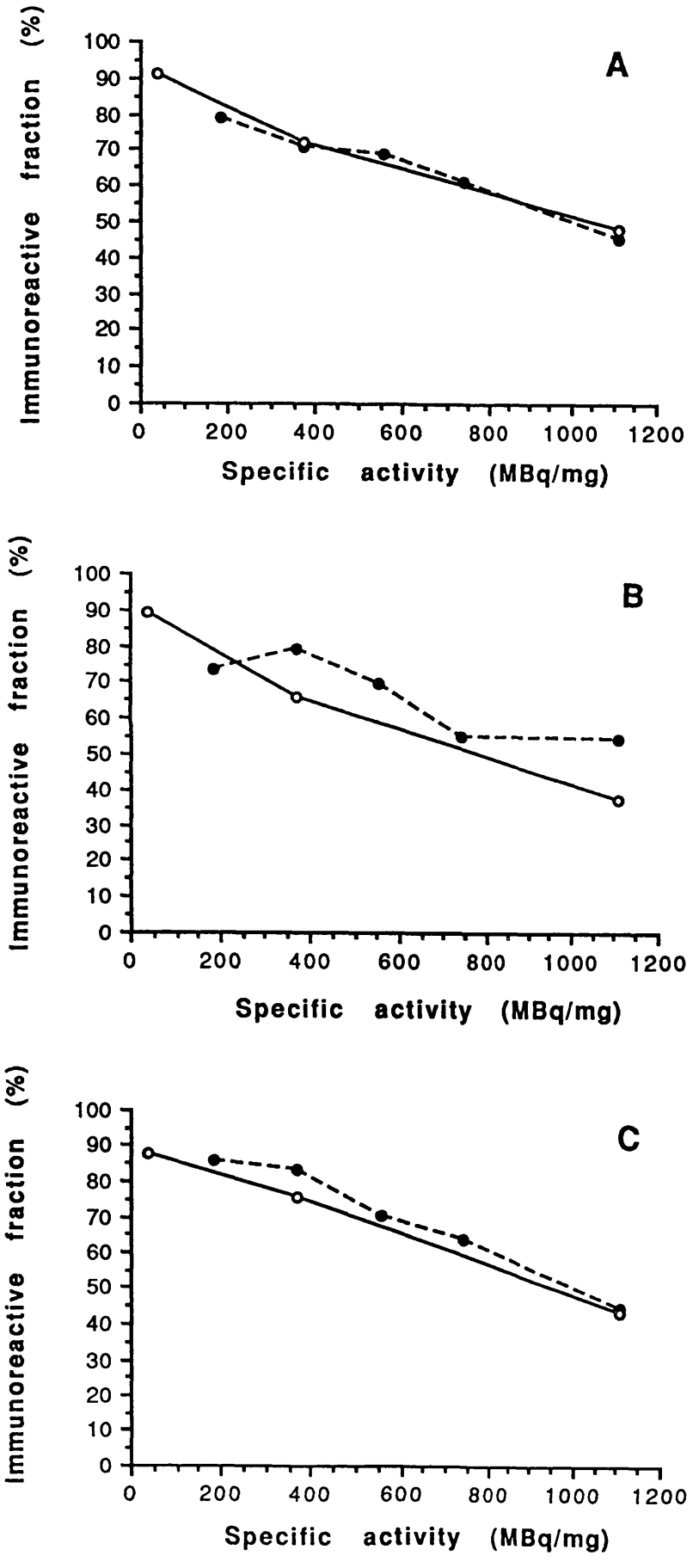
A
B
C
Immunoreactive fraction (%)
Specific activity (MBq/mg)
0
10
20
30
40
50
60
70
80
90
100
0
200
400
600
800
1000
1200

(ii) Effect of time following radiolabelling on immunoreactive fraction.

Table 4.3 depicts the data from binding assays performed on days 0, 1 and 7 following radiolabelling. By 24 hours after iodination, most conjugates demonstrated relatively small losses in IRF, with only five out of 23 showing falls greater than 10%. Four of these were for conjugates of WT1, with a maximum decrease of 27.5% for ^{125}I-WT1 labelled to a specific activity of 185 MBq/mg protein. By seven days after radiolabelling, significant loses of IRF of between 20.3 and 25.5 were observed for ^{131}I conjugates of WCMH and between 4.9 and 25.7 for WT1 radiolabellings. By contrast, no conjugate of HD37 sustained a fall in IRF of greater than 10%.

(iii) Structural integrity following radiolabelling.

Autoradiographs were examined for evidence of both protein aggregation and fragmentation. Figure 4.4 shows the autoradiographs of ^{125}I-HD37 and ^{131}I-WT1 following incubation for 0 and 7 days at 37°C in PBS, serum and CSF. For each product, intense bands are seen, equivalent to the molecular weight of IgG. The multiple bands observed probably represent differential glycosylation of antibodies. For ^{131}I-WT1, higher molecular weight bands are visualized in each lane, indicative of protein aggregation. These figures are representative for all antibodies radiolabelled with ^{125}I and ^{131}I to each specific activity. Each autoradiograph demonstrated excellent preservation of IgG structure in terms of molecular weight. Aggregation of protein was noted, but in no case was significant fragmentation of labelled antibodies observed, thus excluding significant *in-vitro* proteolysis.

Figure 4.4

Demonstration of the structural integrity of radioiodinated antibodies with respect to time following radiolabelling.

WT1 and HD37 were labelled with ^{131}I and ^{125}I respectively, to a specific activity of 1110 MBq/mg protein. Radioconjugates were diluted in PBS, normal human serum and normal human CSF, and incubated at 37°C. After 0 and 7 days, samples (2 x 10^4 cpm) were run, together with ^{14}C-labelled molecular weight markers, on a 5% polyacrylamide gel subjected to autoradiography.

Lanes: A, CSF - day 0; B, PBSA - day 0;
C, serum - day 0; D, CSF - day 7;
E, PBSA - day 7; F, serum - day 7;
G, ^{14}C-molecular weight markers.

Molecular weight markers:

Protein	Molecular Weight
Myosin	200,000
Phosphorylase b	92,500
Bovine serum albumin	69,000
Ovalbumin	46,000
Carbonic anhydrase	30,000
Trypsin inhibitor	21,500
Lysozyme	14,300

Figure 4.4

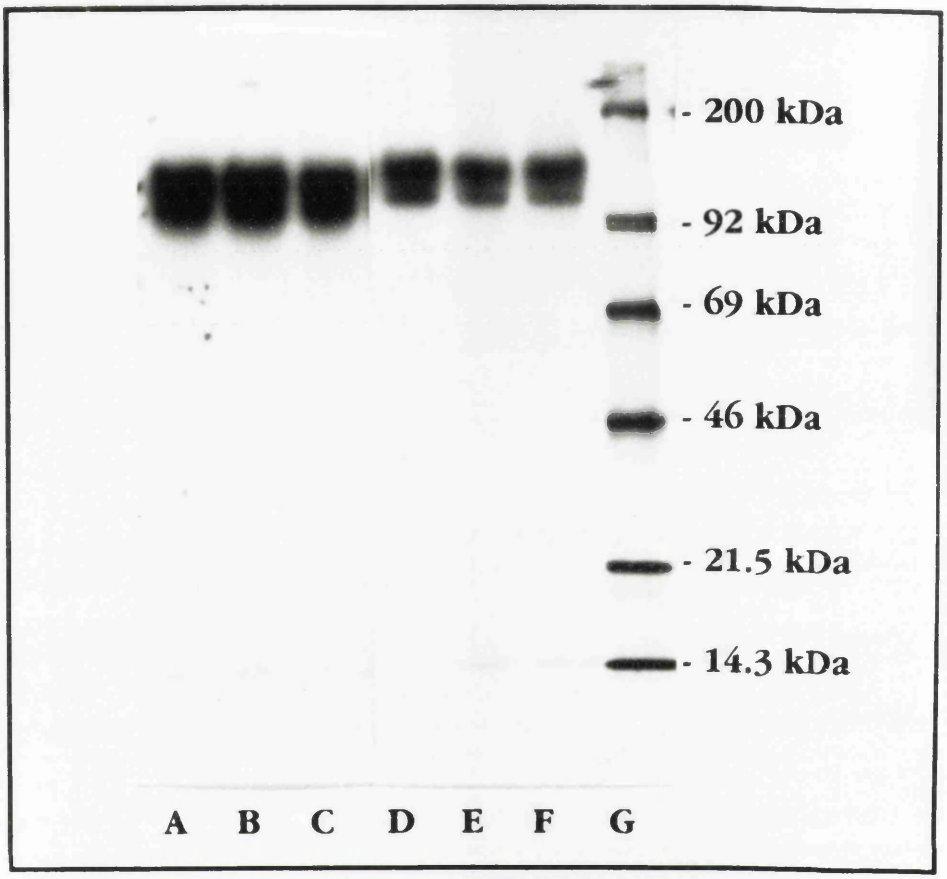

^{125}I-HD37

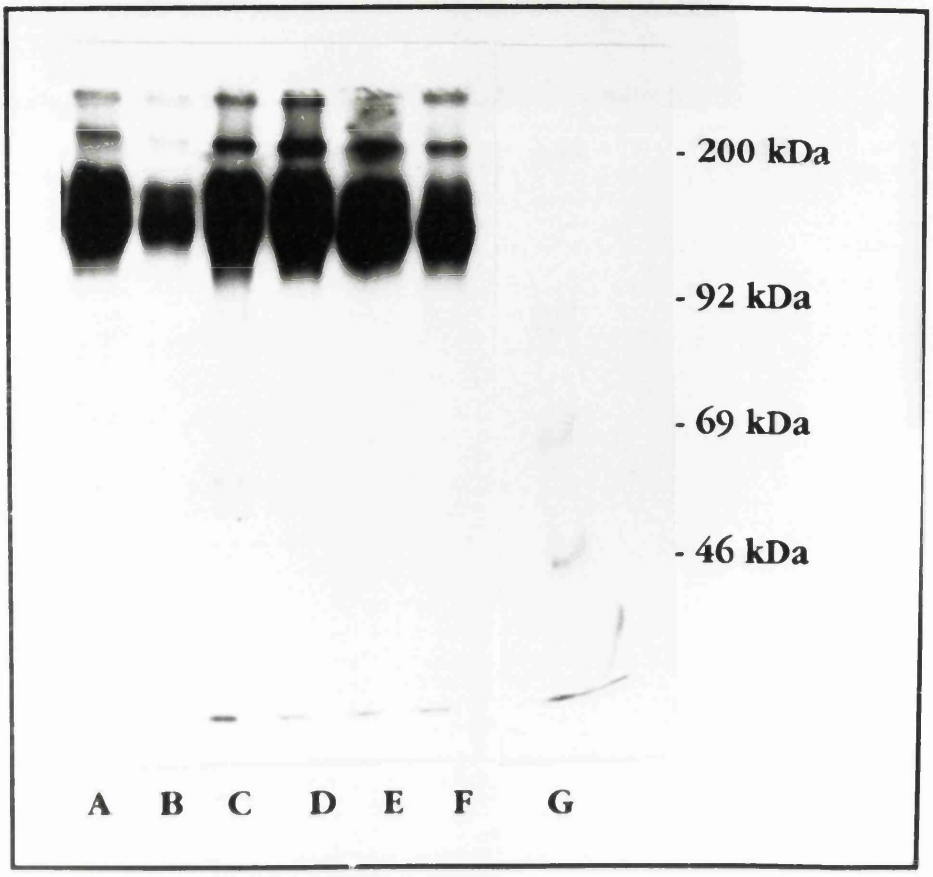

^{131}I-WT1

3. Discussion.

One of the main factors behind the sustained popularity of isotopes of iodine, for studies of both radiolocalisation and radioimmunotherapy, is their well established and relatively uncomplicated chemistry of conjugation to protein molecules. Protein iodination techniques can be broadly divided into two groups; direct methods, in which radioiodine is directly incorporated into amino acid residues, and indirect methods in which a radioiodinated moiety, eg. the Bolton and Hunter reagent, is conjugated to a specific side-chain of the protein [238].

Direct methods are most widely used, having the advantages of being easier to perform, involving a single reaction stage and having a higher level of incorporation of radioactivity. These techniques involve the oxidation of NaI and subsequent incorporation of radioiodine into amino acid residues, principally tyrosine, although some iodine may also react with histidine, tryptophan and sulphydryl groups [239]. Oxidation of NaI may be achieved chemically, as in the Chloramine-T [211] and iodogen techniques [210], enzymatically (lactoperoxidase) [240] or by electrolysis [241]. Direct methods of iodination may, however, be limited by an increased risk of reduced biological activity if iodinated residues lie within areas such as the antibody hypervariable region. This risk will be increased as the number of iodine molecules incorporated into the protein is raised, i.e. with increasing specific activity. Further damage from the iodination reagents, radiolysis and denaturing of proteins as a result of storage and handling is possible [239].

The Chloramine-T method was, for some time, the method of choice in our laboratory. Concern was expressed, however, with regard to oxidative damage caused by this and other soluble oxidising agents. We thus investigated a solid phase system of radiolabelling using the water-insoluble, chloramide, Iodogen™ [210]. This study demonstrates a clear superiority for

the iodogen technique as compared with the Chloramine-T method, in terms of both labelling efficiency and conjugate immunoreactivity for ^{125}I labellings of WCMH and HD37, confirming the results of other investigators [210] [236] [237]. This work also demonstrates that all three antibodies selected for use in both *in-vitro* and clinical studies could be satisfactorily radiolabelled with iodogen over a range of specific activities up to 1110 MBq/mg, for which labelling efficiencies of at least 45% were observed.

For all three reagents, a clear trend towards decreased IRF with increasing specific activity was noted. Nevertheless, even at a specific activity of 1110 MBq/mg protein, a mean IRF of at least 37.5% was observed. This specific activity is equivalent to an average incorporation of two iodine atoms per immunoglobulin molecule. No significant differences in initial IRFs were observed when the three anti-leukaemic antibodies were compared, and when comparing ^{125}I and ^{131}I antibody conjugates. Very few similar studies have been reported. However, Matzhu *et al.*, observed a similar trend of decreased immunoreactivity of anti-melanoma antibodies labelled with ^{125}I up to a specific activity of 1036 MBq/mg protein [242].

The effect of time on immunoreactivity was investigated by comparing initial values with those obtained 24 hours after radiolabelling. This time point was chosen as previous clinical studies indicated that by 24 hours post injection approximately 90% of the injected activity had cleared from the CSF [67]. At this time, preservation of immunoreactivity was observed. By seven days, when approximately 0.01% of injected activity remains in the CSF, significant losses in IRF were noted. Differences between antibodies were seen with regard to this effect, with HD37 relatively resistant to damage as compared with either WCMH or WT1. Such a variation is possibly explained by the positioning of tyrosine residues. Radiolysis was not expected to result in gross structural damage such as antibody fragmentation. This was confirmed by SDS-PAGE and autoradiography.

These studies were performed using relatively low amounts of ^{125}I and ^{131}I, i.e. 37 MBq. Radiation protection considerations did not permit these comparative investigations to be undertaken with the amounts of isotope used in clinical studies, i.e. 370 - 2220 MBq. Quality control data of clinically used radioconjugates indicated that their respective IRFs were lower than those observed here (Chapter 10; 3c).

The relatively small free iodine content of labelled products, even after prolonged incubation *in-vitro,* may not reflect the clinical situation. *In-vivo* de-halogenation is well recognized and has been attributed, in part, by the action of iodinases, eg. iodotyrosinases [243]. Attempts to overcome this problem have included the development of alternative labelling technologies. Zalutsky *et al.,* have described a method of iodination using acylation agents to protect iodine from the action of de-halogenase enzymes [244]. Significantly enhanced tumour localization and *in-vivo* stability was observed in a nude mouse model for antibody labelled using these reagents as compared to Cloramine-T [76]. However, a similar advantage was not reproduced in clinical studies (Personal communication, Mr H Coakham, Imperial Cancer Research Fund, Bristol).

Following these investigations, antibodies were labelled to a specific activity of 370 MBq/mg for both *in-vitro* and patient studies. It was felt that the advantage of delivering a higher activity to the cell surface for each bound antibody molecule at this level, as compared with lower specific activities, would more than compensate for the relatively small decrease in immunoreactivity. Concern was felt with regard to antibody damage at higher specific activities than this, particularly when using therapeutic amounts of ^{131}I. However, subsequent data from *in-vitro* investigations suggest that, despite lower immunoreactivity, cell kill is increased using antibody labelled to a specific activity of 1110 MBq/mg as compared with 370 and 37 MBq/mg (Chapter 6; 3h). Our group is thus again considering iodination to this level in our clinical program.

CHAPTER 5.

DEVELOPMENT OF AN *IN-VITRO* MODEL FOR THE DETERMINATION OF THE SURVIVAL FRACTION OF LEUKAEMIA CELL LINES.

The soft agar clonogenic assay of Courtenay and Mills [245] was modified for leukaemia cell lines to allow the *in-vitro* investigation of targeted radiotherapy. Suitable cell lines were selected where the colony forming efficiency remained constant over a range of cell concentrations.

1. Method.

Leukaemia cell lines were harvested in exponential growth phase, washed twice, resuspended in Hams F-12 complete medium and the viability estimated by Trypan Blue exclusion. The concentration of live cells was adjusted to 5 x that required finally and cells were maintained at 37°C.

5 g Agar Noble (5 ml displacement) was mixed with 95 ml double distilled water in a conical flask and sterilised by boiling for 15 minutes. The flask was covered to prevent evaporation. 5 ml of agar solution was diluted in 45 ml complete medium, pre-warmed to 44°C and kept at this temperature prior to use.

Red blood cells from August rats were obtained by cardiac puncture using preservative-free heparin. Red cells were washed three times in PBS (1000 x g for eight minutes) and resuspended to the original blood volume in complete medium. To inactivate nucleated cells, the suspension was heated to 44°C for one hour and stored at 4°C for up to one month. A 1 in 8 dilution in complete medium was carried out immediately before use.

For cloning, 2 ml of cell suspension was added to 1 ml of the red cell suspension, 1 ml of complete medium and 6 ml of agar suspension (final agar concentration of 0.3%). Aliquots of 1 ml were pipetted into 14 ml plastic tubes (Falcon), care being taken to avoid the formation of bubbles. Tubes were capped and placed in crushed ice for 10 minutes to facilitate setting of the agar. Tubes were subsequently placed in the rack of a Modular Incubator Chamber™ (Flow Laboratories). This was gassed for 10 minutes with a mixture of 90% nitrogen, 5% oxygen and 5% carbon dioxide and incubated at 37°C. Following red cell lysis at five to seven days, 2 ml of complete medium was added to the agar plug in each tube and the chamber regassed. After 14 days incubation, colonies were fixed with 1 ml of a 2.5% aqueous solution of glutaraldehyde and stored at 4°C prior to counting.

For colony counting, the liquid layer was decanted off and the agar pellet tipped into the inverted lid of a 6 cm tissue culture plate marked with a 2 mm grid (Costar) to aid counting. The base of the lid was pushed down on to the agar pellet to form a thin layer. Colonies containing more than 50 cells were counted under an Olympus inverted microscope. To eliminate observer bias, tubes were coded before counting using a computer program to generate a series of four digit random numbers (Courtesy of Dr K Elsom).

2. Results.

(a) Selection of cell lines.

A variety of human leukaemia and lymphoma cell lines were screened to determine their ability to clone in the Courtenay assay system. These included the B-lineage ALL lines, Nalm 6, KM3, Reh and Nalm 16, and the lymphoma cell line, Daudi. T-ALL cell lines included JM, MOLT 4 and GH1. Between one and 5000 cells were plated and the mean colony forming

Table 5.1

Cloning of human ALL and lymphoma cell lines in soft agar.

Cell Line	Number of Cloning Experiments	Number of Experiments in which Colonies Demonstrated	Colony Forming Efficiency (%) [Mean]	Disaggregation*
Nalm 6	7	4	Expt. 1. 67 2. 51 [47] 3. 37 4. 32	Expt. 1. + 2. ++ 3. ++ 4. ++
Reh	6	3	1. 18 2. 62 [44] 3. 51	1. +++ 2. ++ 3. +++
KM3	5	2	1. 10 [23] 2. 35	1. +++ 2. +++
Daudi	5	1	1. 7	1. ++
Nalm 16	3	0	-	-
JM	4	4	1. 56 2. 55 [52] 3. 46 4. 60	1. + 2. ++ 3. + 4. ++
GH1	3	2	1. 50 [58] 2. 65	1. ++++ 2. +++
MOLT 4	4	2	1. 47 [51] 2. 55	1. +++ 2. +++

* Abitary scale: 0 - ++++

efficiency (CFE) determined from six replicate tubes (Table 5.1). This was repeated on at least three occasions for each line.

Cell lines were selected on the basis of reliability of cloning, CFE and colony appearance in terms of cell morphology and disaggregation. Of the B-cell lines tested, Nalm 6 cloned in four of seven attempts, with the least disaggregated colonies and the highest mean CFE of 47%. Reh and KM3 exhibited clonogenicity in 50% and 40% of attempts respectively, but colonies demonstrated greater cellular disaggregation. Cloning was demonstrated in only one out of five attempts for Daudi and on no occasion for Nalm 16 (n=3). Of the T-ALL lines investigated, JM cloned on each occasion and consistently demonstrated colonies with the least disaggregation, as opposed to either MOLT 4 and GH1, whose colonies disaggregated to such an extent that counting proved inaccurate based on repeated measurements (Figure 5.1). Nalm 6 and JM were thus selected for subsequent cell survival experiments. For both lines, linearity of cloning was repeatedly observed when plating between one and 5000 cells per tube, and CFEs obtained of between 32 and 67% for Nalm 6 (Figure 5.2) and between 46 and 60% for JM. This allowed a two to three log kill to be demonstrated in subsequent experiments from 2×10^3 plated cells.

(b) Variables associated with cloning.

(i) Mycoplasma infection.

Sub-optimal cloning of Nalm 6 in terms of CFE and colony morphology was intermittently demonstrated. This was found to be due to mycoplasma contamination. Mycoplasma-free cells (Courtesy of Dr F Katz, Institute of Child Health, London) were recovered from liquid nitrogen at approximately four weekly intervals for use in subsequent cell survival experiments.

Figure 5.1

Photomicrographs of T-ALL colonies in soft agar.

T-ALL cell lines, JM and MOLT 4 were plated in a modified Courtenay assay. Colonies were photographed using a Zeiss Axiovert 10™ inverted microscope.

A = JM.

B = MOLT 4. Marked disaggregation of colonies is observed.

Figure 5.2

Cloning efficiency of Nalm 6 in soft agar.

Groups of six cultures containing between one and 5000 untreated Nalm 6 cells, were plated in a modified Courtenay assay. The mean number of colonies observed is plotted against plated cell number. Regression analysis by the method of least squares reveals a mean colony forming efficiency of 32% (R^2 = 0.998). Data was representative of a total of four experiments. Error bars represent +/- 2 SD.

Figure 5.1

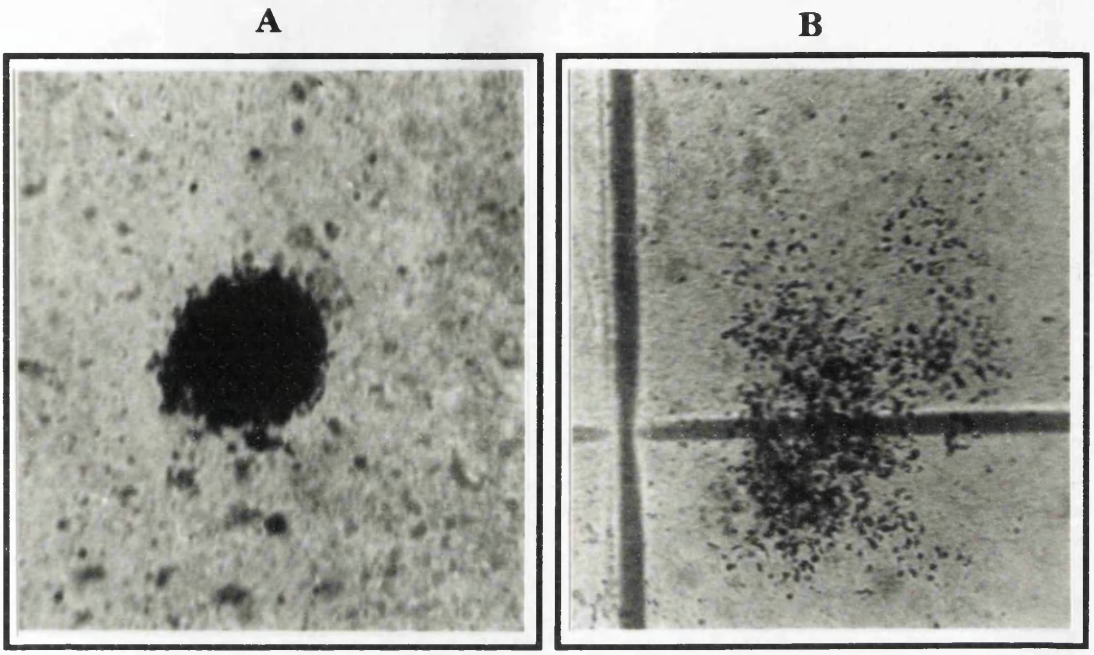

Figure 5.2

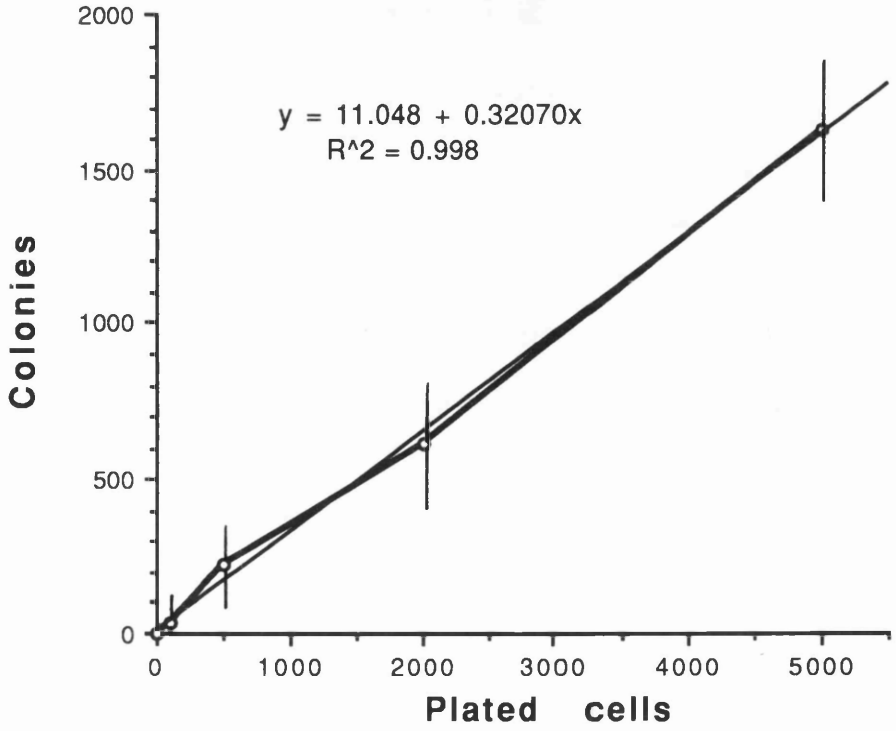

Following adoption of this policy, cloning of Nalm 6 became markedly more reliable.

(ii) Cloning medium.

All colonies formed in agar demonstrated some degree of disaggregation. To investigate whether an alternative matrix would affect colony appearance, Nalm 6 and JM cells were cloned in Agarose Noble (Difco). Colonies in this medium were often eliptical in shape, with smooth edges and very little cellular disaggregation. However, these colonies were smaller than those observed in Agar Noble, which made counting more difficult against the granular background. In a direct comparison, CFEs of 26 and 30% were obtained in Agarose Noble for Nalm 6 and JM respectively, as opposed to respective values of 51 and 60% for these cells lines cloned in agar. In view of these results, Agar Noble continued to be used as the cloning media.

3. Discussion.

Clonogenic assays form the basis for the *in-vitro* investigation of tumour radiobiology [246] and have been extensively used to study the effect on cell survival following exposure to chemotherapeutic and other cytotoxic agents. Such systems have the advantages of both reliability and reproducibility. As opposed to other methods, they examine the effect of toxic agents not only with respect to immediate cell death or metabolic injury, but also on inherited damage, which may only manifest as death of the progeny after several cell divisions, i.e. reproductive death. This loss of cellular capacity for indefinite proliferation is the most relevant criterion by which to asses cell lethality. Several studies have directly compared cell cloning with other assays for cytotoxicity (vital dye exclusion, ^{51}Cr release, protein and DNA synthesis) and have confirmed that they provide the most reliable dose-dependent index of

cell damage [247] [248]. Disadvantages include the length of time taken for colony formation, and technical difficulties, particularly the time-intensive nature of colony counting.

A clonogenic assay is especially applicable for the *in-vitro* investigation of targeted radiotherapy of leukaemia, as opposed to bulky tumours for which a spheroid system may be more appropriate. Data from colony forming assays also offer the potential for direct comparison of cell kill induced by targeted radiotherapy with radiobiological data for leukaemic cells exposed to external beam irradiation.

The soft agar clonogenic assay of Courtenay and Mills is associated with high CFEs and offers an advantage in terms of colony counting within a small agar pellet. Hill and Whelan undertook a direct comparison of this method with either a "Conventional" assay, in which cells are plated in simple agar/complete medium mixture, or the two layer plate stem cell assay described by Hamburger and Salmon [249]. For each of six human tumour cell lines studied, use of the Courtenay assay resulted in a statistically greater CFE as compared with the other systems [250]. Modification of the Hamburger and Salmon assay by the addition of August rat blood cells and gassing with a low oxygen mixture increased the CFEs, but these did not reach the levels observed in the Courtenay assay.

Consistent with convention, a colony was defined as containing at least 50 cells, equivalent to approximately six cell divisions. Manual counting was chosen in preference to mechanical means, which are disadvantaged by high cost and inaccuracies due to edge effects and colony disaggregation (Personal communication, Mr R. Whelan, Imperial Cancer Research Fund, London).

An anticipated problem of leukaemic cell cloning was disaggregation of colonies due to the relatively low adhesive nature of these tumours. All cell lines studied exhibited this phenomenon, but variability between lines was observed. Nalm 6 and JM cloned most consistently, with least disaggregation

and highest CFEs. Counting was deemed accurate for at least 3000 colonies in each 1 ml agar pellet.

Agarose appeared to present a more restrictive medium to colony formation. Disaggregation was diminished but colony size was reduced, which resulted in difficulties with counting. Alternative media such as methylcellulose were not investigated.

When comparing treated cells with controls, it is important that the CFE should not change significantly with decreasing cell number. Linearity of cloning was repeatedly observed for both Nalm 6 and JM, for between one and 5000 plated cells.

CHAPTER 6.

IN-VITRO STUDIES OF ^{131}I TARGETED RADIATION THERAPY OF LEUKAEMIA.

1. Introduction.

The modified clonogenic assay of Courtenay and Mills was used to investigate the radiobiology of targeted radiation therapy for ALL. This model served as a means of pre-clinical evaluation of radioimmunoconjugates and to complement the clinical programme by exploring strategies to improve efficacy.

2. Methods.

(a) Radiolabelling.

Monoclonal antibodies were radiolabelled with ^{131}I (37 - 148 MBq) using the iodogen technique (Chapter 2; 5a) to a specific activity of 370 MBq/mg of protein. Radiolabelled antibody present in the Sephadex G-25™ gel filtration peak was collected and passed through a 0.22 μm Millex™ filter to ensure sterility. To accurately determine the activity concentration of the labelled product, three 1:100 dilutions were made in 6 ml PBS and three 100 μl aliquots from each dilution counted in a gamma counter.

The mean activity of the nine aliquots was determined and the activity concentration calculated for each labelled antibody. $Na^{131}I$, used as a control in cell survival experiments, was similarly treated. For each product, the free-iodine content was determined and the immunoreactive fraction (IRF) estimated using an appropriate radiobinding assay. Only those with an IRF greater than 50% and free iodine of less than 10% were used in subsequent

experiments. Conjugates were kept at 4°C and used within six hours of radiolabelling.

(b) Irradiation of cell lines.

Cell lines were harvested in exponential growth phase, washed twice in Hams F-12 complete medium and diluted to a viable cell concentration of 5×10^5/ml. This represents the median concentration of lymphoblasts present in the CSF in meningeal relapse of ALL [125]. 2 ml of cell suspension was incubated with either radiolabelled antibody solution or $Na^{131}I$ (maximum volume 500 µl) in 35 mm plastic tissue culture plates (Falcon). The plates were maintained at 37°C in a 6%CO_2/94% air incubator on a orbitally rotating R100 Luckham Rotatest™ shaker. After one to 24 hours incubation, the suspension was placed in 6 ml plastic tubes, washed three times and resuspended in 1 ml of complete medium. To account for cell proliferation during incubation, the viable cell concentration of untreated control cells was estimated by Trypan Blue exclusion and adjusted to 1×10^6/ml with complete medium. The same volume of medium was added to the treated cell suspensions. The cell bound activity in all tubes was estimated in a gamma counter. 200 µl of cell suspension, equivalent to 2×10^5 control cells, was diluted in 20 ml complete medium, mixed and 2 ml added to the stock solution of the Courtenay assay (Chapter 5; 1).

(c) Statistical analysis.

Between four and six replicate cultures of treated cells, and between eight and 12 of untreated controls were included in each experiment. The per cent surviving cells of each replicate culture was calculated as:

$$\text{Percent surviving cells} = \frac{\text{Number of colonies in "test" culture}}{\text{Mean number of colonies in control cultures}} \times 100$$

In the initial series of experiments, variation in cell survival were calculated as the Standard Error (SE). For subsequent experiments, in which cells were incubated in tubes (including the comparison of plate and tube methods of incubation), statistical analysis was performed by Dr B De Stavola (Medical Statistics Laboratory, Imperial Cancer Research Fund, London). A logistic model [251] was used to analyse the relationship between the percentage of surviving cells and the amount of incubated radioactivity or, where applicable, time of incubation. Estimate survival curves were subsequently computed and plotted against activity or time on a semi-log scale. 95% confidence bands were computed on the basis of the variances of the parameters in the logistic model. It is of note, that using this method, confidence limits are not symmetrical. The statistical computer package STATA™ was used on an IBM compatible computer for the computations and the plots constructed using Cricket Graph™ software on an Apple Macintosh II™ computer.

3. Results.

(a) Determination of the optimum number of washes to remove unbound activity.

4 MBq of the specific antibody conjugate, ^{131}I-HD37, was incubated with Nalm 6 cells for 24 hours. The activity (cpm) of the cell pellet was determined after initial centrifugation and after eight subsequent washes (Table 6.1).

Table 6.1 Variation of cell bound activity of Nalm 6 with number of washes following incubation with 4 MBq ^{131}I-HD37.

Number of Washes	Cell Bound Activity (cpm)
0	3,040,040
1	335,519
2	99,300
3	68,554
4	63,516
5	56,210
6	54,232
7	52,032
8	57,544

From this data, three washes were considered sufficient to remove unbound activity. This policy was thus maintained for all cell survival experiments.

(b) Survival of ALL cell lines incubated in plates with ^{131}I-labelled monoclonal antibodies.

Initially, the effect of incubating cells with ^{131}I-labelled antibodies for different times was determined. 1 MBq ^{131}I-HD37 was incubated with Nalm 6

for between two and 24 hours (n=2), and ^{131}I-WT1 with JM for between one and 24 hours (n=2). Cell survival associated with specific conjugates was compared with that for the same activity of a ^{131}I-labelled irrelevant monoclonal antibody, UJ13A (IgG_{2a}, anti-NCAM) [252] or $Na^{131}I$. This activity was chosen as it corresponds to 5% of an injected activity of 1480 MBq in patients, assuming a CSF volume of 150 ml. In previous clinical studies, this approximated to the beginning of the second phase of the biexponential clearance of radioisotope from the CSF [67] [253].

For Nalm 6 incubations, the survival curves were exponential with specific conjugates demonstrating biphasic configuration with an increased gradient between eight and 24 hours incubation (Figure 6.1). Following 24 hours incubation, a significantly ($p < 0.05$) lower cell survival of 22.9% was observed for Nalm 6 incubated with ^{131}I-HD37, as compared with 52.0 and 56.3% for ^{131}I-UJ13A and $Na^{131}I$ respectively (Table 6.2). A difference in cell survival was not observed between specific and control reagents for an eight hour incubation period.

Table 6.2 Time response survival data for cell line Nalm 6 incubated in plates with 1 MBq ^{131}I-labelled antibodies.

Time of Incubation (hours)	*Cell Survival % (SEM)		
	Conjugate		
	^{131}I-HD37	^{131}I-UJ13A	$Na^{131}I$
2	89.0 (4.7)	-	-
4	70.1 (6.7)	-	-
8	69.9 (6.0)	74.1 (13.6)	86.1 (13.1)
24	22.9 (6.4)	52.0 (3.9)	56.3 (4.5)

* Data is the mean cell survival from two experiments, each consisting of four cultures per time point.

Figure 6.1

Time response of cell survival for Nalm 6 incubated with ^{131}I-labelled antibodies.

1 x 10^6 Nalm 6 cells, in 2 mls complete medium, were incubated for between 2 and 24 hours with 1 MBq of ^{131}I-labelled antibodies. Cell survival was calculated by comparing the number of colonies in each of six replicate tubes with that of the mean of untreated controls. Survival curves were plotted from the mean cell survival of two experiments. For clarity, confidence limits are excluded (see Table 6.2).

Figure 6.1

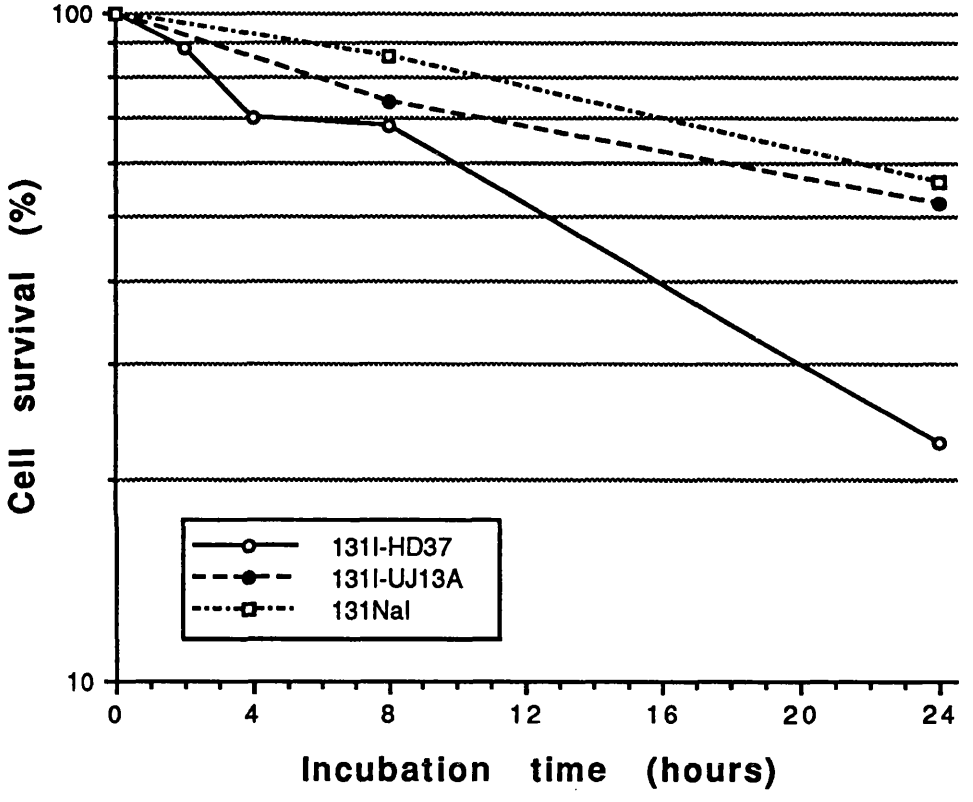
100
10
Cell survival (%)
0
4
8
12
16
20
24
Incubation time (hours)
131I-HD37
131I-UJ13A
131NaI

Similarly shaped cell survival curves were noted after incubation of JM with 1 MBq of ^{131}I-WT1 and control reagents (n=2) (Figure 6.2). Survival data was similar to that of the Nalm 6 experiment, with a cell survival at 24 hours of 21.1% for ^{131}I-WT1 treated cells, again significantly lower ($p < 0.05$) than that for control reagents.

Table 6.3 Time response survival data for cell line JM incubated in plates with ^{131}I-labelled antibodies.

Activity (MBq)	Conjugate	*Cell Survival % (SEM) Time of Incubation (hours)				
		1	2	4	8	24
1	^{131}I-WT1	96.7 (0.5)	79.0 (6.1)	77.5 (4.0)	70.4 (4.6)	21.1 (3.0)
	^{131}I-UJ13A	93.6 (2.9)	-	-	86.2 (8.3)	50.5 (8.4)
	Na^{131}I	89.2 (3.3)	-	-	80.2 (6.5)	49.1 (4.9)
2	^{131}I-WT1	-	-	43.9 (4.4)	36.4 (2.2)	4.54 (0.27)
	^{131}I-UJ13A	-	-	72.0 (10.1)	49.1 (5.0)	14.2 (0.6)
	Na^{131}I	-	-	-	38.0 (3.6)	13.5 (0.5)
4	^{131}I-WT1	-	-	32.8 (1.9)	26.7 (2.6)	1.00 (0.12)
	^{131}I-UJ13A	-	-	51.8 (5.0)	35.2 (4.0)	2.77 (0.19)
	Na^{131}I	-	-	43.3 (3.3)	32.1 (5.3)	3.21 (0.23)

* Data is the mean cell survival of two experiments, each consisting of four cultures per time point.

Further time response experiments were performed using increased activities of 2 and 4 MBq of both ^{131}I-WT1 and controls, incubated with JM for between four and 24 hours (n=2) (Table 6.3). At both activities, survival curves were approximately monoexponential, with the biphasic configuration for control reagents less obvious (Figure 6.2). After 24 hours incubation of JM

Figure 6.2

Time response of cell survival of JM incubated with ^{131}I-labelled antibodies.

1 x 10^6 JM cells were incubated for between 1 and 24 hours with 1, 2 or 4 MBq ^{131}I-labelled antibodies. Cell survival (see Figure 6.1) is plotted against time of incubation (n=2). For clarity confidence limits are excluded (see Table 6.3).

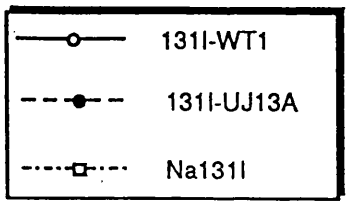

Figure 6.2

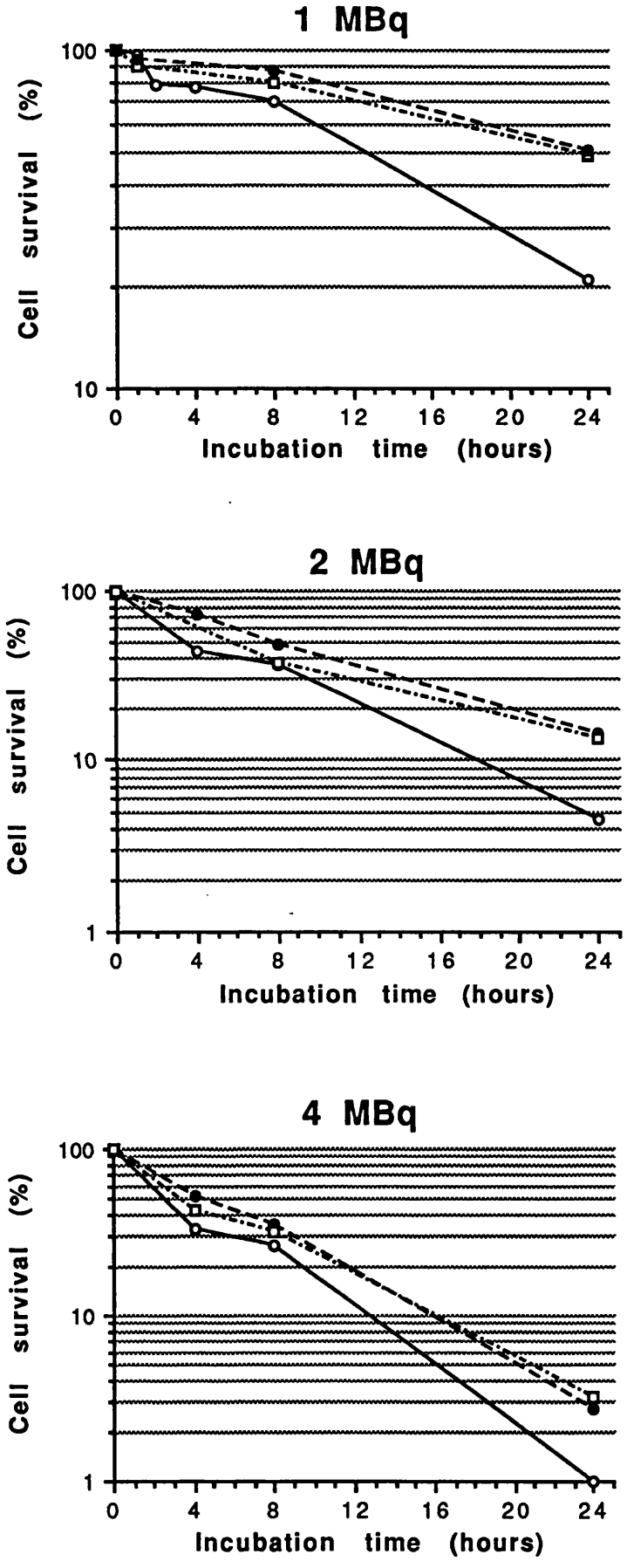
1 MBq
Cell survival (%)
100
10
0
4
8
12
16
20
24
Incubation time (hours)
2 MBq
Cell survival (%)
100
10
1
0
4
8
12
16
20
24
Incubation time (hours)
4 MBq
Cell survival (%)
100
10
1
0
4
8
12
16
20
24
Incubation time (hours)

with both 2 and 4 MBq ^{131}I-WT1, significantly lower ($p < 0.05$) cell survivals of 4.54 and 1.00% respectively were observed, as compared with control reagents.

The data from these experiments was used to construct activity response curves for a treatment time of 24 hours (Figure 6.3). These curves were approximately monoexponential for all three reagents.

These experiments demonstrate a clear advantage in terms of cell kill for specific radioconjugates incubated with target cells for 24 hours, as compared with control reagents. A possible explanation for this phenomenon lay in the method of incubation of cells with radiolabelled antibodies. Due to the orbital rotatory action of the plate shaker, cells amass in the centre of the plate. In addition, under microscopy, numerous cell clumps, many of greater than 10 cell diameters, were observed, although this was not quantified accurately. Such artificially induced cell aggregation may theoretically increase cell kill from bound radionuclide as a result of a crossfire effect of β-particles "hitting" a greater number of adjacent cells than would be found in a homogeneous single cell suspension.

An alternative system was thus developed by which cells were incubated in 6 ml plastic tubes (Falcon) rotating about their long axis on a Luckham Multimix Major™ tube roller, and angled at 20° to prevent the suspension coming in contact with the tube cap. The *in-vitro* assay was otherwise identical to that described for plate incubation. As expected from the mechanism of tube rotation, macroscopically homogeneous cell suspensions of both JM and Nalm 6 cell lines were repeatedly observed.

(c) Comparison of plate and tube methods of incubation, in respect of cell kill from ^{131}I-labelled antibodies.

To determine whether the method of incubation of cells with radioconjugates affects cell survival, JM cells were incubated for 24 hours with

Figure 6.3

Activity response of cell survival for JM incubated with ^{131}I-labelled antibodies.

Cell survival (see Figure 6.1) of JM following incubation for 24 hours is plotted against activity of ^{131}I-labelled antibodies. For clarity, confidence limits are excluded (see Table 6.3)

Figure 6.3

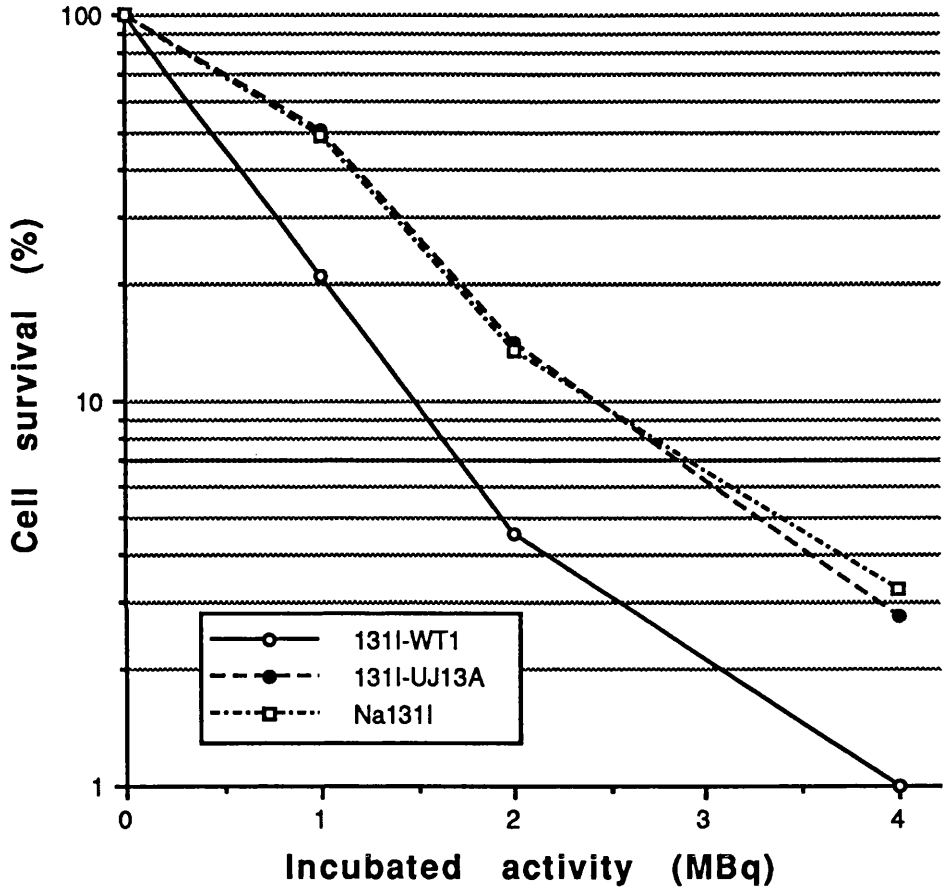
100
10
1
Cell survival (%)
0
1
2
3
4
Incubated activity (MBq)
131I-WT1
131I-UJ13A
Na131I

between 1 and 4 MBq ^{131}I-WT1, ^{131}I-UJ13A and Na^{131}I in either plates or tubes (n=1). Cell survival data was analysed using a logistic model.

Table 6.4 Cell survival data for cell line JM incubated with ^{131}I-labelled antibodies. Comparison of plate and tube methods of incubation.

Method of Incubation	Conjugate	Cell Survival (%) Incubated Activity (MBq)		
		1	2	4
Plate	^{131}I-WT1	[+3.38] *19.13 [-2.98]	[+1.07] 4.96 [-0.88]	[+0.26] 1.14 [-0.21]
	^{131}I-UJ13A	[+3.43] 33.48 [-3.27]	[+2.39] 15.32 [-2.12]	[+0.46] 2.93 [-0.40]
	Na^{131}I	[+3.53] 39.06 [-3.42]	[+1.67] 12.31 [-1.49]	[+0.67] 3.79 [-0.57]
Tube	^{131}I-WT1	[+3.16] 24.9 [-2.91]	[+1.84] 12.18 [-1.63]	[+0.75] 4.51 [-0.65]
	^{131}I-UJ13A	[+6.21] 61.0 [-6.59]	[+7.25] 33.37 [-6.54]	[+3.49] 13.55 [-2.87]
	Na^{131}I	[+4.22] 49.87 [-4.21]	[+3.64] 29.69 [-3.40]	[+1.38] 8.33 [-1.20]

* Data is the mean cell survival of six cultures per activity level. Figures in parentheses give upper and lower 95% confidence limits.

Apart from one instance (1 MBq ^{131}I-WT1), survival was significantly lower ($p < 0.05$) for cells incubated in plates as compared with tubes (Table 6.4, Figure 6.4).

Figure 6.4

Comparison of cell survival for plate and tube methods of incubation.

1×10^6 JM cells were incubated in either 35 mm tissue culture plates or 6 ml tubes, with between 1 and 4 MBq ^{131}I-labelled antibodies (n=1). Cell survival (see Figure 6.1) is plotted against activity of incubation. For clarity, confidence limits are excluded (see Table 6.4).

Figure 6.4

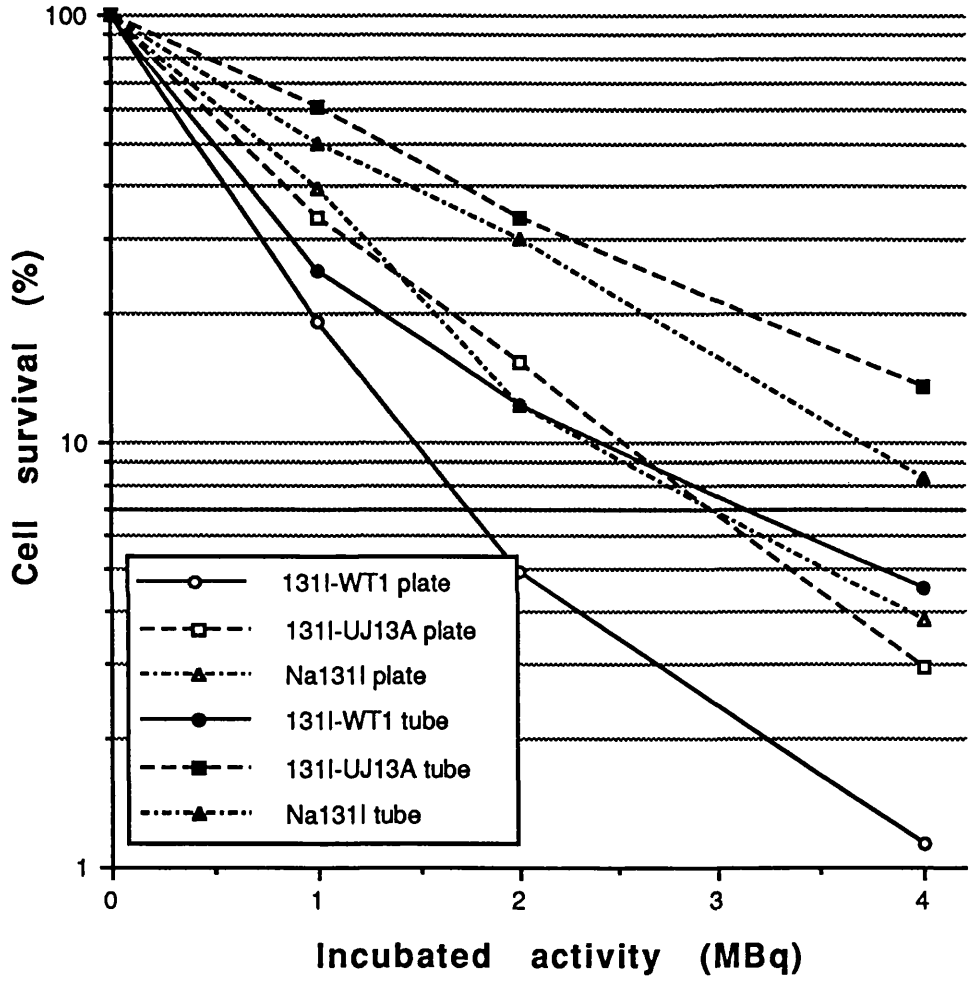
100
10
1
Cell survival (%)
0
1
2
3
4
Incubated activity (MBq)
131I-WT1 plate
131I-UJ13A plate
Na131I plate
131I-WT1 tube
131I-UJ13A tube
Na131I tube

For each incubated activity of each reagent, an "advantage in cell kill" of plate versus tube incubations was calculated by dividing the mean cell survival following incubation in tubes by that for cells incubated in plates (Table 6.5).

Table 6.5 Advantage in cell kill of plate versus tube methods of incubation of JM with ^{131}I-labelled antibodies.

Conjugate	Incubated Activity (MBq)					
	1		2		4	
^{131}I-WT1	*1.30	[0.14]	2.46	[0.33]	3.96	[0.51]
^{131}I-UJ13A	1.80	[0.18]	2.18	[0.12]	4.62	[0.42]
Na^{131}I	1.28	[0.08]	2.41	[0.21]	2.20	[0.21]

* Mean cell survival following incubation in tubes is divided by that for cells incubated in plates (Table 6.4). Figures in parentheses represent the approximate standard error of the ratio.

In this single experiment, the conditions established in the plate system appear to result in a similar increase in cell kill for both specific and control agents. This was unexpected, as the "advantage in cell kill" for plate incubations would have been expected to be greater for the specific conjugate. However, to obtain a more accurate analysis of the cytotoxicity of targeted radiation therapy against a homogeneous cell suspension, the tube method of incubation was used in subsequent experiments.

(d) Aggregation of cells incubated in rotating tubes.

To confirm that cell lines incubated in rotating tubes did not exhibit significant aggregation, untreated JM and Nalm 6 cells were incubated using conditions employed in cell survival experiments. After 24 hours, the cell suspension was gently decanted into the base of a 6 cm tissue culture dish marked with a 2 mm grid. The number of cells in each aggregate (including

Figure 6.5

Aggregation of JM and Nalm 6 cell lines incubated in roller tubes.

Either JM or Nalm 6 were incubated in roller tubes for 24 hours. The number of cells in each aggregate (including single cells) is plotted against the total number of aggregates counted. Three tube counts (A-C) were performed for each of three separate incubations (1-3).

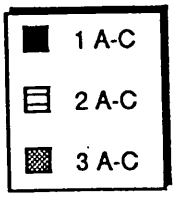

Figure 6.5

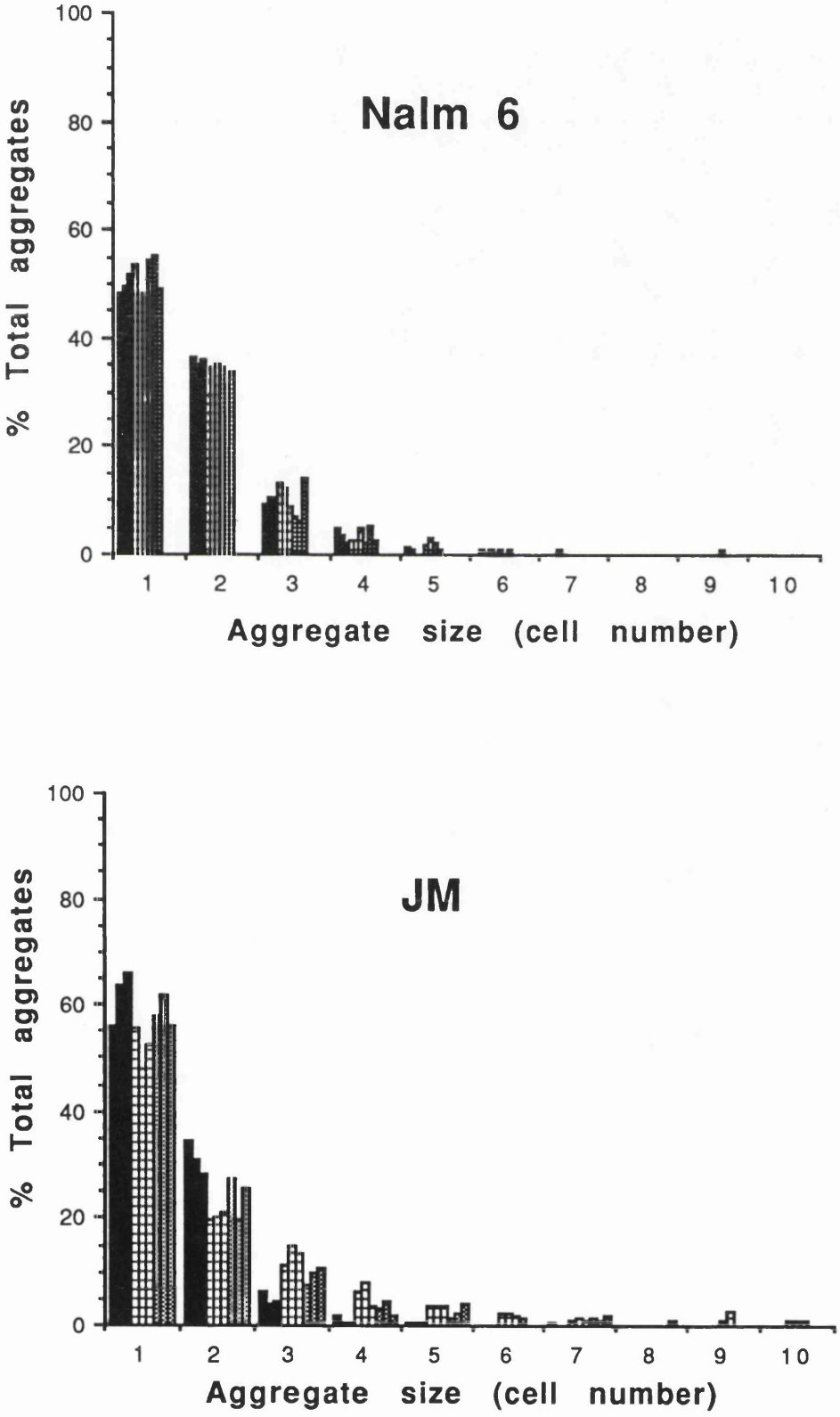
Nalm 6
% Total aggregates
100
80
60
40
20
0
1
2
3
4
5
6
7
8
9
10
Aggregate size (cell number)
JM
% Total aggregates
100
80
60
40
20
0
1
2
3
4
5
6
7
8
9
10
Aggregate size (cell number)

single cells) was counted and expressed as a percentage of the total number of aggregates counted (100 - 200 per tube). Three tubes were examined for each of three separate incubations. In addition, for each incubation, cells from one tube were counted to determine cell proliferation, the proportion of viable cells being determined by Trypan Blue exclusion.

For Nalm 6, a mean of 50.8% of groups counted were single cells, and 33.9%, doublets (Figure 6.5). A slightly higher proportion of JM groups were single cells, 57.6%, with less as doublets; 25.3%. Overall, of the total cell groups counted, only 17.1% and 14.5% consisted of aggregates of three cells or more for Nalm 6 and JM respectively.

At 24 hours, the population of JM cells had increased from an initial 1×10^6 to between 1.2 and 2.0×10^6 (mean 1.6×10^6), and of Nalm 6 to between 1.55 and 1.65×10^6 (mean 1.6×10^6). Greater than 95% of cells were viable in every case.

(e) Survival of ALL cell lines incubated in tubes with ^{131}I-labelled monoclonal antibodies.

(i) Time response experiments.

Time response data was generated for Nalm 6 cells incubated in tubes for between two and 24 hours. Cell survival following incubation with either 1 or 2 MBq of specific conjugates, ^{131}I-HD37 or ^{131}I-WCMH, was again compared to that with either ^{131}I-UJ13A or Na^{131}I (n=1) (Table 6.6; Figure 6.6).

In contrast to the plate incubation experiments, curves for 1 MBq of specific radiolabelled antibodies demonstrated a decreased gradient between time points of eight and 24 hours. All other cell survival curves were approximately monophasic.

Figure 6.6

Time response of cell survival for Nalm 6 incubated in roller tubes with ^{131}I-labelled antibodies.

1 x 10^6 Nalm 6 cells were incubated in roller tubes for between 2 and 24 hours, with either 1 or 2 MBq ^{131}I-labelled antibodies (n=1). Cell survival (see Figure 6.1) is plotted against time of incubation. For clarity, confidence limits are excluded (see Table 6.6).

Figure 6.6

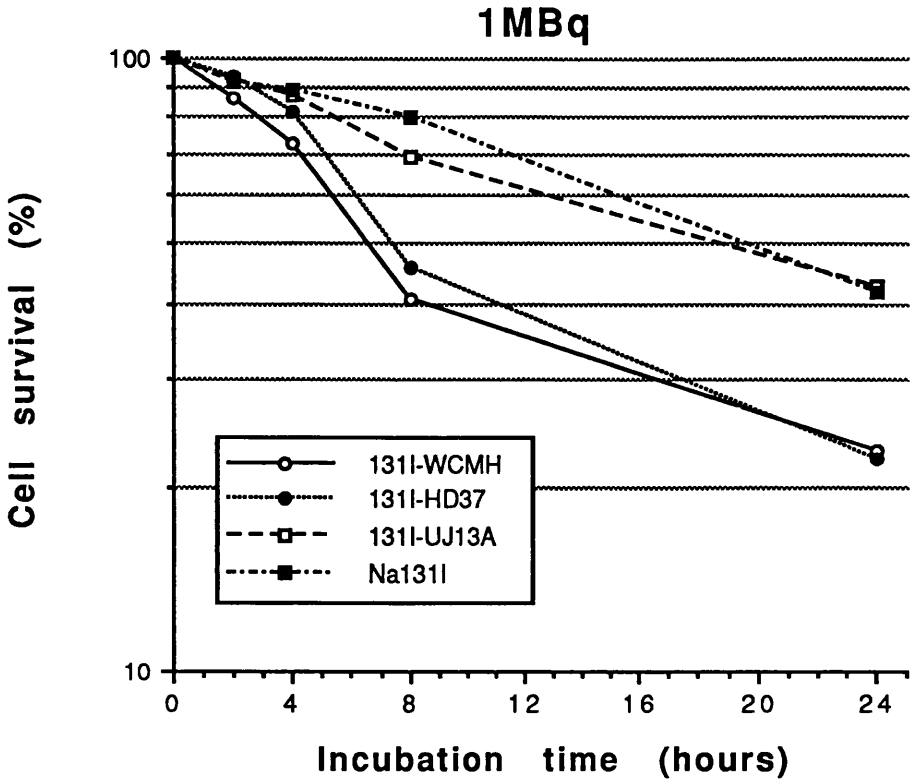
1MBq
100
10
Cell survival (%)
0
4
8
12
16
20
24
Incubation time (hours)
131I-WCMH
131I-HD37
131I-UJ13A
Na131I

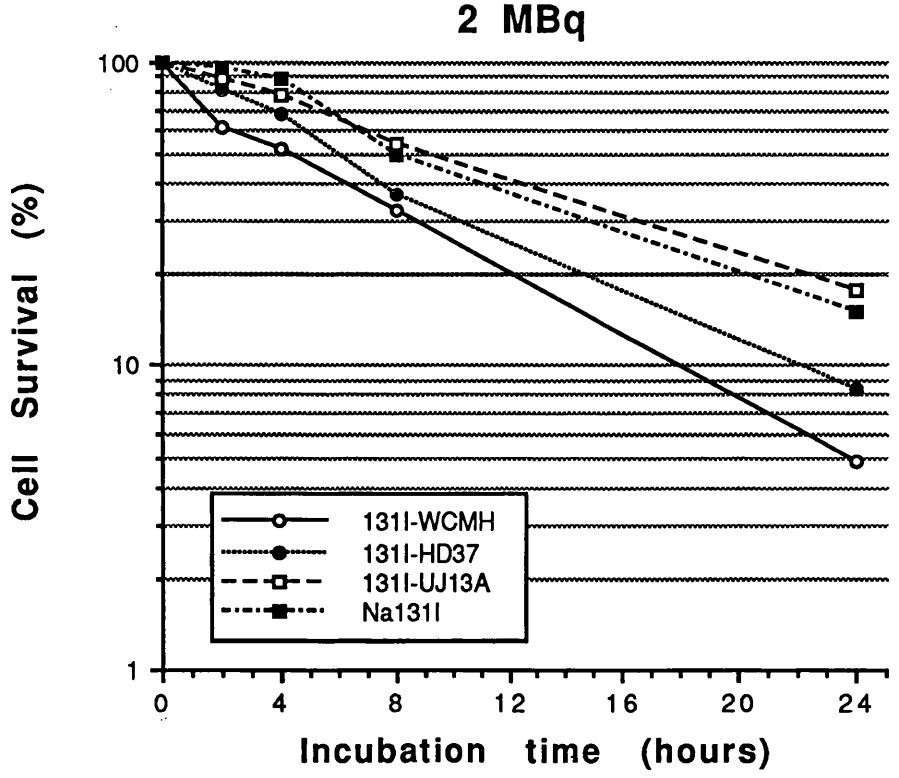
2 MBq
100
10
1
Cell Survival (%)
0
4
8
12
16
20
24
Incubation time (hours)
131I-WCMH
131I-HD37
131I-UJ13A
Na131I

Table 6.6 Time response survival data for Nalm 6 incubated in tubes with ^{131}I-labelled monoclonal antibodies.

Activity (MBq)	Conjugate	Cell Survival (%) Time of Incubation (hours)			
		2	4	8	24
1	^{131}I-WCMH	*85.7 [+6.1] [-4.5]	72.3 [+5.5] [-6.2]	40.7 [+11.5] [-10.6]	22.9 [+9.8] [-7.2]
	^{131}I-HD37	92.9 [+3.1] [-5.3]	82.1 [+5.4] [-7.0]	45.9 [+16.4] [-15.5]	22.2 [+14.5] [-9.9]
	^{131}I-UJ13A	92.4 [+3.3] [-5.5]	86.5 [+3.8] [-5.0]	69.4 [+9.8] [-12.0]	42.8 [+11.5] [-10.6]
	Na^{131}I	91.6 [+2.5] [-3.5]	88.5 [+2.4] [-2.8]	80.2 [+5.9] [-7.6]	42.0 [+9.7] [-9.2]
2	^{131}I-WCMH	62.0 [+3.5] [-3.5]	51.7 [+2.5] [-2.5]	32.9 [+3.7] [-3.4]	4.9 [+0.9] [-0.7]
	^{131}I-HD37	81.6 [+4.8] [-6.0]	67.6 [+5.1] [-5.5]	37.0 [+9.4] [-8.5]	8.4 [+3.8] [-2.7]
	^{131}I-UJ13A	88.5 [+3.3] [-4.6]	79.2 [+3.9] [-4.7]	54.0 [+10.0] [-10.3]	17.9 [+7.4] [-5.6]
	Na^{131}I	96.1 [+2.6] [-7.2]	87.9 [+5.8] [-9.8]	50.0 [+25.0] [-25.0]	15.2 [+17.8] [-9.1]

* Data is the mean cell survival of six cultures. Figures in parentheses represent upper and lower 95% confidence limits.

Incubation of cells with 1 MBq ^{131}I-WCMH for four, eight and 24 hours was associated with a significantly decreased ($p < 0.05$) cell survival as compared to that with both ^{131}I-UJ13A and Na^{131}I. Probably as a result of the large variance in cell survival for this single experiment, a significantly

decreased survival was only observed for 1 MBq ^{131}I-HD37 when compared with Na^{131}I after eight hours incubation. After 24 hours incubation, survivals of 22.9 and 22.2% were observed for ^{131}I-WCMH and ^{131}I-HD37 respectively, and 42.8 and 42.0% for ^{131}I-UJ13A and Na^{131}I respectively.

Incubation of cells with 2 MBq ^{131}I-WCMH showed a significantly ($p < 0.05$) lower cell survival at all time points when compared to that with both ^{131}I-UJ13A and Na^{131}I. Survival of cells treated with 2 MBq ^{131}I-HD37 was significantly lower ($p < 0.05$) when compared with ^{131}I-UJ13A at 4 and 24 hours and with Na^{131}I at eight and 24 hours. For 24 hour incubations, cell survivals of 4.9 and 8.4% were observed for ^{131}I-WCMH and ^{131}I-HD37 respectively, and 17.9 and 15.2% for ^{131}I-UJ13A and Na^{131}I respectively. In this experiment, the difference in survival of cells incubated with either ^{131}I-WCMH or ^{131}I-HD37 was significant at the 5% level.

(ii) Activity response experiments.

A further series of experiments were performed to determine cell survival following incubation with increasing amounts of ^{131}I-labelled monoclonal antibodies. All incubations were performed in tubes for a period of 24 hours. Both targeting of Nalm 6 and JM cells was investigated.

(iia) ^{131}I targeting of Nalm 6.

Between 1 and 4 MBq of either ^{131}I-WCMH or ^{131}I-HD37 was incubated with Nalm 6 cells as described above, and cell survival data compared with that following treatment with control reagents, ^{131}I-UJ13A and Na^{131}I (n=6) (Table 6.7). A plot of mean cell survival is depicted in Figure 6.7, and to aid visualisation of confidence limits, 1 x 1 comparisons of all four reagents are shown in Figure 6.8.

Figure 6.7

Activity response of cell survival for Nalm 6 incubated in roller tubes with ^{131}I-labelled antibodies.

1 x 10^6 Nalm 6 cells were incubated in roller tubes for 24 hours, with between 1 and 4 MBq ^{131}I-labelled antibodies (n=6). Mean cell survival (see Figure 6.1) is plotted against activity of incubation. For clarity, confidence bands are excluded (see Figure 6.8, Table 6.7).

Figure 6.7

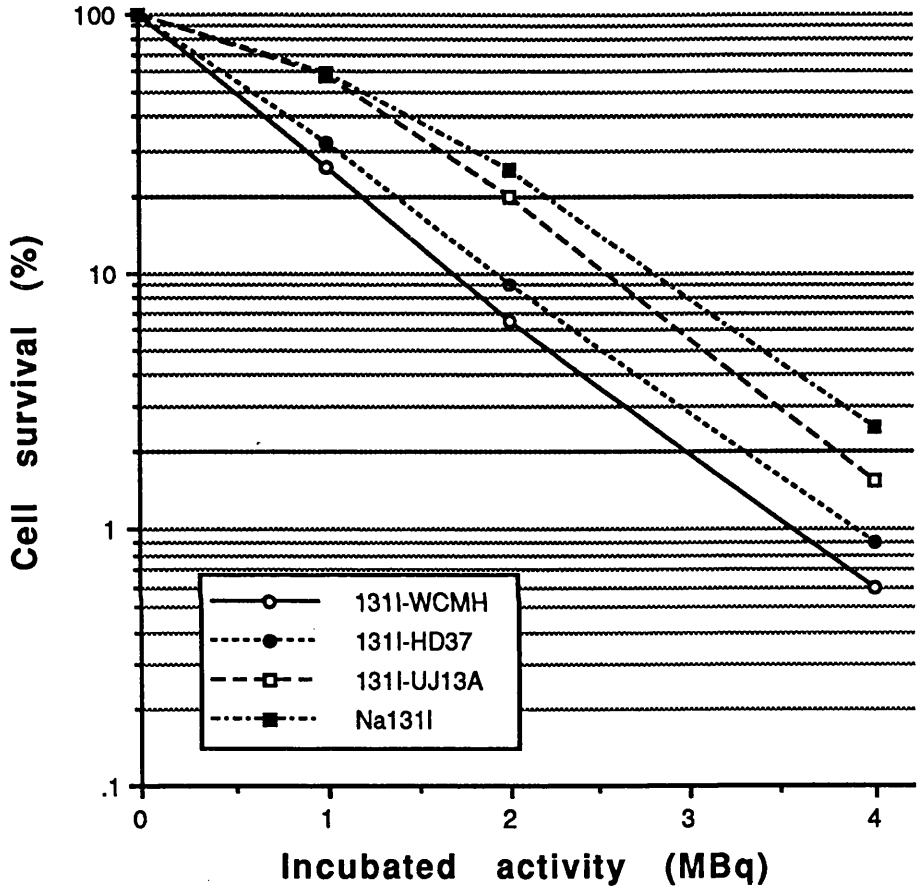
100
10
1
.1
Cell survival (%)
0
1
2
3
4
Incubated activity (MBq)
131I-WCMH
131I-HD37
131I-UJ13A
Na131I

Figure 6.8

Activity response cell survival for *in-vitro* targeting of Nalm 6. 1 x 1 comparisons of ^{131}I-labelled antibodies (data from Table 6.7).

_____ Mean cell survival

---------- 95% confidence limits

A = ^{131}I-WCMH v ^{131}I-HD37

B = ^{131}I-WCMH v ^{131}I-UJ13A

C = ^{131}I-WCMH v Na^{131}I

D = ^{131}I-HD37 v ^{131}I-UJ13A

E = ^{131}I-HD37 v Na^{131}I

F = ^{131}I-UJ13A v Na^{131}I

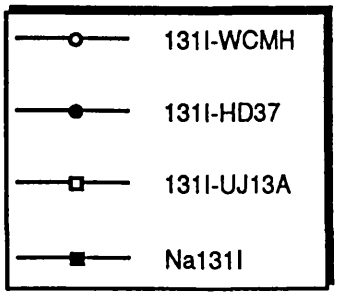

Figure 6.8

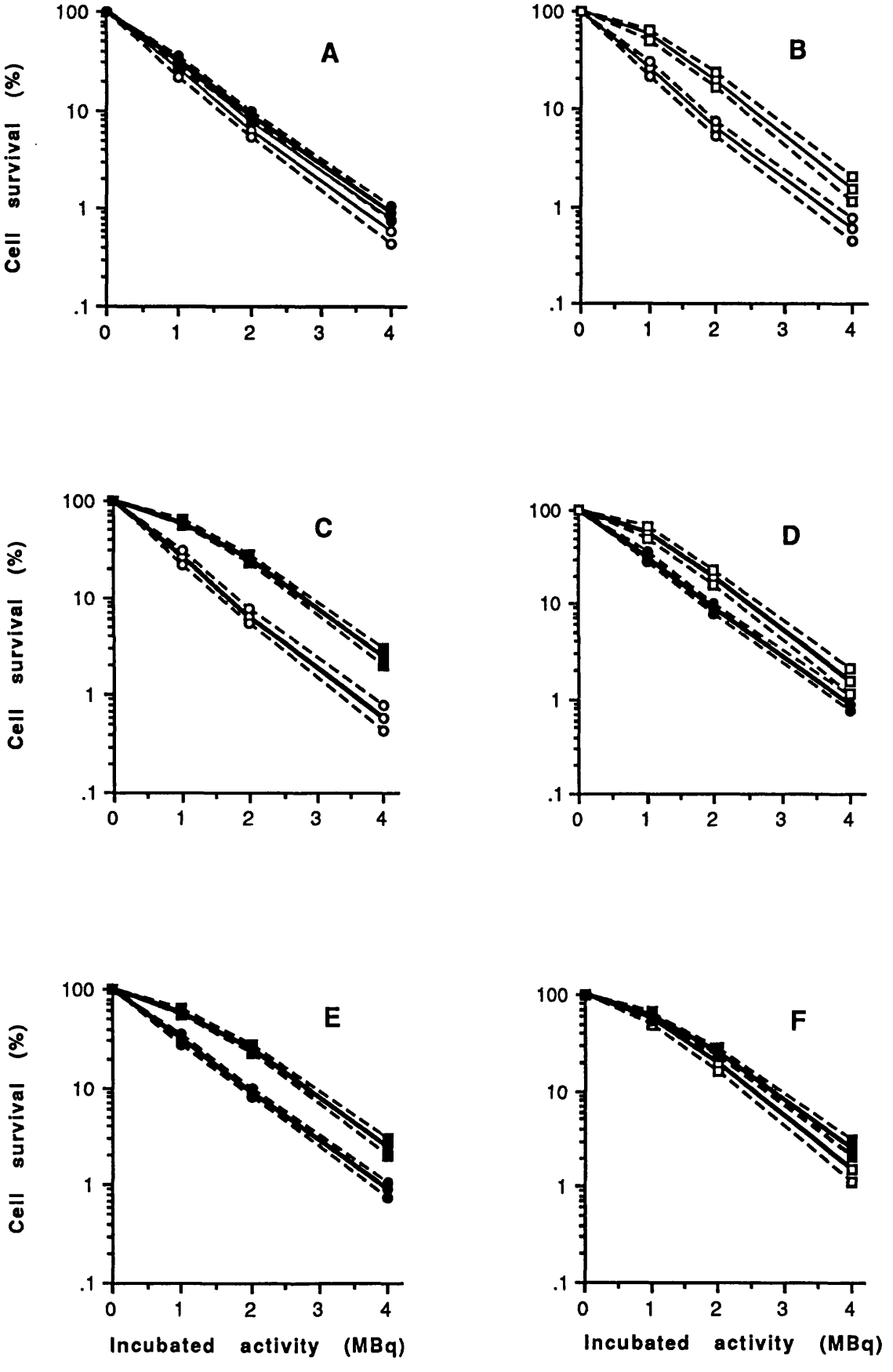
A
B
C
D
E
F
Cell survival (%)
100
10
1
.1
0
1
2
3
4
Incubated activity (MBq)

Table 6.7 Activity response survival data for Nalm 6 incubated with ^{131}I-labelled antibodies.

Conjugate	Cell Survival (%) Incubated Activity (MBq)		
	1	2	4
^{131}I-WCMH	*25.86 [+5.23] [-4.62]	6.45 [+1.19] [-1.02]	0.59 [+0.19] [-0.15]
^{131}I-HD37	31.62 [+4.02] [-3.76]	8.99 [+1.07] [-0.97]	0.90 [+0.18] [-0.15]
^{131}I-UJ13A	57.93 [+7.30] [-7.66]	19.61 [+3.56] [-3.13]	1.55 [+0.57] [-0.42]
Na^{131}I	59.56 [+4.93] [-5.13]	25.34 [+2.80] [-2.61]	2.51 [+0.56] [-0.46]

* Data is the mean of six experiments, each consisting of six cultures per activity level. Figures in parentheses represent upper and lower 95% confidence limits.

For specific ^{131}I-labelled antibodies, activity response survival curves appear monophasic. In contrast, curves for both control agents appear multiphasic with initial shallow gradients. At each activity level, a statistically significant ($p < 0.05$) increase in cell kill was observed for both ^{131}I-WCMH and ^{131}I-HD37 as compared with control reagents. Following incubation of cells with 4 MBq of conjugate, a 2.23 log kill for ^{131}I-WCMH and a 2.05 log kill for ^{131}I-HD37, was observed. For ^{131}I-UJ13A and Na^{131}I, 1.81 and 1.70 log kills were noted respectively. This constitutes a 2.63 fold increase in cell kill for ^{131}I-WCMH compared with ^{131}I-UJ13A, and a 4.24 fold increase compared with Na^{131}I. For ^{131}I-HD37, this advantage was 1.71 and 2.79 fold respectively. As demonstrated in the time response experiment (Section 6.1b), a significantly ($p < 0.05$) increased cell kill was observed for 2 MBq ^{131}I-WCMH

as compared with ^{131}I-HD37. A similar advantage for 4 MBq ^{131}I-WCMH over ^{131}I-HD37 failed to reach statistical significance ($p < 0.1$).

(iib) ^{131}I targeting of JM.

Between 1 and 4 MBq ^{131}I-WT1 was incubated with JM for 24 hours, and cell survival compared with that for control reagents (n=3) (Table 6.8, Figure 6.9). 1 x 1 comparisons of survival curves are depicted in Figure 6.10.

Table 6.8 Activity response survival data for JM incubated with ^{131}I-labelled antibodies.

Conjugate	Cell Survival (%) Incubated Activity (MBq)		
	1	2	4
^{131}I-WT1	*24.40 [+2.52] [-2.35]	9.07 [+0.77] [-0.71]	1.43 [+0.20] [-0.18]
^{131}I-UJ13A	42.63 [+2.58] [-2.54]	16.97 [+1.04] [-0.99]	2.61 [+0.30] [-2.68]
Na^{131}I	43.29 [+3.06] [-3.01]	18.27 [+1.36] [-1.29]	3.00 [+0.46] [-0.40]

* Data is the mean cell survival of three experiments, each consisting of six cultures per activity level. Figures in parentheses represent upper and lower 95% confidence limits.

In contrast to the activity response survival curves observed for Nalm 6 cells, that for JM targeted with the specific conjugate, ^{131}I-WT1, appears biphasic with an increased gradient between an activity of 0 and 1 MBq. Curves for control radiolabels appear monoexponential.

At each activity level, a significantly ($p < 0.05$) decreased survival was observed for cells incubated with ^{131}I-WT1 as compared with control agents.

Figure 6.9

Activity response of cell survival for JM incubated in roller tubes with ^{131}I-labelled antibodies.

1 x 10^6 JM cells were incubated in roller tubes for 24 hours, with between 1 and 4 MBq ^{131}I-labelled antibodies (n=3). Mean cell survival (see Figure 6.1) is plotted against activity of incubation. For clarity, confidence bands are excluded (see Figure 6.10, Table 6.8).

Figure 6.9

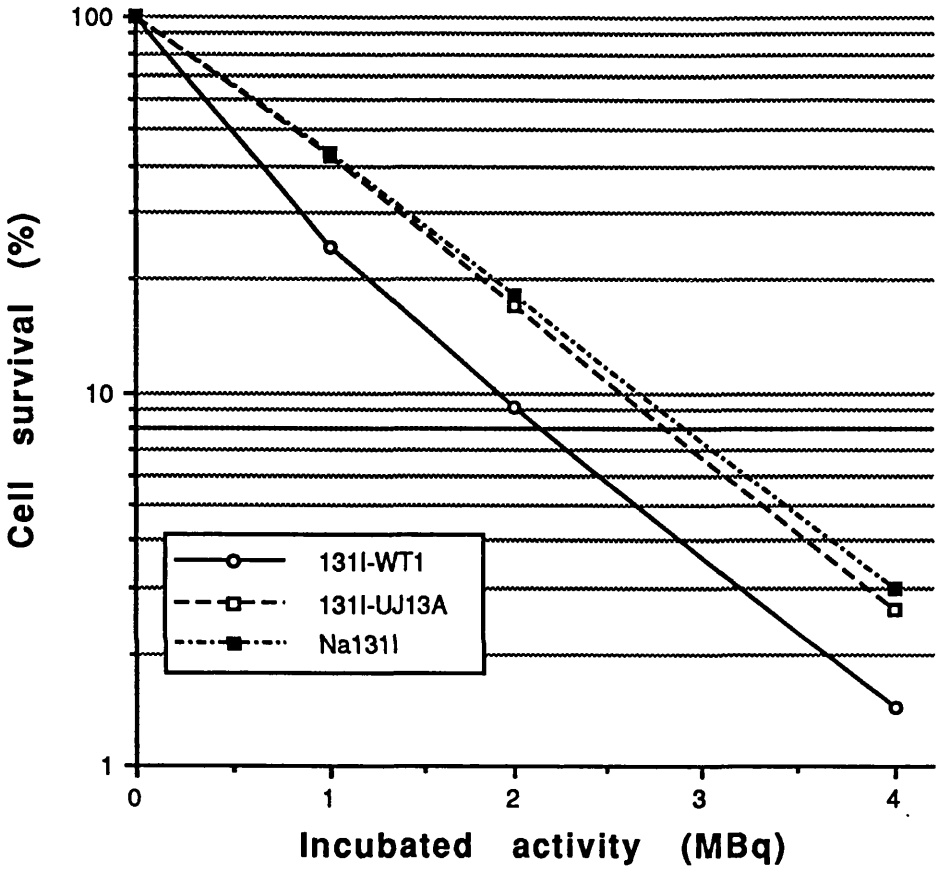
100
10
1
Cell survival (%)
0
1
2
3
4
Incubated activity (MBq)
131I-WT1
131I-UJ13A
Na131I

Figure 6.10

Activity response cell survival data for *in-vitro* targeting of JM. 1 x 1 comparisons of ^{131}I-labelled antibodies (data from Table 6.8).

———— Mean cell survival.

---------- 95% Confidence limits.

A = ^{131}I-WT1 v ^{131}I-UJ13A

B = ^{131}I-WCMH v Na^{131}I

C = ^{131}I-UJ13A v Na^{131}I

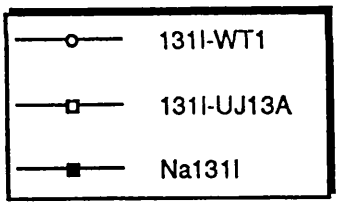

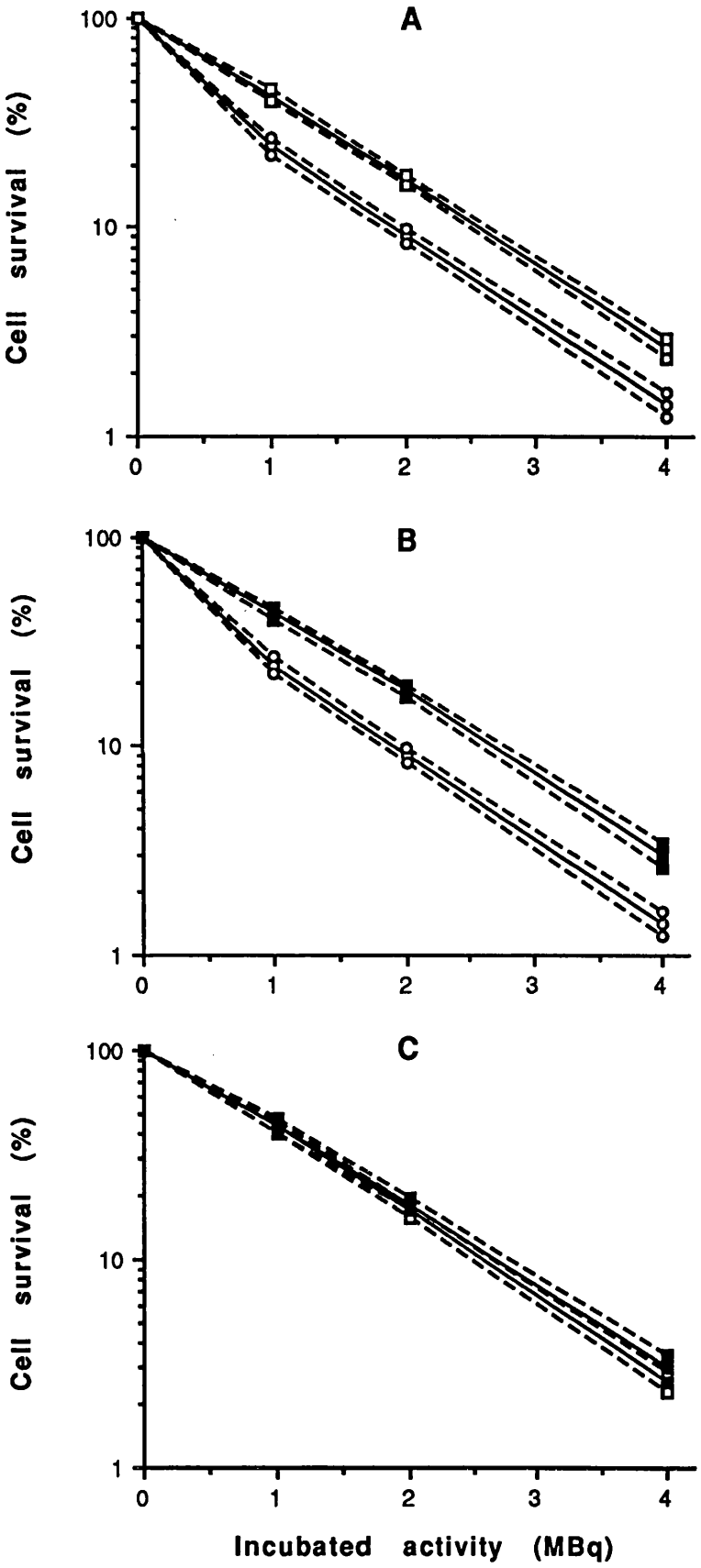
A
B
C
Cell survival (%)
100
10
1
0
1
2
3
4
Incubated activity (MBq)

No difference in cell survival between control reagents at any activity was noted. At 4 MBq, a 1.85 log kill was observed for ^{131}I-WT1, as compared with 1.53 and 1.52 log kills for ^{131}I-UJ13A and Na^{131}I respectively. This constitutes a cell kill advantage of 1.83 and 2.10 fold for ^{131}I-WT1 over ^{131}I-UJ13A and Na^{131}I respectively.

(iic) Comparison of Nalm 6 and JM survival data.

Activity response cell survival data following ^{131}I-targeting of Nalm 6 and JM was compared to explore possible differences in the sensitivity of cell lines to β-irradiation and/or the efficacy of specific conjugates.

For 24 hour incubations with 1 MBq, survival of JM incubated with ^{131}I-WT1 was similar to that of Nalm 6 targeted with ^{131}I-WCMH, but significantly less ($p < 0.05$) than for Nalm 6 incubated with ^{131}I-HD37 (Tables 6.7, 6.8). Both control reagents were associated with a significantly lower cell survival ($p < 0.05$) for JM as compared with Nalm 6. These differences between sets of experiments are reflected in the initial gradients of the cell survival curves. When comparing the advantage in cell kill (see above) for specific over control reagents at this activity (Table 6.9), that for ^{131}I-WCMH (but not ^{131}I-HD37) is significantly greater ($p < 0.05$) than the advantage for ^{131}I-WT1.

At the highest activity of 4 MBq, a significantly increased cell kill ($p < 0.05$) is observed for both ^{131}I-WCMH and ^{131}I-HD37 targeting of Nalm 6 cells as compared with ^{131}I-WT1 targeting of JM. However, the cell kill associated with both control reagents is higher for Nalm 6 than for JM incubations, for which a significant difference ($p < 0.05$) is observed for ^{131}I-UJ13A. Correspondingly, there is no significant difference in the cell kill advantage for specific versus control radiolabels between the two sets of experiments at this activity.

Table 6.9 Advantage in cell kill for specific over control ^{131}I radioconjugates incubated with ALL cell lines.

Cell Line	Specific Conjugate	Control Conjugate	Incubated Activity (MBq)		
			1	2	4
Nalm 6	^{131}I-WCMH	^{131}I-UJ13A	*2.24 [0.15]	3.04 [0.46]	2.62 [0.85]
		$Na^{131}I$	2.30 [0.17]	3.93 [0.60]	4.23 [1.16]
Nalm 6	^{131}I-HD37	^{131}I-UJ13A	1.83 [0.07]	2.18 [0.24]	1.71 [0.43]
		$Na^{131}I$	1.88 [0.11]	2.82 [0.32]	2.77 [0.53]
JM	^{131}I-WT1	^{131}I-UJ13A	1.75 [0.06]	1.87 [0.11]	1.83 [0.19]
		$Na^{131}I$	1.78 [0.06]	2.01 [0.10]	2.10 [0.24]

* The mean cell survival following incubation with control conjugate is divided by that for specific conjugate. Figures in parentheses represent the approximate standard error of the ratio. See Table 6.7 for data for Nalm 6 incubations and Table 6.8 for JM incubations.

(iid) The effect of monoclonal antibody cocktails.

In view of the advantage of using single specific ^{131}I-labelled antibodies to kill leukaemic cells in this model system, the effect of a combination of MoAbs was explored, to investigate whether a change in cell kill would result from increasing the amount of surface bound ^{131}I by targeting two different leukaemia-associated antigens. A combination of ^{131}I-WCMH and ^{131}I-HD37 was incubated with Nalm 6 cells for 24 hours, each conjugate contributing to half of the total activities of 1, 2 and 4 MBq (n=6). Activity response data (Table 6.10) was compared with that from experiments in which a single ^{131}I-labelled antibody was targeted (Table 6.7).

Table 6.10 Activity response cell survival data for Nalm 6 incubated with a cocktail of ^{131}I-labelled antibodies.

Cell Survival (%)		
Incubated Activity (MBq)		
1	2	4
[+3.11] *12.54 [-2.57]	[+1.08] 3.65 [-2.57]	[+0.13] 0.33 [-0.10]

* Data is the mean cell survival of six experiments, each consisting of six cultures per activity level. Figures in parentheses represent upper and lower 95% confidence limits.

The survival curve for ^{131}I-cocktail targeted cells was biphasic, with an initial steeper gradient (Figure 6.11). A significantly increased cell kill ($p < 0.05$) was observed for the cocktail at each activity level when compared with ^{131}I-HD37, and at 1 and 2 MBq when compared with ^{131}I-WCMH.

For an incubated activity of 4 MBq a mean of 2.67 log kill was observed for ^{131}I-cocktail as compared with a 2.23 log kill for ^{131}I-WCMH alone and a 2.05 log kill for ^{131}I-HD37 alone. This amounts to a 1.79 fold increase in cell kill over ^{131}I-WCMH alone and a 2.74 fold increase over ^{131}I-HD37 alone.

(f) The nature of the targeting effect.

Mathematical modelling suggests that antibody targeting ^{131}I to single cell suspensions should not result in a significant specific killing effect [92] [93]. Further experiments were thus designed to investigate the nature of cell kill observed in the culture system.

(i) The effect of non-radiolabelled reagents.

JM and Nalm 6 cells were incubated for 24 hours with non-radiolabelled antibody (WT1 and HD37), "cold" NaI or antibody radiolabelled with non-

Figure 6.11

Activity response of cell survival for Nalm 6 incubated with ^{131}I-cocktail.

1 x 10^6 Nalm 6 cells were incubated in roller tubes for 24 hours with between 1 and 4 MBq of a cocktail of ^{131}I-WCMH and ^{131}I-HD37. Mean cell survival, together with 95% confidence limits (See Figure 6.1) is plotted against activity of incubation (n=6) together with activity response survival curves for incubations with either ^{131}I-WCMH or ^{131}I-HD37 (See Figure 6.8).

A = ^{131}I-cocktail v ^{131}I-WCMH.

B = ^{131}I-cocktail v ^{131}I-HD37.

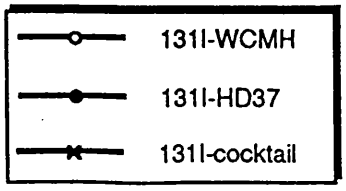

Figure 6.11

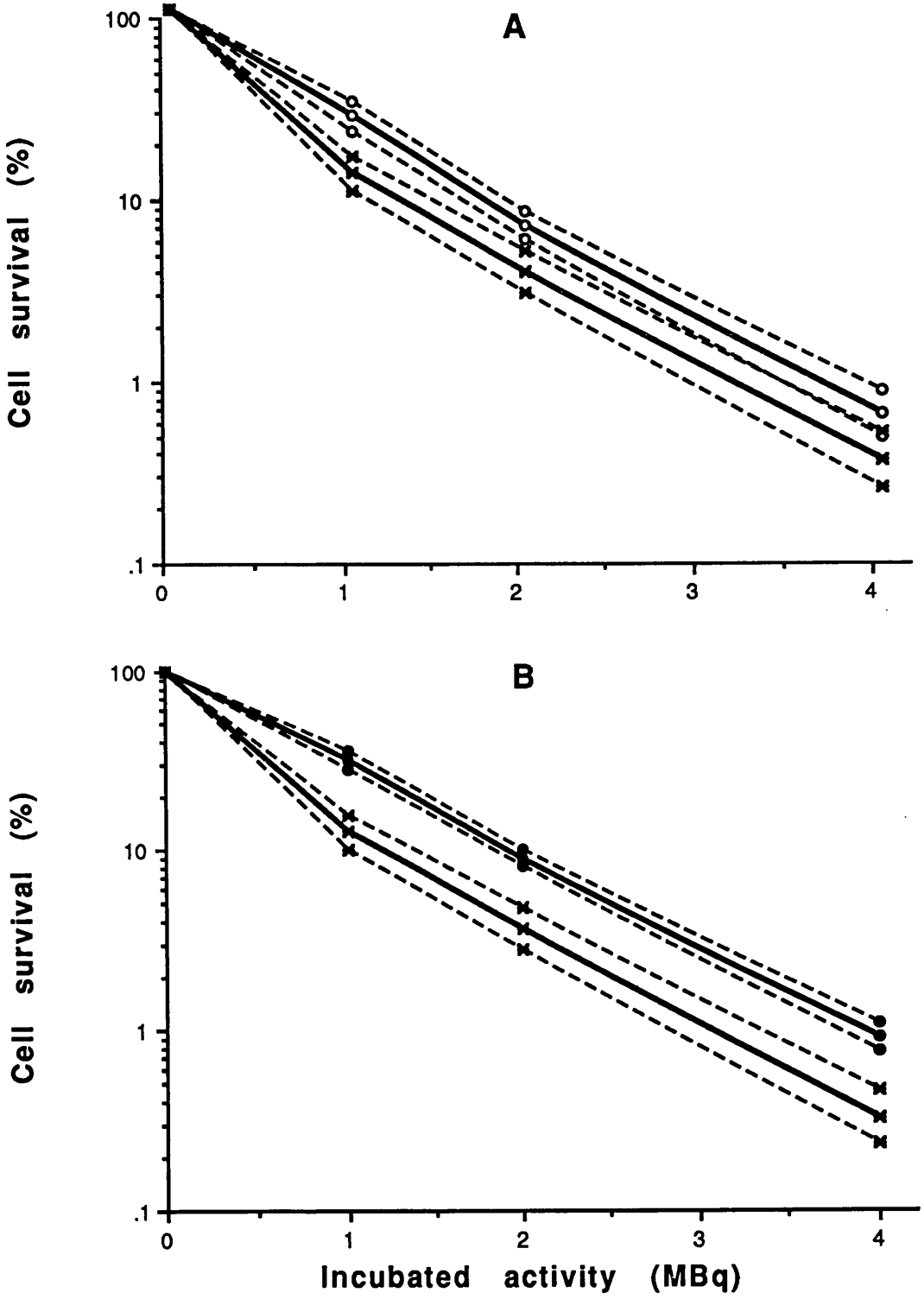

radioactive NaI, under conditions described for ^{131}I-targeting experiments. To ensure collection of the "cold-labelled" protein peak, a trace amount of $Na^{125}I$ (400 Bq) was included in the reaction procedure. Concentrations of these reagents were equivalent to 1 and 10 x those used in ^{131}I studies, assuming an incubated activity of 4 MBq, a labelling efficiency of 50% and a specific activity of $Na^{131}I$ of 740 MBq/μg (Personal communication, Mr S Davenport, Amersham International). Cell survival following incubation with each reagent was calculated for Nalm 6 (n=2) and JM (n=2) cells as previously described (Tables 6.11, 6.12).

Table 6.11

Survival of Nalm 6 incubated with non-radioactive reagents.

Reagent	*Concentration	**Cell Survival (%) (SEM)
I-HD37	x 1	94.4 (0.1)
	x 10	91.1 (0.1)
HD37	x 1	94.2 (0.1)
	x 10	93.6 (0.6)
NaI	x 1	93.9 (0.9)
	x 10	95.6 (0.5)

* Relative to that used in ^{131}I targeting experiments.

** Data is the mean of two experiments, each consisting of four cultures per reagent concentration.

Table 6.12

Survival of JM incubated with non-radioactive reagents.

Reagent	*Concentration	**Cell Survival (%) (SEM)
I-WT1	x 1	96.8 (1.1)
	x 10	95.6 (2.2)
WT1	x 1	95.4 (1.6)
	x 10	96.7 (2.2)
NaI	x 1	95.3 (1.6)
	x 10	98.3 (1.9)

* Relative to that used in ^{131}I targeting experiments.

** Data is the mean of two experiments, each consisting of four cultures per reagent concentration.

Less than 10% cell kill was observed for any of these reagents, excluding a significant non-radioactive cytotoxic effect.

(ii) Determination of cell-bound ^{131}I activity.

To investigate a possible relationship with cell survival, cell-bound ^{131}I activity was estimated in a gamma counter following incubation with radiolabelled antibodies and removal of unbound activity by washing (Section 2b). Data was collected for both time and activity response experiments of ^{131}I targeted to cells incubated in tubes.

For the time response experiments (n=1), binding of both 1 and 2 MBq of specific conjugates to Nalm 6 reached a point of saturation between two and four hours incubation, although the difference between bound activity at these times was greater for ^{131}I-WCMH than for ^{131}I-HD37 (Table 6.13, Figure 6.12).

Figure 6.12

Variation of Nalm 6 cell bound activity with time of incubation with ^{131}I-labelled antibodies.

1 x 10^6 Nalm 6 cells in 2 ml complete medium were incubated for between 2 and 24 hours with either 1 or 2 MBq of ^{131}I-labelled antibodies (n=1). Cell bound activity was determined in a gamma counter and the mean plotted against time of incubation.

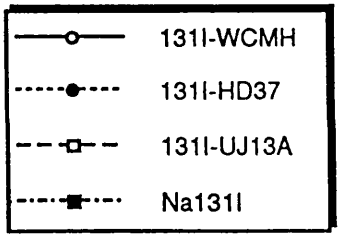

Figure 6.12

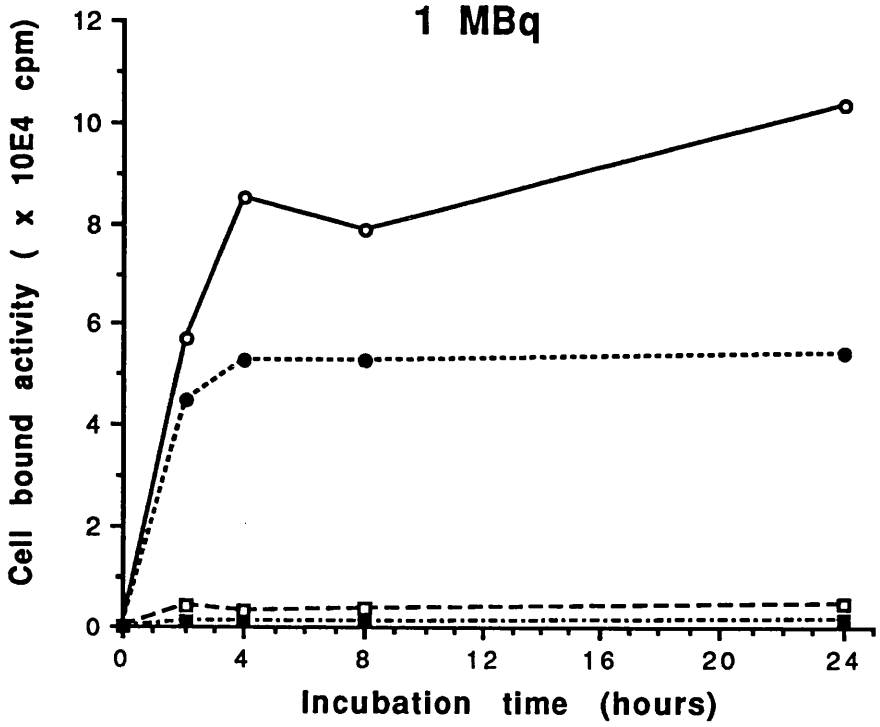
1 MBq
Cell bound activity (x 10E4 cpm)
12
10
8
6
4
2
0
0
4
8
12
16
20
24
Incubation time (hours)

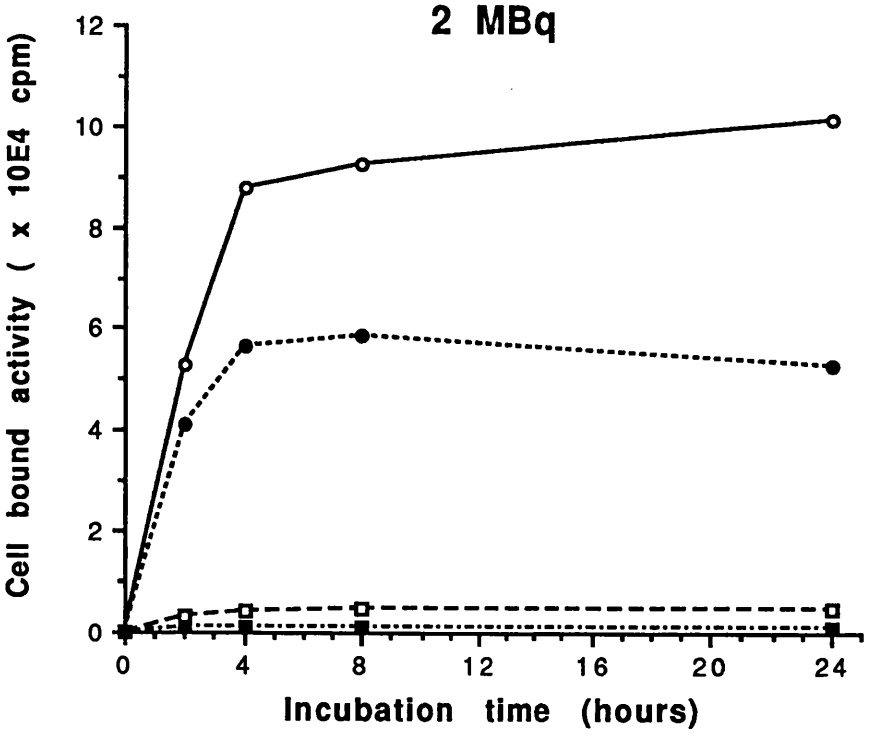
2 MBq
Cell bound activity (x 10E4 cpm)
12
10
8
6
4
2
0
0
4
8
12
16
20
24
Incubation time (hours)

Table 6.13 Nalm 6 bound activity following incubation for between 2 and 24 hours with 1 or 2 MBq ^{131}I-labelled antibodies.

Activity (MBq)	Conjugate	Cell Bound Activity (x 10^4 cpm)			
		Time of Incubation			
		2	4	8	24
1	^{131}I-WCMH	5.71	8.50	7.87	10.37
	^{131}I-HD37	4.51	5.31	5.26	5.46
	^{131}I-UJ13A	0.41	0.30	0.38	0.47
	Na^{131}I	0.10	0.08	0.09	0.15
2	^{131}I-WCMH	5.30	8.79	9.27	10.14
	^{131}I-HD37	4.10	5.68	5.89	5.26
	^{131}I-UJ13A	0.32	0.42	0.46	0.50
	Na^{131}I	0.12	0.08	0.10	0.10

Table 6.14 JM bound activity following incubation for 24 hours with 1 - 4 MBq ^{131}I-labelled antibodies.

Conjugate	* Cell Bound Activity (x 10^4 cpm) (SD)		
	Total Incubated Activity (MBq)		
	1	2	4
^{131}I-WT1	23.4 (6.3)	25.3 (6.3)	26.5 (7.4)
^{131}I-UJ13A	1.3 (0.9)	1.9 (1.0)	3.3 (1.7)
Na^{131}I	0.2 (0.2)	0.5 (0.4)	0.9 (0.5)

* Data is the mean of three experiments.

Table 6.15 Nalm 6 bound activity following incubation for 24 hours with 1 - 4 MBq ^{131}I-labelled antibodies.

Conjugate	* Cell Bound Activity (x 10^4 cpm) (SD) Total Incubated Activity (MBq)		
	1	2	4
^{131}I-cocktail	25.4 (3.4)	24.4 (3.2)	24.3 (2.8)
^{131}I-WCMH	15.7 (4.3)	15.1 (3.8)	16.2 (2.8)
^{131}I-HD37	9.7 (4.3)	11.3 (4.9)	13.0 (4.4)
^{131}I-UJ13A	1.3 (1.3)	1.4 (0.8)	2.6 (1.1)
Na^{131}I	0.3 (0.2)	0.4 (0.3)	0.7 (0.7)

* Data is the mean of six experiments.

This *in-vitro* model represents a situation of gross antibody excess. Thus, as expected, data from activity response experiments revealed saturable binding of all three single specific antibodies and the cocktail of WCMH and HD37, at all activities investigated after 24 hours incubation.

For JM cells, a mean of 2.34 x 10^5 cpm of ^{131}I-WT1 equivalent to 15.6 kBq or 1.56% of an incubated activity of 1 MBq remained bound, as compared with 0.09 and 0.01% for ^{131}I-UJ13A and Na^{131}I respectively (Table 6.14, Figure 6.13). For ^{131}I-WT1, bound activity fell to 0.93% of a total of 4 MBq, in comparison to 0.06 and 0.02% of ^{131}I-UJ13A and Na^{131}I respectively.

For Nalm 6, a mean of 1.04 and 0.65% of an incubated activity of 1 MBq ^{131}I-WCMH and ^{131}I-HD37 remained bound respectively (Table 6.15, Figure 6.14). This fell to 0.27 and 0.22 % of 4 MBq ^{131}I-WCMH and ^{131}I-HD37 respectively. This compares with 0.09 and 0.01% of 1 MBq, and 0.04 and 0.01% of 4 MBq, for ^{131}I-UJ13A and Na^{131}I respectively .

At each activity, increased bound activity was noted for ^{131}I-cocktail as compared with either single antibody component. For 1 MBq ^{131}I-cocktail,

Figure 6.13

Variation of JM cell bound activity with activity of incubated ^{131}I-labelled antibodies.

1 x 10^6 JM cells in 2 ml complete medium were incubated for 24 hours with between 1 and 4 MBq of ^{131}I-labelled antibodies. The mean cell bound activity (See Figure 6.12) of three experiments is plotted against incubated activity.
Error bars represent +/- 1 SD.

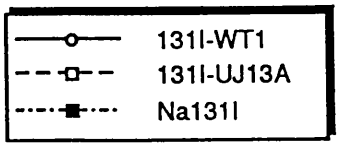

Figure 6.14

Variation of Nalm 6 cell bound activity with activity of incubated ^{131}I-labelled antibodies.

1 x 10^6 Nalm 6 cells in 2 ml complete medium were incubated for 24 hours with between 1 and 4 MBq of ^{131}I-labelled antibodies. The mean cell bound activity (See Figure 6.12) of six experiments is plotted against incubated activity.
Error bars represent +/- 1 SD.

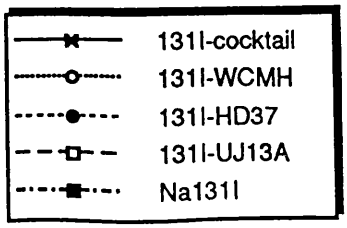

Figure 6.13

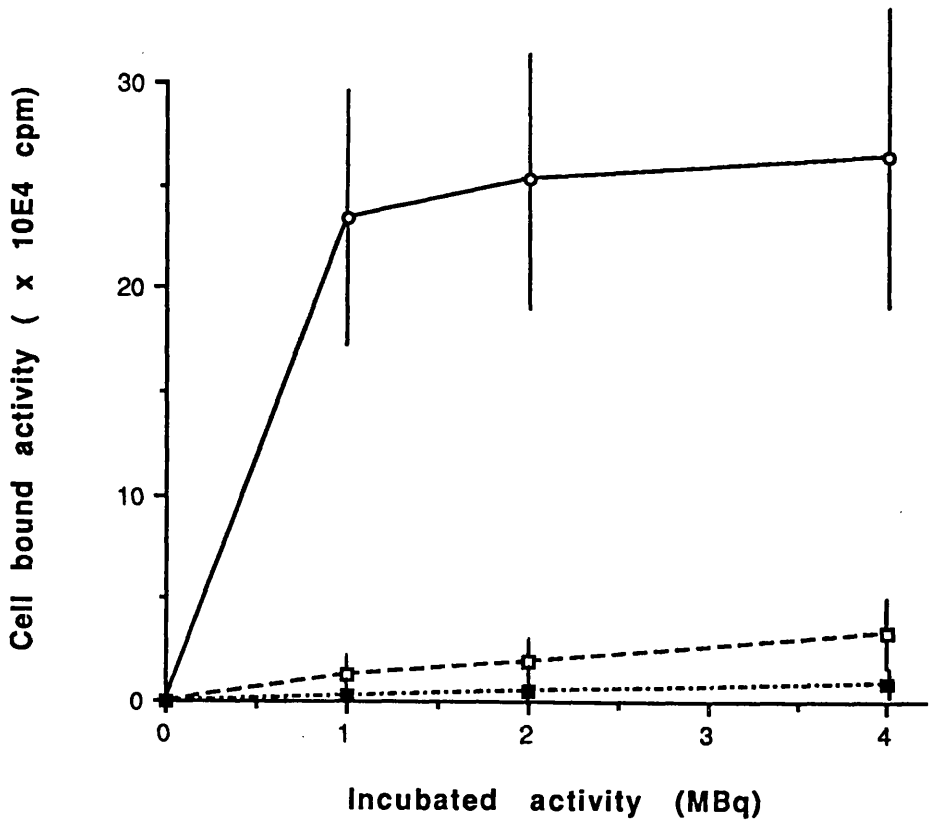

Figure 6.14

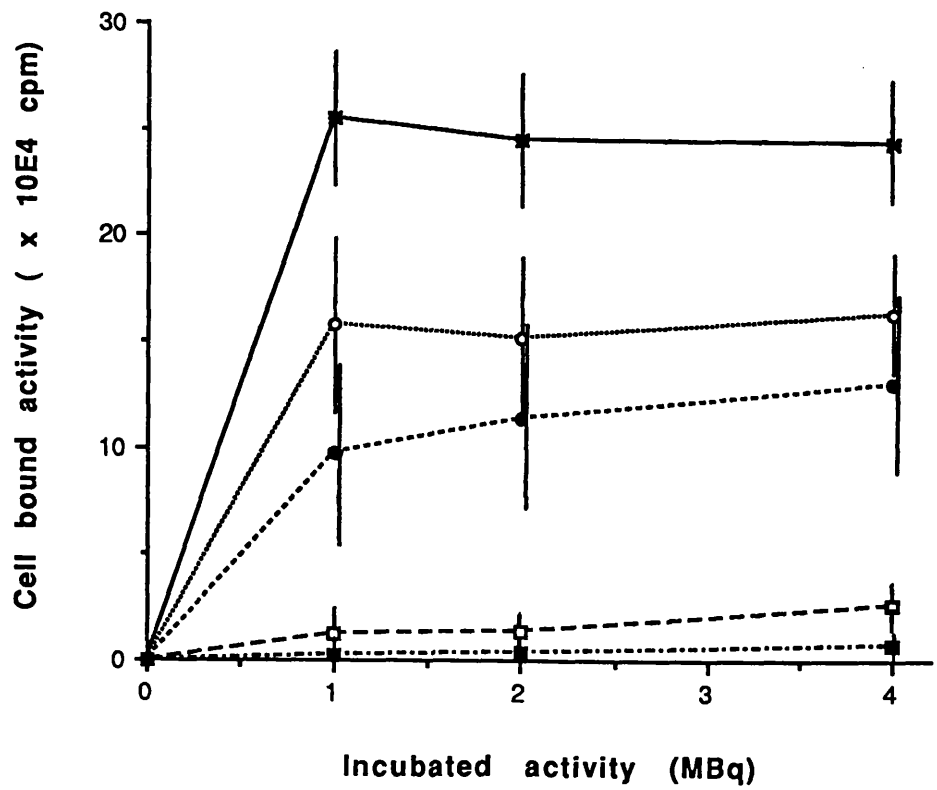

1.67% was noted to be bound to Nalm 6, equal to the sum of bound activities of ^{131}I-WCMH and ^{131}I-HD37.

(iii) The crossfire effect of bound activity in the clonogenic phase of the *in-vitro* system.

During the 14 day cloning period, cells in the Courtenay assay will continue to be irradiated by β-emissions from surface bound ^{131}I. Because cell are artificially trapped in soft agar, it was necessary to investigate radiation crossfire during this phase as an addition to the targeting effect.

JM cells were incubated in roller tubes with 1, 2 and 4 MBq of either ^{131}I-WT1 or Na^{131}I for 24 hours. The cell bound activity for both groups of cells was determined. An amount of Na^{131}I equivalent to the difference between the bound activities of ^{131}I-WT1 and Na^{131}I was added to cells incubated with Na^{131}I for 24 hours (n=3). These cells were placed in the Courtenay assay and cell survival (Table 6.16) compared with that from JM activity response experiments in which cells were irradiated without this additional isotope (from Table 6.8).

Table 6.16

Survival of JM cells incubated for 24 hours with $Na^{131}I$. The effect of a "targeted-equivalent activity" of ^{131}I in the clonogenic phase.

Activity of Incubation (MBq)	Cell Survival (%)	
	* With Additional $Na^{131}I$ in the Clonogenic Phase (SEM)	** Without Additional $Na^{131}I$ in the Clonogenic Phase
1	41.64 (1.56)	43.29 [+3.06] [-3.01]
2	21.57 (1.41)	18.27 [+1.36] [-1.29]
4	2.81 (0.24)	3.00 [+0.46] [-0.40]

* Data is the mean of three experiments, each consisting of six cultures per activity level.

** Data from activity response survival experiments (from Table 6.8).

No difference in survival between cells incubated with $Na^{131}I$, with or without the additional targeted-equivalent amount of ^{131}I, was observed. This excludes radiation crossfire from bound β-particles as a major contributory factor to radiation dose.

(g) Variation in cell survival with volume of incubation.

The effect of increasing the volume of incubation, whilst maintaining a constant incubated activity and cell population, was examined. 1 x 10^6 JM cells were incubated in complete Hams F-12 medium with between 1 and 8 MBq of either with ^{131}I-WT1 or $Na^{131}I$ in a volume of either 8 (n=3) or 20 ml (n=2) .

Incubations were undertaken in either 14 ml (Falcon) or 50 ml (Becton Dickinson) gas permeable tubes under conditions described for cell suspensions of 2 ml (Section 2.2). After 24 hours, cells were centrifuged, resuspended in 3 ml complete medium and transferred to 6 ml tubes. Three further washes were performed prior to incorporation of cells into the clonogenic assay. Variation in mean cell survival was calculated as the SEM.

Table 6.17

Cell survival data from JM incubated in a volume of 8 ml with ^{131}I-labelled antibodies.

Conjugate	* Cell Survival (%) (SEM)			
	Incubated Activity (MBq)			
	1	2	4	8
^{131}I-WT1	63.61 (3.16)	51.41 (2.90)	36.26 (3.17)	16.07 (0.77)
Na^{131}I	74.75 (1.44)	70.69 (0.72)	53.50 (1.62)	24.60 (1.49)

* Data is mean cell survival of three experiments, each consisting of four cultures per activity level.

Table 6.18

Cell survival data for JM incubated in a volume of 20 ml with ^{131}I-labelled antibodies.

Conjugate	* Cell Survival (%) (SEM)			
	Incubated Activity (MBq)			
	1	2	4	8
^{131}I-WT1	82.50 (1.69)	71.70 (1.87)	69.40 (3.05)	49.70 (2.19)
Na^{131}I	98.75 (0.35)	83.60 (1.10)	80.14 (2.36)	68.50 (0.71)

* Data is the mean of two experiments, each consisting of four cultures per activity level.

Survival curves for cells incubated in a volume of 8 ml with both ^{131}I-WT1 and Na^{131}I were exponential, with possible increased gradients between 0 and 1 MBq (Figure 6.15). For each incubated activity, a significantly lower ($p < 0.05$) cell survival was observed for JM incubated with ^{131}I-WT1 as compared with Na^{131}I (Table 6.17). Cell survival following incubation with both reagents in a volume of 8 ml was considerably higher as compared with cells treated in a 2 ml volume (Table 6.8). For an incubated activity of 4 MBq, survival of JM treated in 8 ml with ^{131}I-WT1 was 36.26% as compared with 1.43% for cells irradiated in 2 ml volume. Respective survivals for cells treated with Na^{131}I were 53.50 and 3.00%.

For irradiation in a volume of 20 ml, survival was again lower for cells incubated with ^{131}I-WT1 as compared with Na^{131}I (Table 6.18, Figure 6.16). This difference was significant ($p < 0.05$) for activities of 1, 2 and 8 MBq. For each incubated activity of both reagents, survival of JM cells was significantly greater ($p < 0.05$) when treated in a volume of 20 ml as compared with 8 ml irradiations.

The overall effect of increasing the volume of cell suspension was examined by constructing a plot of cell survival against the activity concentration (MBq/ml) within the cell suspension. This was undertaken for cells irradiated with either ^{131}I-WT1 or Na^{131}I in volumes of 2, 8 and 20 ml (Figure 6.17). This demonstrates a clear relationship between cell survival and activity concentration for both the specific and the control reagent.

In a single experiment, the cell bound activity (cpm) after three washes was recorded for JM cells incubated with either ^{131}I-WT1 or Na^{131}I in a volume of 2, 8 or 20 ml (Table 6.19, Figure 6.18).

Figure 6.15

Activity response of cell survival for Nalm 6 incubated with ^{131}I-labelled antibodies in a volume of 8 ml.

1 x 10^6 Nalm 6 cells were incubated in 8 ml complete medium for 24 hours with between 1 and 8 MBq ^{131}I-labelled antibodies (n=3). Mean cell survival (see Figure 6.1) is plotted against activity of incubation. Error bars represent +/- 2 SE.

Figure 6.16

Activity response of cell survival for Nalm 6 incubated with ^{131}I-labelled antibodies in a volume of 20 ml.

1 x 10^6 Nalm 6 cells were incubated in 20 ml complete medium for 24 hours with between 1 and 8 MBq ^{131}I-labelled antibodies (n=2). Mean cell survival (see Figure 6.1) is plotted against activity of incubation. Error bars represent +/- 2 SE.

Figure 6.15

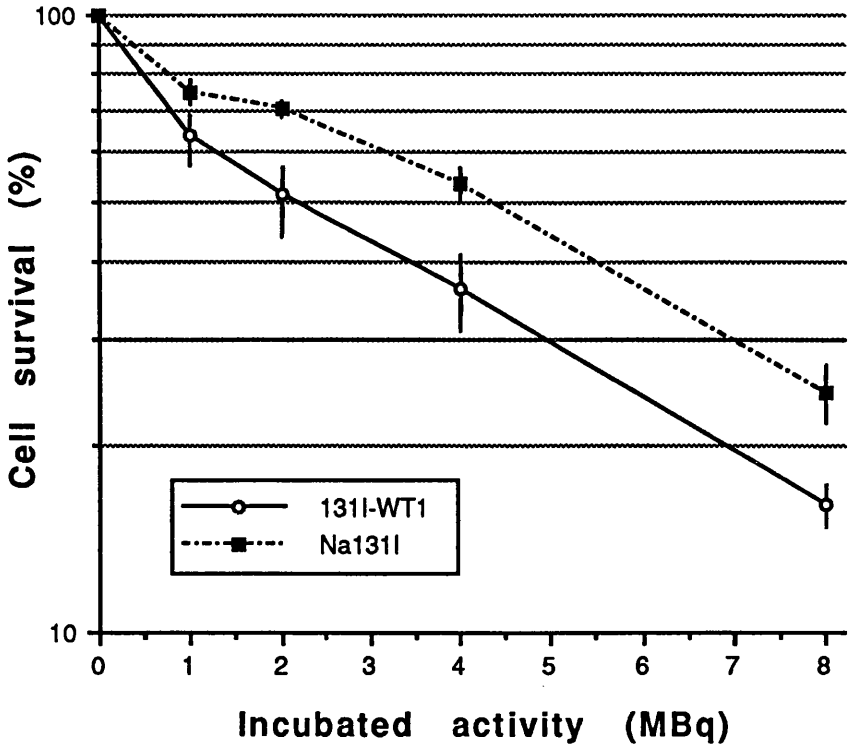

Figure 6.16

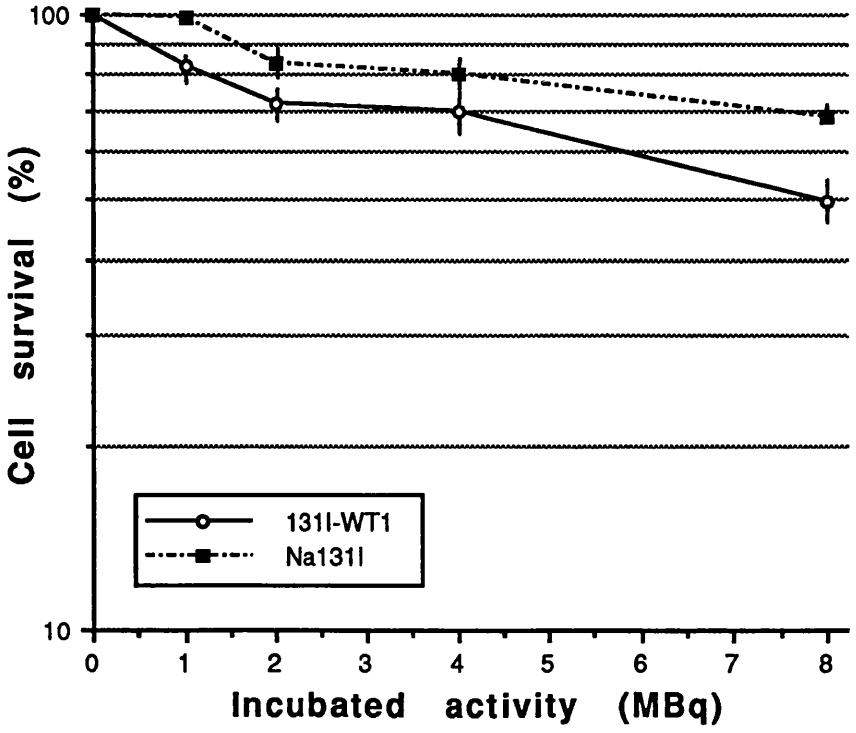

Figure 6.17

Variation in JM cell survival with activity concentration of incubated ^{131}I-labelled antibodies.

Mean cell survival of JM incubated with either ^{131}I-WT1 or ^{131}NaI, in volumes of 2, 8 and 20 ml, was plotted against activity concentration (MBq/ml) within the cell suspension (see Tables 6.8, 6.17 and 6.18).

Figure 6.18

Variation of JM cell bound activity with volume of cell suspension incubated with ^{131}I-labelled antibodies.

1 x 10^6 JM cells in 2, 8 or 20 ml complete medium were incubated for 24 hours with between 1 and 4 MBq of ^{131}I-labelled antibodies (n=1). Cell bound activity (see Figure 6.12) was plotted against incubated activity for each volume of incubation.

Figure 6.17

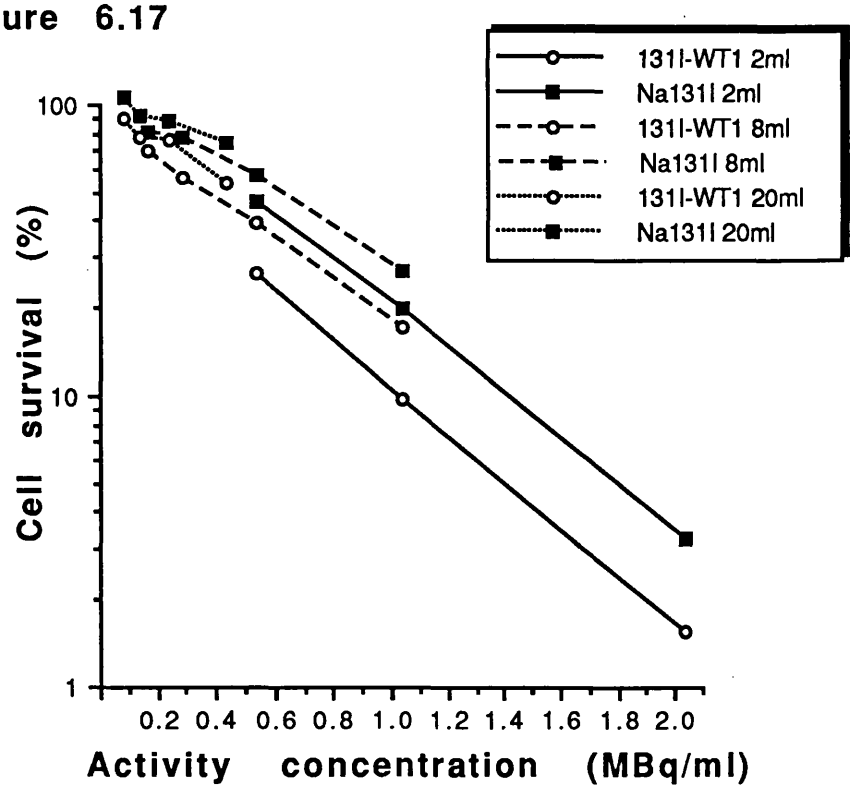

Figure 6.18

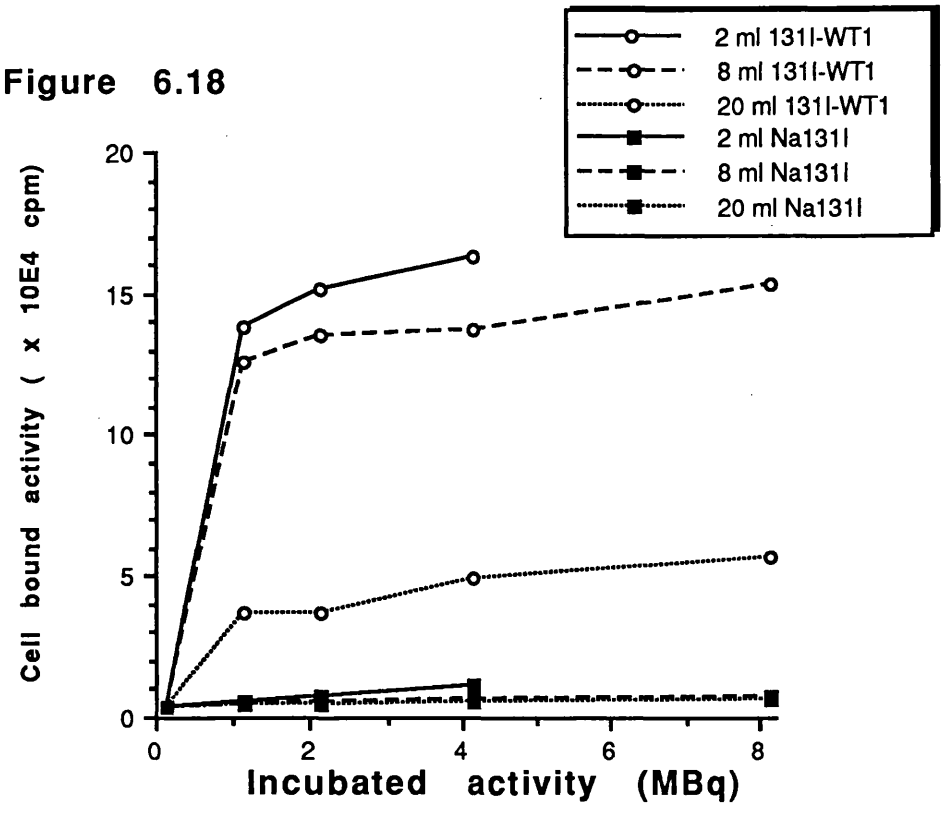

Table 6.19

Variation in cell bound activity of JM cells with volume of cell suspension incubated with ^{131}I-labelled antibodies.

Volume of Cell Suspension (ml)	Incubated Activity (MBq)	Cell Bound Activity (x 10^4 cpm)	
		Conjugate	
		^{131}I-WT1	Na^{131}I
2	1	13.46	0.22
	2	14.81	0.37
	4	15.92	0.80
8	1	12.20	0.12
	2	13.21	0.18
	4	13.40	0.26
	8	15.00	0.42
20	1	3.33	0.09
	2	3.32	0.11
	4	4.51	0.19
	8	5.32	0.32

As compared with those observed for incubations in a 2 ml volume, cell bound activities of ^{131}I-WT1 was slightly lower for 8 ml incubations, but considerably lower for cell irradiated in a volume of 20 ml. Saturable binding of WT1 was again noted at all activities for each volume of cell suspension investigated.

(h) Variation in cell survival with the specific activity of ^{131}I-radiolabelled antibodies.

A potential strategy for increasing the cytotoxicity of targeted radioconjugates is to increase the incorporation of radioiodine into each antibody molecule.

1 x 10^6 JM cells were incubated for 24 hours in a volume of 2 ml with 1, 2 or 4 MBq of WT1 radiolabelled with ^{131}I to a specific activity of 37, 370 or

1110 MBq/mg protein. A radiobinding assay (Chapter 2; 5f) performed immediately following iodination revealed immunoreactive fractions of 94, 61 and 28% for antibody labelled to these respective specific activities. Labelling efficiencies were 73, 54 and 42% respectively.

Table 6.20 Cell survival data for JM incubated with different specific activities of ^{131}I-WT1.

Specific Activity (MBq/mg)	Cell Survival (%)		
	Incubated Activity (MBq)		
	1	2	4
37	[+3.44] *35.24 [-3.29]	[+1.79] 14.00 [-1.62]	[+0.65] 4.31 [-0.57]
370	[+3.26] 30.33 [-3.07]	[+1.44] 10.01 [-1.27]	[+0.41] 2.72 [-0.36]
1110	[+3.23] 26.43 [-3.00]	[+1.13] 7.77 [-1.03]	[+0.33] 1.95 [-0.28]

* Data is the mean of twelve cultures per activity level. Figures in parentheses give upper and lower 95% confidence limits.

For each incubated activity, a significantly lower ($p < 0.05$) cell survival was observed when WT1 labelled to a specific activity of 1110 MBq/mg protein is compared with antibody at a specific activity of 37 MBq/mg protein (Table 6.20, Figure 6.19). Significantly lower ($p < 0.05$) survival was also noted for JM when treated with 4 MBq of antibody labelled to 1110 MBq/mg protein as compared with 370 MBq/mg, and when irradiated with either 2 or 4 MBq of WT1 at 370 MBq/mg protein as compared with 37 MBq/mg protein.

Figure 6.19

Variation in JM cell survival, with specific activity of incubated ^{131}I-WT1.

1 x 10^6 JM cells were incubated in roller tubes for 24 hours, with between 1 and 4 MBq ^{131}I-WT1 (n=1). Mean cell survival (see Figure 6.1) is plotted against activity of incubation. For clarity, confidence limits are excluded (see Table 6.20).

Figure 6.19

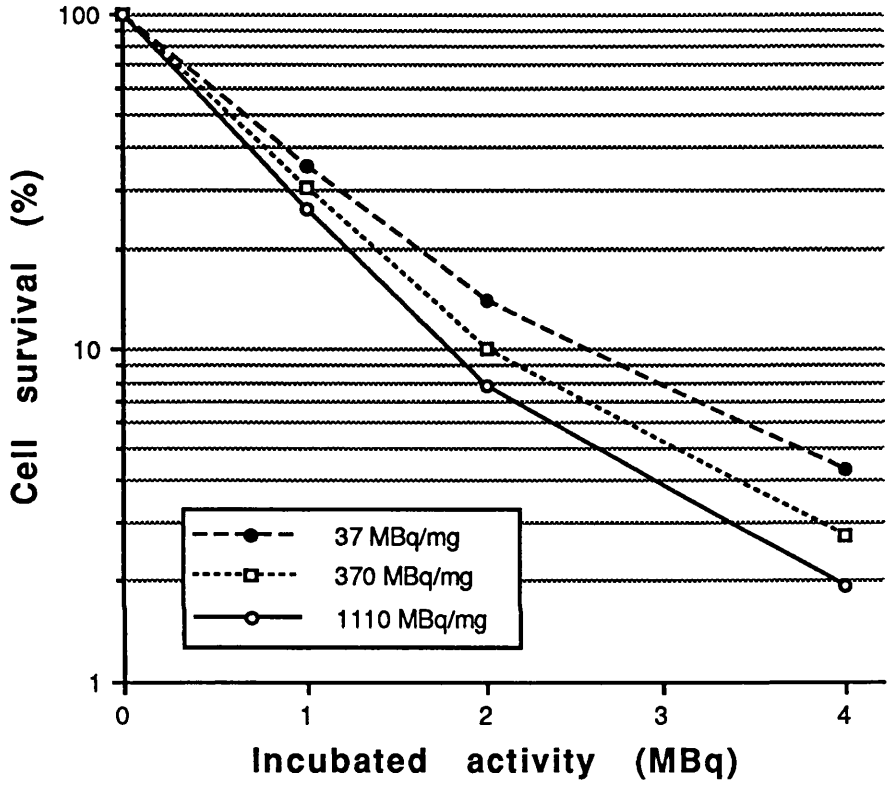
100
10
1
Cell survival (%)
0
1
2
3
4
Incubated activity (MBq)
37 MBq/mg
370 MBq/mg
1110 MBq/mg

For an incubated activity of 4 MBq, an advantage in cell kill of 1.39 and 2.21 fold was noted for WT1 labelled to 1110 MBq/mg, as compared with 370 and 37 MBq/mg protein respectively.

Table 6.21

Variation in JM cell bound activity with specific activity of incubated ^{131}I-WT1.

Specific Activity (MBq/mg)	Cell Bound Activity (x 10^4 cpm)		
	Incubated Activity (MBq)		
	1	2	4
37	5.74	5.74	7.35
370	16.45	18.26	21.63
1110	28.88	36.57	40.62

Saturable binding was again observed for all reagents at each incubated activity, with a marked increase in cell bound activity with increasing specific activity of incubated radioconjugate (Table 6.21). This increase, however, was not as large as expected relative to the elevation in specific activity of radiolabelling. For WT1 labelled to a specific activity of 1110 MBq/mg, bound activities equivalent to 1.93, 1.24 and 0.68 % of incubated activities of 1, 2 and 4 MBq respectively, were observed.

4. Discussion.

This *in-vitro* model was developed to investigate the radiobiology of antibody-targeted ^{131}I radiotherapy against a single cell suspension of human tumour cells. The issue of specificity of antibody mediated therapy is crucial to this concept and this series of experiments were designed to address this question.

The irradiation of a cell suspension *in-vitro* is especially applicable to meningeal leukaemia which, unless at an advanced stage, presents as a single cell disease or as small clumps of tumour. This is in contrast to more bulky tumours in which a spheroid system would be more appropriate. The conditions of incubation of cells with radioconjugates were chosen to mimic the clinical situation as closely as possible, in terms of both cell concentration and administered radioactivity. Such models are, however, inevitably limited as they cannot take into account anatomical and physiological considerations, and the complex clearance kinetics of immunoconjugates from the CSF.

In these studies, a clear advantage in terms of cell kill by targeting ^{131}I to leukaemic cells was demonstrated. The cell kill associated with ^{131}I-WCMH, ^{131}I-HD37 and ^{131}I-WT1 was consistently greater than that for either ^{131}I-UJ13A or $Na^{131}I$. The contribution of non-radiolabelled components was shown to be unimportant in relation to specific cell kill.

To explain the cytotoxicity of targeted therapy observed, it is important to consider the components of the radiation dose delivered to cells from β-particles emitted from ^{131}I conjugated to antibody (Figure 6.20). In the suspension phase of the assay, cells will be irradiated from both ^{131}I bound to the cell surface as a result of antibody targeting, and from unbound radionuclide, which in a situation of gross antibody excess, contributes to the majority of the energy. An additional consideration is the crossfire effect; the irradiation of non-targeted cells by radionuclide bound to neighbouring

Figure 6.20 ß-particle irradiation from specific ^{131}I-monoclonal antibody conjugates

Direct targeting effect from bound radionuclide:

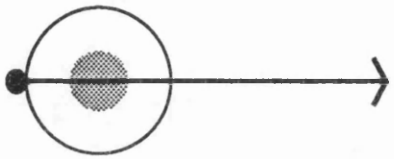

Crossfire effect from bound radionuclide:

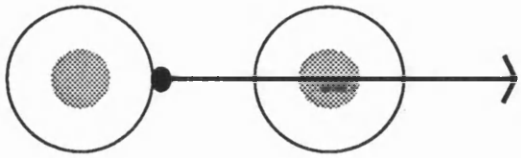

Effect from unbound radionuclide:

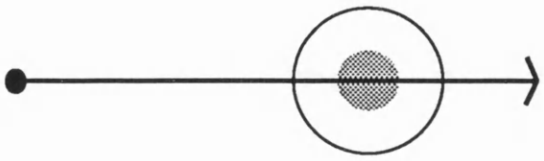

targeted cells. In a homogeneous cell suspension, the radiation dose due to crossfire will be equivalent to that of unbound radionuclide, and in gross antibody excess, this component will be small compared with that of unbound radionuclide. Such considerations do not apply to targeted agents such as drugs and toxins which require both cell binding and internalization. The specificity of targeting observed for these agents in similar culture systems [15] [229] is, therefore, clearly expected.

During the clonogenic phase of the assay, bound radionuclide continues to irradiate cells. This applies to all *in-vitro* investigations of targeted therapy in which cell damage is estimated at a time point greater than that of the treatment period. As well as providing a continued direct radiation source, bound activity may potentially contribute to the overall cell dose by crossfire within the confines of the soft agar matrix. However, for JM cells, the addition of an activity of $Na^{131}I$ in the clonogenic phase, equivalent to that targeted with antibody, did not decrease the survival of cells incubated in suspension with $Na^{131}I$. This experiment therefore excludes a significant crossfire effect within the soft agar. Although not confirmed, this should equally apply to Nalm 6 cells. Moreover, because the difference between the bound activity of ^{131}I-WT1 and that of $Na^{131}I$ is greater than that of $Na^{131}I$ alone, this experiment excludes a significant cytotoxic effect of $Na^{131}I$ bound to cells within the clonogenic phase.

In the experimental system, therefore, cell-bound isotope irradiates cells in both the suspension and clonogenic phases, whereas unbound radionuclide only exerts an effect during the period when cells are in liquid phase. This reflects the situation *in-vivo* where cells are initially exposed to a high concentration of unbound radionuclide, which clears more rapidly than that bound to tumour cells. This results in an environment in which a lower overall activity is present, but one in which a greater proportion of radionuclide is cell-associated.

From the data, it is impossible to define what proportion of the observed cell kill results from the radiation dose received during either the incubation or cloning phases. Data indicating a significant effect during the incubation phase comes from the time response experiments, in which the advantage for specific conjugates in terms of cell kill, increases with time of incubation (Tables 6.2, 6.3 and 6.6). As the majority of antibody binding to cells occurs within four hours of incubation, this result would not be expected if the effect of targeting results solely from bound radiation during the clonogenic phase. The amount of bound activity carried over into the soft agar is independent of the incubation time after saturation of antigen binding sites.

An additional consideration is the contribution to cell kill by unbound radionuclide on cells receiving a sub-lethal radiation dose from targeted radionuclide. This effect may only be significant within the incubation phase. Thus, the advantage of antibody targeting per unit time may be disproportionately greater during this period as opposed to during cloning..

Repeating cell kill experiments using an alternative assay such as the MMT-Tetrazolium Blue system [254] may resolve some of the above issues, despite the disadvantages of methods utilising metabolic injury as an index of cell lethality. The specificity observed has also been explored on a theoretical basis using a mathematical model (Chapter 7).

Further experiments were performed to investigate additional factors that may potentially contribute to the targeting effect. In contrast to the plate method of incubation, the roller tube system provides a macroscopically homogeneous cell suspension. Nevertheless, naturally or artificially induced cell aggregation will enhance the effect of targeting by the introduction of a significant crossfire effect. Quantification of the size of tumour aggregates excluded this as an explanation.

These studies imply that the increased cell kill associated with specific conjugates result from a direct effect of targeting ^{131}I to the cell surface,

significantly increasing the probability of a nuclear "hit" from bound, as compared with unbound radionuclide. The existence of a direct targeting effect is supported by the increased cell kill associated with the use of a cocktail of ^{131}I-WCMH and ^{131}I-HD37 as compared with individual reagents. This result has important clinical implications, and as a direct result of these studies, we have incorporated the use of a WCMH/HD37 cocktail into our clinical programme (Chapter 10; 3b). It is probable that cytotoxicity will be increased using combinations of more than two antibodies (Chapter 13; 2b).

Relatively little attention has been paid to either the pre-clinical or clinical investigation of antibody combinations. Using a paired labelling approach, Pimm *et al.*, demonstrated enhanced localisation of isotope using two specific radioimmunocojugates in a human osteogenic sarcoma nude mouse xenograft [255]. In patients, Chatel *et al.*, evaluated two ^{131}I- labelled MoAbs, 17-1A and 19-9, for the localisation of colonic cancer [256]. For MoAb 17-1A, 59% of the known cancer sites were detected by scintigraphy, while for 19-9, 66% were detected. When a combination of these two antibodies were administered, the detection rate was increased to 77%. White *et al.*, showed synergy between unmodified anti-transferrin receptor antibodies in inhibiting growth of CCRF-CEM leukaemic T-cells in both an *in-vitro* HL-colony forming assay and nude mice bearing the same tumour [257]. A cocktail of three immunotoxins have been successfully used to remove CALLA positive cells from bone marrow infiltrated with leukaemia [258]. A mixture of three ricin-bonded antibodies has also been shown to enhance *in-vitro* toxicity when targeted to a T-lymphocytes, as compared with single immunotoxins [259].

Using Nalm 6 as target cells, an increased cell kill was noted for ^{131}I-WCMH over ^{131}I-HD37. This may reflect the higher epitope density of CD10 on this cell line. This suggests that antibodies used clinically should be selected with greater attention to epitope density on the target cell. As with the use of antibody combinations, this approach is strongly supported on a theoretical

basis using mathematical modelling (Chapter 7). The sensitivity of target cells to irradiation by ^{131}I is also important, as JM cells consistently bound more antibody than Nalm 6. However, less cell kill was observed for the T-cell line treated with both specific and control reagents, implying a reduced radiation sensitivity of JM to β-irradiation.

Further evidence for a direct targeting effect is provided by a single experiment indicating decreased survival of JM cells when targeted with ^{131}I-WT1 of increasing specific activity. This occurred despite a reduction in both labelling efficiency and immunoreactivity. If substantiated, this result suggests that antibodies radiolabelled to higher specific activities (eg. 1110 MBq/mg) should be introduced into clinical trials. A specific activity of 1110 MBq/mg protein corresponds to approximately two iodine atoms per immunoglobulin molecule. Each Ig molecule may contain up to 50 tyrosine residues [242] and, therefore, there may be scope for the investigation of conjugates of even higher specific activity. Limitations to such an approach may result from a further reduction in immunoreactivity, requiring the use of alternatives to direct oxidation methods of radiolabelling.

Time response survival curves showed an exponential configuration, but as each experiment was only undertaken on one or two occasions, further studies are necessary to allow detailed analysis of the shape of the curves. Investigation of treatment times in excess of 24 hours was not undertaken, as the viability of untreated cells incubated at an initial concentration of 5 x 10^5/ml is compromised after 36 - 48 hours.

Activity response curves, which have much smaller confidence limits than the time-response curves, also conform to an exponential function, consistent with curves for cells exposed to X-irradiation [246]. Those for Nalm 6 and JM treated with either ^{131}I-cocktail or ^{131}I-WT1 exhibited an initial increased gradient. This was predicted given the fact that antigen saturation is achieved with an activity of 1 MBq of radiolabelled antibodies. The

corresponding curves for ^{131}I-HD37 and ^{131}I-WCMH do not, however, exhibit this phenomenon, which may be related to reduced cell bound activity. Alternatively, the shape of the curves for Nalm 6 incubated with single specific conjugates may be due to cell recovery from sub-lethal damage at lower activities. This may explain the initial shallow gradients of curves for Nalm 6 incubated with ^{131}I-UJ13A and Na^{131}I, and may reflect the typical "shoulder" of survival curves for X-irradiated cells. A potential increased gradient for ^{131}I-WCMH and ^{131}I-HD37 may thus be offset by this mechanism. However, as the curves for JM incubated with control reagents do not exhibit this phenomenon, it implies that JM cells do not demonstrate increased recovery from low activity β-irradiation. This is in contrast to experiments in which JM and Nalm 6 were exposed to X-rays at a dose rate of 100 cGy/minute, for which the shoulder of the respective survival curves was more evident for JM (data not presented).

As incubated activity is increased, the contribution of unbound activity should become proportionately greater, and the advantage of targeting decrease correspondingly. This was not observed over the range of activities used in these studies. Further experiments are planned to address this issue, employing higher activities of radioconjugates. Such studies will require the demonstration of linearity of cloning in soft agar for a considerably greater number of plated cells than currently investigated.

Cell bound activity of ^{131}I-WCMH and ^{131}I-HD37 reached relative saturation after four hours incubation with target cells. This was unexpected, as it is generally accepted that the majority of antibody-antigen binding occurs within minutes. Thus, these observations require confirmation. Possible explanations for this phenomenon may be either the effect of incubating cells with reagents in a relatively large volume (2 ml), or antigen modulation followed by regeneration of antigen, recruiting further surface bound antibody.

As expected, cell bound activity of all three specific conjugates reached relative saturation for an incubated activity of 1 MBq of antibody. The bound activity of WT1 was consistently greater than that for either WCMH and HD37. This was not predicted using data from Scatchard analysis (Chapter 3; 6). If the number of binding sites as determined by Scatchard analysis is used to calculated the expected per cent cell-bound activity, then 5.25, 0.37 and 0.26% of an incubated activity of 1 MBq would be expected to be bound for ^{131}I-WCMH, ^{131}I-HD37 and ^{131}I-WT1 respectively, as opposed to observed values of 1.04, 0.65 and 1.56% respectively. This discrepancy is difficult to explain, but may result from changes in the epitope expression on both Nalm 6 and JM over a two year period.

Few studies, similar to those detailed here, have been undertaken on tumour cells in either cell suspension or monolayer culture. Tsai *et al.*, used a radioiodinated anti-CEA antibody, C27, to target a colorectal carcinoma cell line, LS174T, [260]. Cytotoxicity associated with specific conjugates was assessed by counting viable cells and compared with either ^{131}I-labelled normal mouse IgG (MOPC21) or Na^{131}I. A significantly decreased cell survival was noted for incubation with specific reagents. After 12 days, the mean number of cells following treatment with ^{131}I-C27 was 0.8 x 10^4, in comparison to 97.4 and 101.5 x 10^4 for cells incubated with ^{131}I-MOPC21 and Na^{131}I respectively, and 123.5 x 10^4 for non-treated cells.

Capala *et al.*, employed a clonogenic assay to investigate the effect of ^{131}I-labelled Epidermal Growth Factor (EGF) on the survival of a human glioma cell line, U-343MGa C12.6, growing as a monolayer culture [261]. At the higher activity used (0.6 MBq/ml), mean survival of ^{131}I-EGF treated cells was significantly lower than that for cells incubated with ^{131}I-BSA.

The majority of *in-vitro* studies of antibody-mediated ^{131}I therapy have employed a multicellular tumour spheroid model, in which the efficiency of targeting is more readily explained by the size of these cell aggregates. A

specific effect of antibody targeting against human malignant melanoma spheroids [262] and of a ^{131}I-labelled anti-CEA antibody against a human colon adenocarcinoma spheroids [263] has been demonstrated. Walker *et al.*, established spheroids from the human neuroblastoma cell line, NB1-G. 200 μm spheroids were exposed for two hours to between 5 and 28 MBq of a ^{131}I-labelled specific monoclonal antibody [264]. A clear effect of targeting was observed, in terms of both the proportion of spheroids sterilized and the time taken for spheroids to reach 10 x their original volume. The authors concluded that the overall radiation dose delivered to spheroids resulted from spheroid irradiation during both the incubation and the spheroid growth periods.

In addition to exploring the response to higher activities, further experiments are underway to investigate the effect of altering cell concentration whilst maintaining a constant incubated activity and volume of incubation. This may relate to the situation *in-vivo* with respect to treating a range of CSF blast cell concentrations. An initial experiment has been performed in which JM cells at concentrations of 0.1, 0.5 and 2.5 x 10^6/ml, in a volume of 2 ml, were incubated for 24 hours with between 1 and 4 MBq of either ^{131}I-WT1 or Na^{131}I. Whilst decreased cell survival was again noted for cells treated with the specific conjugate, no differences were observed when comparing survival between cells irradiated at any concentration. This result is predicted from mathematical modelling (Chapter 7), although additional assays will examine both higher and lower concentrations than those treated here.

CHAPTER 7.

APPLICATION OF THE HUMM MODEL FOR MICRODOSIMETRY OF RADIOLABELLED ANTIBODIES FOR THE TREATMENT OF NON-SOLID TUMOURS.

1. Introduction.

In 1986, Humm published a manuscript detailing dosimetric aspects of targeted radiation therapy [92]. This concentrated on the relationship between the physical characteristics of radionuclides used in targeted therapy and the morphology of the targeted tumour.

Humm's microdosimetric calculations for non-solid tumours were designed to investigate the dose advantage due to antibody binding in terms of a tumour to non-tumour radiation dose ratio. The formulae used apply equally to the study of the specificity of targeted therapy for tumour cells in suspension, as they assume no cell clumping and hence no crossfire effect.

In collaboration with a co-worker (Mr V Papanastassiou, Imperial Cancer Research Fund, Bristol), Humm's model was used to determine the theoretical dose advantage of antibody targeting of ^{131}I for CNS ALL. The model was extended to examine the effect of variation in cell concentration and the degree of antibody binding.

2. Methods.

(a) Humm's model.

The energy deposition in cell nuclei, E_1, from radiolabelled antibodies not bound to tumour cells is given by:

$$E_1 = V_V \cdot r_o \cdot LET, \qquad (1)$$

where, V_V is the fraction of the tissue volume occupied by cell nuclei,

r_0 is the mean particle range of the radionuclide used,

and **LET** is the linear energy transfer.

This indicates that the fraction of the particle's path length spent in the nucleus is equal to the fraction of the tissue volume occupied by nuclei, V_V. The product $V_V \times r_0$ gives the length of particle track contributing to nuclear damage. This multiplied by the linear energy transfer, **LET**, gives the energy deposition, E_1, contributing to cell inactivation. The remaining energy is wasted in the cytoplasm and extracellular space.

For a tumour cell with a radiolabelled antibody bound to its surface, the energy deposition in the nucleus, E_2, is given by:

$$E_2 = pr \cdot l \cdot LET, \qquad (2)$$

where, **pr** is the probability that a particle traverses the nucleus

and **l** is the mean path length of a linear track across the nucleus.

The product $pr \times l$ is the average particle path length across the tumour cell nucleus. As above, multiplication by the **LET** gives the energy deposition contributing to cell inactivation.

Assuming the crossfire effect to be negligible, the dose advantage due to antibody binding, D_A, can be expressed as the ratio of the equations, **(1)** and **(2)**:

$$D_A = \frac{pr \cdot l}{V_V \cdot r_0} \qquad (3)$$

The values of the parameters in equation **(3)** depend on the physical characteristics of the tumour cells and the radionuclide used.

The probability, **pr**, that a particle from a targeted radionuclide traverses the cell nucleus is a fraction represented by the solid angle, ω, subtended by the nucleus from a point of decay on the cell surface membrane (Figure 7.1). This will depend on the nuclear/cytoplasmic ratio of the particular tumour cell. The mean length of a straight line particle track through the nucleus, **l**, is dependent on nuclear size and will approximate to:

$$\mathbf{l} = \frac{4}{3}\mathbf{R},$$

where, **R** is the radius of the cell nucleus .

The nuclear volume fraction, $\mathbf{V_V}$, will vary with the degree of tumour infiltration, as well as with the nuclear size. The mean particle range, $\mathbf{r_0}$, is characteristic for individual radionuclides. It corresponds to the distance in water in which half the emitted energy is deposited (R_{50}).

Humm calculated a representative value of dose advantage, $\mathbf{D_A}$, for a medium range β-particle emitter. Using the equation above and values for **pr** of 1 in 16 (for a cell with nuclear and cellular diameters of 10 μm and 20 μm respectively), $\mathbf{V_V}$ of 0.1 and $\mathbf{r_0}$ of 500 μm, he found $\mathbf{D_A}$ to be only 0.008. He therefore concluded that:

"... the dose enhancement to tumour cells is inexploitably small when the gain from cross-fire present in a solid tumour is lost."

(b) Application of Humm's model to ^{131}I targeted therapy of CNS ALL.

When the above parameters are considered in the context of single cell disease within the intrathecal space, it is apparent that some of the values used by Humm in his calculations of "typical" $\mathbf{D_A}$ are inappropriate. This particularly applies to the nuclear volume fraction, $\mathbf{V_V}$. In cases of malignant infiltration of the CSF , $\mathbf{V_V}$ for the free floating cells will be dependent on the cell concentration within the CSF and the size of the cell nucleus:

Figure 7.1 **Illustration of the solid angle, ω, subtended by the nucleus from a point of radioactive decay on the cell surface membrane.**

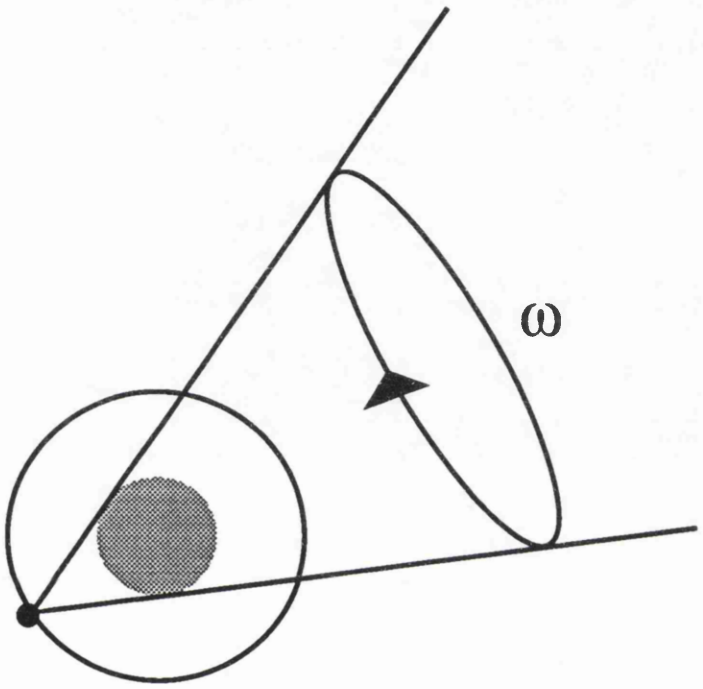

Figure 7.2 Calculation of the probability of a nuclear hit by a particle originating at a point (A) on the cell membrane

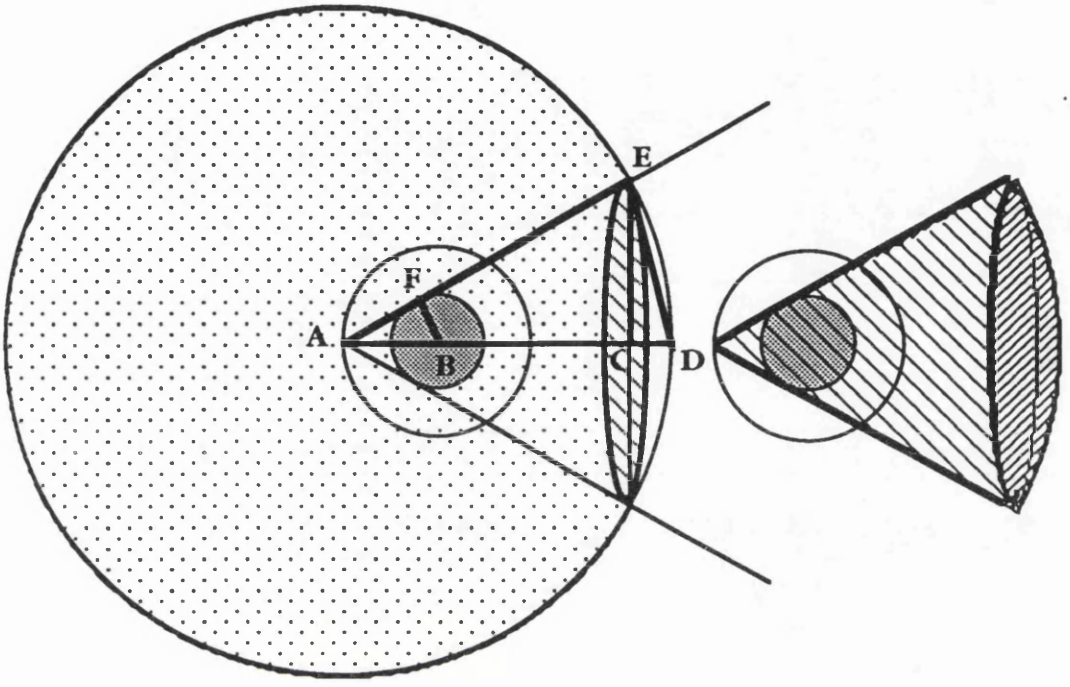

AB = Cell radius, R_c

BF = Nuclear radius, R_n

AE = AD = Sphere radius, r

CD = Spherical segment height, h

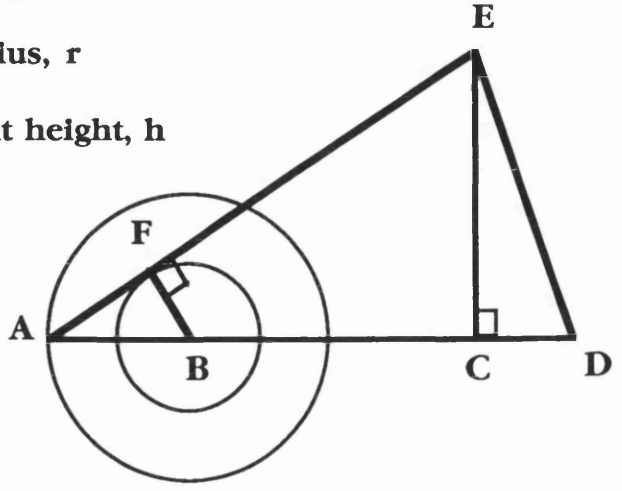

$$V_V = \frac{c \cdot \frac{4}{3}\pi R^3}{10^{-6}} \qquad (4)$$

where,

c is the cell concentration in cells per ml,

R is the radius of the cell nucleus,

and $\frac{4}{3}\pi R^3$ is the volume of an individual cell nucleus.

The cell concentrations encountered in CNS ALL are in the range of 5×10^3 to 1×10^6 cells per ml. Given a nuclear radius of 5 μm [265], this would give values of V_V ranging from 2.6×10^{-6} to 5.2×10^{-4}. These are 5000 to 100000-fold smaller than the value of 0.1 used by Humm.

For ^{131}I, r_o is equal to 285×10^{-6} m [91].

For a nuclear radius of 5×10^{-6} m, **l** = $4/3 \times 5 \times 10^{-6}$ m = 6.667×10^{-6} m

A method for calculating values of **pr**, for a cell of given nuclear and cellular dimensions, was provided by Mr V Papanastassiou (Imperial Cancer Research Fund, Bristol), and is presented below.

The probability, **pr**, of a particle originating at **A** hitting the nucleus is a fraction represented by the solid angle, ω (Figure 7.2). This can be defined as the ratio of the volume of a spherical segment subtended by this angle, to the volume of the sphere from which the segment arises. This being a ratio, will hold true for any given sphere. The probability **pr** is, therefore, given by:

$$pr = \frac{\textbf{Volume of spherical segment height h}}{\textbf{Volume of sphere radius r}}$$

$$pr = \frac{\frac{2}{3}\pi r^2 h}{\frac{4}{3}\pi r^3}$$

where, **r** is the radius of the sphere

and **h** is the height of the spherical segment.

This can be simplified to:

$$\mathbf{pr} = \frac{1}{2}\left[\frac{\mathbf{h}}{\mathbf{r}}\right] \qquad (5)$$

To obtain an expression for **pr** in terms of the cell dimensions, $\mathbf{R_c}$ and $\mathbf{R_n}$, the relationship between the four parameters **h**, **r**, $\mathbf{R_c}$ and $\mathbf{R_n}$ needs to be established. This is done using simple geometry by considering Figure 7.2:

ABF and **AEC** are similar triangles

(Right angle triangles with an equal angle **<A**),

therefore:

$$\frac{\mathbf{AB}}{\mathbf{AE}} = \frac{\mathbf{AF}}{\mathbf{AC}} \qquad (6)$$

Applying Pythagoras's theorem to triangle **ABF**:

$$\mathbf{AB^2 = AF^2 + BF^2}$$

$$\mathbf{AF^2 = AB^2 - BF^2}$$

$$\mathbf{AF = \sqrt{AB^2 - BF^2}}$$

$$\mathbf{AF = \sqrt{R_c^2 - R_n^2}} \qquad (a)$$

From the same diagram:

$$\mathbf{AC = AD - CD}$$

$$\mathbf{AC = r - h} \qquad (b)$$

Substituting **(a)** and **(b)** in formula **(6)**:

$$\frac{\mathbf{R_c}}{\mathbf{r}} = \frac{\sqrt{\mathbf{R_c^2 - R_n^2}}}{\mathbf{r-h}} \qquad (7)$$

Re-arranging expression **(7)**:

$$r\text{-}h = \frac{\sqrt{R_c^2 - R_n^2}}{R_c} \times r$$

Solving the equation for **h**:

$$h = \left[1 - \frac{\sqrt{R_c^2 - R_n^2}}{R_c}\right] \times r \qquad (8)$$

Substituting **h** from equation **(8)** into equation **(5)**:

$$pr = \frac{1}{2} \frac{\left[1 - \frac{\sqrt{R_c^2 - R_n^2}}{R_c}\right] \times r}{r}$$

r can be cancelled out, leaving an expression for probability, **pr**, in terms of the cell and nuclear radii, R_c and R_n, and independent of **h** and **r**:

$$pr = \frac{1}{2}\left[1 - \frac{\sqrt{R_c^2 - R_n^2}}{R_c}\right] \qquad (9)$$

For a L_1 lymphoblast (FAB system of classification) of cell diameter 12 μm and nuclear diameter 10 μm [265], **pr** is equal to 1/4.47 (0.224). It is of note that **pr** (and hence D_A) will be greater for leukaemic cells than for the majority of tumour cells due to their large nuclear : cytoplasmic ratio. **pr** is even higher if radionuclide is internalised within the cell, as has been shown for antibodies used in these studies.

3. Results and Discussion.

The dose advantage, $\mathbf{D_A}$, for an individual β-particle (or radiolabelled antibody) can thus be calculated for a range of tumour cell concentrations relevant to ^{131}I targeting of CNS ALL, i.e. 5×10^3 to 1×10^6/ml (Table 7.1).

Table 7.1 Variation of radiation dose advantage with leukaemic cell concentration for targeting an individual ^{131}I-radiolabelled antibody.

Cell Concentration (c) (ml^{-1})	Nuclear Volume Fraction (V_V)	Dose Advantage (D_A)
5×10^3	2.618×10^{-6}	1999
1×10^4	5.236×10^{-6}	999
5×10^4	2.618×10^{-5}	200
1×10^5	5.236×10^{-5}	100
5×10^5	2.618×10^{-4}	20.0
1×10^6	5.236×10^{-4}	10.0

Thus, $\mathbf{D_A}$ increases markedly with decreasing cell concentration. Even for a cell concentration of 1×10^6/ml, much greater values of $\mathbf{D_A}$ than in the example given by Humm are obtained.

These values of $\mathbf{D_A}$ apply to an individual ^{131}I-radiolabelled antibody molecule, and will be relevant to the *in-vitro* or clinical situation only if 100% of antibody is bound (as in Humm's calculations). In a situation of antibody excess, the degree of antibody bound should be considered. For a given number of antibody molecules, this will be dependent on both the number of binding sites per cell and the cell concentration. The overall dose advantage, **A**, can be calculated as the ratio of an increased dose, due to a proportion of the activity being targeted, over the dose that would have been received if none of the radiolabel was cell bound. The dose delivered in the first instance

can be obtained by considering it as the sum of two parts; a bound component, enhanced by a factor $(1+D_A)$, and an unbound component with no enhancement. Therefore, **A**, for a given number of radiolabelled antibody molecules (and hence constant activity) for which a varying proportion was bound is given by:

$$A = \frac{B \times [\,1 + D_A\,] + [\,100 - B\,] \times 1}{100 \times 1} \qquad (10)$$

where, **B** is the percentage of activity bound to the cell surface,

hence, **(100-B)** is the percentage of unbound activity

and D_A is the dose advantage for the given cell concentration.

For a cell concentration of 5×10^5/ml, as investigated in the *in-vitro* model, **A** was calculated over a range of **B** of between 0.1 and 50% (Table 7.2).

Figure 7.2 Variation of overall dose advantage due to targeting with per cent of bound radiolabelled antibody, for a cell concentration of 5×10^5/ml.

Per cent Bound (B)	Overall Dose Advantage (A)
0.1	1.02
0.5	1.10
1.0	1.20
5.0	2.00
10	3.00
50	10.99

Thus, for a tumour cell of the above dimensions at a concentration of 5×10^5/ml, the tumour dose will be doubled if 5% of antibody is bound.

The effect of changing cell concentration on overall dose advantage for a constant number of radiolabelled antibody molecules was examined by

consideration of equations **(4)** and **(10)**. This relates to the situation *in-vivo*, in which the same amount of antibody is used to treat varying tumour loads. Assuming antigen saturation, for a given number of antibody molecules the per cent of bound Ig decreases proportionately with decreasing cell number. This parallels the increase in dose advantage, $\mathbf{D_A}$, as a consequence of decreasing nuclear volume fraction, $\mathbf{V_V}$, (Table 7.1). There is therefore no increase in overall dose advantage, **A**.

This is in contrast to the effect of increasing the proportion of cell bound antibody for a given cell concentration. In the *in-vitro* model, bound activity for ^{131}I- labelled antibodies varied between 0.22 and 1.56% over the range of incubated activities. However, higher values of cell-associated activity, of up to 5.87% (1 MBq ^{125}I-WCMH binding to Nalm 6) were noted for ^{125}I conjugates using the same assay system (Chapter 8; 3c). For a cell concentration of 5 x 10^5/ml, a theoretical overall dose advantage of 1.2 and 2.0 is noted for 1.0% and 5.0% antibody binding respectively (Table 7.2).

Such calculated values may give an estimate of the expected advantage of targeting in the liquid phase of the *in-vitro* system. However, in the clinical situation, the proportion of bound activity will probably increase to levels significantly greater than those seen *in-vitro*, as unbound radiolabelled antibody is cleared more rapidly from the CSF.

It is clear from the model that the specificity of targeted therapy can be increased by increasing the number of antigenic sites occupied by conjugate molecules. In turn, this can be achieved by either selecting antibodies binding to a greater number of cell surface epitopes or by using a cocktail of radiolabelled antibodies. This is reflected in data from *in-vitro* investigations (Tables 6.7, 6.10).

An increase in JM cell kill *in-vitro* was observed for ^{131}I-WT1 labelled with increasing specific activity (Table 6.21). Whilst this approach does not increase the proportion of antibody bound to tumour cells, it does enable a

higher percentage of the total radioactivity to be targeted, and thus provides an alternative strategy by which targeting specificity can be increased.

This mathematical model is applicable not only to intrathecal targeting of diffuse leptomeningeal disease, but also to other situations in which compartmentalisation of therapy is appropriate, eg. intraperitoneal therapy for ovarian carcinoma [108]. It gives cause for optimism with regard to the specificity achieved with ^{131}I antibody-mediated therapy against single cell or small volume disease, and provides a theoretical basis by which specificity may be improved.

CHAPTER 8.

IN-VITRO STUDIES OF ^{125}I TARGETED RADIOTHERAPY OF LEUKAEMIA.

1. Introduction.

Radioactive iodine-125 decays by electron capture ($T_{1/2}$ = 60.1 days) to an excited state of tellurium-125, which undergoes immediate decay by internal conversion (93%) or by a 35-keV gamma ray emission (7%) to the tellurium-125 daughter ground state [14]. Due to inner shell vacancies produced, a complex series of electron shell rearrangements occur, resulting in the emission of low-energy X-rays and a cascade of ultra-short range (1 - 20 nm), low energy electrons.

These "Auger" electrons have been shown to cause specific chromosomal damage to dividing cells when nucleotide precursors are radiolabelled with ^{125}I [266] [267], and to result in cell killing by irreversible damage to DNA [268] [269]. It is proposed that the cell killing efficiency of ^{125}I following its incorporation into DNA is similar to that of high LET radiations [270], while extracellular or cell surface bound ^{125}I shows minimal or no damage [267] [271]. Based on such evidence, ^{125}I and other emitters of Auger electrons such as ^{77}Br, have been proposed as suitable radionuclides for use in antibody targeted therapy [92] [93].

It is clear that to obtain tumouricidal effects, ^{125}I-labelled antibodies, in addition to specific cell binding, must undergo significant internalisation into the cell, and that the radionuclide be conveyed to, and probably incorporated within the nucleus [14]. If such requirements are met by the conjugate in respect of the tumour cell target, but not normal tissue, then targeted ^{125}I therapy offers the scope for exquisite specificity of treatment. In this case, radiation dose from the effect of crossfire and from unbound radionuclide will be negligible.

Antigen modulation and internalisation of antibody has been demonstrated for all three antigens targeted in these studies (Chapter 3; 8). Investigation of ^{125}I-labelled antibodies, using the model system described for ^{131}I conjugates, was thus appropriate.

2. Methods.

The methods employed for cell survival assays were identical to those for studies in which leukaemic cells were incubated in tubes with ^{131}I conjugates (Chapter 6; 2). Targeting of both Nalm 6 and JM cell lines was investigated.

3. Results.

(a) ^{125}I targeting of Nalm 6.

Between 1 and 20 MBq of either ^{125}I-WCMH or ^{125}I-HD37 were incubated with Nalm 6 cells in roller tubes for 24 hours and cell survival data compared to that following treatment with control reagents, ^{125}I-UJ13A and Na^{125}I (n=3) (Table 8.1, Figure 8.1). 1 x 1 comparisons of survival curves are depicted in Figure 8.2.

Figure 8.1

Activity response of cell survival for Nalm 6 incubated with ^{125}I-labelled antibodies.

1 x 10^6 Nalm 6 cells were incubated in roller tubes for 24 hours with between 1 and 20 MBq ^{125}I-labelled antibodies (n=3). Mean cell survival (see Figure 6.1) is plotted against activity of incubation. For clarity, confidence limits are excluded (see Figure 8.2, Table 8.1).

Figure 8.1

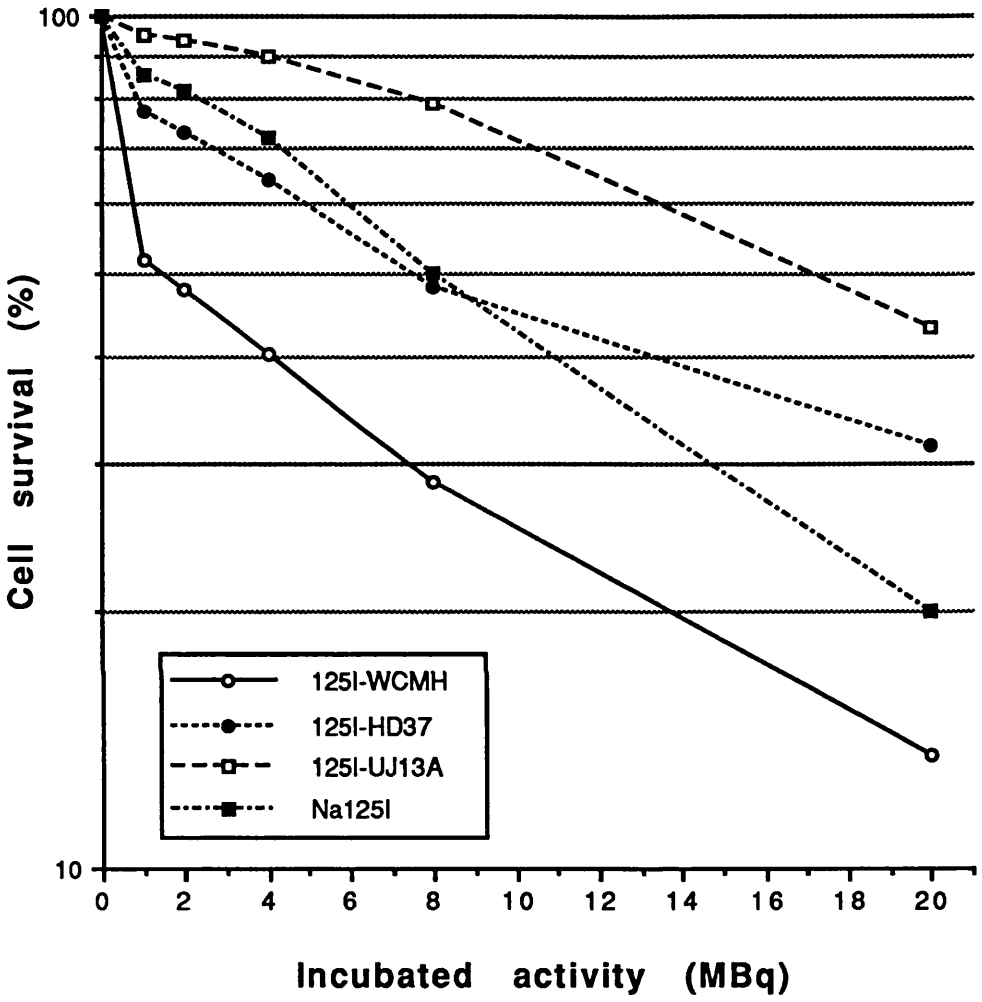
100
10
Cell survival (%)
0
2
4
6
8
10
12
14
16
18
20
Incubated activity (MBq)
125I-WCMH
125I-HD37
125I-UJ13A
Na125I

Figure 8.2

Activity response cell survival for *in-vitro* targeting of Nalm 6. 1 x 1 comparisons of ^{125}I-labelled antibodies (data from Table 8.1).

_____ Mean cell survival

---------- 95% confidence limits

A	=	^{125}I-WCMH	v	^{125}I-HD37
B	=	^{125}I-WCMH	v	^{125}I-UJ13A
C	=	^{125}I-WCMH	v	Na^{125}I
D	=	^{125}I-HD37	v	^{125}I-UJ13A
E	=	^{125}I-HD37	v	Na^{125}I
F	=	^{125}I-UJ13A	v	Na^{125}I

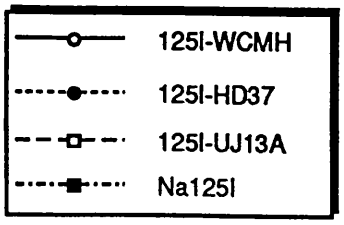

Figure 8.2

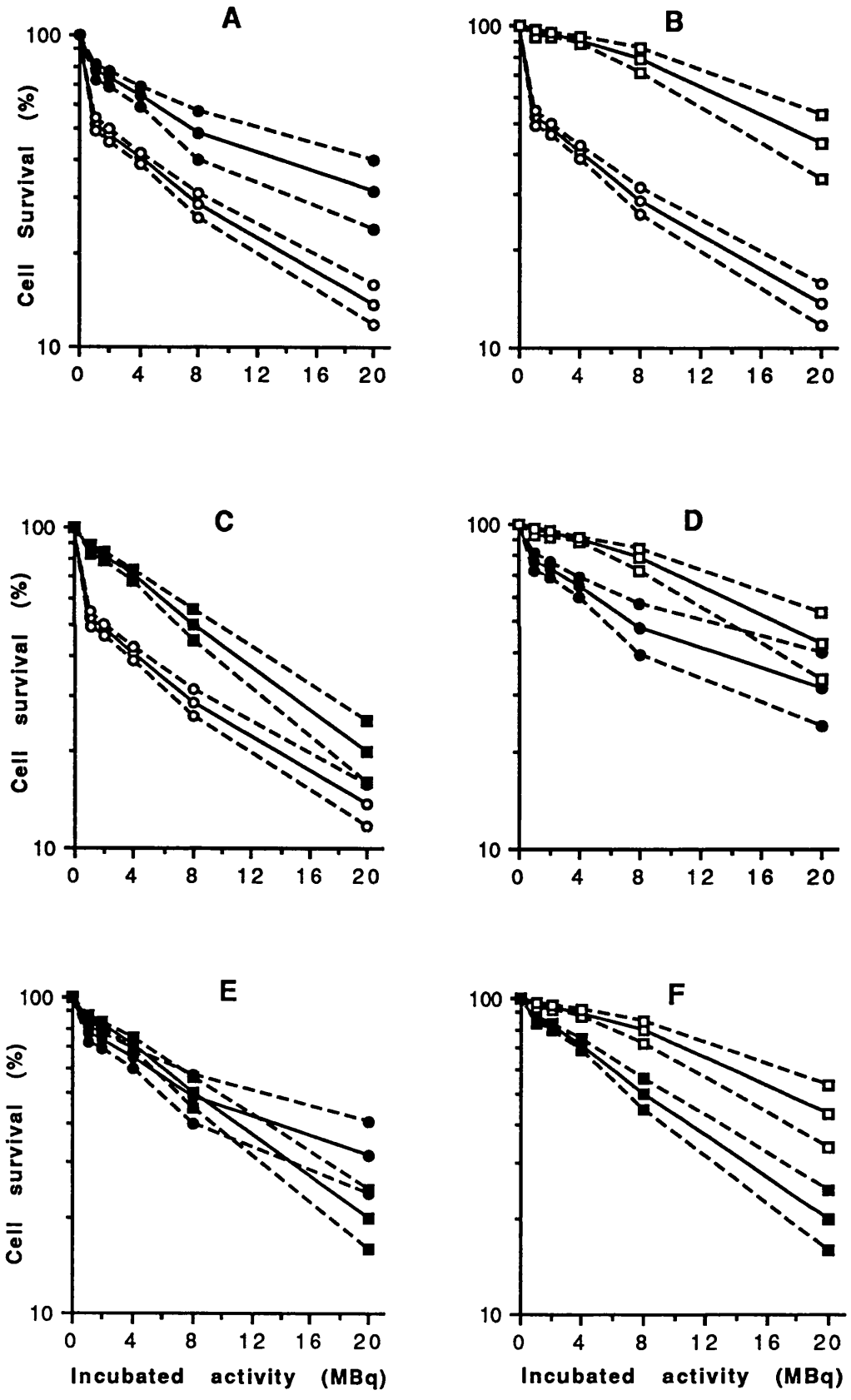
A
B
C
D
E
F
100
10
0
4
8
12
16
20
Cell Survival (%)
Cell survival (%)
Incubated activity (MBq)

Table 8.1 Survival data for Nalm 6 incubated with ^{125}I-labelled antibodies.

Conjugate	Cell Survival (%)				
	Incubated Activity (MBq)				
	1	2	4	8	20
^{125}I-WCMH	[+2.70] *51.76 [-2.71]	[+2.13] 47.80 [-2.12]	[+1.87] 40.22 [-1.84]	[+2.67] 28.50 [-2.53]	[+2.12] 13.64 [-1.88]
^{125}I-HD37	[+4.07] 77.02 [-4.64]	[+3.57] 72.95 [-3.90]	[+4.37] 64.12 [-4.61]	[+8.68] 48.23 [-8.56]	[+8.64] 31.40 [-7.52]
^{125}I-UJ13A	[+1.46] 94.83 [-1.98]	[+1.43] 93.47 [-1.80]	[+1.85] 89.80 [-2.20]	[+5.63] 79.18 [-7.03]	[+9.97] 43.10 [-9.44]
Na^{125}I	[+2.29] 85.66 [-2.64]	[+2.22] 81.66 [-2.45]	[+2.66] 71.65 [-2.82]	[+5.51] 49.88 [-5.51]	[+4.86] 20.11 [-4.12]

* Data is the mean cell survival of three experiments, each consisting of four cultures per activity level. Figures in parentheses represent 95% confidence limits.

A striking feature of the survival curves for cells incubated with specific conjugates is the steep initial gradients between 0 and 1 MBq, this being greater for cells treated with ^{125}I-WCMH than with ^{125}I-HD37. Cell survival was 51.76 and 77.02% for Nalm 6 treated with 1 MBq ^{125}I-WCMH and 1 MBq ^{125}I-HD37 respectively. Thereafter, the curves for both specific conjugates are exponential, with a possible reduced gradient between incubated activities of 8 and 20 MBq. Curves for both control reagents are approximately monoexponential, with possibly increased gradients between 0 and 1 MBq Na^{125}I, and between 8 and 20 MBq ^{125}I-UJ13A.

In contrast to that seen for ^{131}I targeting experiments, the overall gradient of the Na^{125}I curves is much steeper than that for ^{125}I-UJ13A, such that for an

incubated activity of 20 MBq, survival for cells incubated with $Na^{125}I$ is less than that for cells irradiated with ^{125}I-HD37.

For each incubated activity, survival of cells treated with ^{125}I-WCMH was significantly lower ($p < 0.05$) than that for those incubated with ^{125}I-HD37 or with either control reagent. For an incubated activity of 1 MBq, an advantage in cell kill of 1.49, 1.83 and 1.66 was observed for ^{125}I-WCMH over ^{125}I-HD37, ^{125}I-UJ13A and $Na^{125}I$ respectively (Table 8.3).

A mean cell survival of 13.64% was observed for Nalm 6 irradiated with 20 MBq ^{125}I-WCMH as compared with 31.40, 43.10 and 20.11% for ^{125}I-HD37, ^{125}I-UJ13A and $Na^{125}I$ respectively. This amounts to an advantage in cell kill of 2.30, 3.16 and 1.47 fold for ^{125}I-WCMH over ^{125}I-HD37, ^{125}I-UJ13A and $Na^{125}I$ respectively, and 1.56 and 2.14 fold for $Na^{125}I$ over ^{125}I-HD37 and ^{125}I-UJ13A respectively.

(b) ^{125}I targeting of JM.

JM cells were incubated for 24 hours with between 0.5 and 20 MBq ^{125}I-WT1, and cell survival compared with that following treatment with ^{125}I-UJ13A and $Na^{125}I$ (n=2) (Table 8.2). 1 x 1 comparisons of survival curves are depicted in Figure 8.3.

Figure 8.3

Activity response cell survival data for *in-vitro* targeting of JM. 1 x 1 comparisons of ^{125}I-labelled antibodies (data from Table 8.2).

_____ Mean cell survival.

---------- 95% confidence limits.

A = ^{125}I-WT1 v ^{125}I-UJ13A

B = ^{125}I-WT1 v Na^{125}I

C = ^{125}I-UJ13A v Na^{125}I

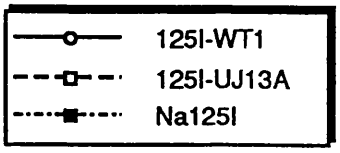

Figure 8.3

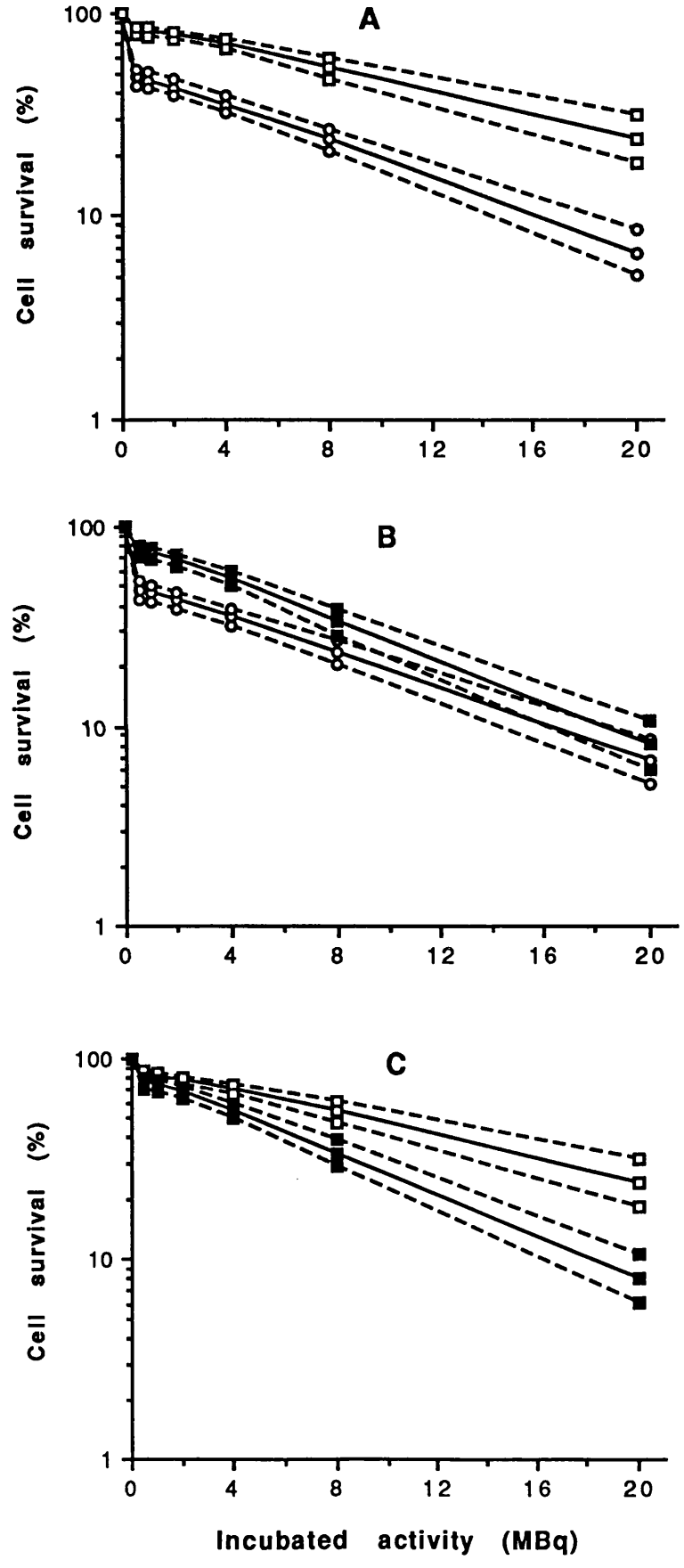
A
B
C
100
10
1
Cell survival (%)
0
4
8
12
16
20
Incubated activity (MBq)

Table 8.2

Survival data for JM incubated with ^{125}I-labelled antibodies.

Conjugate	Cell Survival (%)					
	Incubated Activity (MBq)					
	0.5	1	2	4	8	20
^{125}I-WT1	[+4.80] *48.11 [-4.77]	[+4.52] 46.23 [-4.47]	[+4.04] 42.55 [-3.94]	[+3.38] 35.37 [-3.24]	[+3.18] 23.37 [-2.91]	[+1.90] 6.65 [-1.50]
^{125}I-UJ13A	[+3.37] 82.72 [-3.99]	[+3.34] 81.16 [-3.86]	[+3.27] 77.81 [-3.65]	[+3.57] 70.12 [-3.83]	[+6.23] 54.04 [-6.36]	[+7.39] 24.24 [-6.12]
Na^{125}I	[+4.71] 75.69 [-5.43]	[+4.73] 73.11 [-5.32]	[+4.68] 67.62 [-5.06]	[+4.61] 55.43 [-4.71]	[+5.26] 33.65 [-4.89]	[+2.58] 8.12 [-2.00]

* Data is the mean cell survival of two experiments, each consisting of four cultures per activity level. Figures in parentheses represent 95% confidence limits.

The survival curve for JM incubated with ^{125}I-WT1 was again biphasic, with a steep initial gradient between 0 and 0.5 MBq. The gradient of the curve for cells treated with Na^{125}I was again higher than for cells irradiated with ^{125}I-UJ13A, and higher than that of the second phase of the curve for ^{125}I-WT1. Cell survival was significantly lower ($p < 0.05$) for JM incubated with ^{125}I-WT1 at all activities investigated as compared with ^{125}I-UJ13A, and for activities of between 0.5 and 8 MBq as compared with Na^{125}I. No significant difference was noted in the survival of cells treated with 20 MBq of either ^{125}I-WT1 or Na^{125}I.

For an activity of 0.5 MBq, survival of JM was 48.11, 82.72 and 75.69% for cells incubated with ^{125}I-WT1, ^{125}I-UJ13A and Na^{125}I respectively. Respective mean survivals for a 20 MBq incubated activity were 6.65, 24.24 and 8.12%. The advantage in cell kill for ^{125}I-WT1 as compared with ^{125}I-UJ13A and Na^{125}I was 1.72 and 1.57 respectively for an activity of 0.5 MBq, and 3.64 and 1.22 respectively for an activity of 20 MBq (Table 8.3).

Table 8.3 Advantage in cell kill for specific over control ^{125}I radioconjugates.

Cell Line	Specific Conjugate	Control Conjugate	Incubated Activity (MBq)					
			0.5	1	2	4	8	20
Nalm 6	^{125}I-WCMH	^{125}I-UJ13A	-	*1.83	1.96	2.23	2.78	3.16
		$Na^{125}I$	-	1.66	1.71	1.78	1.75	1.47
Nalm 6	^{125}I-HD37	^{125}I-UJ13A	-	1.23	1.28	1.40	1.64	1.37
		$Na^{125}I$	-	1.11	1.12	1.20	1.03	0.64
JM	^{125}I-WT1	^{125}I-UJ13A	1.72	1.76	1.83	1.98	2.28	3.64
		$Na^{125}I$	1.57	1.58	1.59	1.57	1.42	1.22

* The mean cell survival following incubation with control conjugate is divided by that for cells treated with specific conjugate. See Table 8.1 for Nalm 6 incubations and Table 8.2 for JM incubations.

(c) Determination of cell bound ^{125}I activity.

The activity of ^{125}I bound to cells was determined for Nalm 6 (n=3) and JM (n=1) in a similar fashion to that for ^{131}I targeting experiments (Chapter 6; 3f). Nalm 6 cell bound activity of ^{125}I-WCMH demonstrated saturable binding at all activities, of between 108 and 116 x 10^4 cpm, although the variance for these observations is large (Table 8.4, Figure 8.4). A mean of 42.5 x 10^4 cpm of ^{125}I-HD37 was bound to Nalm 6 for an incubated activity of 1 MBq. Thereafter, in contrast to that observed for ^{131}I-WCMH, binding appeared to increase in a linear fashion to a maximum of 81.4 x 10^4 cpm for an incubated activity of 20 MBq. Binding of both control reagents also increased linearly.

These bound counts are equivalent to a mean of 2.22 and 1.15% of an incubated activity of 1 MBq ^{125}I-WCMH and ^{125}I-HD37 respectively, as compared with 0.09 and 0.01% of ^{125}I-UJ13A and $Na^{125}I$ respectively. For Nalm 6 treated with 20 MBq of conjugate, a mean of 0.2 and 0.08% of ^{125}I-WCMH and ^{125}I-HD37 was bound respectively, in comparison to 0.03% for both control reagents.

As observed for ^{131}I targeting, JM cell bound activity of ^{125}I-WT1 was greater than that for Nalm 6 of ^{125}I-WCMH, reaching 146.7 and 223.3 x 10^4 cpm, which corresponds to 5.87 and 0.22% of total incubated activities of 0.5 and 20 MBq respectively (Table 8.5, Figure 8.5). Apart from one instance (20 MBq $Na^{125}I$), binding of control reagents to JM was similar to that to Nalm 6.

Table 8.4 Nalm 6 bound activity following incubation with ^{125}I-labelled antibodies.

Conjugate	*Cell Bound Activity (x 10^4 cpm) (SD)				
	Total Incubated Activity (MBq)				
	1	2	4	8	20
^{125}I-WCMH	111.0 (48.2)	112.8 (50.0)	115.8 (51.2)	116.0 (50.1)	108.4 (57.0)
^{125}I-HD37	42.5 (12.5)	42.1 (10.4)	48.1 (11.0)	57.6 (12.1)	81.4 (15.3)
^{125}I-UJ13A	4.3 (1.9)	7.0 (2.7)	8.8 (1.2)	17.7 (5.7)	37.1 (10.1)
$Na^{125}I$	1.7 (1.1)	3.4 (1.9)	5.2 (2.8)	9.2 (4.7)	25.9 (3.1)

* Data is the mean of three experiments.

Table 8.5 JM bound activity following incubation with ^{125}I-labelled antibodies.

Conjugate	Cell Bound Activity (x 10^4 cpm)					
	Total Incubated Activity (MBq)					
	0.5	1	2	4	8	20
^{125}I-WT1	146.7	159.0	176.8	182.2	203.3	223.3
^{125}I-UJ13A	2.5	3.4	6.7	17.5	18.3	35.2
$Na^{125}I$	1.2	1.8	1.7	4.0	7.7	8.9

Figure 8.4

Variation of Nalm 6 cell bound activity with activity of incubated ^{125}I-labelled antibodies.

1 x 10^6 Nalm 6 cells, in 2 ml complete medium, were incubated for 24 hours with between 1 and 20 MBq of ^{125}I-labelled antibodies. The mean cell-bound activity (see Figure 6.12) of three experiments is plotted against incubated activity. Error bars represent +/- 1 SD.

Figure 8.5

Variation of JM cell bound activity with activity of incubated ^{125}I-labelled antibodies.

1 x 10^6 JM cells, in 2 ml complete medium, were incubated for 24 hours with between 0.5 and 20 MBq of ^{125}I-labelled antibodies (n=1). Cell bound activity (see Figure 6.12) is plotted against incubated activity.

Figure 8.4

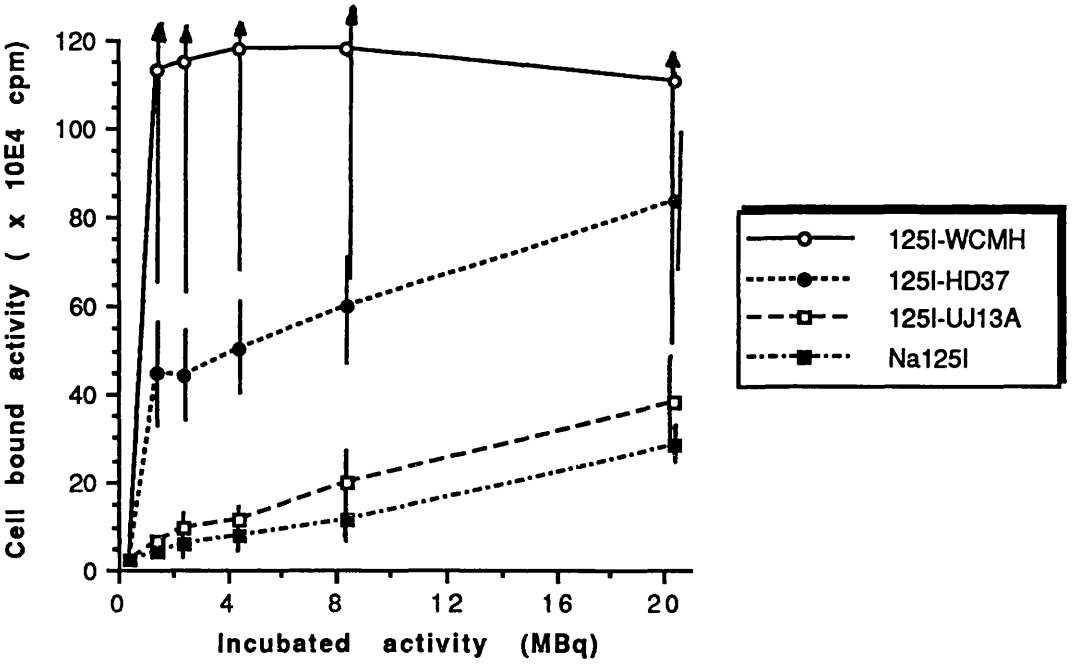

Figure 8.5

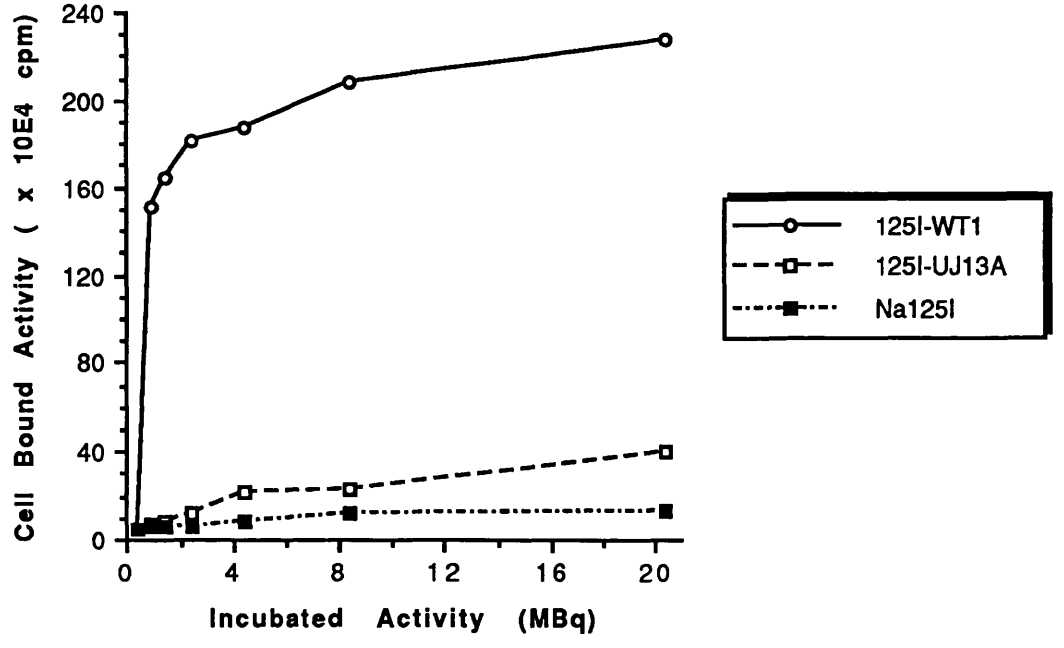

4. Discussion.

Using this assay system, the cytotoxic effect of ^{125}I-WCMH, ^{125}I-HD37 and ^{125}I-WT1 antibody conjugates was clearly demonstrated. This was predicted as internalisation of CD10, CD19 and CD7 antibodies has been observed previously (Chapter 3; 8). An additional factor by which the toxicity of ^{125}I to leukaemic cells may be enhanced is their relatively sparse cytoplasmic content, which, for the majority of lymphoblasts, occupies a space of less than 3 - 4 μm between the nuclear and cell membranes [265]. Thus, at least in respect of passive diffusion, internalised radionuclide may reach the nucleus more readily than for the majority of tumour cells.

The steep initial gradient of the survival curves observed for these reagents probably reflects the degree of cell kill occurring due to saturation of both antigen binding sites and mechanisms involved in antibody internalisation. Saturation of antigen binding sites occurs at lower incubated activities than those used here and thus further studies are required to define this point precisely. An alternative explanation for the shape of the survival curves shapes may be provided by heterogeneity of antigenic expression, for which a proportion of non- or sparsely antigen-expressing cells will be relatively resistant to injury. A similar result would be predicted if heterogeneity of putative internalisation mechanisms also occurred.

Survival data for both JM and Nalm 6 irradiated with ^{125}I-UJ13A illustrate a degree of cell kill. This may result from either non-specific endocytosis, or de-halogenation with passive diffusion of free ^{125}I entering the cytoplasm. We have subsequently observed a much greater degree of *in-vitro* de-halogenation of radioiodine conjugates of UJ13A as compared with that for several other antibodies (Personal Communication, Mr V Papanastassiou, Imperial Cancer Research Fund, Bristol).

The gradient of the survival curves for both JM and Nalm 6 incubated with $Na^{125}I$ was greater than that for the second phase of the curves for cells incubated with each specific conjugate. This probably reflects a continuing process of passive diffusion of ^{125}I into tumour cells, within the range of activities investigated. The probability of incorporation of ^{125}I into leukaemic cell nuclei will again be theoretically greater than for other cell lines by virtue of a paucity of cytoplasm. This may well explain the discrepancy between data from this and other similar studies, in which only minimal cytotoxicity due to free ^{125}I was observed [272]. However, $Na^{125}I$ alone would be unsuitable for clinical use, due to a greatly increased rate of clearance from the CSF, as compared with ^{125}I conjugated to immunoglobulin.

Experiments are planned to confirm the mechanism of antibody internalisation, and to attempt to define the nuclear deposition of ^{125}I. Appropriate techniques include microautoradiography, and acid cell lysis with differential centrifugation of cellular components [14].

For each specific conjugate, cell-bound activity again reached a point of relative saturation at the lowest incubated activity. The per cent cell-associated activity of these ^{125}I-labelled antibodies was, however, consistently greater than that observed for their ^{131}I counterparts (Chapter 6; 3f). This discrepancy may be accounted for by a different epitope density on both Nalm 6 and JM between these two sets of experiments.

In comparison with experiments using ^{131}I-labelled antibodies, a lower cell kill was observed following therapy with ^{125}I conjugates over the range of comparable activities investigated. However, as a result of the different mechanisms of cell damage due to these isotopes, it is possible that at lower activities than those used here, or by using incubation times of less than 24 hours, the cytotoxicity of ^{125}I conjugates may approach or exceed that of their ^{131}I counterparts. Work is planned to generate additional cell survival data from both activity- and time-response experiments. As for ^{131}I-conjugates, it is envisaged

that the use of cocktails of ^{125}I-labelled antibodies will result in a greater cell kill than that associated with single reagents.

With regard to other *in-vitro* studies of ^{125}I targeted therapy, Woo *et al.*, have conducted a series of experiments examining the survival of the human colon carcinoma cell line, SW1116, and the human epidermoid line, A-431, targeted with ^{125}I conjugated to the respective specific antibodies, 17-1a and EGF-425 [14]. Survival curves for both SW1116 and A-431 conformed to an exponential function, with a possible slight "shoulder" on the curve for SW1116. No steep initial phase was noted, despite saturation of ^{125}I-17-1a binding occurring at a radioactivity concentration of 10 μCi/ml and within a one hour time period. At the highest activity concentrations, 40 μCi/ml of ^{125}I-17-1a was associated with a cell survival for SW1116 of approximately 1%, and 30 μCi/ml of ^{125}I-EGF-425 with a survival for A-431 of 0.5%. Incubation of SW1116 cells with a ^{125}I-labelled irrelevant antibody, R11D10, resulted in greater than 90% cell survival. Na^{125}I was not used as a control reagent in these survival experiments. The authors also documented a specific effect of ^{125}I-17-1a on the number of chromosome breaks of SW1116. Based on this data, a clinical programme has been established in which patients with malignant glioma are treated with intra-arterial injections of ^{125}I-EGF-425 as an adjuvant to external beam radiotherapy and surgery [273]. Initial response and toxicity data appears encouraging

In a report by Sugiyama *et al.*, a ^{125}I-labelled antibody was observed to have a specific growth inhibition effect on tumour cell lines expressing a gp 160 surface antigen, which when bound by its specific antibody, also underwent internalisation [274].

These experiments indicate a clinical potential for antibody-mediated ^{125}I therapy of CNS leukaemia, which may have an advantage over targeting of ^{131}I due to reduced radiation doses to normal tissues and improved radiation protection conditions. Investigation of ^{125}I targeted therapy in an animal model appears justified, for which the guinea pig/L_2C meningeal leukaemia model

described in Chapter 9 may be appropriate, as antigen modulation and presumed endocytosis has been demonstrated when L_2C cells are exposed to specific antibody [275].

CHAPTER 9.

AN ANIMAL MODEL FOR THE INVESTIGATION OF TARGETED RADIOTHERAPY FOR CENTRAL NERVOUS SYSTEM LEUKAEMIA.

1. Introduction.

To complement *in-vitro* experimentation, an animal model of leptomeningeal lymphoproliferative disease was developed for the pre-clinical investigation of intrathecally administered targeted radiotherapy. In addition to providing information on both the efficacy and specificity of therapy, the model was established to examine both pharmacokinetics and treatment variables such as dose-response and the effect of repeated therapy. The model selected was that the of B-cell leukaemia, L_2C, injected intrathecally into Strain 2 guinea pigs.

Congdon and Lorenz first described the metastasis of systemically inoculated L_2C to the leptomeninges [276]. In 1974, Perk *et al.*, demonstrated CNS deposits in an animal inoculated intraperitoneally (IP) with L_2C and treated systemically with cyclophosphamide. This drug suppressed systemic disease whilst enabling CNS metastases to develop [277]. The cells metastasised through arachnoid veins on the brain surface and grew extensively along the leptomeninges, only invading through the pia mater into the brain parenchyma at a late stage. This pattern of metastasis has been confirmed by others using this and alternative models of leptomeningeal lymphoproliferative disease [278] [279] [280], and correlates well with that seen in CNS disease of human ALL [132].

Zovikian and Youle demonstrated that direct IT inoculation of L_2C into the cisterna magna produced the same meningeal pattern of growth, but in a shorter time than that previously observed [136]. Intrathecally administered therapy with ricin-A chain conjugated to an anti-idiotypic antibody yielded a mean of 5.5 days prolongation of survival. Interpretation of results from this study was, however, complicated by systemic leukaemia which arose in an unspecified number of animals. Urch *et al.,* modified this model for the investigation of the toxin, saporin, linked to the anti-idiotypic antibody, anti-Id-1 and injected one day after tumour inoculation [281]. Systemic disease was temporarily suppressed by an IP injection of cyclophosphamide (20 mg/kg) on days one and eight, a dose previously shown not to affect the growth of meningeal L_2C leukaemia [282]. All 10 animals receiving anti-Id-1-saporin at a dose of either 5 or 0.5 μg responded to therapy, survived for more than 150 days and were presumed cured. Three out of 10 animals receiving a lower dose of 0.05 μg were long term survivors, whereas those receiving either no therapy or treatment with a control IgG-saporin conjugate, died with systemic leukaemia within 30 days .

A modification of Urch's L_2C meningeal leukaemia model was used to investigate targeted radiation therapy. By the administration of continuous weekly cyclophosphamide, the model was extended further to enable the effect of therapy on the development of CNS leukaemia to its terminal stage.

2. Methods

(a) Leukaemic cells.

The Strain 2 guinea pig lymphoblastic leukaemia, L_2C, arose spontaneously [276], and has been maintained by *in-vivo* passage. All attempts to establish a long-term culture of this cell line have been unsuccessful. Ten cells injected systemically cause leukaemia in all recipient animals, followed by death within four days [283]. L_2C cells express monomeric surface IgM at a density of 1.0 - 1.5 x 10^5 molecules/cell [275] and, in short-term culture, secrete free lambda chain together with small amounts of idiotypic 19S IgM. Immunological studies reveal a close relationship between the L_2C and human B-cell malignancies [204].

Cryopreserved L_2C cells (kindly donated by Dr A Preece, Bristol Royal Infirmary) were recovered, resuspended in RPMI 1640 complete medium, washed and diluted to a viable cell concentration of 5 x 10^5 cells/ml (Chapter 2; 1e, 1f). 200 µl (1 x 10^5 cells) of cell suspension was injected IP into adult Strain 2 guinea pigs. From day seven, the peripheral blood white cell count (WCC) was monitored daily and when greater than 50 x 10^9/litre, the animal was exsanguinated under anaesthesia (ether inhalation). Using an aseptic technique, 15 to 25 ml of blood was obtained by cardiac puncture into a pre-heparinized syringe. White cells were isolated from fresh leukaemic blood by differential density centrifugation on Ficoll-Isopaque at 1000 x g for 15 minutes. The buffy coat was removed, cells washed twice in PBS and diluted in PBS to the required viable cell concentration. Cells for IT injection were used within six hours of harvesting and were more than 95% viable. Cells were cryopreserved in in 10% DMSO/RPMI 1640 complete medium (Chapter 2; 1e).

(b) Monoclonal antibodies.

The monoclonal antibody, anti-Id-1 (Courtesy of Dr M Glennie, Tenovus Research Laboratory, Southampton), a murine IgG_1 specific for the surface IgM idiotype of the L_2C tumour, was raised by Hamblin *et al* [284]. At 37°C, the affinity constant of anti-Id-1 is $1.1 \times 10^9\ M^{-1}$, as demonstrated by Scatchard analysis [275]. Antibody was supplied as either purified material, or was purified from mouse ascites by Protein-A affinity chromatography (Chapter 2; 2b).

The murine IgG_1 monoclonal antibody, M340 [231], was used as a control for therapeutic studies. It recognizes an antigen expressed selectively on neuroectodermal tissue. Both anti-Id-1 and M340 were shown not to bind to normal guinea pig cerebrum or spinal cord, as determined by indirect immunofluorescence (n=3).

(c) Radiolabelling.

Monoclonal antibodies were radiolabelled with ^{131}I using the iodogen technique (Chapter 2; 5a) to a specific activity of 370 MBq/mg protein. The activity of the pooled Sephadex G-25™ gel filtration peak was determined in a Vinten radionuclide assay calibrator and the final radiolabelled product passed through a 0.22 μm Millex™ filter to ensure sterility. For each product, the free iodine content and the immunoreactive fraction (IRF) was determined. For binding assays, fresh L_2C cells were used as the target for ^{131}I-anti-Id-1, and a homogenate of human adult brain was used for ^{131}I-M340 (Chapter 2; 5f). Only those radiolabelled antibodies with an IRF of greater than 50% and a free iodine content of less than 10% were used in subsequent experiments. Conjugates were kept at 4°C and used within six hours of radiolabelling.

(d) Animals.

Pure-bred adult Strain 2 guinea pigs of either sex, weighing between 300 and 700 gm, were supplied from the Animal Unit, University of Bristol Medical School. Studies using radioisotopes were undertaken in a designated controlled area. Experimental animals were ear tagged and inspected daily. All animal experimentation was undertaken under Home Office Project and Personal Licences.

(e) Determination of peripheral blood white cell count.

20 µl of blood was taken by ear vein puncture into heparinized capillary tubes (Hemocaps™, Drummond Scientific Ltd) and diluted in 20 ml Isoton™ together with four drops of Zaponin™ lysing reagent. The mean of two measurements of white cell count was determined using a Model DN Coulter Counter™ (Coulter Electronics Ltd). Full blood count analysis (FBC) (including haemoglobin and platelet concentration and differential white cell count) was undertaken using 150 µl blood, similarly obtained (Courtesy of the Dept. of Haematology, Bristol Royal Infirmary).

(f) Protocol for intrathecal injection.

To induce surgical anaesthesia for IT injections, a combination of Hypnorm™:Hypnovel™:sterile water (1:1:2), at a dose of 4 ml/kg, was injected IP. This gave acceptable muscle relaxation and analgesia. Surgical anaesthesia took 15 minutes to induce and lasted for approximately 45 minutes, full recovery taking between three and four hours.

For the IT injection, a modification of the method of Zovickian and Youle was used [136]. Guinea pigs were anaesthetized, their necks shaved and disinfected with chlorhexidine. With the animal lying prone, the external occipital protuberance was located and a midline 1 cm cutaneous incision made from the protuberance caudially. The head was flexed at 90° to the

spine and a 25-gauge Butterfly™ needle (Butterfly-25 short, venesystem, Abbott Ireland Ltd) was inserted 1 cm below the external occipital protuberance at an angle of 60° to the spine, until the base of the occiput was reached. The needle was inserted below the occiput at an angle of 80° to the spine, through the posterior atlanto-occipital membrane and into the cisterna magna. A change in pressure was detected as the needle passed through the membrane. As soon as CSF was observed, the plastic tubing was clamped using fine artery forceps and 50 - 120 µl of solution injected from a 1 ml syringe via a 25-gauge needle (Gillette) into the side of the tubing. On withdrawal of the needle, the neck was de-flexed and pressure applied over the injection site until the cutaneous incision was closed using a 4/0 silk suture (Ethicon Ltd). All procedures were performed using a strictly aseptic technique.

For therapeutic studies, between 200 and 500 µl of whole blood was taken by ear vein puncture prior to each injection. The serum from each sample was separated by centrifugation and stored at -20°C for subsequent analysis of a guinea pig anti-mouse Ig response. This procedure was repeated at three to four weeks after injection.

(g) Histological techniques.

(i) Preparation of histological material.

Guinea pigs were killed by an IP injection of pentobarbitone (240 mg/kg) and organs removed at post mortem examination, either with or without prior cardio-perfusion. Where appropriate, perfusion was undertaken with 200 ml warm (37°C) 10% buffered neutral formalin (BNF) followed by a similar volume at 4°C. Histological samples (brain, spinal cord and systemic organs) were fixed in 20% BNF for at least a further 24 hours. The brain was cut in coronal section at the level of the mammilary bodies and at the level of posterior trigeminal nerve root. The spinal cord was cut in coronal

section at the levels, $C_{2/3}$ and $L_{4/5}$, and other organs were cut in transverse section. Specimens were placed in metal cassettes and processed on a Histokinette 2000™ automatic tissue processor (Rechert-Jung) prior to embedding in Fibrowax™. 7 μm sections were cut using a Leitz base sledge microtome, placed on albumin/glycerol coated slides and dried overnight at 37°C.

(ii) Staining with haematoxylin and eosin.

Sections were de-waxed in a 60°C oven for three minutes followed by immersion in xylene. Sections were washed sequentially in 100% ethanol (x 2), 70% ethanol and tap water, prior to staining in Capazzi's Haematoxylin for ten minutes. Sections were rinsed with tap water and developed in 1% HCl/70% ethanol for ten seconds, followed by Scott's reagent to "blue". Counter staining was performed using a 2% aqueous solution of eosin (three minutes), prior to sequential immersion in water, 70% ethanol, 100% ethanol (x 2) and xylene (x 2). Cover slips were finally applied using DPX mountant. Sections were examined under an Olympus BH2™ light microscope (x 16 - x 160).

3. Results - Establishment of the Animal Model

(a) Confirmation of the injection technique.

To establish that injection into the cisterna magna, as described above, was a viable route for IT inoculation, 100 µl of methylene blue was injected into the cisterna magna of 15 animals. Five to 10 minutes later, the animal was killed, followed by cardiac perfusion and extraction of the brain and spinal cord. Dye was seen along the needle tract, with staining of the surrounding tissues to a depth of up to 2 mm. On cutting the brain, dye was confined to the ventricles and sub-arachnoid space. On no occasion was dye observed within the brain parenchyma. Dye was also present within the spinal sub-arachnoid space, usually to the lower thoracic level, further caudal extension of dye probably being prevented as a result of the short time between injection and death.

(b) Pattern of L_2C growth following systemic inoculation.

20 guinea pigs were systemically (IP) inoculated with 10^5 fresh L_2C cells to expand tumour cell stocks and provide material for IT injection. Systemic leukaemia (WCC greater than 30 x 10^9/litre) was demonstrated at between 10 and 17 days (mean = 13.2 days) (Table 9.1).

Table 9.1 Development of systemic leukaemia in guinea pigs following IP injection of 10^5 L_2C cells.

Time Taken for WCC to Exceed 30 x 10^9/litre (days)	Number of Animals
10	2
11	2
12	3
13	5
14	3
15	2
16	2
17	1

Three animals in the terminal stage of leukaemia were killed and subjected to post mortem examination. In each case, the spleen was grossly enlarged, providing an additional sign of systemic disease. Systemic organs (liver, spleen, kidney and lung) were noted to be heavily infiltrated with tumour in all cases (Figure 9.1). On two occasions, examination of the brain and spinal cord (days 14 and 15) revealed no evidence of leptomeningeal or parenchymal leukaemia.

(c) Pattern of L_2C growth following intrathecal inoculation.

10^5 fresh L_2C cells, in 100 µl PBS, were injected intrathecally into eight guinea pigs. All animals recovered from anaesthesia and remained well following injection until the development of systemic leukaemia. A WCC greater than 30 x 10^9/litre was noted in seven animals at between 13 and 17 days (mean = 15.3 days) after inoculation (Table 9.2). Leukaemia failed to develop in one animal who remained well for over 100 days.

Figure 9.1

Light microscopy photographs of guinea pig organs, 14 days after systemic inoculation of 10^5 L_2C cells.

Liver, spleen, kidney and lung were removed at post mortem examination. Tissue sections were stained with haematoxylin and eosin (magnification x 290). Heavy leukaemic infiltration of each organ is demonstrated.

A = Lung (a = alveolar space)

B = Liver

C = Kidney (g = glomerulus, t = tubule)

D = Spleen

Figure 9.1

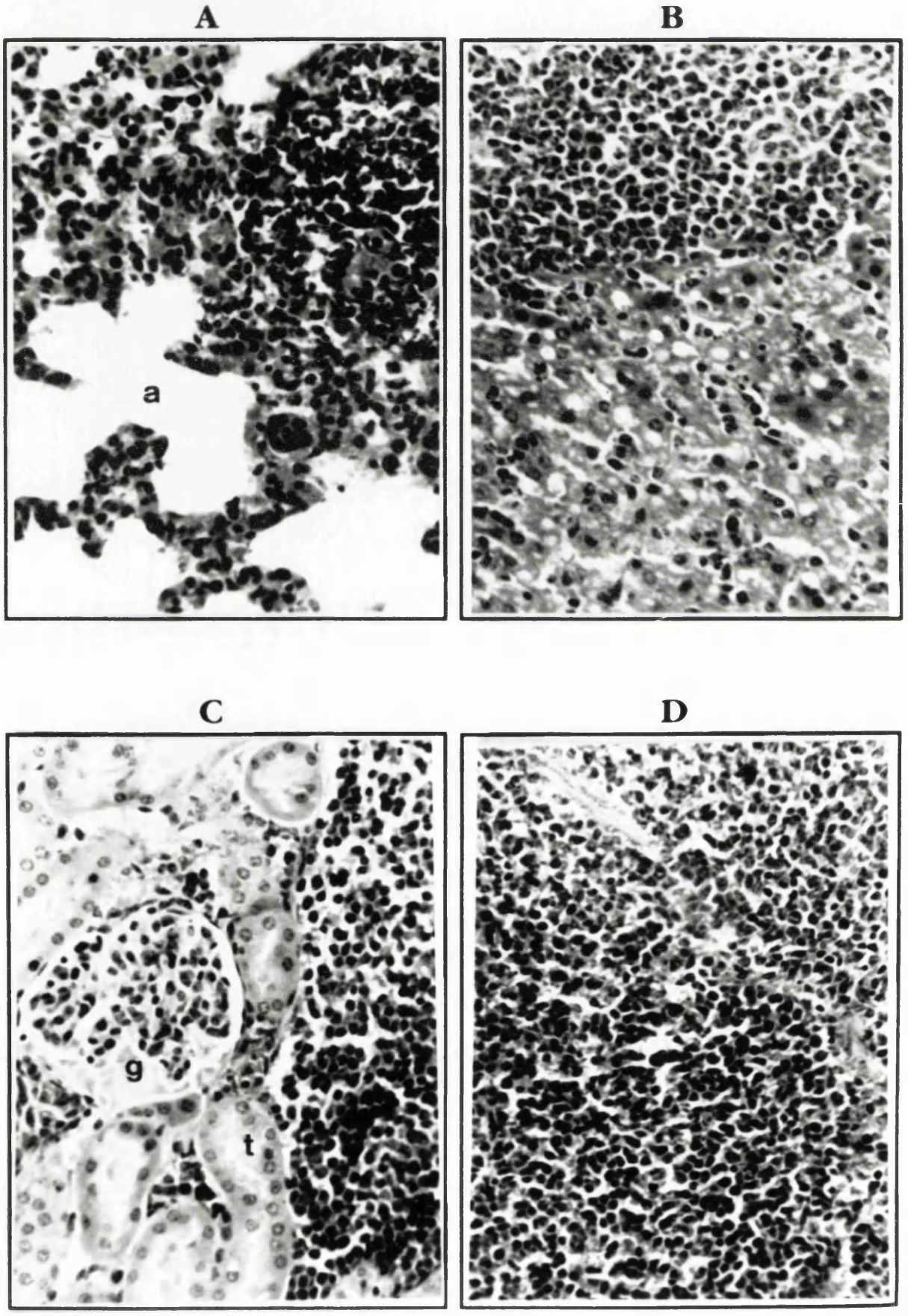

Table 9.2 Development of systemic leukaemia in guinea pigs following IT injection of 10^5 L_2C cells.

Time Taken for WCC to Exceed 30 x 10^9/litre (days)	Number of Animals
13	2
14	1
15	1
16	1
17	1
18	0
19	1

Four animals were subjected to post mortem examination at 14 to 19 days after IT inoculation. In each case, the spleen was grossly enlarged and microscopic tumour infiltration was noted in the spleen, liver, kidney and lung. Examination of both the cerebrum and hindbrain demonstrated leptomeningeal infiltration of tumour, with extension along the Virchow-Robin spaces. Leukaemia cells were also observed within blood vessels, with occasional evidence of tumour extravasation. Apart from this, no tumour penetration of the brain parenchyma was seen (Figure 9.2). A similar pattern was noted on examination of the cervical and lumbar spinal cord, again with no evidence of parenchymal disease.

In order to investigate further the natural history of CNS leukaemia following IT inoculation of L_2C cells, the *in-vitro* model was modified as described by Urch *et al.* [281]. Five guinea pigs received an IT injection of 10^5 fresh leukaemic cells. On days one and eight following tumour inoculation, animals were injected IP with 20 mg/kg cyclophosphamide (1 ml/kg). This was given to suppress or eradicate L_2C cells seeding from the needle tract at the time of injection. As a result, the appearance of systemic leukaemia was

Figure 9.2

Light microscopy photograph of guinea pig brain, 14 days after IT inoculation of 10^5 L_2C cells.

Tissue section stained with haematoxylin and eosin. Leptomeningeal infiltration of tumour is demonstrated, but there is no evidence of parenchymal extension (magnification x 290).

b = brain, t = tumour, sas = subarachnoid space.

Figure 9.2

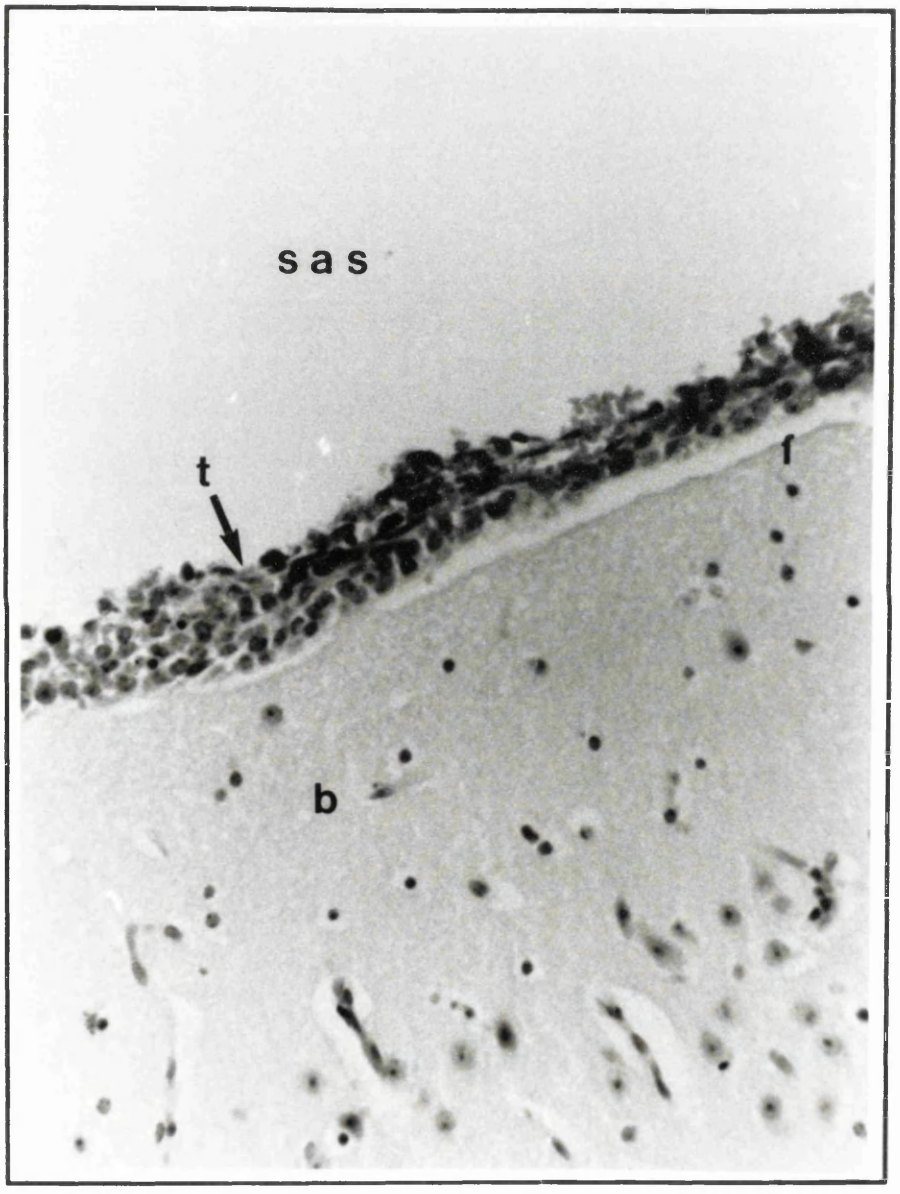

presumed to arise from leptomeningeal tumour re-seeding the systemic circulation.

This group remained well until the development of systemic leukaemia (WCC greater than 30 x 10^9/litre) in all animals on days 23 to 27 (mean 25.2 days). Histological examination of the CNS revealed more extensive leptomeningeal infiltration than that observed previously. Penetration of leukaemic cells into the brain parenchyma was also noted, appearing predominantly as either extension of disease from Virchow-Robin spaces or as perivascular cuffing, often several cells thick (Figure 9.3 A). Penetration of the pia and ependymal layers was also noted (Figure 9.3 B). Extension of leptomeningeal disease was also observed on examination of both cervical and lumber spinal cord, again with evidence of parenchymal infiltration (Figure 9.3 C).

To follow the progression of CNS leukaemic to its terminal stage, six guinea pigs received an IT injection of 10^5 fresh L_2C cells, followed by a weekly IP injection of 20 mg/kg cyclophosphamide, commencing on day one. The WCC was monitored once or twice weekly. CNS leukaemia failed to develop in one animal. The other five showed signs of disease after approximately 30 days, manifest by loss of appetite, gradually progressive lethargy and loss of weight. A normal WCC and no other neurological signs were recorded until the onset, over two to three days, of rapidly progressive paralysis. This was followed by death within five days, at 61, 63, 66, 68 and 69 days after tumour inoculation. Histological examination in each case revealed massive infiltration of tumour cells throughout the parenchyma of both brain and spinal cord (Figure 9.4). At death, the spleen was normal in size or slightly enlarged, with no evidence of leukaemic infiltration.

Figure 9.3

Light microscopy photographs of guinea pig CNS, 26 days after IT inoculation of 10^5 L_2C cells.

Tissue sections stained with haematoxylin and eosin.

A = Marked perivascular cuffing of tumour cells (magnification x 290).

B = Leptomeningeal infiltration of the brain, with tumour penetration of the pial-glial membrane (magnification x 733).

C = Leptomeningeal infiltration of the cervical spinal cord, with tumour penetration of parenchyma (magnification x 733).

Figure 9.3

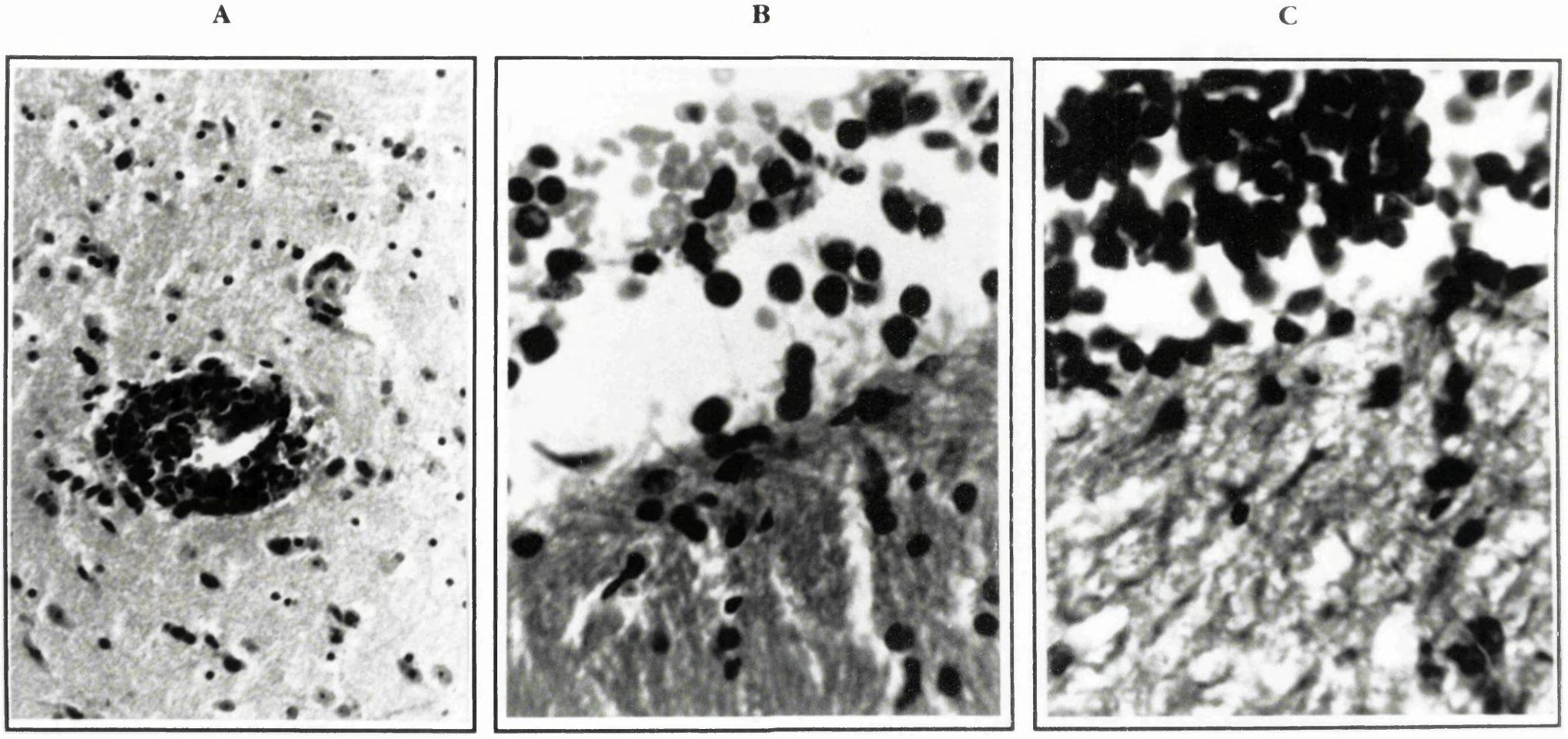

Figure 9.4

Light microscopy photographs of guinea pig CNS, 66 days after IT inoculation of 10^5 L_2C cells.

Tissue section stained with haematoxylin and eosin. Massive tumour cell infiltration of parenchyma is demonstrated.

A = Cerebrum (magnification x 116).

B = Cervical spinal cord (magnification x 290).

Figure 9.4

A

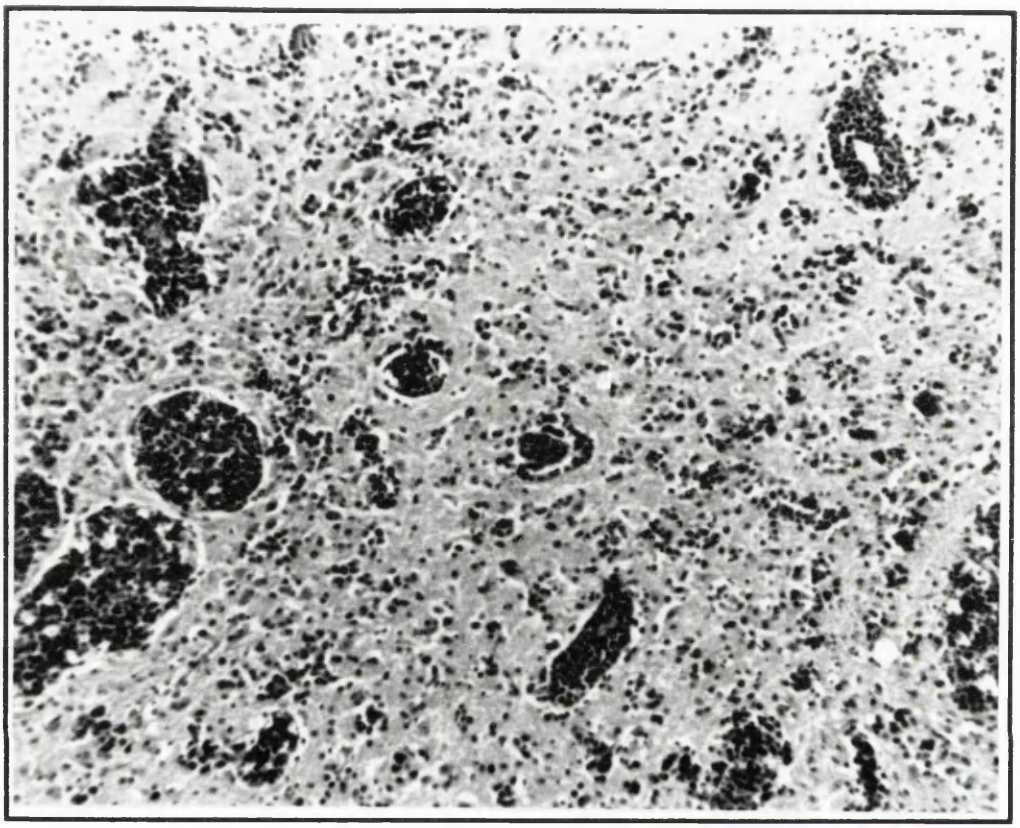

B

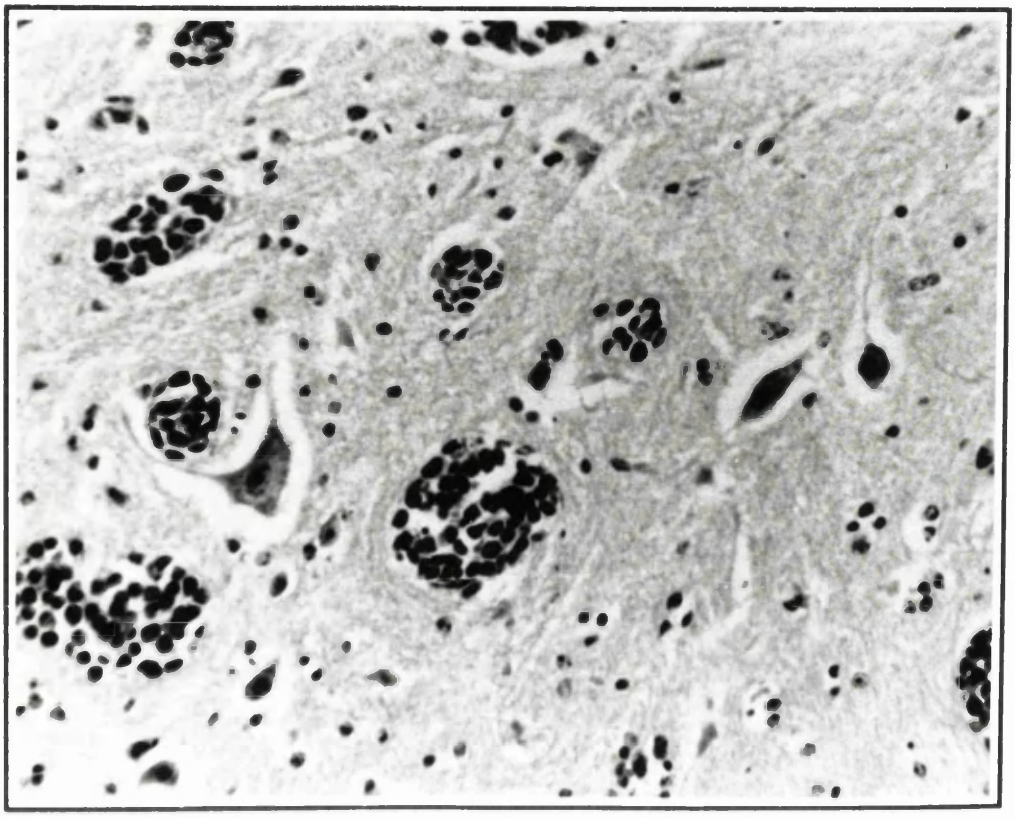

4. Therapeutic Studies.

(a) Intrathecal ^{131}I-anti-Id-1 therapy of CNS L_2C leukaemia in guinea pigs receiving cyclophosphamide on days 1 and 8.

Initial experiments designed to investigate the efficacy and specificity of ^{131}I-anti-Id-1 were based on those undertaken by Urch *et al.* (see above). Twelve guinea pigs were inoculated with 10^5 fresh L_2C cells in 100 µl PBS. After 24 hours, animals received a further IT injection of either ^{131}I-anti-Id-1 (n=3) or a control reagent (n=9). Controls consisted of PBS alone (n=3), ^{131}I-M340 (n=2), Na^{131}I (n=2) or 26 µg non-radiolabelled anti-Id-1 (n=2). 4.9 MBq (26 µg protein) ^{131}I was administered, an activity chosen to result in an equivalent activity concentration within the CSF to that in patients receiving 1480 MBq, assuming an adult human CSF volume of 150 ml and a guinea pig CSF volume of 500 µl [285]. Animals received 20 mg/kg IP cyclophosphamide on days one and eight and the peripheral blood WCC was monitored on alternate days from day 12. Where possible, animals were killed if death appeared imminent (less than one day).

Table 9.3

Survival of guinea pigs following IT injection of ^{131}I-anti-Id-1 one day after IT inoculation of L_2C cells.

Animal Number	Injected Reagent	Survival (days)	
		Experiment 1: Injected Activity 4.9 MBq	Experiment 2: Injected Activity 9.9 MBq
1 2 3	PBS	24 23 24	25 24 32
4 5 6	^{131}I-anti-Id-1	25 25 25	25 26 26
7 8	^{131}I-M340	26 25	26 26
9 10	Na^{131}I	24 31	24 24
11 12	Anti-Id-1	23 25	24 32

No difference in survival was observed between animals in any treatment group (Table 9.3). In addition, no differences were noted between the overall survival of this group and that of previously untreated animals.

This experiment was repeated using an increased injected radioactivity of 9.9 MBq (52 μg protein). No difference was again noted in survival time between treatment groups, or in survival of these 12 animals in comparison with those receiving either an injected activity of 4.9 MBq ^{131}I or no IT therapy (Table 9.3). No toxicity was observed on inspection of guinea pigs in either

experiment prior to the development of systemic leukaemia. No instance of a WCC of less than 3.0 x 10^9/litre was recorded in animals receiving an injected activity of 4.9 MBq. Only three animals treated with 9.9 MBq ^{131}I were noted to have a fall in WCC to less than 3.0 x 10^9/litre, as determined by measurement with either a DN Coulter Counter™ or by FBC analysis on days 11 and 16. In no case was the haemoglobin concentration less than 13.0 gm/dl or the platelet concentration less than 200 x 10^9/litre. Histopathological examination of the CNS in animals receiving ^{131}I-anti-Id-1 (n=2) revealed a similar degree of leptomeningeal infiltration to that of untreated controls.

These experiments reveal a lack of efficacy for IT ^{131}I therapy in preventing leptomeningeal leukaemia seeding the systemic circulation. However, it was also apparent that dose-limited toxicity had not been reached using injected activities of up to 9.9 MBq.

(b) Intrathecal ^{131}I-anti-Id-1 therapy of CNS L_2C leukaemia in guinea pigs receiving continuous cyclophosphamide.

A further series of therapeutic experiments were undertaken in which CNS leukaemia was allowed to develop to its terminal stage by the continuous weekly IP administration of 20 mg/kg cyclophosphamide. The effect of increased injected activities of ^{131}I and of repeated therapy, was investigated. Survival in treated animals was compared with those receiving PBS, a comparison with radiolabelled control antibodies being withheld until the efficacy of specific conjugate therapy could be demonstrated. The WCC was monitored at weekly intervals.

A relatively short interval (one to five days) between the development of paralysis and death was noted previously in animals receiving continuous cyclophosphamide. As a result, paralysis was taken as the end point for the determination of guinea pig survival, following which the animal was sacrificed.

(i) IT therapy on days 1 and 29.

Twenty guinea pigs were inoculated with 10^5 fresh L_2C cells. After 24 hours, animals received a further IT injection of either 20 MBq ^{131}I-anti-Id-1 (n=14) or PBS (n=6), in a volume of 120 µl. On day 29 following L_2C inoculation, seven of the treatment group received a further injection of 20 MBq ^{131}I-anti-Id-1 and seven, PBS alone. At this time, PBS was administered to control animals, one of which died during anaesthesia.

Table 9.4

Survival of guinea pigs following ^{131}I-anti-Id-1 therapy on days 1 and 29 after IT inoculation of L_2C cells.

IT Therapy	Animal Number	*Survival (days)
PBS - Days 1 and 29	1	58
	2	69
	**3	-
	4	61
	5	80
	6	72
20 MBq ^{131}I-anti-Id-1 Day 1 PBS - Day 29	7	79
	8	69
	9	82
	10	91
	11	80
	12	71
	13	65
20 MBq ^{131}I-anti-Id-1 Days 1 and 29	14	76
	15	72
	16	80
	17	71
	18	59
	19	58
	20	58

* Defined as time to onset of paralysis.

** Died during anaesthesia on day 29.

Survival of controls ranged between 58 and 80 days (mean = 68.0 days), consistent with that observed previously (Table 9.4). In the treatment groups, a slightly increased survival for those receiving a single injection of active conjugate of between 65 and 91 days (mean = 76.7 days), was observed. The survival of guinea pigs receiving two injections of conjugate was, however, between 58 and 80 days (mean = 67.7 days), identical to that of controls. There were no significant differences ($p > 0.05$) between these three groups in terms of survival (Mann Whitney U test).

Despite the increased activity of ^{131}I administered, little evidence of myelosuppression was observed. A WCC of less than 3.0×10^9/litre was noted at between 21 and 28 days in four animals receiving ^{131}I and in one control. No similar leucopaenia was noted following the second therapy injection, nor were there signs of myelosuppression on inspection of any animal.

(ii) IT therapy on days 21 and 44.

The efficacy of IT ^{131}I-anti-Id-1 administered on days 21 and 44 was investigated in a similar fashion to that described for therapeutic injections on days 1 and 29. 20 MBq ^{131}I-anti-Id-1 was administered to 14 guinea pigs on day 21, seven of these receiving a further injection of 20 MBq ^{131}I-anti-Id-1 on day 44. The remaining seven were injected with PBS. Six control animals were give two injections of PBS, one of which died during anaesthesia on day 21.

Table 9.5

Survival of guinea pigs following ^{131}I-anti-Id-1 therapy on days 21 and 44 after IT inoculation of L_2C cells.

IT Therapy	Animal Number	*Survival (days)
PBS - Days 21 and 44	1	70
	2	61
	3	59
	4	72
	5	69
	**6	-
20 MBq ^{131}I-anti-Id-1 Day 21 PBS - Day 44	7	57
	8	62
	9	62
	10	65
	11	78
	12	86
	13	84
20 MBq ^{131}I-anti-Id-1 Days 21 and 44	14	64
	15	85
	16	58
	17	84
	18	85
	19	77
	20	85

* Defined as time to onset of paralysis.

** Died during anaesthesia on day 21.

Control animals survived for between 59 and 72 days (mean = 66.2 days), comparable with previous observations (Table 9.5). Guinea pigs treated with a single injection of conjugate survived for a slightly longer period, of between 57 and 86 days (mean = 70.6). Survival in animals receiving two therapeutic injections was increased further at between 58 and 85 days (mean = 76.9). However, differences in survival between any of these groups were not statistically significant ($p > 0.05$, Mann Whitney U Test). Again, there was little

evidence of myelosuppression, a WCC of less than 3.0 x 10^9/litre only being noted in three animals.

(iii) IT therapy on days 14, 21 and 28.

As a result of the lack of both response and major toxicity in either of the experiments described above, a further study utilised even higher injected activities of ^{131}I. In addition, the effect of therapy injected at different time points to those used previously, namely 14, 21 and 28 days, was examined.

10^5 fresh L_2C cells were inoculated into four groups of six guinea pigs. Pre-therapy WCC's were normal (> 3.0 x 10^9/litre) in all animals. Control animals (Group A) received three injections of 100 µl PBS on days 14, 21 and 28. Test animals were administered 50 MBq ^{131}I-anti-Id-1 (100 - 120 µl) on day 14 (Group B), days 14 and 21 (Group C) or on days 14, 21 and 28 (Group D). Survival was again defined as the time to onset of paralysis.

Table 9.6

Survival of guinea pigs following ^{131}I-anti-Id-1 therapy on days 14, 21 and 28 after IT inoculation of L_2C cells.

Group	Therapy	Animal Number	Survival (days)
A	PBS - Days 14, 21 and 24	1 2 3 4 5 6	44 58 63 56 51 58
B	50 MBq ^{131}I-anti-Id-1 Day 14 PBS - Days 21 and 28	7 8 9 10 11 12	62 65 79 51 58 >200
C	50 MBq ^{131}I-anti-Id-1 Days 14 and 21 PBS - Day 28	13 14 15 16 17 18	71 65 60 57 50 >200
D	50 MBq ^{131}I-anti-Id-1 Days 14, 21 and 28	19 20 21 22 23 24	60 65 70 >200 78 72

Controls survived for between 44 and 63 days (mean = 55.0 days) (Table 9.6). This represents a significantly shorter overall survival time than that for the nine control animals in the two previous experiments ($p < 0.005$, Mann Whitney U test). The guinea pig dying at 44 days demonstrated typical progression of disease, with a rapid development of severe paralysis followed

by death within two days. Post mortem examination in this animal revealed no cause of death other than that due to extensive tumour infiltration of the parenchyma of the brain and spinal cord. In each of groups B, C and D, one guinea pig remained alive and well at more than 200 days following tumour inoculation and was presumed cured.

Of the remaining five animals in each group, survival in group B ranged between 51 and 79 days (mean = 63.0 days), in group C between 57 and 71 days (mean = 62.2 days) and in group D between 60 and 78 days (mean = 70.6 days). Statistical analysis was undertaken by Dr D Altman (Medical Statistics Laboratory, Imperial Cancer Research Fund, London) using logrank tests to compare survival times in the four groups. In the first analysis, A v B v C v D was compared, giving a chi squared value of 9.63 on three degrees of freedom, giving $p = 0.02$. The survival times of group A was then compared with those of group B, C or D. This gave a chi squared value of 9.27 on one degree of freedom, giving $p = 0.002$. Finally, B v C v D was compared resulting in a chi squared value of 0.62 on two degrees of freedom, giving $p = 0.73$. This analysis indicates that treated guinea pigs survived longer than those untreated, but there is no evidence to suggest differences between groups B, C and D.

Despite the level of radioactivity administered, a surprising lack of toxicity was observed. No signs of acute toxicity were documented following any injection in terms of behavioural changes. Peripheral WCC, recorded at weekly intervals, only fell to between 2.0 and 3.0 x 10^9/litre in six animals (one group A, two group B and three group D) with no signs of myelosuppression observed. Apart from signs of CNS leukaemia, no other toxicity was documented in any case, either on inspection or on post mortem examination.

A guinea pig anti-mouse Ig assay is being developed. Both pre- and post-injection blood samples have been collected and stored for subsequent analysis.

5. Pharmacokinetic Studies.

Experiments were undertaken to determine the clearance kinetics of radiolabelled IgG from the guinea pig subarachnoid space and vascular compartments. Similar investigations of an IgM conjugate were performed to determine whether the CSF clearance of this molecule is delayed relative to that of IgG, potentially resulting in a larger radiation dose to the CSF and tumour cells.

(a) Scintigraphic examination following IT injection of radioconjugates.

It was intended to use gamma camera scintigraphy as a modality for studying the biodistribution of intrathecally injected radiolabelled antibodies. In a preliminary experiment, 10 MBq (100 µl) of ^{131}I-anti-Id-1, ^{131}I-M340 or Na^{131}I was injected into two non-tumour-bearing guinea pigs. 90 minutes after injection, animals were imaged on a General Electric Maxicamera II™ using a high energy collimator, interfaced with a Links Systems MAPS 2000™ computer using Med 256™ software. At this time, no animal had passed urine. The mean of three whole body counts (acquisition time 120 seconds) was recorded. Region of interest analysis was not possible. Scanning revealed isotope limited to the craniospinal axis in all animals receiving either ^{131}I-anti-Id-1 or ^{131}I-M340. In contrast, a significant proportion of isotope was present in the systemic circulation and abdominal organs, probably concentrating in the stomach, in guinea pigs injected with Na^{131}I, confirming its rapid clearance from the CSF (Figure 9.5).

Imaging was repeated at 115 and 210 hours after injection. In animals receiving either antibody conjugate, scanning revealed a dense concentration of residual isotope in the CNS at 115 hours together with a lower level of systemic activity, which cleared by 210 hours. At 210 hours, the majority of

Figure 9.5

Scintigrams of guinea pigs following IT injection of radioconjugate.

10 MBq of either ^{131}I-anti-Id-1 or Na^{131}I was injected intrathecally into guinea pigs. Images were taken at 1.5, 115 and 210 hours post injection. Acquisition times were 120, 180 and 300 seconds respectively (see text- images for animals injected with ^{131}I-M340 are not shown).

Figure 9.5

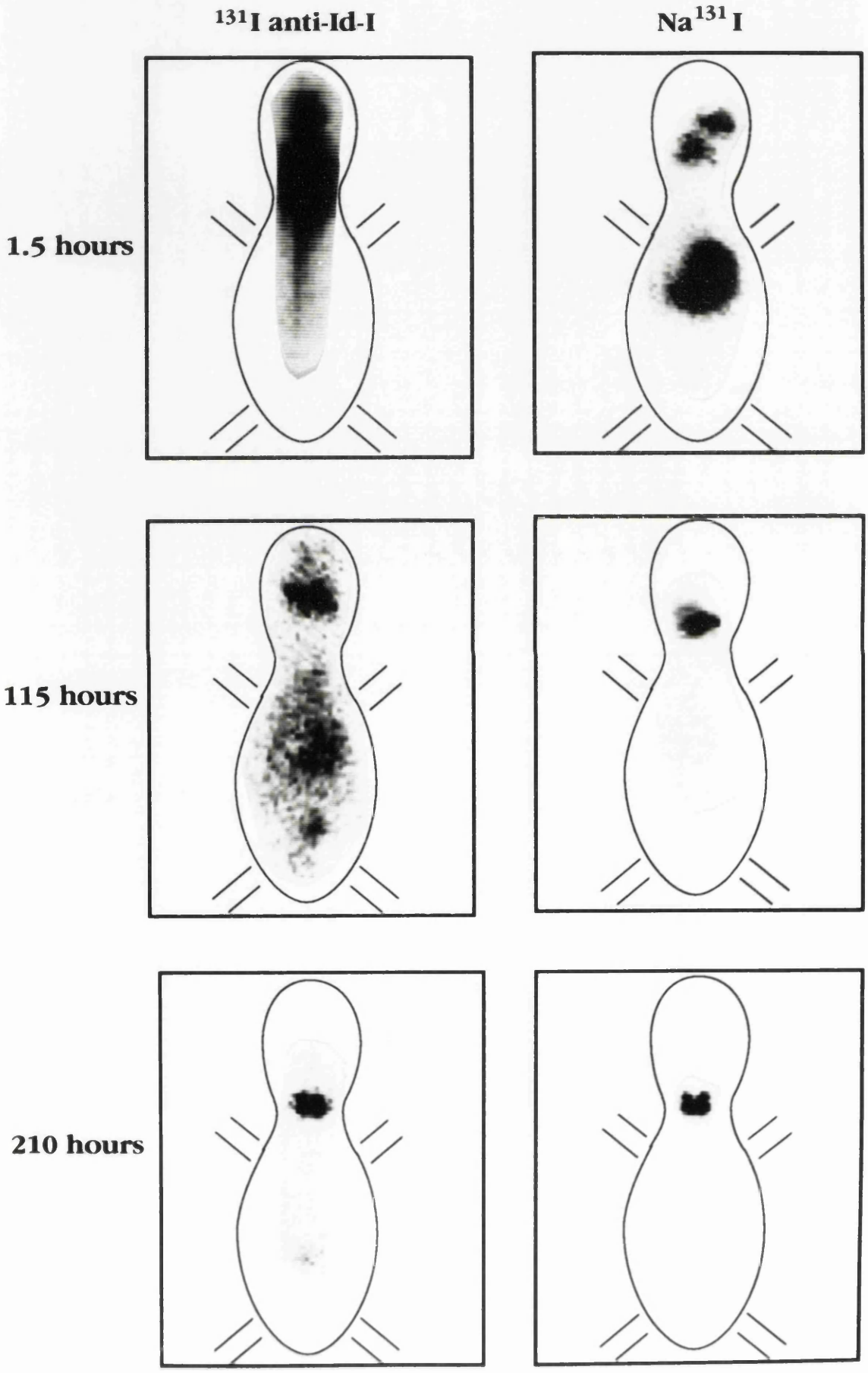

residual activity appeared to be concentrated in the unblocked thyroid gland. Residual brain activity was also noted at 115 hours following injection of $Na^{131}I$, with marked thyroid uptake at 210 hours. Systemic activity was less evident, presumably as a result of rapid clearance.

The mean biological whole body retention at 115 hours was 30.8 (SD = 5.8), 25.4 (3.1) and 12.2 (3.5)% for ^{131}I-anti-Id-1, ^{131}I-M340 and $Na^{131}I$ respectively. At 210 hours respective values were 16.5 (2.1), 15.4 (2.9) and 11.6 (1.5)%. More frequent imaging was precluded, making detailed analysis of whole body clearance rates unreliable.

The use of the gamma camera facility was subsequently withdrawn and thus further pharmacokinetic work was based upon the clearance of isotope from the blood.

(b) Determination of blood clearance kinetics of IgG and IgM radioconjugates.

(i) Methods

(ia) Antibodies.

The murine IgG, WCMH, and IgM, RFAL3 [286], were used in pharmacokinetic experiments. Both recognise the CD10 (CALLA) antigen, which is not expressed on normal guinea pig cerebrum or spinal cord, as determined by indirect immunofluorescence (n=2). The RFAL3 hybridoma was obtained from the European Collection of Animal Cell Cultures, Porton Down. Antibody was produced in mouse ascites (Chapter 2; 1).

To purify RFAL3, the Ig fraction was initially isolated by precipitation with ammonium sulphate (Chapter 2; 2a). To remove contaminating IgG, the Ig solution was subjected to Protein-A affinity chromatography (Chapter 2; 2b), and the unbound fraction collected and dialysed against PBS at 4°C overnight. The antibody solution was analysed by FPLC Superose-12™ gel

filtration (Chapter 2; 3h). This demonstrated a large peak, equivalent in molecular weight to IgM, as determined by an IgM standard on FPLC gel filtration using a Sephacryl S-300 HR™ column. A smaller peak of 150 kDa was also noted. The Ig solution was thus concentrated to approximately 10 mg/ml and re-subjected to FPLC gel filtration. The fractions of equivalent molecular weight to IgM were pooled, re-analysis revealing a single high molecular weight species. A biological activity of RFAL3 of at least 1/100 was noted by indirect immunofluorescence on the cell line, Nalm 6 (Chapter 2; 4c).

(ib) Radiolabelling.

Both WCMH and RFAL3 were labelled with ^{131}I using the iodogen technique (Chapter 2; 5a) to a specific activity of 185 MBq/mg protein. RFAL3 was found to radiolabel satisfactorily, with a resulting immunoreactive fraction of at least 40% (n=5). In all experiments, the free iodine content of conjugates was less than 10%.

(ic) Determination of radioactivity in blood.

At pre-determined intervals after either IT or IV injection of radioconjugate, 100 µl of blood was sampled by ear vein puncture into pre-heparinized capillary tubes (Hemocaps™, Drummond Scientific Ltd) and transferred to 1 ml conical test tubes. Samples were counted in a gamma counter and the radioactivity, given as counts per minute (cpm), corrected for physical decay to give biological activity, using the equation:

$$\mathbf{cpm_{corrected} = cpm_{uncorrected} \times 10^{1.5609 \times 10^{-3} \times t}}$$

where,

t = time of counting from injection (hours).

$\mathbf{1.5609 \times 10^{-3}}$ = the decay constant (base 10) for ^{131}I.

Activity in MBq/ml was calculated (Chapter 2; 5c), and the total whole blood radioactivity was determined assuming a blood volume of 6.96 ml/100 gm body weight [287]. This was expressed as a percentage of the injected activity. Time-activity concentration curves were then constructed.

Curve fitting was undertaken in collaboration with Dr A Renwick (Clinical Pharmacology Group, University of Southampton) using the ELSFIT™ software package on an IBM P2™ computer. This program generates absorption ($\mathbf{k_a}$) and elimination ($\mathbf{k_e}$) rate constants by the "method of residuals" [288] (Chapter 11; 3b). Half-times for each phase ($T_{1/2}$ α and $T_{1/2}$ β respectively) were calculated from the relationship:

$$T_{1/2} = \frac{\log_{(e)} 2}{k} = \frac{0.693}{k}$$

where, **k** is the rate constant.

(ii) Results.

(iia) Blood clearance of ^{131}I radiolabelled antibodies following intrathecal injection.

Eight adult guinea pigs, designated GP-1 to GP-8, were injected intrathecally with either 5 MBq ^{131}I-WCMH (n=4) or 2.5 MBq ^{131}I-RFAL3 (n=4). Blood was sampled at hourly intervals for 14 hours, and then at 23 hours and 46 hours post-injection. Table 9.7 gives the per cent injected activity present in circulating blood at each time point. Figure 9.6 presents this data in graphical form for each animal, together with a graph depicting the mean per cent injected activity against time for each reagent.

Table 9.7 Blood activity of ^{131}I following IT injection of either ^{131}I-WCMH or ^{131}I-RFAL3.

Time Post-Injection (hours)	% Injected Activity of ^{131}I in Blood							
	^{131}I-WCMH				^{131}I-RFAL3			
	GP-1	GP-2	GP-3	GP-4	GP-5	GP-6	GP-7	GP-8
1	9.94	4.99	5.86	6.18	17.17	16.09	10.01	11.79
2	15.31	8.40	6.69	16.05	24.68	18.23	13.92	17.13
3	19.66	9.41	8.46	14.47	24.60	17.29	15.01	14.35
4	20.79	10.85	9.56	16.48	22.80	15.26	14.46	13.15
5	22.52	12.28	8,39	14.85	20.81	15.00	16.96	12.39
6	22.44	13.23	10.58	15.52	18.43	12.88	11.40	11.10
7	21.96	13.26	9.95	15.57	18.49	12.46	12.01	10.11
8	21.90	13.86	9.65	17.10	15.91	11.49	10.14	9.96
9	23.44	13.32	10.45	16.27	14.50	11.27	9.24	8.41
10	23.00	13.59	10.26	15.71	13.58	9.59	9.28	8.07
11	23.40	14.35	9.29	15.95	13.08	10.67	8.77	8.06
12	22.71	14.69	12.15	16.20	12.85	10.07	9.64	7.12
13	21.70	14.25	10.88	16.24	11.54	9.18	N/E	6.64
14	22.17	13.36	11.42	15.99	10.97	8.88	8.36	5.71
23	19.34	10.48	7.13	14.00	7.97	5.98	4.86	3.57
46	9.14	N/E	N/E	6.58	1.32	1.64	0.94	0.80

N/E = Not estimated

For animals injected with ^{131}I-WCMH, mean blood activity increased rapidly to a level of 14.4% at four hours. Thereafter, a relative plateau was observed, with a peak blood activity of 16.4% at 12 hours after injection. ^{131}I was then eliminated from the blood by monoexponential kinetics. For guinea pigs injected with ^{131}I-RFAL3, blood activity rose even more steeply to a mean peak activity of 18.5% at two hours. No plateau was noted, activity clearing again by monoexponential kinetics, but at a faster rate than that observed for ^{131}I-WCMH.

Figure 9.6

Blood clearance of intrathecally injected ^{131}I-labelled antibodies in guinea pigs.

Either 5 MBq ^{131}I-WCMH (GP-1 to GP-4) or 2.5 MBq ^{131}I-RFAL3 (GP-5 to GP-8) was injected intrathecally into guinea pigs. Blood (100 µl) was sequentially sampled and radioactivity measured in a gamma counter. Blood activity is expressed as per cent injected activity in the vascular compartment and plotted against time post-injection.

A = GP-1 to GP-4

B = GP-5 to GP-8

C = Mean per cent injected activity against time for ^{131}I-WCMH (GP-1 to GP-4) and ^{131}I-RFAL3 (GP-5 to GP-8).

Figure 9.6

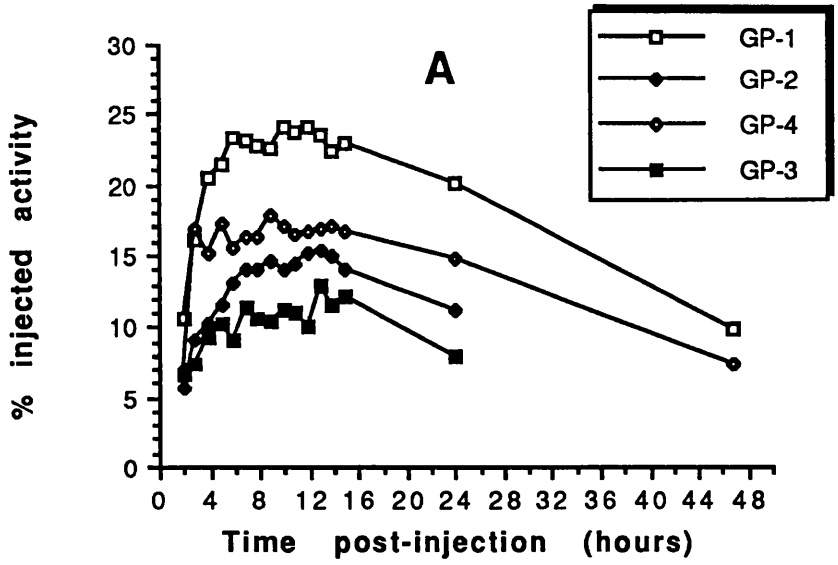
A
GP-1
GP-2
GP-4
GP-3
% injected activity
0
5
10
15
20
25
30
0 4 8 12 16 20 24 28 32 36 40 44 48
Time post-injection (hours)

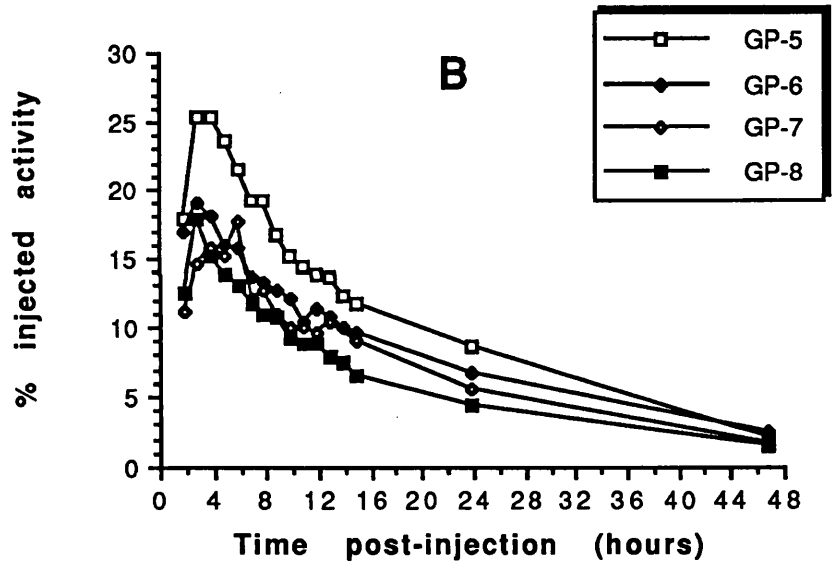
B
GP-5
GP-6
GP-7
GP-8
% injected activity
0
5
10
15
20
25
30
0 4 8 12 16 20 24 28 32 36 40 44 48
Time post-injection (hours)

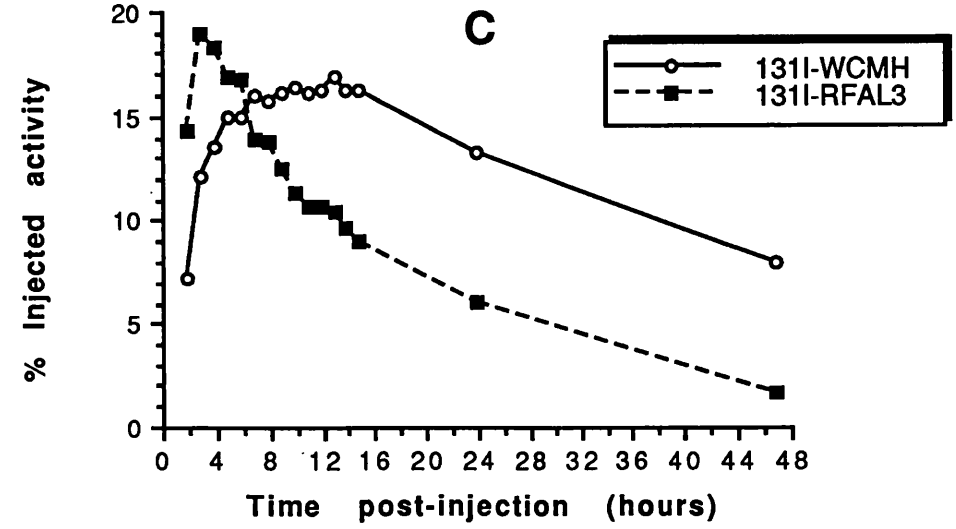
C
131I-WCMH
131I-RFAL3
% Injected activity
0
5
10
15
20
0 4 8 12 16 20 24 28 32 36 40 44 48
Time post-injection (hours)

Table 9.8 Pharmacokinetic analysis of blood clearance of ^{131}I-labelled antibodies following IT injection .

Injectate	No.	Absorption Rate Constant k_a (x 10^{-2} hour^{-1})	Elimination Rate Constant k_e (x 10^{-2} hour^{-1})	Half-time (hours)			
				$T_{1/2}$ α	$T_{1/2}$ β	$T_{1/2}$ α mean (SD)	$T_{1/2}$ β mean (SD)
^{131}I-WCMH	GP-1	40.11	2.22	1.73	31.22	1.68 (0.86)	37.09 (10.76)
	GP-2	25.71	2.76	2.70	25.11		
	GP-3	40.74	1.43	1.70	48.46		
	GP-4	117.05	1.59	0.59	43.58		
^{131}I-RFAL3	GP-5	269.11	7.06	0.26	9.82	0.28 (0.25)	10.10 (1.39)
	GP-6	660.40	5.94	0.10	11.67		
	GP-7	115.99	6.58	0.60	10.53		
	GP-8	453.01	8.29	0.153	8.36		

The blood absorption rate constant (k_a) of ^{131}I-WCMH varied between 25.71 and 117.05 x 10^{-2} hour^{-1}, and the elimination rate constant (k_e) between 1.43 and 2.76 x 10^{-2} hour $^{-1}$ (Table 9.8). For ^{131}I-RFAL3, k_a was between 115.99 and 660.40, and k_e between 5.94 and 8.29 x 10^{-2} hour^{-1}. This equates to values of $T_{1/2}$ α of ^{131}I-WCMH of between 0.59 and 2.70 hours (mean = 1.68 hours, standard deviation (SD) 0.86 hours), and of $T_{1/2}$ β of between 25.11 and 48.46 hours (mean = 37.09 hours, SD = 10.76 hours). For ^{131}I-RFAL3, $T_{1/2}$ α was shorter at between 0.10 and 0.60 hours (mean = 0.28, SD = 0.25 hours) as was $T_{1/2}$ β at between 8.36 and 11.67 hours (mean = 10.10, SD = 1.39 hours).
To compare respective half-times, the Students t test was applied with a log transformation of the data to stabilize the variance. This gives:

$T_{1/2}$ α ^{131}I-WCMH v T1/2 α ^{131}I-RFAL3 : t = 3.77 on 6 degrees of freedom,

p = 0.01

$T_{1/2}$ β ^{131}I-WCMH v T1/2 ß ^{131}I-RFAL3 : t = 7.65 on 6 degrees of freedom,

p = 0.003

This suggests that following IT injection, radiolabelled IgM is more rapidly absorbed from the subarachnoid space into the blood, and more rapidly eliminated from the blood than IgG. These results also indicate that for both reagents, blood elimination is rate-limiting.

The accurate computation of rate constants and half-times for intrathecally injected compounds depends on the assumption of a one-compartment (blood) model with first order absorption and elimination kinetics. The clearance of radioconjugates following IV injection was thus investigated to determine whether this assumption is valid.

(iib) Blood clearance of ^{131}I radiolabelled antibodies following intracardiac injection.

Five guinea pigs (GP-9 to GP-13) received a systemic injection of either 2.5 MBq ^{131}I-WCMH (n=3) or 1.4 MBq ^{131}I-RFAL3 (n=2). Antibodies were injected into the right ventricle, injection into a peripheral vein having been shown to be unreliable. Blood was sampled at 0.083, 0.25, 0.5 and 1.0 hours and thereafter at hourly intervals for a total of five hours, with a final sample at 22 hours (Table 9.9).

Table 9.9 Blood activity of ^{131}I following intracardiac injection of either ^{131}I-WCMH or ^{131}I-RFAL3.

Time Post Injection (hours)	% Injected Activity of ^{131}I in Blood				
	^{131}I-WCMH			^{131}I-RFAL3	
	GP-9	GP-10	GP-11	GP-12	GP-13
0.083	102.90	101.2	90.58	65.60	52.95
0.25	60.66	74.03	56.54	50.41	45.04
0.5	N/E	55.36	55.36	46.49	43.24
1.0	35.73	52.67	48.28	45.86	40.45
2.0	35.53	44.36	N/E	39.06	35.71
3.0	N/E	39.14	37.46	34.32	35.09
4.0	27.12	35.50	36.68	35.15	N/E
5.0	26.77	34.25	34.69	29.65	28.87
22.0	22.68	19.48	27.18	10.03	10.76

N/E = Not estimated

Table 9.10

Pharmacokinetic analysis of blood clearance of ^{131}I-labelled antibodies following intracardiac injection.

Injectate	No.	Distribution Rate Constant k_d (x 10^{-2} hour^{-1})	Elimination Rate Constant k_e (x 10^{-2} hour^{-1})	Half-time (hours)			
				$T_{1/2}$ α	$T_{1/2}$ β	$T_{1/2}$ α mean (SD)	$T_{1/2}$ β mean (SD)
^{131}I-WCMH	GP-9	620.8	1.60	0.11	43.31	0.093 (0.047)	35.37 (12.63)
	GP-10	539.8	3.33	0.13	20.81		
	GP-11	1598.5	1.65	0.04	42.00		
^{131}I-RFAL3	GP-12	1128.7	6.62	0.06	10.47	0.070 (0.014)	10.21 (0.37)
	GP-13	859.2	6.07	0.08	9.94		

Figure 9.7

Blood clearance of intracardiac injected ^{131}I-labelled antibodies in guinea pigs.

Either 2.5 MBq ^{131}I-WCMH (GP-9 to GP-11) or 1.4 MBq ^{131}I-RFAL3 (GP-12 and GP-13) was injected into the right cardiac ventricle of guinea pigs. Blood (100 µl) was sequentially sampled and radioactivity measured in a gamma counter. Blood activity is plotted against time post-injection (see Figure 9.6).

A = Clearance curves for each animal

B = Mean per cent injected activity against time for ^{131}I-WCMH (GP-9 to GP-11) and ^{131}I-RFAL3 (GP-12 and GP-13).

Figure 9.7

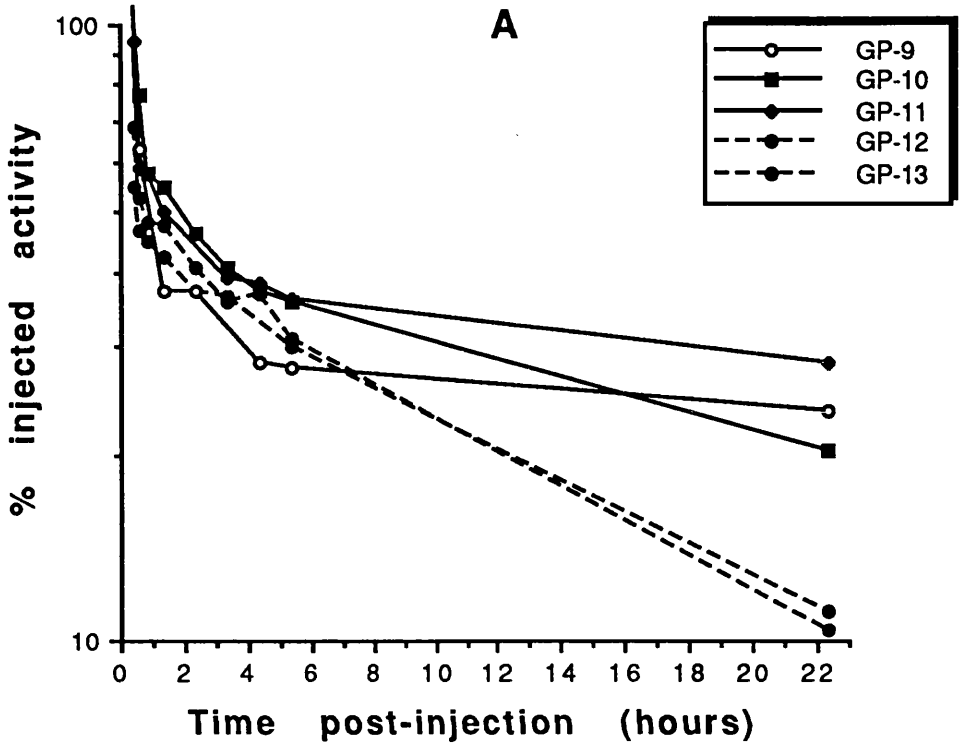
A
100
10
% injected activity
0 2 4 6 8 10 12 14 16 18 20 22
Time post-injection (hours)
GP-9
GP-10
GP-11
GP-12
GP-13

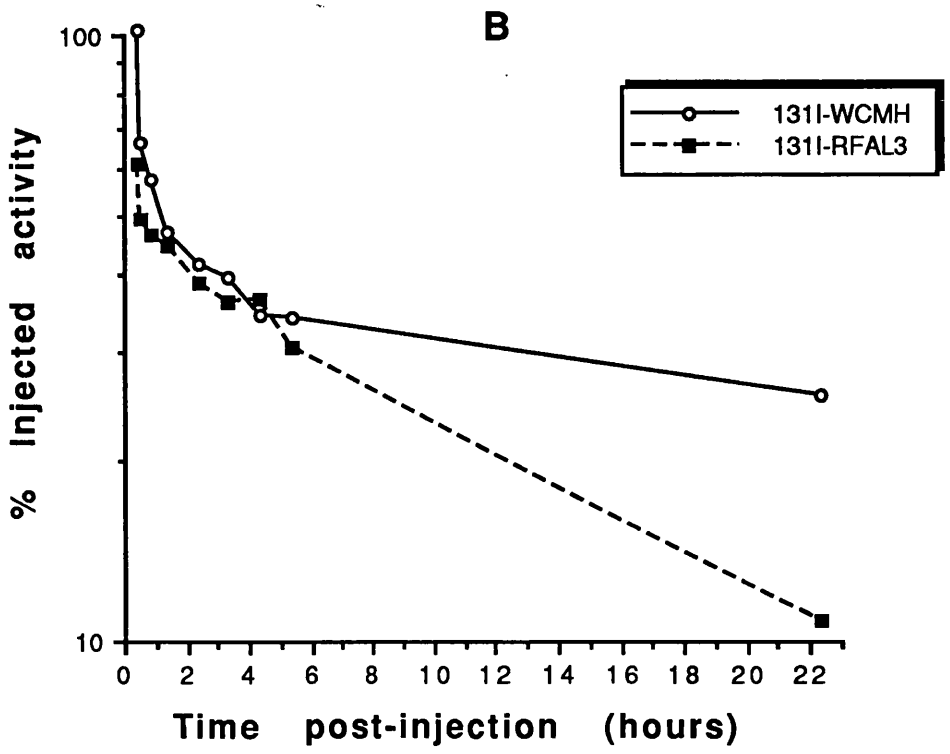
B
100
10
% Injected activity
0 2 4 6 8 10 12 14 16 18 20 22
Time post-injection (hours)
131I-WCMH
131I-RFAL3

Blood clearance curves for animals injected with ^{131}I-RFAL3 conformed to a similar pattern; a rapid distribution phase followed by a slower, monoexponential elimination phase (Figure 9.8). Following the distribution phase, clearance of ^{131}I-WCMH mirrored closely that of ^{131}I-RFAL3 for up to five hours, but thereafter the gradient of the elimination phase curve was noticeably less than that for the IgM conjugate.

The distribution rate constants ($\mathbf{k_d}$) for ^{131}I-WCMH were 620.8, 539.8 and 1598 x 10^{-2} hour^{-1} and the elimination rate constants ($\mathbf{k_e}$), 1.60, 3.33 and 1.65 x 10^{-2} hour^{-1} respectively (Table 9.10). For ^{131}I-RFAL3, $\mathbf{k_d}$ was 859.2 and 1128.7 x 10^{-2} hour^{-1} and $\mathbf{k_e}$, 6.62 and 6.07 x 10^{-2} hour^{-1} respectively. This gave mean values for $T_{1/2}$ α of 0.093 and 0.077 hours, for ^{131}I-WCMH and ^{131}I-RFAL3 respectively. Respective values for mean $T_{1/2}$ β were 35.37 and 10.21 hours. To compare respective half-times, the Students t test was again applied with a log transformation of the data. This gives:

$T_{1/2}$ α ^{131}I-WCMH v $T_{1/2}$ α ^{131}I-RFAL3 : t = 0.37 on 3 degrees of freedom, p = 0.7

$T_{1/2}$ β ^{131}I-WCMH v $T_{1/2}$ β ^{131}I-RFAL3 : t = 3.85 on 3 degrees of freedom, p = 0.03

Despite the small number of animals used, differences in $\mathbf{k_e}$ between reagents again reached significance. In retrospect, further blood samples should have been taken both between five and 22 hours, and after 22 hours. Nevertheless, the rate constant for the rate-limiting elimination phase is similar following IV and IT injection. This implies that the "method of residuals" can be applied to the calculation of the blood absorption rate for intrathecally administered radioconjugates in this model.

6. Discussion.

Results from culture systems have clearly demonstrated the efficacy and specificity of both ^{131}I and ^{125}I targeted radiotherapy for leukaemia (Chapters 6, 8). Such models have, however, obvious limitations with regard to the pharmacokinetic, anatomical and physiological considerations present in the clinical situation. An animal model was thus developed to re-address issues such as specificity, which is unable to be investigated in a clinical study, as a comparison between therapeutic amounts of radiolabelled specific and control antibodies would be required. Due to the relatively low incidence of isolated CNS relapse of ALL and NHL, an *in-vivo* model may also allow information with regard to treatment variables, such as the benefit of repeated therapy, to be more readily obtained.

Several models of meningeal leukaemia have been developed. Lynch *et al.*, observed meningeal leukaemia in AKR mice following IV injection of a transplantable murine leukaemia [289]. Systemic disease was suppressed by the co-administration of Amphotericin B and BCNU. CNS leukaemia was also noted in WF rats who sustained a systemic remission following IV chemotherapy for a WF rat AML cell line [280], and in the BD IX rat following intracerebral inoculation of L5222 rat leukaemia cells [279]. Hoogerbrugge and Hagenbeek compared the pattern of leptomeningeal proliferation of transplantable rat AML and ALL cell lines injected intrathecally (cisterna magna) into Brown Norway rats [278]. The pattern of CNS growth of ALL lines was similar to that observed in this study, with animals dying from systemic leukaemia at around 30 days.

The L_2C/Strain 2 guinea pig model, however, appeared most appropriate for use in this study, the feasibility of IT administered immunotoxin therapy having been demonstrated in two previous studies. Models using larger animals and those in which immunosuppressive regimens

are required to establish to leptomeningeal tumour, were considered inappropriate.

This study demonstrates a consistent pattern of growth within the CNS of L_2C cells injected into the cisterna magna. Whereas no microscopic evidence of parenchymal extension of leptomeningeal disease was noted at between 14 and 19 days after tumour inoculation, this was observed by 23 to 27 days. This is consistent with the observations of Urch *et al.*, who noted a similar progression of disease at 14 and 28 days post-inoculation [281].

In initial experiments, no benefit was noted from IT radioconjugate therapy in terms of preventing the development of systemic leukaemia as a result of re-seeding from meningeal tumour. We were thus unable to reproduce the results of Urch *et al.*, who demonstrated a cure of all animals receiving an IT dose of either 0.5 or 5 μg anti-Id-1 saporin on day one. If 10 remaining meningeal L_2C cells are assumed to result in systemic leukaemia, this result equates to a greater than a four log kill as a result of therapy.

It is clear, however, that the higher dose of 9.9 MBq radioconjugate used in these studies is well below that necessary to cause significant toxicity. This is born out in a subsequent experiment, in which six animals receiving 150 MBq ^{131}I-anti-Id-1 over a two week period also demonstrated minimal toxicity. Injected activities of at least 100 MBq should be employed in further studies using this modification of the model system.

It is also of note that in Urch's preliminary studies, an IT dose of above 10 μg immunotoxin was shown to be lethal to all of four to six animals treated in each group. These developed a severe systemic illness on about day two, dying at between eight to 10 days following therapy. The nature of this toxicity is a cause for concern in relation to clinical studies of IT immunotoxin therapy. In addition, therapy was administered only one day after tumour inoculation and, given a doubling time of L_2C *in-vivo* of 18 to 20 hours [290], a maximum of 2.5×10^5 cells would be present at the time of therapy. Moreover, these cells

may not be fully established on the leptomeninges and will be thus more amenable to treatment with immunotoxins, which require direct cell binding to exert their cytotoxic effect. With more established disease as in human CNS leukaemia (Chapter 1; 2b), accessibility to immunotoxins will assume more importance, either with regard to antibody penetration of sheets of leptomeningeal tumour or to cells in relatively inaccessible sites such as the neuro-capillary spaces. In this case, β-emitting radionuclides may have an advantage over toxins, by virtue of the cytotoxic effect of emissions from unbound conjugate or as a result of the crossfire effect.

When the model was extended by the administration of weekly cyclophosphamide, a lack of efficacy was again demonstrated for 20 MBq ^{131}I-anti-Id-1 injected on either day one or day 21. It is probable that by day 21, parenchymal disease is present, which may be unresponsive to IT therapy. A second injection on either day 29 or 43 respectively had no effect on survival. This is not surprising as surviving L_2C cells would have had sufficient time (28 or 22 days) to proliferate and enter the CNS parenchyma. In retrospect, these treatment times were inappropriate for the investigation of repeated therapy.

In the final experiment, 50 MBq ^{131}I-anti-Id-1 administered on day 14 was associated with a significantly increased survival. In each of three groups of six animals treated, one was cured. It is unlikely that this resulted from the tumour failing "to take" in each case, as this had only been observed in one out of 44 guinea pigs followed to the terminal state in previous experiments. It should be noted, however, that mean survival of the control group was significantly shorter than that previously observed. The reason for this is unclear, but the same suspension of tumour cells was used for both control and treatment groups. Of the treated animals that died, survival was only significantly greater ($p < 0.05$) than controls in group D. However, there was no significant difference in survival between treated animals. These findings may be explained by a sufficient cytoreduction of L_2C cells in one animal in

each group to result in cure. In the remaining guinea pigs a critical number of cells remained, resulting from either an insufficient radiation dose to leptomeningeal cells or the existence of cells inaccessible to antibody. The lack of response to repeated therapy may indicate that inaccessibility of antibody to tumour cells is an important factor, resulting from parenchymal disease either present on day 14 or occurring from cells surviving the initial therapy.

Results from a single experiment involving small numbers of animals must be interpreted with caution. Nevertheless, the observation of three cured animals suggests a useful basis for further experimentation. Further work will attempt to increase therapeutic efficacy. This will involve single injections of at least 100 - 150 MBq ^{131}I-anti-Id-1, with dose escalation until significant toxicity is observed. The timing of injection also needs consideration. Injection of conjugate at an earlier point following tumour inoculation eg. between days seven and 10 may be more appropriate. This will ensure that therapy is directed against established meningeal disease, but will increase the likelihood of accessibility to leptomeningeal tumour. If the efficacy of this approach is demonstrated, then further experiments will include the investigation of the antibody specificity, by comparing survival associated with ^{131}I-anti-Id-1 and a ^{131}I-labelled irrelevant antibody. The issue of repeated therapy needs reconsideration with attention to therapeutic response, pharmacokinetics and the generation of an anti-mouse Ig response, once a reliable assay has been developed.

This model is also appropriate for the investigation of alternative agents such as short-range β- or α-emitters (Chapter 13; 2c). As discussed in Chapter 8, internalisation of anti-Id-1 has been previously reported, making this model also suitable for the *in-vivo* investigation of ^{125}I targeted radiotherapy.

The mean absorption half-time of 1.68 hours, for ^{131}I-WCMH injected into the cisterna magna, is comparable to that determined by Urch *et al.*, who

derived a value for anti-Id-1 of 1.83 hours [281]. This corresponds to the expected value, given that guinea pig CSF is replaced at the rate of 30 - 40% per hour [291], and should allow adequate time to permit binding of antibody to tumour cells.

The considerably faster clearance of radiolabelled IgG from both the subarachnoid and vascular compartments, relative to that noted in clinical studies, clearly explains the lack of myelosuppression in guinea pigs, even following IT injected activities of 150 MBq over a two week period. This is equivalent to a injected activity in patients of 45000 MBq, on an equivalent CSF volume basis, or over 30 times the activity initially proposed for our clinical studies (Chapter 10; 2f).

Two basic strategies are available for increasing the dose to the CSF, and hence tumour cells, following IT injection of radioconjugate; either to increase the injected activity or to decrease the clearance of radioconjugate from the subarachnoid space. It was hypothesized that clearance might be inversely related to molecular size. These experiments indicate that a larger Ig molecule, IgM (molecular weight approximately 900 kDa), is conversely cleared more rapidly from the CSF than IgG, and that on this basis, conjugates of IgM do not have a role to play in IT targeted radiotherapy. This conclusion is supported by data from a co-worker, Mr V Papanastassiou, who has conducted similar experiments using a larger animal model, the small pig (body weight approximately 15 kg). The reason for this faster CSF elimination of IgM is unclear. Evidence from animal studies, including primate models, suggest that the size of the drainage pathways of the arachnoid villi are sufficiently large to freely allow polystyrene microspheres as large as 2 μm in size and erythrocytes (7.5 μm) to exit from the CSF [292]. One explanation for these observations is that radiolabelled IgM may undergo increased de-halogenation either before or after IT injection, following which free iodine will be cleared rapidly from the CSF.

Pharmacokinetic experiments were conducted in non-tumour bearing animals. Similar studies will be undertaken during future therapeutic experiments. In particular, the rate of CSF clearance of isotope will be compared between specific and control radiolabelled IgG. If clearance of the conjugate is delayed as a result of tumour binding, this will provide indirect evidence as to the specificity of conjugate therapy.

CHAPTER 10.

CLINICAL STUDIES OF TARGETED RADIOTHERAPY IN THE TREATMENT OF LEPTOMENINGEAL LYMPHOPROLIFERATIVE DISEASE.

1. Introduction

Since 1980, our group has been involved in the development of intrathecally administered targeted radiotherapy in the treatment of leptomeningeal malignancy. In our initial pilot study, 15 patients with a variety of meningeal neoplasms received a single IT injection of 407 - 2220 MBq ^{131}I conjugated to an appropriate monoclonal antibody [118]. Toxicity was acceptable and tumour responses were observed in six of nine evaluable patients (Chapter 1; 1e). Meningeal lymphoproliferative disease appeared an obvious condition in which to investigate further this novel therapeutic modality.

Our group thus established a Phase I/II study of ^{131}I-targeted therapy in the treatment of meningeal relapse of either ALL or non-Hodgkin's lymphoma (NHL). A detailed discussion of the background and rationale for this study is presented in Chapter 1. Presented here is a summary of the study protocol, together with toxicity and response data from six patients receiving a single injection of radiolabelled antibody. Therapy in the seventh and final patient, represents the second phase of our studies, in which we are attempting to prolong remission time by dose escalation, the use of a radiolabelled antibody cocktail and by the repeated injection of radioconjugate. Pharmacokinetic and dosimetric investigations are described in Chapters 11 and 12 respectively.

2. Methods

STUDY PROTOCOL

(a) Patient selection.

(i) Patients are eligible for entry into the study if in second or subsequent CNS relapse of ALL or NHL, and in systemic remission. At present, it is not normally considered justifiable to enter patients in first meningeal relapse, as treatment with conventional chemoradiotherapy is associated with a rate of long term CNS remission of up to 50% (Chapter 1; 2g). Patients are, however, eligible for study in first CNS relapse if they have received prior cranial external beam irradiation as part of total body irradiation for systemic relapse, in addition to initial cranial irradiation.

(ii) Patients must have measurable disease involving the leptomeninges. For the large majority of patients, this will be on the basis of CSF cytology. Patients with solid leptomeningeal relapse of NHL may be entered, providing that tumour deposits can be clearly defined using an appropriate imaging technique.

(iii) The tumour must be reactive with a proposed targeting antibody, preferably from cells sampled at relapse. If no current cytology is available from CSF or on biopsy, patients may be included if their tumour has been demonstrated to express the relevant antigen at some point during their clinical history.

(iv) No spinal block must be present at the time of therapy. Patients with spinal block as a result of solid deposits of NHL may be treated with localised external beam radiotherapy to create free-flowing CSF pathways. In this case, the patient's disease status must be reassessed prior to targeted therapy.

(v) The last course of IT chemotherapy must be at least four weeks before the proposed targeted therapy. External beam radiotherapy to evaluable disease must be at least six weeks from treatment. These conditions may, however, be waived if there is clear evidence of progressive disease.

(vi) The patient must be at least two years of age at the time of entry into the study. Significant difficulties with regard to patient care are anticipated when treating children younger than this. There is no upper age limit.

(vii) No prior treatment with any rodent antibody is permitted.

(viii) A history of anaphylactic reaction or other allergic/hypersensitivity disorder (eg. asthma, eczema, food or drug allergy not resulting in anaphylaxis) should be carefully considered, but does not constitute a strict contra-indication.

(ix) Patients should have a peripheral blood haemoglobin (Hb) concentration of at least 10 g/dl, a neutrophil count of at least 1×10^9/litre and a platelet count of at least 100×10^9/litre. In terms of renal function, blood urea should be less than 7 mmol/litre and blood creatinine less than 120 µmol/litre.

(x) Ethical Committee approval must be obtained for this study at each treatment centre.

(xi) Fully informed patient/parental consent must be obtained. Consent forms, specifically designed for this study, should be completed.

(b) Patient assessment.

(i) A full clinical history, including details of prior radiotherapy and chemotherapy, must be obtained. Each patient should undergo a complete clinical examination prior to therapy.

(ii) CSF must be examined for total and differential cell count prior to administration of therapy. CSF protein and glucose concentrations should be determined. An aliquot (1 - 2 ml) of CSF should be stored for subsequent analysis of a human anti-mouse antibody (HAMA) response.

(iii) Myelography should be performed in cases of CNS NHL where solid disease is suspected.

(iv) CT scan of the head with contrast and/or MRI of head should be performed in all patients as a baseline investigation for the assessment of potential neurotoxicity, and in cases of CNS lymphoma to determine disease status.

(v) Pre-therapy peripheral blood should be taken for:

- Full blood count (FBC) with differential white cell count and examination of blood film.
- Estimation of plasma urea, creatinine and electrolyte concentrations.
- Serum liver function tests (LFTs) (bilirubin, alkaline phosphatase, alanine transferase, albumin and globulin).
- Plasma thyroid function tests (TFTs) (thyroid stimulating hormone, thyroxine)

5 - 10 ml of serum should be stored for subsequent analysis of a HAMA response.

(c) Patient preparation.

(i) Anticonvulsants.

In our initial pilot study, two patients experienced convulsions following IT therapy [118]. Patients should, therefore, be placed on anticonvulsant therapy, eg. phenytoin, for a minimum of three days before and one week following conjugate administration.

(ii) Thyroid blockade.

Drug therapy to prevent the uptake of ^{131}I into the thyroid gland is to be selected by the individual participating centres. At our institution, patients are given supersaturated potassium iodide, at a dose of 0.5 - 1 ml three times daily. Thyroid blockade must be started 72 hours before administration of the radioconjugate and continued for a minimum of 14 days after treatment.

(iii) Cannula.

An indwelling intravenous catheter should be fitted before therapy to facilitate drug administration and the taking of subsequent blood samples.

(iv) Hydration/catheterisation.

Patients must be fully hydrated before administration. Very young or incontinent patients must be catheterised in order to minimise the problems of radiation safety and staff exposure.

(v) Systemic chemotherapy (eg. oral 6-mercaptopurine and methotrexate)

This should be discontinued for up to two weeks before and at least four weeks following conjugate administration. This is to enable an evaluation of the

toxicity associated with targeted radiotherapy. Inability to comply with this criterion does not exclude patients from the study, but it must be appreciated that a combination of targeted therapy and systemic chemotherapy may result in enhanced myelosuppression.

(d) Selection of monoclonal antibodies.

The purified MoAbs, WCMH, HD37 and WT1 are to be used in clinical studies (Chapter 3). Batches of antibody for patient administration are selected on the basis of a high degree of purity (> 98% IgG) and biological activity (> 1/1000) (Chapter 3; 5b). All preparations are sterile, as determined by a routine microbiological screen (Courtesy of the Department of Pathology, Frenchay Hospital, Bristol) and contain less than 0.05 ng/ml of endotoxin as determined by the LAL assay (Chapter 2; 3k).

Antibodies are selected on the basis of the immunoreactivity of each individual's tumour, as determined by indirect immunofluorescence staining of air-dried cytospin preparations or frozen tumour sections (Chapter 2; 4e, 4f).

(e) Radiolabelling.

Radiolabelling is undertaken in a purpose-built radioisotope suite in our laboratory or, when appropriate, at the collaborative centre. Antibodies are radiolabelled using the iodogen technique to a specific activity of 370 MBq/mg protein (Chapter 2; 5a). To reduce potential antibody damage and the radiation risk to personnel, antibodies are radiolabelled in batches. 148 - 185 MBq $Na^{131}I$ is placed together with antibody in each iodogen tube, and the product from four or five tubes loaded on to each Sephadex G-25™ gel filtration column.

The labelled product from each column is pooled and the radioactivity measured in a Vinten Isocal™ radionuclide calibrator. A small aliquot (10 - 20 MBq) is taken for quality control and the final product (5 - 15 ml) collected into

11 ml sterile evacuated vials (Mallinckrodt Diagnostica) after further passage through a 0.22 μm Millex™ filter.

The final product is analysed for estimation of free iodine by precipitation with 10% TCA (Chapter 2; 5d) and of conjugate aggregation using FPLC Superose-12™ gel filtration (Chapter 2; 5e). The immunoreactive fraction is estimated using a liquid phase radiobinding assay (Chapter 2; 5f).

(f) Injected activity

(i) Adults and adolescents

In a pilot study of 15 patients, three adults developed reversible myelosuppression, having received 2220, 2072 and 2072 MBq ^{131}I respectively. For this study, we proposed to administer a lower initial activity than this; 1480 MBq to adults and adolescents (age 10 years and above), an activity at which tumour responses were noted previously. It was anticipated that in the case of B-lineage disease, increased myelosuppression may be observed when using antibodies recognising a subset of differentiating lymphocytes within the bone marrow.

(ii) Dose reduction for children.

A dose-reduction schedule was constructed for patients younger than ten years of age. This was devised following consideration of both changes in body surface area and CSF volume with age (Table 10.1, Figure 10.1). Ideally, the dose of cytotoxic agents administered into the CSF should be related to either CSF volume or CNS surface area/volume, both of which rise rapidly with age, reaching approximately 80% of the adult value at three years [152]. This forms the basis for the currently used regimen for IT administered drugs such as methotrexate. However, we did not feel that we can base the dose schedule for radioconjugates solely on these parameters, as this may result in relatively

Figure 10.1

Illustration of CSF volume and body surface area with respect to age. The injected activity of ^{131}I relative to that for adults is included.

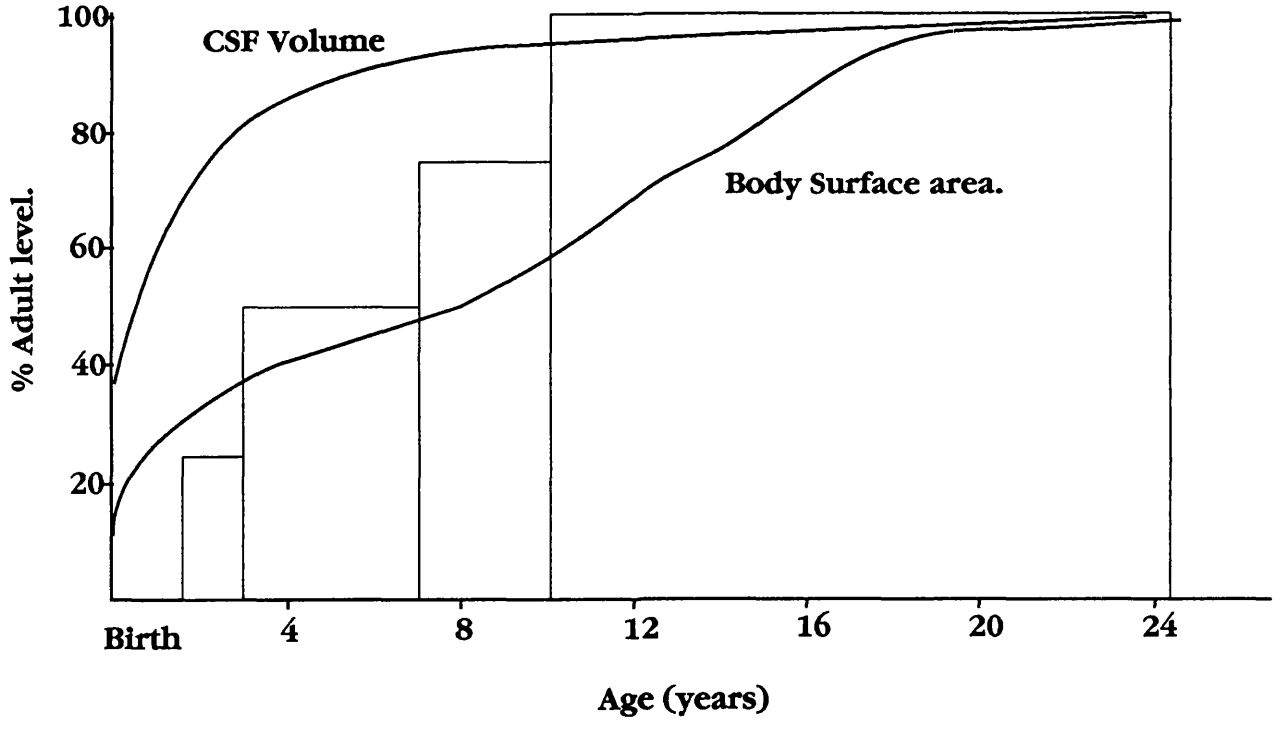

increased myelosuppression in young children following clearance of ^{131}I into the systemic circulation.

Table 10.1 **Schedule for initial injected activity of ^{131}I-labelled antibodies.**

Age (years inclusive)	Initial Activity (MBq)
2	370
3-6	740
7-9	1110
>9	1480

(g) Administration of Conjugate.

Where possible, therapy is delivered within eight hours of radiolabelling, to limit potential radiolysis. It is recommended that conjugate is administered by the intraventricular route, via an Ommaya Reservoir. This is to ensure optimum distribution of conjugate, throughout the subarachnoid space [293]. If this method is considered inappropriate, then conjugate may be given by lumbar puncture (LP). The choice of route should be made by the consultant in charge of the patient, following discussion with a study group member and the patient/parents.

Administration is to be performed using a strictly aseptic technique. Conjugate is dispensed into a 20 - 30 ml syringe and the activity re-estimated. Injection into an Ommaya reservoir is performed by connecting the syringe to a 23 or 25 gauge Butterfly™ needle via a 0.22 μm Millex™ filter. For injection by LP, a length of extension tubing is connected between the syringe/filter and the LP needle. All connections should be luer locking and checked for leakage before administration. A volume of CSF, equivalent to the volume of conjugate, is removed, the solution injected over one to two minutes and the needle/tubing finally flushed with 2 ml of sterile 0.9% saline.

Full resuscitation facilities must be available in case of an anaphylactic or other acute severe reaction. The patient's condition should be closely observed following therapy, especially within the first 72 hours. Temperature, pulse rate, respiration rate and blood pressure should be recorded at least every four hours. It is not anticipated that hospitalisation should last more than seven days.

(h) Radiation protection.

Patients will be nursed in a designated isolation room until the whole body radioactivity has fallen to a level determined by the local Radiation Protection Officer, who will be responsible for all aspects of radiation safety according to local procedures.

(i) Post-treatment investigations.

Investigations relating to pharmacokinetic studies are detailed in Chapter 11. Those undertaken to monitor toxicity and tumour response are presented below:

(i) Full clinical review at 1, 2, 4, 6, 8 and 12 weeks post-therapy and thereafter at monthly intervals, or more frequently if clinically indicated.

(ii) FBC including differential WCC count at weekly intervals for 8 weeks.

(iii) Urea, electrolytes, creatinine and LFTs at 2, 4, 6, 8 and 12 weeks post-therapy. These should be repeated at 6 and 12 months from therapy.

(iv) TFTs at 12 weeks, and at 6 and 12 months from therapy.

(v) Myelography should be performed at 4 and 8 weeks following therapy if disease is demonstrated by initial myelography. This should

be repeated at 12 weeks, unless progressive disease is demonstrated at 8 weeks post-therapy.

(vi) CT scan with contrast or MRI of the head is to be performed at 4 and 8 weeks post-injection if disease is demonstrated by the initial scan. This should be repeated at 12 weeks, unless progressive disease is demonstrated at 8 weeks post-therapy. CT scan of the head with contrast and/or MRI of the head should be performed in all patients at six months post-injection to assess delayed neurotoxicity.

(vii) CSF examination for total and differential cell count, immunocytochemistry and protein and glucose estimations should be undertaken at 2, 4, 6, 8 and 12 weeks after antibody administration.

(viii) At 4 and 8 weeks, both serum and CSF should be taken and stored for estimation of a HAMA response.

Where appropriate, toxicity will be graded according to the WHO system and recorded on a specific pro forma. In the event of death, a full post mortem examination will be requested, including complete macroscopic and histological examination of the CNS.

(j) Study documentation

Each participating centre is supplied with a clinical protocol, a summary of the clinical protocol, a physics protocol, an investigation check list, patient data sheets and consent forms.

3. Results

(a) Patient recruitment

Seven children/adolescents, aged 3 - 16 years, have been entered into the study to date (January 1992). Five children were in isolated second CNS relapse of B-lineage ALL and two, in third relapse. All except patients 1 and 7 had had two courses of cranial irradiation. Five patients had the common ALL phenotype, and two, CD 19 positive, CD 10 negative, null ALL. No patient with CNS relapse of either T-ALL or NHL has so far been referred. A summary of each patient's clinical history is presented in Table 10.2.

(b) Injected activity and administration of radiolabelled antibodies.

Only the first two patients received conjugate by lumbar puncture (Table 10.3). In the other individuals, Ommaya reservoirs were inserted without complication, all patients fully recovering from surgery within 24 hours. In the first six patients, injected activity ranged between 629 and 1480 MBq, conjugated to between 1.7 and 4.0 mg of protein. Five received an injected activity within 185 MBq of that proposed by the study protocol. As a result of an error in radiolabelling, patient 2 received only 962 MBq (intended activity of 1480 MBq). The seventh child was the first to enter a dose escalation programme. He initially received an activity of 1702 MBq, somewhat greater than the proposed activity of 1480 MBq. Following relapse, he received, at weekly intervals, 1276, 1178 and 1138 MBq respectively (proposed activity, 1110 MBq x 3), commencing 12 weeks after his initial injection.

Of the first six patients, four with common ALL received WCMH and two, with null ALL, HD37. Although CD10 positive lymphoblasts always co-expressed CD19, WCMH was selected due to the higher epitope density of CD10 on leukaemic cell lines (Chapter 3; 6). This probably relates to the

Table 10.2

Details of patients receiving ^{131}I targeted radiotherapy.

Pt No	Age	Sex	Tumour Phenotype	Event	Previous Therapy
1	6	M	cALL	Diagnosis	BFM, Cr DXT 18 Gy, IT MTX
				1st CNS Relapse	IT MTX, HC, CA
2	16	F	null ALL	Diagnosis	UKALL V, Cr DXT 24 Gy, IT MTX
				BM+CNS Relapse	UKALL VIII, Cr DXT 18 Gy, IT MTX
				2nd BM Relapse	UKALL VIII
				2nd CNS Relapse	IT MTX, HC, CA
				3rd BM Relapse	UKALL X
3	13	M	cALL	Diagnosis	PLOD, Cr DXT 18 Gy
				BM+CNS Relapse	UKALL X, TBI 9 Gy, HD Cyclo, BMT
				2nd CNS Relapse	IT MTX, HC, CA
4	14	M	cALL	Diagnosis	Manchester 1 Protocol, Cr DXT 24 Gy
				BM Relapse	GOS,UKALL X
				1st CNS Relapse	Cr DXT 24 Gy, Sp DXT 12 Gy, IT MTX
				2nd BM Relapse	UKALL X
5	7	F	cALL	Diagnosis	UKALL X, Cr DXT 18 Gy, IT MTX
				1st CNS Relapse	UKALL X , Cr DXT 24 Gy, Sp DXT 12Gy
6	3	F	null ALL	Diagnosis	UKALL X, Cr DXT 18 Gy, IT MTX
				1st CNS Relapse	Cr DXT 24 Gy, Sp DXT 12 Gy, IT MTX
7	3	M	cALL	Diagnosis	UKALL X, Cr DXT 18 Gy, IT MTX
				1st CNS Relapse	UKALL X, IT MTX

cALL = Common Acute Lymphoblastic Leukaemia
BFM = Berlin, Frankfurt, Münster Protocol
Cr DXT = Cranial external beam radiotherapy
MTX = Methotrexate
HC = Hydrocortisone
CA = Cytosine Arabinoside
UKALL = United Kingdom Acute Lymphoblastic Leukaemia Protocol
Sp DXT = Spinal external beam radiotherapy
PLOD = Prednisolone, L-Asparaginase, Vincristine, Daunorubicin
TBI = Total body irradiation
BMT = Bone marrow transplant
HD Cyclo. = High dose cyclophosphamide
GOS = Great Ormond Street Hospital relapsed leukaemia protocol

increased cell kill associated with the CD10 over the CD19 reagent observed in *in-vitro* cell survival experiments (Chapter 6; 4). Again, as a direct result of *in-vitro* investigations, the final patient was administered a radiolabelled cocktail of WCMH and HD37, each antibody conjugate contributing to half of the total activity.

Table 10.3 Details of administration of ^{131}I-labelled antibodies.

Patient	Antibody	Proposed Injected Activity (MBq)	Actual Injected Activity (MBq)	Route of Administration
1	WCMH	740	629	Lumbar
2	HD37	1480	962	Lumbar
3	WCMH	1480	1480	Ventricular
4	WCMH	1480	1295	Ventricular
5	WCMH	1110	1110	Ventricular
6	HD37	740	777	Ventricular
7(i)	WCMH/HD37	1480	1702	Ventricular
7(ii - iv)	WCMH/HD37	1110 x 3	*1276, 1178, 1138	Ventricular

* Administered at weekly intervals

(c) Quality control of radioconjugates.

Analysis revealed less than 5% aggregation of all ten radiolabelled conjugates (Table 10.4). In each case, less than 10% contamination with free iodine was noted (mean = 3.1%), with only two conjugates having greater than 5% contamination. Radiobinding assays were performed on eight occasions, the immunoreactive fraction ranging between 21% and 72% (mean = 56%). This is somewhat less than observed for radiolabellings using lower activities of ^{131}I (Chapter 4; 2b).

Table 10.4 Quality control of injected radioconjugates.

Patient	Immunoreactive Fraction (%)	Free ^{131}I (%)	Aggregates (%)
1	N/E	9	5
2	58	6	2
3	64	2	1
4	21	4	<1
5	N/E	2	4
6	69	0	<1
7(i)	42	1	2
7(ii)	42	2	1
7(iii)	72	3	4
7(iv)	57	2	3

N/E = Not estimated

(d) Acute toxicity.

Of the first six patients, four experienced acute toxicity with symptoms of aseptic meningitis, namely; headache, nausea and vomiting (Table 10.5). Neck stiffness was not observed. Transient tachycardia (pulse rate 100 - 150/minute) was seen, but there was no evidence of alteration in blood pressure or signs of respiratory distress. Toxicity was deemed mild in three patients and of moderate severity in one child (patient 5). Two patients (3 and 5) developed a transient pyrexia which resolved within 72 hours. In both cases, there was no evidence of infection. The onset of all acute symptoms was between four and 12 hours, and all resolved by 72 hours. Two patients remained completely asymptomatic. All patients were able to be discharged from hospital within seven days.

Following his first injection of conjugate, patient 7 experienced mild acute toxicity of similar nature and timing to that observed previously. After each of three further injections, he experienced moderately severe headache

Table 10.5 Toxicity following targeted radiotherapy.

Patient	Acute Toxicity	Myelosuppression						
		**WHO Grading				Timing (weeks)		
		Anaemia	Leuco-paenia	Neutro-paenia	Thrombo-cytopaenia	Onset	Nadir	Recovery
1	None	1	1	2	1	N/E	5	7
2	Mild	0	2	1	1	2	4 - 8	10
3*	Mild (temp 38.5 °C)	4	3	3	4	3	4-5	8
4	Mild	0	0	0	1	4	4	4
5	Moderate (temp 39.5 °C)	2	1	1	2	4	4 - 6	7
6	None	0	0	0	1	N/E	7	N/E
7(i)	Mild	2	2	1	2	3	4 - 6	9
7(ii) 7(iii) 7(iv)	Moderate (temp 38.4 °C) Moderate (temp 39.0 °C) Moderate (temp 39.0 °C)	1	1	0	0	-	-	-

* Received concurrent oral 6-mercaptopurine and methotrexate.
** Grading in patient 7 was performed nine days after last IT injection.
Bone marrow relapse diagnosed 22 days after last IT injection.
N/E = Not estimated

commencing at four, three and 1.5 hours respectively. Vomiting of moderate severity, requiring intravenous antiemetic therapy, began at six, four and one hour respectively. On each occasion, pyrexia was noted within 12 - 24 hours, reaching a maximum of between 38.4 and 39.0°C. All acute symptoms improved by 36 hours post-therapy and had resolved by 72 hours. No neck stiffness was observed, and apart from tachycardia, no other acute toxicity was recorded.

(e) Delayed toxicity.

This was manifest primarily as myelosuppression (Table 10.5). All patients developed some degree of bone marrow toxicity, first noted at two to four weeks post-injection, with nadir counts at between four and eight weeks. In patients 4 and 6, only transient (one occasion) grade 1 thrombocytopaenia was recorded. Patients 1, 2 and 5 had grade 1 - 2 myelosuppression.

Despite being the smallest child (body weight 17.1 kg), only grade 1 - 2 myelosuppression was observed in patient 7, after having received the highest injected activity (1702 MBq). He subsequently received a total of 3592 MBq over a two week period. Nine days after the last injection, only grade 1 anaemia and leucopaenia was noted. Further assessment of myelotoxicity was complicated by bone marrow relapse of ALL occurring 13 days later, associated with elevated WCC and thrombocytopaenia.

Grade 3 - 4 myelosuppression was noted in patient 3. Following onset at three weeks, nadir counts were seen at between four and six weeks post-therapy; Hb 6.7 gm/dl, WCC 1.9 x 10^9/litre, neutrophils 0.4 x 10^9/litre, platelets 18 x 10^9/litre. Both blood and platelet transfusions were given but, in common with all other patients, he remained asymptomatic. This child, however, was the only one who was taking oral continuation therapy throughout the post-treatment period.

The other delayed toxicity was the occurrence of elevated plasma urea in patient 3, indicative of renal impairment. This may relate to his marked renal uptake of radioiodine (Chapter 11; 3d) and consequent high radiation dose to the kidneys (Chapter 12; 2e). Pre-therapy renal biochemistry was normal. Four months after therapy, a plasma urea of 7.7 mmol/litre (reference range 2.3 to 6.7) was noted, increasing to a maximum recorded value of 9.4 mmol/litre two weeks later. Following this, the plasma urea has remained high at between 8.0 and 9.0 mmol/litre (October 1991, 26 months post-therapy). Plasma creatinine and other biochemical investigations have been consistently normal, with no evidence of hypertension or other clinical signs of renal insufficiency. No neurological, hepatic, thyroid or other toxicity has been recorded in five patients surviving for more than nine months following therapy.

(f) Therapeutic response.

Therapeutic response was assessed by reduction of the CSF blast cell count (Table 10.6). In six patients, pre-therapy counts varied between 10 and 4000 x 10^6 lymphoblasts/litre. In a seventh (patient 2), the CSF white cell count was less than 1 x 10^6/litre, but numerous blast cells were seen on CSF cytospin preparations.

Following targeted therapy, a response was seen in all but one patient. In patient 1, despite an initial CSF lymphoblast count of 4000 x 10^6/litre, a complete absence of blast cells was noted at both two and four weeks post-therapy, with a return of malignant cells at six weeks. This pattern of response was also observed in patient 3. Patients 4 and 5 also had markedly elevated pre-therapy counts of 1310 and 2380 x 10^6/litre respectively. Their CSF was clear at two weeks post-therapy, but blast cells, at a concentration of less than 10 x 10^6/litre, appeared at four weeks from therapy, with a marked increase in the cell count at six weeks. In patient 2, CSF cytospin preparations showed only occasional blast cells at two, four and six weeks post-treatment. At eight weeks,

the CSF was deemed clear of cells, but an elevated blast cell count of 160 x 10^6/litre was noted at 12 weeks.

The final patient to respond (patient 7), had a complete absence of blast cells in the CSF at two, four and six weeks following injection of a cocktail of ^{131}I-labelled antibodies. Malignant cells were, however, seen at eight weeks. Following a course of three further injections, the CSF again cleared at two weeks after the last injection. One week later he was noted to be in systemic relapse. CSF analysis at this time revealed "occasional abnormal cells" on a cytospin preparation. IT chemotherapy was thus administered. These cells were presumably lymphoblasts, either seeding from peripheral blood or representing a true CSF relapse. This event precludes, therefore, a true evaluation of the CNS response to repeated targeted therapy.

Table 10.6

Tumour response in patients receiving targeted radiotherapy.

Patient	CSF Lymphoblast Count (x 10^6/litre)					
	Pre Therapy	Post-therapy				
		Week 2	Week 4	Week 6	Week 8	Week 12
1	4000	0	0	81	-	-
2	CP	Occ.	Occ.	Occ.	0	160
3	10	0	0	10	0	0
4	1310	0	2	145	-	-
5	2380	0	7	1520	-	-
6	63	40	149	-	-	-
7(i)	10	0	0	0	10	-
7(ii - iv)	10	0	SR	-	-	-

CP = Cytospin positive.

Occ. = Occasional cells on cytospin examination.

SR = Systemic relapse.

4. Discussion.

These studies demonstrate the feasibility of IT targeted radiotherapy for childhood CNS ALL. Acute toxicity was consistent with that noted in our 15 patient study [118]. However, in contrast to previous patients, no neck stiffness was documented and in no case were symptoms deemed severe. Acute meningeal irritation occurs as a result of foreign material injected into the CSF and is noted, albeit to a lesser degree, following the IT injection of chemotherapeutic agents such as methotrexate [127].

Aseptic meningitis was also observed in 10% of 73 patients receiving ^{198}Au colloid by lumbar puncture for the prevention of overt CNS ALL [116]. This has also been noted following the introduction of other proteins such as radioiodinated human serum albumin for cisternography [294]. In the latter case, the frequency of aseptic meningitis was diminished by changing the source of albumin, for which reduction in endotoxin contamination of the preparation was proposed as a possible factor. It remains to be seen whether differences in quality control between batches of antibody prove to be associated with an alteration in acute toxicity.

In patient 7, increased acute toxicity occurred during the course of repeated therapy. In addition, the time between injection and the onset of both headache and vomiting became progressively shorter with each injection. This probably results from the development of an increasing HAMA response (Chapter 11; 4) with leptomeningeal deposition of immune complexes. All his symptoms resolved within 72 hours, but nevertheless, this observation has implications with regard to the development of repeated targeted therapy.

Significant myelosuppression (WHO grade 3 - 4) was noted in only one child, who was taking oral continuation therapy throughout the post-therapy period. This almost certainly contributed to his toxicity, and confirms our impression that myelosuppressive chemotherapy should be discontinued at the

time of therapy. There is a theoretical increased risk of systemic relapse if such therapy is discontinued, especially in patients who have sustained such an event previously. It is impossible to determine whether this was responsible for the systemic relapse in patient 7, but further patients will be carefully monitored for this occurrence. Of the first six patients, the lack of significant myelosuppression (other than in patient 3) suggested that dose escalation could safely continue. This was confirmed by the relative lack of toxicity in patient 7 following an injected activity of 1702 MBq, over twice that proposed in the initial dose schedule. Myelosuppression is further discussed in relation to red bone marrow dosimetry in Chapter 12.

The renal toxicity in patient 3, manifest by an elevated plasma urea concentration, is of cause for concern. In this patient, marked renal uptake of ^{131}I was demonstrated by scintigraphy, with an estimated radiation dose to the kidney of 7 Gy (Chapters 11; 3d, 12; 2e). Similar uptake of isotope was noted in patient 4, although no clinical or biochemical toxicity has been evident.

Renal accumulation of ^{131}I probably results from WCMH binding to CD10 expressed on normal kidney (Chapter 3; 5c). Why this was only noted in two of five patients treated with this antibody is unclear. No similar uptake has been noted on any occasion in 40 other patients treated with intrathecally injected conjugates of other antibodies. At present we feel justified in continuing to use WCMH, however antibodies recognizing alternative antigens eg. CD 22 and CD 20 are being considered for investigation (Chapter 13; 2b).

It is too early to determine whether delayed neurotoxicity will be associated with this mode of treatment. No such toxicity has been recorded to date (October 1991) in five patients surviving for more than nine months post-therapy. In particular, there has been no incidence of the post-radiation somnolence syndrome, often experienced following cranial external beam radiotherapy (Chapter 1; 2i). No post mortem examination was undertaken in the four children that have died.

All seven patients receiving a single injection of radioconjugate were evaluable for therapeutic response. Complete disappearance of CSF lymphoblasts for between two and six weeks was noted in five children, the longest response in a child who received the highest activity of ^{131}I, conjugated to an antibody cocktail.

Although remission times are relatively short, these results should be viewed in the light of a high response rate to a single injection of a new agent for a second or third relapse of a highly malignant tumour. Results compare favourably to those in D'Angio's report of two children with overt CNS ALL, who showed no response to treatment with IT ^{198}Au colloid [113].

Further studies will be directed towards increasing the length of remission. A major problem in this respect is the low rate of patient accrual. This, in turn, reflects the low incidence of isolated second CNS relapse of ALL. Pinkerton and Chessells noted only four such cases presenting to the Hospital for Sick Children, Great Ormond Street, London, over an eight year period [295]. Of 1600 children entered into the Medical Research Council (MRC) UKALL X trial between 1985 and 1990, 70 (4.4%) have experienced an isolated first CNS relapse, whereas only 14 (0.875%) have so far experienced a second isolated CNS relapse (August 1991, personal communication, Dr S Richards, Clinical Trials Service Unit, Oxford).

Our group has now entered into a collaboration with the United Kingdom Children's Cancer Study Group (UKCCSG). This enables us to enhance patient accrual and to benefit from input from UKCCSG members. A joint clinical co-ordinating committee has been established to oversee this study. We are also actively seeking to enrol patients from the adult population.

The dose escalation programme will continue, to enable determination of the maximum tolerated activity (MTA) of a single injection of radioconjugate. At present, this will relate to each age group treated. In retrospect, the dose reduction schedule for children should probably have been constructed on the

basis of either body surface area or body weight alone, and not have taken into account changes in the volume of the CNS with age. Whilst this would have resulted in a relatively lower CSF dose/unit injected activity in young children, such a schedule would have been more appropriate to what is predominantly a toxicity study. We are currently considering this revision to our dose schedule. Providing that pharmacokinetics between young children and adults do not differ significantly, this will enable us to determine the MTA across the whole age range. It may also allow a more ready comparison in terms of toxicity between study groups i.e. lymphoproliferative disease and primitive neuroectodermal tumours.

Patients who relapse following either complete or partial response (defined at present as a reduction of greater than 75% of the pre-therapy CSF blast cell concentration) will be considered for further therapy. It is probable that once the MTA of a single injection has been determined, that a course of multiple injections may be investigated as "primary" therapy for second CNS relapse. Assuming myelotoxicity to be dose-limiting, these will probably be scheduled to allow recovery of bone marrow function prior to each injection. This may may offer an advantage over a single injection by virtue of increased accessibility of radioconjugate to tumour cells, and an increased probability of targeting leukaemic cells in a radiosensitive phase of the cell cycle.

A further consideration is that of dose fractionation, the role of which, in targeted radiotherapy, is not yet clear [93]. Additional factors influencing dose scheduling will include pharmacokinetic and dosimetric aspects of therapy, particularly with respect to the development of a HAMA response (Chapter 11; 3f). Logistic factors including radiation protection, bed occupancy and the requirements for systemic chemotherapy in relation to the risk of systemic relapse will also need consideration. Should the results of these studies prove encouraging in terms of both tumour response and toxicity, then therapy may be offered to patients in first CNS relapse (Chapter 13; 1). This will result in a

greatly increased rate of patient accrual, from the population of approximately 5% of children with ALL who present with isolated first CNS relapse.

CHAPTER 11.

PHARMACOKINETIC STUDIES OF TARGETED RADIOTHERAPY FOR MENINGEAL ACUTE LYMPHOBLASTIC LEUKAEMIA.

1. Introduction.

In addition to recording toxicity and response data (Chapter 10), pharmacokinetic studies were undertaken during the clinical investigation of targeted radiotherapy in seven children with CNS ALL. These were performed to define the biodistribution of intrathecally administered radiolabelled antibodies, as well as to provide data for dosimetric models (Chapter 12). Studies in patient 7 provide the opportunity for investigating the pharmacokinetics of repeated therapy, to determine the influence of factors such as the HAMA response.

Conjugate injected into an Ommaya reservoir enters one of the lateral ventricles. The volume of ventricular CSF is approximately 25 ml in normal adults [296] and thus distribution within this space is rapid. Radiolabelled antibody is cleared via the third and fourth ventricles into the basal cisterns and then into the cerebral and spinal subarachnoid space. This flow is essentially unidirectional, partly because of gravity, but mainly due to the continuous production of CSF by the choroid plexus of the lateral ventricles. This accounts for the relatively low ventricular activity of radiolabel following lumbar injection, in contrast to the high levels of activity in the subarachnoid space following ventricular administration [293]. The ventricular space can thus be considered, in pharmacokinetic terms, to be a single compartment system with first order elimination kinetics. It can also be assumed to be connected

in series with the subarachnoid space, so that the elimination rate from the ventricular system is identical to the absorption rate into the subarachnoid space. The normal turnover rate constant for CSF formation in man is 0.0026 $minute^{-1}$, giving a half-time for CSF renewal of 4.5 hours [297].

The mechanisms by which macromolecules are cleared from the CSF are not fully understood, but this process is thought mainly to result from bulk flow via the subarachnoid villi and granulations into the venous sinuses [298]. A smaller component of CSF exits at the lumbar region via the nerve root sheaths, and probably by the lymphatic system, the choroid plexus and via the extravascular space of the brain parenchyma. In this study, these processes are assumed to be governed by first order kinetics, with a blood absorption rate constant identical to the subarachnoid CSF elimination rate constant.

Conjugate is primarily eliminated from the body by renal excretion. A smaller proportion (5 - 10%) may be excreted within bile after metabolism in the liver, or in saliva, gastric secretions and sweat [299]. Conjugate may also enter the extravascular spaces or be taken up by tissues such as those of the reticuloendothelial system, from which they may re-enter the vascular compartment in an intact or metabolized form. Absorption and elimination (back into blood) from these "peripheral compartments" are governed by separate kinetics.

On a mathematical basis, it is useful to regard the body either as a one or a two compartment open system. In a one compartment open model, the radiolabel is assumed to be evenly distributed within a single compartment (blood), elimination from which is by a first order process.

In a two compartment open model, the radiolabel initially enters a central compartment (blood), in which distribution is instantaneous, and is subsequently distributed to peripheral compartments. Elimination occurs from the central compartment only and, therefore, any activity in a peripheral

compartment must transfer back to the central compartment to be eliminated. In these studies, a one compartment model is assumed, i.e. there is no differential flow to and from any slow equilibrating tissues.

2. Methods

Pharmacokinetic investigations were undertaken at individual treatment centres according to the study protocol, under the supervision of the local Medical Physics department. Data was collected and processed centrally in our laboratory.

Data analysis for the determination of pharmacokinetic parameters was primarily based upon values of biological radioactivity to reflect the biodistribution of radiolabelled antibody. This is important when comparing antibodies labelled with different radionuclides. In contrast, dosimetric calculations are based upon data for effective radioactivity, to reflect the actual activity contributing to radiation dose (Chapter 12).

For ^{131}I, effective (eff.) activity may be calculated from measured activity (Chapter 2; 5c) using the following:

$$\textbf{Eff. activity} = \textbf{measured. activity} \cdot 10^{1.5609 \times 10^{-3} \cdot (t_{count} - t_{sampling})}$$

and biological (biol.) activity from:

$$\textbf{Biol. activity} = \textbf{measured. activity} \cdot 10^{1.5609 \times 10^{-3} \cdot t_{count}}$$

where,

$\mathbf{t_{count}}$ = time of counting from injection (hours),

$\mathbf{t_{sample}}$ = time of sampling from injection (hours),

and $\mathbf{1.5609 \times 10^{-3}}$ = the decay constant (base 10) for ^{131}I.

Time-activity curves for each data set were plotted using Cricket Graph™ software on an Apple Macintosh II™ computer. Curve-fitting (base 10) was performed using the same software package. In contrast to studies in guinea pigs, specific curve-fitting software was not employed, although we are planning to undertake a comparison between these two methods in the near future.

Where appropriate, rate constants (**k**) (base e) for absorption and elimination are derived from the fitted slope, using the relationship:

$$\mathbf{k} = \frac{\textbf{slope (base 10)}}{\textbf{log (e)}}$$

Half-times ($\mathbf{T_{1/2}}$) are calculated from:

$$\mathbf{T_{1/2}} = \frac{\textbf{ln 2}}{\textbf{k}} = \frac{\textbf{0.693}}{\textbf{k}}$$

Biological and effective rate constants are related by:

$$\mathbf{k_{biological}} = \mathbf{k_{effective}} + \mathbf{k_{physical}}$$

Half-times are related by:

$$\frac{\mathbf{1}}{\mathbf{T_{1/2}\ biological}} = \frac{\mathbf{1}}{\mathbf{T_{1/2}\ effective}} + \frac{\mathbf{1}}{\mathbf{T_{1/2}\ physical}}$$

(a) Whole body retention.

This was generally recorded using either a fixed or hand-held dose rate meter. It was recommended that measurements be undertaken at least daily for seven days following administration. The patient was to be counted in both anterior and posterior positions at a set distance, and a geometrical mean obtained. Each value was expressed as a percentage of the measurement

immediately following injection. The biological whole body retention was calculated and plotted on a semi-logarithmic scale against time.

(b) Whole blood ^{131}I absorption and elimination.

Samples of whole venous blood (3 - 4 ml) were collected into EDTA-coated tubes from a indwelling venous catheter. Suggested times for sampling were 4, 8, 12, 16, 20, 24, 32, 40, 48 and 72 hours and then daily for up to seven days post-injection, with a final sample at 14 days. Radioactivity in 1 ml of blood was determined in a gamma counter, and the effective and biological activity concentration (MBq/ml) calculated. The activity in the vascular compartment was calculated from the blood volume [300] and expressed as a per cent of the injected activity.

(c) Clearance of ventricular CSF.

Sequential CSF sampling was performed in patients with an Ommaya reservoir. It was suggested that 1 ml samples should be taken at 12 and 24 hours and then daily for up to seven days, with a final sample 14 days after administration. The effective and biological ventricular CSF activity concentration (MBq/ml) was calculated as described above.

(d) Gamma camera imaging.

Static images of isotope distribution were taken as soon as the patient's condition allowed, or as governed by local radiation protection rules. It was recommended that at least two scanning procedures be performed during the first week and, in addition, on days seven and 14 after injection. Views of anterior and posterior head, chest, abdomen and pelvis were suggested, together with left and right lateral views of the head. It was proposed that either ^{133}Ba or ^{57}Co skin markers be used on anatomical landmarks (eg. shoulders and iliac crest). Both gamma camera calibration and deadtime

correction, particularly for early scans, was performed by the local Medical Physicist. Region of interest (ROI) analysis was performed on static acquisitions to enable time-activity curves to be constructed, where appropriate.

(e) External probe measurements.

In patient 7, external probe measurements were performed to further define distribution and elimination of isotope within the CNS, particularly at early time points. This was undertaken using a single channel Scalar™ rate meter interfaced with a heavily collimated NaI detector. The mean of three measurements of counts over ten seconds was recorded for the probe placed on the cranial vertex and over the spine at levels $C_{7/8}$ and $L_{4/5}$.

3. Results.

(a) Whole body clearance of radioisotope.

Data for whole body clearance was obtained following all therapeutic injections but one (patient 1). The method of assessing clearance varied between treatment centres. In patients 6 and 7, this was undertaken using a hand-held dose rate meter, but apart from data collected after patient 7's second injection, the clearance pattern was based only on two recordings.

Sequential recordings were undertaken in four patients. In patients 4 and 5, this was by means of a ceiling-mounted dose rate meter and in patients 2 and 3, by whole body scintigraphy, for which the gamma camera was calibrated using a phantom. Of this group, clearance was complex, with multiphasic kinetics noted in patients 2, 4 and 5 (Table 11.1, Figure 11.1). Detailed pharmacokinetic analysis was thus not undertaken.

Analysis of clearance in patient 7 was hindered by a paucity of data. Nevertheless, a faster clearance rate of clearance was suggested following each of the three injections in the course of repeated therapy, as compared with the first injection, compatible with a faster rate of elimination of ^{131}I from blood (see below). Based on between two and four measurements, the biological half-time was 39.7 hours following the first injection and 14.3, 25.3 and 10.6 hours following injections 2, 3 and 4 respectively.

Figure 11.1

Whole body clearance of ^{131}I following targeted radiotherapy.

Whole body retention of ^{131}I was recorded using a ceiling-mounted dose rate meter (patients 4 and 5) or by gamma scintigraphy (patients 2 and 3). Biological whole body activity is expressed as a percentage of that immediately following injection, and plotted against time on a semi-log scale.

Figure11.1

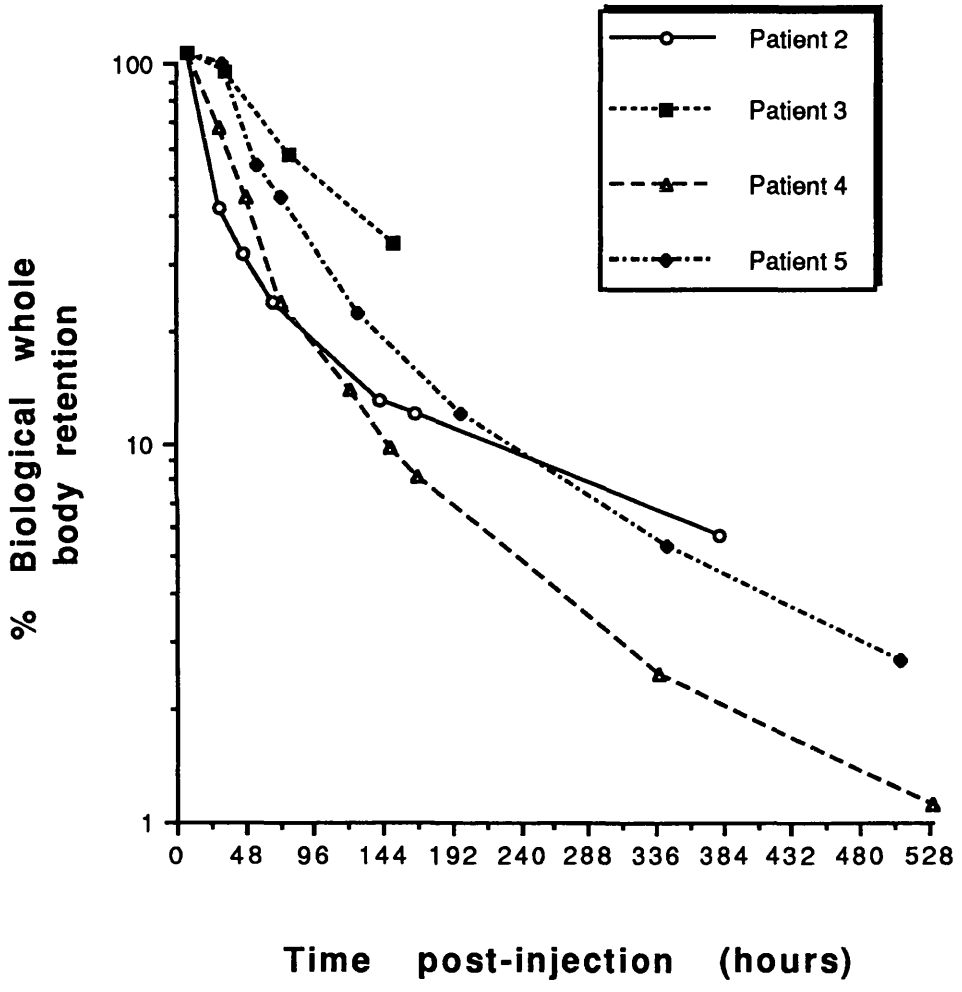
Patient 2
Patient 3
Patient 4
Patient 5
100
10
1
% Biological whole body retention
0
48
96
144
192
240
288
336
384
432
480
528
Time post-injection (hours)

Table 11.1 Whole body clearance data.

Patient	Time Post-Injection (hours)	% Retained Activity-Effective	% Retained Activity-Biological
2	22	36.0	39.0
	40	26.0	30.0
	60	18.0	22.4
	134	7.5	12.2
	158	6.3	11.2
	374	1.4	5.4
3	27	81.0	89.3
	70	42.0	54.0
	144	19.1	32.0
4	22	59.0	63.9
	41	36.0	41.7
	65	21.5	22.2
	113	8.7	13.1
	142	5.5	9.2
	161	4.3	7.7
	331	0.71	2.33
	523	0.16	1.05
5	24	85.4	93.1
	48	42.7	50.7
	66	32.9	41.7
	120	13.5	20.8
	190	5.7	11.3
	336	1.5	5.0
	501	0.41	2.5
6	92	25.0	34.8
7(1)*	68	23.9	30.5
7(2)	21	29.9	32.2
	26	27.0	29.6
	43	10.5	12.3
7(3)	91	6.01	8.3
7(4)	20	25.1	27.0

* Number in parentheses represents injection number.

(b) Blood clearance of radioisotope.

(i) Following a single injection of radiolabelled antibody.

Sequential samples of whole blood were collected from four of six patients receiving a single injection of radioconjugate (patients 1, 3, 4 and 6). Biological and effective blood activity, expressed as per cent injected activity in the vascular compartment, is presented in Table 11.2.

Table 11.2 Blood activity data for patients receiving a single injection of ^{131}I-labelled antibody.

Patient 1

Time Post-Injection (hours)	% Injected Activity in Blood	
	Effective	Biological
5.0	5.70	5.80
12.0	15.20	15.87
17.0	23.20	24.66
29.0	23.80	26.42
35.0	24.40	27.67
41.0	28.20	32.68
47.0	23.60	27.94
59.0	17.80	22.01
71.0	15.40	19.88
83.0	13.80	18.60
159.0	6.90	12.22

Patient 3

Time Post-Injection (hours)	% Injected Activity in Blood	
	Effective	Biological
3.7	8.10	8.21
11.0	21.93	22.81
20.0	20.73	22.28
23.7	19.05	20.74
27.8	17.38	19.20
31.8	16.53	18.26
43.9	13.30	15.57
48.0	11.48	13.64
52.4	10.45	12.62
55.7	9.70	11.85
68.7	8.93	11.43
73.3	8.23	10.71
167.9	3.48	6.36
332.9	0.68	2.33

Patient 4

Time Post-Injection (hours)	% Injected Activity in Blood	
	Effective	Biological
4.0	6.31	6.40
7.3	11.54	11.84
12.8	26.91	28.17
17.0	28.94	30.76
24.0	30.00	32.70
32.0	27.43	30.77
40.7	23.57	27.28
116.8	4.54	6.90
142.8	4.11	6.87

Patient 6

Time Post-Injection (hours)	% Injected Activity in Blood	
	Effective	Biological
9.8	15.99	16.56
19.0	19.30	20.66
24.8	21.18	23.15
34.2	18.72	21.16
43.3	16.38	19.13
50.2	15.43	18.48
69.3	12.64	16.21
91.0	7.63	10.58
122.3	4.38	6.80
166.5	2.60	4.71
333.0	0.99	3.28

Figure 11.2 illustrates time-biological activity curves for this group. Between 5.8 and 16.58% injected activity was noted at the time of the first sample taken at between 3.75 and 9.75 hours. Activity plateaued, reaching a peak of between 20.74 and 32.68% at between 11 and 41 hours post-injection. Blood activity declined more slowly, by biphasic kinetics in patient 6 and by

Figure 11.2

Blood time-activity curves for patients receiving a single injection of ^{131}I-labelled antibody.

Sequential samples of whole venous blood (1 ml) from patients 1, 3, 4 and 6 were counted in a gamma counter and the activity corrected for physical decay for the time between injection and counting. The activity in the vascular compartment was determined for each patient from the blood volume, expressed as a per cent of injected activity, and plotted on a semi-log scale against time.

Figure 11.3

Illustration of curve fitting the elimination phase of biological blood clearance of ^{131}I in patients 1, 3, 4 and 6.

Blood activity for the elimination phase of blood clearance was plotted against time. The exponential equation of best fit together with the goodness of fit was computed.

Figure 11.2

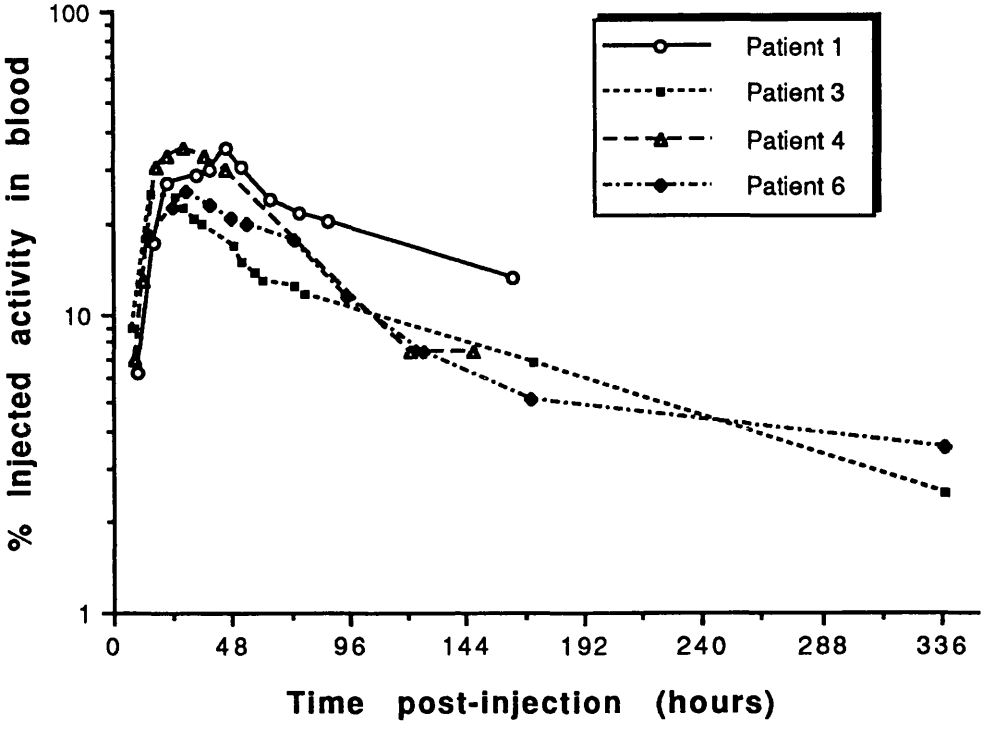

Figure 11.3

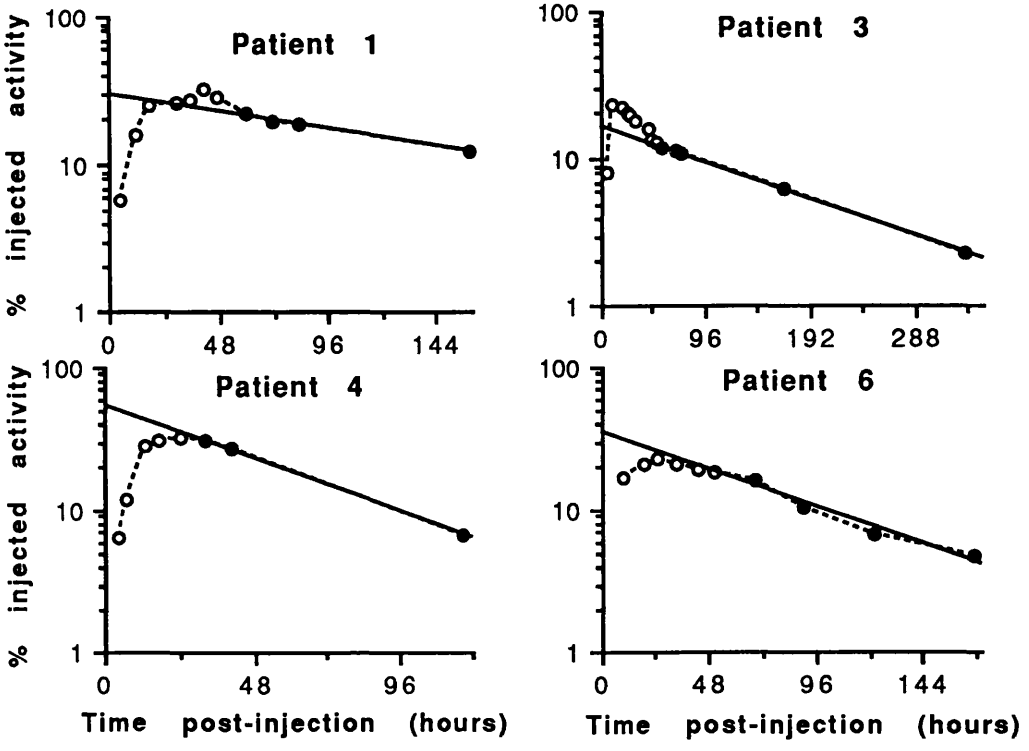

monoexponential kinetics in patients 1, 3 and 4, with a possible second phase of elimination in patient 4.

Calculation of pharmacokinetic parameters.

Assuming the body to be a one compartment system (vascular compartment) governed by first order absorption and elimination kinetics, the various pharmacokinetic parameters are related by the equation [301]:

$$C_{bl} = \frac{F \cdot A_0}{V} \cdot \frac{k_a}{(k_a - k_{el})} \cdot (e^{-k_{el}t} - e^{-k_a t}) \qquad (1)$$

where C_{bl} is the activity concentration in blood

F is the fraction of activity absorbed from the CSF

A_0 is the administered activity

V is the volume of distribution

k_a is the absorption rate constant into the blood

k_{el} is the elimination rate constant from the blood

and t is the time lapsed from injection

In these studies, **F** is assumed to be 1.0 and **V**, equivalent to the blood volume.

Absorption of radiolabel into blood is much faster than elimination. From equation (1), the decrease after peak blood activity is determined by the slower of the two processes (elimination) and for this data, the absorption process is assumed to have negligible influence in the calculation of the elimination rate constant, which is determined directly from the slope of the blood elimination phase. Figure 11.3 illustrates curve-fitting of the elimination phase of biological clearance. The computed equations of best fit, together with elimination rate constants and half-times (calculated from the slope) are

presented in Table 11.3. For patients 4 and 6, the first elimination phase was used in the calculations.

Table 11.3 Blood elimination rate constants and half-times for patients 1, 3, 4 and 6.

Patient No.	Exponential Equation Fitted	R^2	Elimination Rate Constant k_{el} (x 10^{-2} $hour^{-1}$)	Half-time (hours)
1	$y = 30.242 \times 10^{-0.002487x}$	0.996	0.57	**121.1**
3	$y = 16.764 \times 10^{-0.002565x}$	0.999	0.59	**117.5**
4	$y = 55.222 \times 10^{-0.007720x}$	1.000	1.78	**39.0**
6	$y = 34.924 \times 10^{-0.005418x}$	0.964	1.25	**55.5**

In contrast to the calculation of elimination kinetics, measurement of the absorption rate constant must make allowance for excretion of isotope throughout the post-injection period [301]. This problem is solved by use of the "method of residuals", described by Gibaldi and Perrier [288] (see also Chapter 9; 5) and explained in Figure 11.4.

Figure 11.4 Explanation of the method of residuals to calculate the absorption rate constant for a one compartment system.

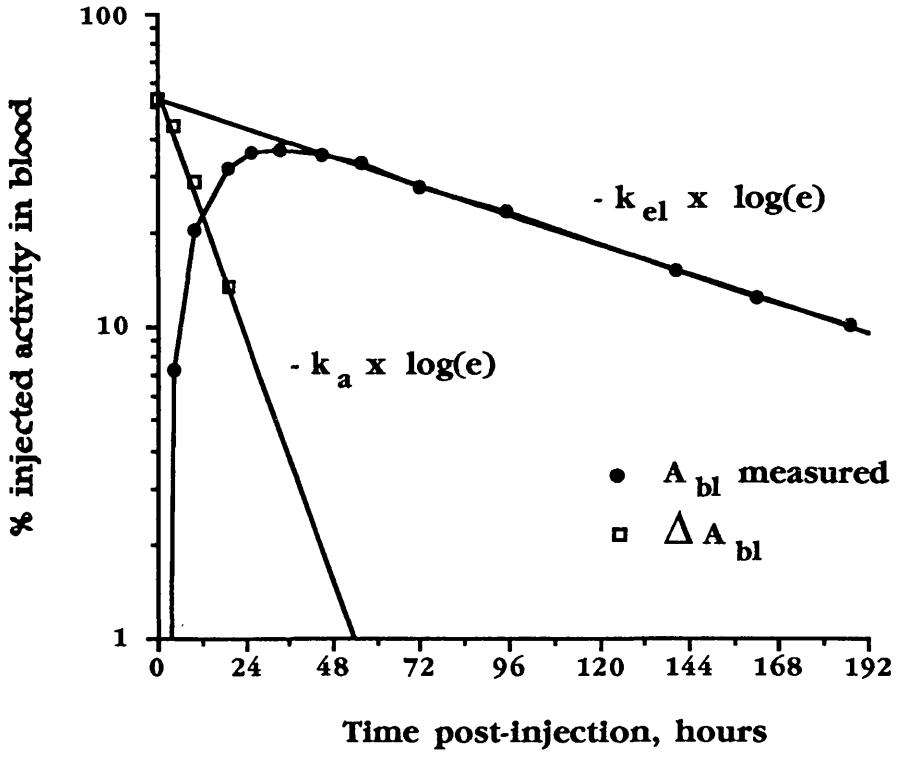

The line of best fit for the linear terminal phase was obtained and used to calculate the extrapolated values on this line corresponding to sampling times for the absorption phase, $\mathbf{A_{blex}}$. The difference values, $\Delta\mathbf{A_{bl}}$ (ΔA_{bl} = A_{blex} - A_{bl} measured), were plotted to yield a line of slope $-\mathbf{k_a} \times \mathbf{log_{(e)}}$. The equation of this curve was obtained and used to calculate the true absorption rate constant and half-time. An example of this method for patient 1 is given below (Table 11.4).

Table 11.4 Determination of the blood absorption rate constant in patient 1, using the method of residuals.

Time (t) (hours)	Activity concentration in Blood-measured (A_{bl}) (% Injected Activity)	Activity Concentration in Blood-extrapolated (A_{blex}) (% Injected Activity)	Difference Between Values (ΔA_{bl}) (% Injected Activity)
0.00	——	30.24	30.24
5.0	5.80	29.34	23.59
12.0	15.87	28.23	12.36

For this patient, the curve of blood activity at times 59 - 159 hours (Table 11.3) describes an equation:

$$A_{bl} = 30.242 \times 10^{(-2.4868 \times 10^{-3}.\ t)}$$

The extrapolated values, A_{blex}, corresponding to the early sampling times (5.0 and 12.0 hours), were then calculated by substituting the early time points for **t** in the equation above. The difference between extrapolated and measured values (ΔA_{bl}) were calculated and plotted against time. The resulting curve describes an equation:

$$\Delta A_{bl} = 31.723 \times 10^{(-3.2865 \times 10^{-2}\ .\ t)}$$

This gives a value for k_a of: 7.6×10^{-2} hour^{-1}

and an absorption rate half-time, $T_{1/2_a}$, of: 9.16 hours.

Values for these parameters were similarly obtained for patients 3, 4 and 6 (Table 11.5). For patients 1, 4 and 6, three extrapolated values were used to curve fit the relevant equation, corresponding to two blood samples taken before the peak of blood activity and the extrapolated value for time 0. As the

method of residuals is subject to significant error if the activity at sampling times at or close to the peak is used to calculate extrapolated values [288], only two values were used to plot curves of "residual activity" for patient 3.

Table 11.5 Blood absorption rate constants and half-times for patients 1, 3, 4 and 6.

Patient No.	Exponential Equation Fitted	Absorption Rate Constant k_a (x 10^{-2} $hour^{-1}$)	Half-time (hours)
1	$y = 31.723 \times 10^{-0.03287x}$	7.57	**9.16**
3	$y = 16.764 \times 10^{-0.08300x}$	19.11	**3.63**
4	$y = 55.222 \times 10^{-0.02425x}$	5.58	**12.41**
6	$y = 33.837 \times 10^{-0.03650x}$	8.41	**8.24**

(ii) Following multiple injections of radiolabelled antibody.

In patient 7, blood was sequentially sampled following all four injections of radioconjugate.

Table 11.6 Blood activity data for patient 7.

Injection 1

Time Post-Injection (hours)	% Injected Activity in Blood	
	Effective	Biological
2.9	3.94	3.99
9.0	9.94	10.26
30.0	14.47	16.11
70.3	5.96	7.67
97.5	3.05	4.33
122.5	1.91	2.97
167.5	0.92	1.67

Injection 2

Time Post-Injection (hours)	% Injected Activity in Blood	
	Effective	Biological
3.5	3.45	3.49
8.8	7.26	7.51
19.9	5.10	5.48
27.8	3.61	3.98
44.1	2.00	2.34
78.8	0.44	0.58
103.0	0.21	0.31

Injection 3

Time Post-Injection (hours)	% Injected Activity in Blood	
	Effective	Biological
1.8	2.11	2.12
3.0	3.69	3.73
9.9	3.92	4.07
19.6	2.22	2.38
28.8	1.57	1.74
50.7	1.01	1.21
70.7	0.59	0.76
93.2	0.37	0.52
144.5	0.19	0.33
168.0	0.13	0.25

Injection 4

Time Post-Injection (hours)	% Injected Activity in Blood	
	Effective	Biological
1.4	1.41	1.41
3.9	4.31	4.36
6.2	5.24	5.36
9.4	4.51	4.66
16.2	2.57	2.72
19.5	1.77	1.90
26.8	1.24	1.37
50.6	0.82	0.99
68.2	0.51	0.66
118.0	0.21	0.31

Following the first injection, 3.99% of the injected activity was noted in the blood at 2.92 hours, increasing to a peak value of 16.11% at 30 hours (Table 11.6, Figure 11.5). In contrast, peak blood activities of 7.51, 4.07 and 5.36% of injected activity were recorded following the second, third and fourth injections respectively, at the earlier time points of 8.8, 9.9 and 6.2 hours respectively.

The blood elimination phase obeyed monoexponential kinetics following the first and second injections (Figure 11.6). Following the third and fourth injections, elimination of ^{131}I was clearly by biphasic kinetics, with the second phase of elimination commencing at 28.8 and 26.8 hours respectively. This indicates a two compartment elimination system [288]. Curves for each phase were thus fitted separately, each having an R^2 value of at least 0.97. Elimination rate constants and half-times were determined as described above (Table 11.7). For injections 3 and 4, values were calculated for both first and second phases of elimination.

Figure 11.5

Blood time-activity curves for patient 7.

The per cent of injected activity is plotted on a semi-log scale against time for each injection (see Figure 11.2).

Figure 11.6

Illustration of curve-fitting the elimination phase of biological blood clearance of ^{131}I in patient 7.

Blood activity during the elimination phase of blood clearance was plotted against time (see Figure 11.3). For injections 3 and 4, the line of best fit for each phase of elimination was computed.

Figure 11.5

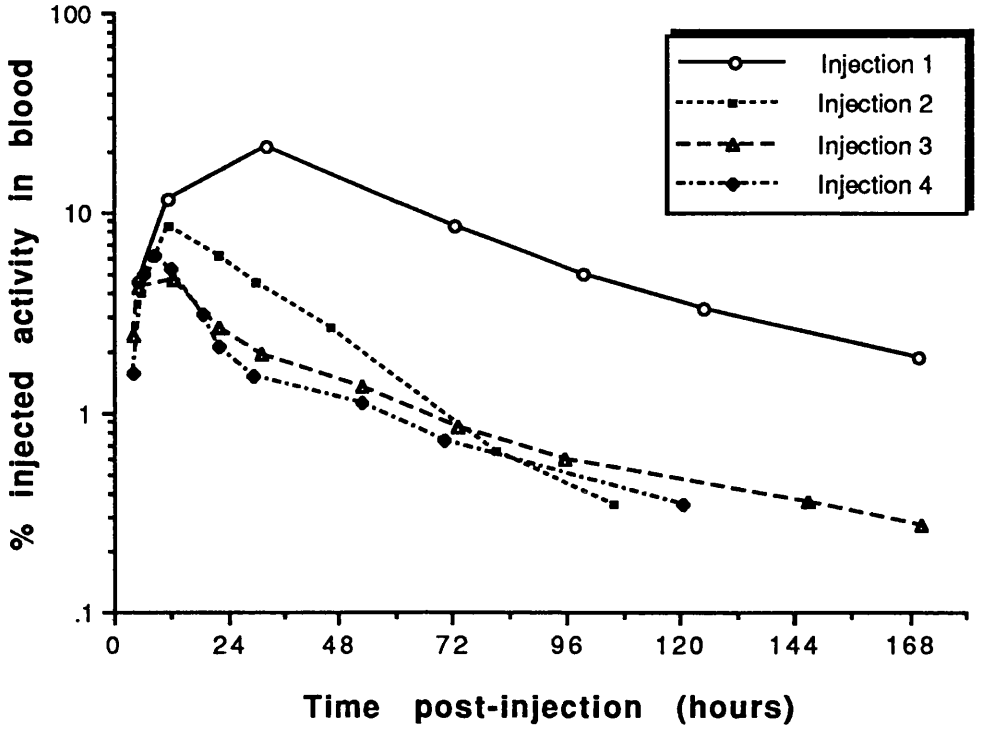

Figure 11.6

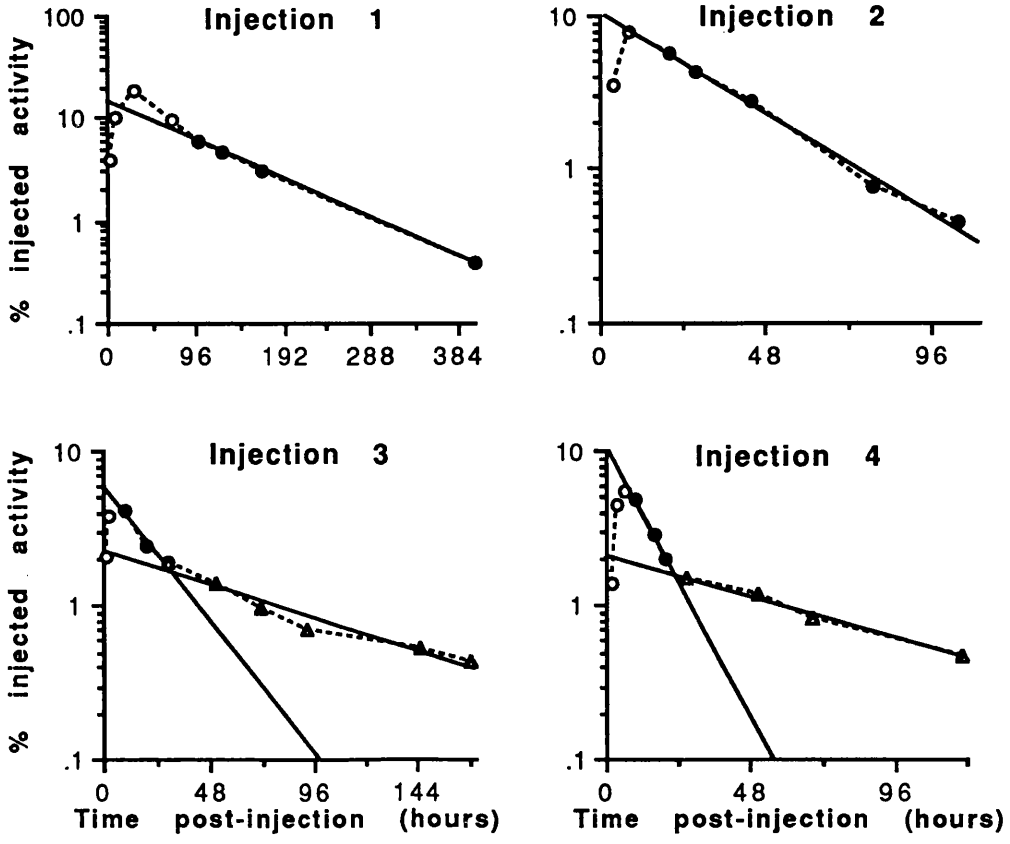

Table 11.7 Rate constants and half-times for biological elimination of ^{131}I from blood in patient 7.

Injection No.	Exponential Equation Fitted	R^2	Rate Constant k_{el} (x 10^{-2} $hour^{-1}$)	Half-time (hours)
1	$y = 20.786 \times 10^{-0.00667x}$	0.985	1.54	**45.11**
2	$y = 10.675 \times 10^{-0.01525x}$	0.995	3.51	**19.74**
3a	$y = 6.148 \times 10^{-0.01956x}$	0.981	4.50	**15.40**
3b	$y = 2.272 \times 10^{-0.00597x}$	0.971	1.37	**50.41**
4a	$y = 8.465 \times 10^{-0.03056x}$	0.983	7.04	**9.85**
4b	$y = 2.134 \times 10^{-0.00711x}$	0.994	1.64	**42.31**

a = First phase of elimination

b = Second phase of elimination

Absorption rate constants were determined by the method of residuals (Table 11.8). For injections 3 and 4, the second elimination phase was assumed to have negligible influence over the absorption rate, k_{el} for this phase being at least three times less than that of the first elimination phase. The equation for the first phase was thus used to determine extrapolated values (A_{blex}). For injection 1, three extrapolated values were used to fit the relevant equation. For reasons discussed above, only two values were able to be used to plot curves of "residual activity" for injections 2, 3 and 4.

Table 11.8 Blood absorption rate constants and half-times for patient 7.

Injection No.	Exponential Equation Fitted	Absorption Rate Constant k_a (x 10^{-2} $hour^{-1}$)	Half-time (hours)
1	$y = 21.220 \times 10^{-0.04758x}$	11.06	**6.33**
2	$y = 10.675 \times 10^{-0.07255x}$	16.71	**4.15**
3	$y = 6.148 \times 10^{-0.13560x}$	31.22	**2.22**
4	$y = 8.465 \times 10^{-0.09341x}$	21.51	**3.22**

This suggests that faster blood absorption, and hence subarachnoid CSF elimination, was associated with each injection in the course of repeated therapy, as compared with that following the first injection.

(c) Clearance of radioisotope from ventricular CSF.

(i) Following a single injection of radiolabelled antibody.

Sequential samples of ventricular CSF were collected from three children receiving a single intraventricular injection of conjugate (patients 4, 5 and 6). Biological and effective ventricular CSF activity data (MBq/ml) is presented in Table 11.9 and time-activity concentration curves are illustrated in Figure 11.7. These curves include a theoretical activity concentration at time 0, based on a ventricular volume of 25 ml. This has been calculated as the approximate normal adult ventricular volume [296] but is assumed to apply to all patients, in line with the increase in overall CSF volume with age, for which approximately 80% of the adult volume is present by three years. In addition, children having received prior cranial irradiation may be expected to have a greater volume of ventricular CSF than untreated children as a result of

cerebral atrophy. Based on this volume, the theoretical activity concentrations at time 0 for patients 4, 5 and 6 are 51.8, 44.4 and 31.08 MBq/ml respectively.

Table 11.9

Ventricular CSF activity data for patients 4, 5 and 6.

Patient 4

Time Post-Injection (hours)	Ventricular concentration of ^{131}I (MBq/ml)	
	Effective	Biological
12.8	0.172	0.180
22.9	2.84×10^{-3}	3.08×10^{-3}
46.4	4.27×10^{-4}	5.04×10^{-4}
96.5	2.7×10^{-5}	3.8×10^{-5}
120.3	1.6×10^{-5}	2.5×10^{-5}
143.0	6.0×10^{-6}	1.0×10^{-5}

Patient 5

Time Post-Injection (hours)	Ventricular concentration of ^{131}I (MBq/ml)	
	Effective	Biological
12.7	0.925	0.968
41.3	3.70×10^{-2}	4.29×10^{-2}
48.8	1.41×10^{-2}	1.68×10^{-2}
332.5	1.63×10^{-4}	5.59×10^{-4}

Patient 6

Time Post-Injection (hours)	Ventricular concentration of ^{131}I (MBq/ml)	
	Effective	Biological
9.8	0.830	0.860
24.8	0.314	0.344
43.5	5.34×10^{-2}	6.24×10^{-2}
69.3	1.21×10^{-2}	1.55×10^{-2}
90.9	6.22×10^{-3}	8.62×10^{-3}
122.5	5.00×10^{-3}	7.76×10^{-3}
165.5	1.44×10^{-3}	2.62×10^{-3}
333.5	3.22×10^{-4}	1.07×10^{-3}

Figure 11.7

Ventricular CSF time-activity curves for patients receiving a single injection of ^{131}I-labelled antibody.

Sequential samples of ventricular CSF (1 ml) from patients 4, 5 and 6 were counted in a gamma counter. The biological activity concentration (MBq/ml) was determined for each patient and plotted on a semi-log scale against time. Curves include a value for activity concentration at time 0, assuming a venticular volume of 25 ml.

Figure 11.7

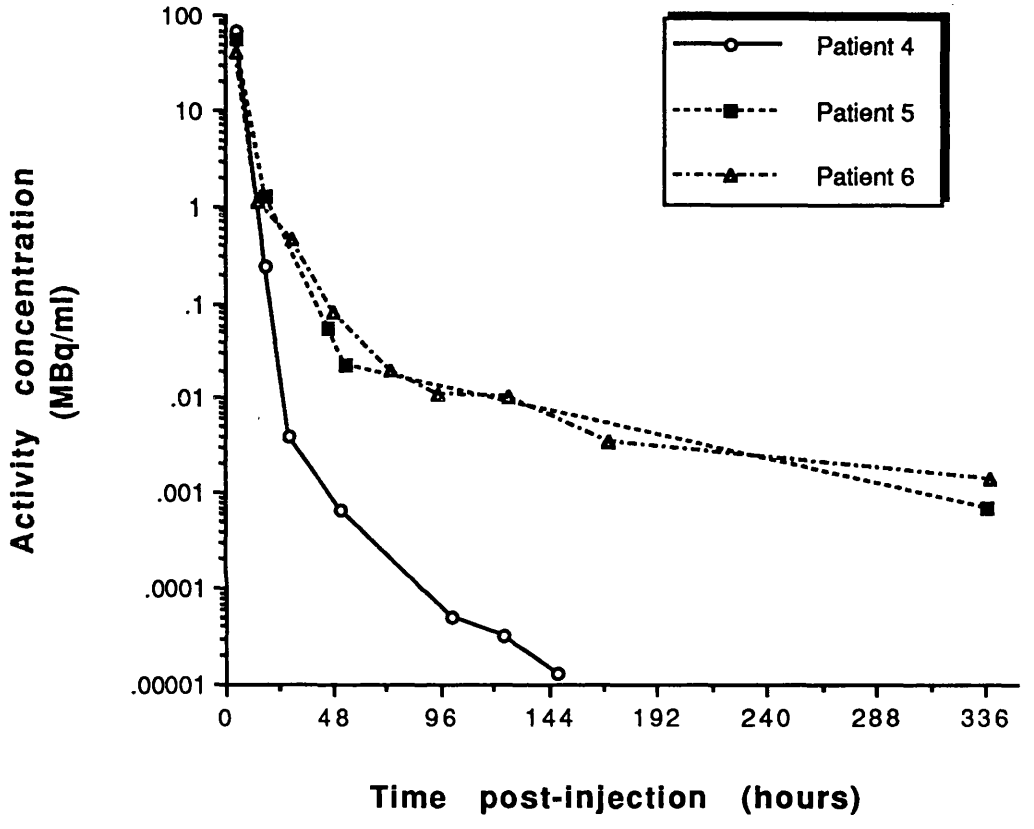
Patient 4
Patient 5
Patient 6
Activity concentration (MBq/ml)
100
10
1
.1
.01
.001
.0001
.00001
0
48
96
144
192
240
288
336
Time post-injection (hours)

Clearance curves for patients 5 and 6 were similar. Based on observed data, radioisotope cleared from the ventricles by biphasic exponential kinetics, the second phase commencing at approximately 49 and 91 hours respectively. In these patients, an apparent rapid phase of clearance is assumed to occur between the time of injection and the first sampling. This probably results from the flushing procedure following conjugate injection. More rapid CSF clearance was noted in patient 4, the reason for which is unclear. This again fitted a biphasic pattern, with the second phase commencing at 23 hours. In this case, a rapid assumed initial phase was not evident. The biological ventricular elimination rate constants and half-times were determined by curve-fitting the observed data (Table 11.10).

Table 11.10

Rate constants and half-times for biological elimination of ^{131}I from ventricular CSF in patients 4, 5 and 6.

Patient No.	Exponential Equation Fitted	R^2	Rate Constant (x 10^{-2} $hour^{-1}$)	Half-time (hours)
4a	$y = 29.501 \times 10^{-0.1740x}$	1.000	40.00	**1.73**
4b	$y = 0.0059 \times 10^{-0.00202x}$	0.971	1.35	**51.20**
5a	$y = 4.026 \times 10^{-0.04832x}$	0.999	11.13	**6.23**
5b	$y = 0.0304 \times 10^{-0.00526x}$	1.000	1.21	**57.18**
6a	$y = 1.252 \times 10^{-0.02559x}$	0.968	5.89	**11.77**
6b	$y = 0.0173 \times 10^{-0.00377x}$	0.900	0.87	**79.92**

a = First clearance phase
b = Second clearance phase

This confirms the much faster first phase of ventricular CSF clearance in patient 4. Half-times for the second phases of clearance were, however, similar between patients.

(ii) Following multiple injections of radiolabelled antibody.

Ventricular CSF activity concentration data for patient 7 is presented in Table 11.11 and time-activity concentration curves are illustrated in Figure 11.8. As above, clearance curves include a projected activity concentration at time 0 of 68.08, 51.04, 47.12 and 45.52 MBq/ml for injections 1, 2, 3 and 4 respectively.

Table 11.11 Ventricular CSF activity data for patient 7.

Injection 1

Time Post-Injection (hours)	Ventricular concentration of ^{131}I (MBq/ml)	
	Effective	Biological
9.0	0.898	0.927
32.8	0.311	0.349
44.0	6.35×10^{-2}	7.44×10^{-2}
70.3	2.06×10^{-2}	2.65×10^{-2}
97.5	6.44×10^{-3}	9.14×10^{-3}
122.5	4.29×10^{-3}	6.66×10^{-3}
167.5	3.22×10^{-3}	5.87×10^{-3}
400.0	8.77×10^{-4}	3.69×10^{-3}

Injection 2

Time Post-Injection (hours)	Ventricular concentration of ^{131}I (MBq/ml)	
	Effective	Biological
3.5	12.358	12.51
8.8	5.742	5.925
19.9	1.227	1.318
27.8	0.118	0.138
44.1	9.99×10^{-2}	0.117
78.8	5.29×10^{-3}	7.02×10^{-3}
103.5	3.29×10^{-3}	4.78×10^{-3}
170.0	1.81×10^{-3}	3.34×10^{-3}

Injection 3

Time Post-Injection (hours)	Ventricular concentration of ^{131}I (MBq/ml)	
	Effective	Biological
1.8	3.233	3.253
3.0	2.658	2.687
9.9	1.264	1.310
19.6	0.406	0.435
28.8	9.65×10^{-2}	0.107
50.7	2.27×10^{-2}	2.73×10^{-2}
70.7	6.03×10^{-3}	7.78×10^{-3}
93.2	1.55×10^{-3}	2.17×10^{-3}
144.5	5.22×10^{-4}	8.77×10^{-4}
168.8	1.89×10^{-4}	3.46×10^{-4}

Injection 4

Time Post-Injection (hours)	Ventricular concentration of ^{131}I (MBq/ml)	
	Effective	Biological
3.9	4.711	4.778
9.4	1.838	1.901
19.5	0.504	0.541
26.8	7.23×10^{-2}	7.96×10^{-2}
50.6	2.28×10^{-2}	2.73×10^{-2}
68.2	7.14×10^{-3}	9.12×10^{-3}
118.0	1.77×10^{-3}	2.70×10^{-3}

Following the first injection, clearance of radioisotope was similar to that noted previously, approximating to a biphasic pattern, with a second phase commencing 98 hours post-injection. A similar clearance pattern was observed after each of the following three injections, but with slightly steeper initial gradients for observed data, and with slightly less residual CSF activity noted at later time points. A probable third phase was, however, noted following injection 3. For all four injections, a rapid initial clearance phase was predicted by extrapolation to the theoretical activity concentration at time 0. The biological elimination kinetics of radioisotope from the ventricles were determined by plotting and curve-fitting the observed data (Table 11.12, Figure 11.9).

Figure 11.8

Ventricular CSF time-activity curves for patient 7.

The biological ventricular CSF activity concentration (MBq/ml) was plotted on a semi-log scale against time for each injection (see Figure 11.7).

Figure 11.9

Illustration of curve-fitting ventricular CSF time-activity concentration curves in patient 7.

Curve-fitting was undertaken on each phase of ventricular CSF clearance of ^{131}I for each injection.

Figure 11.8

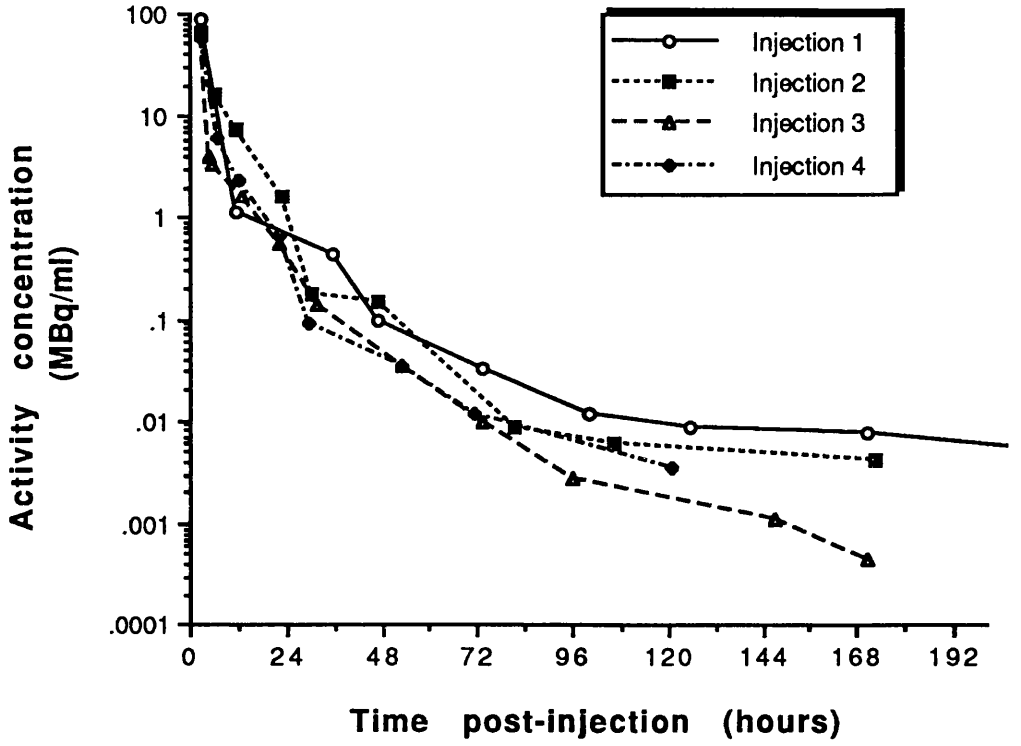

Figure 11.9

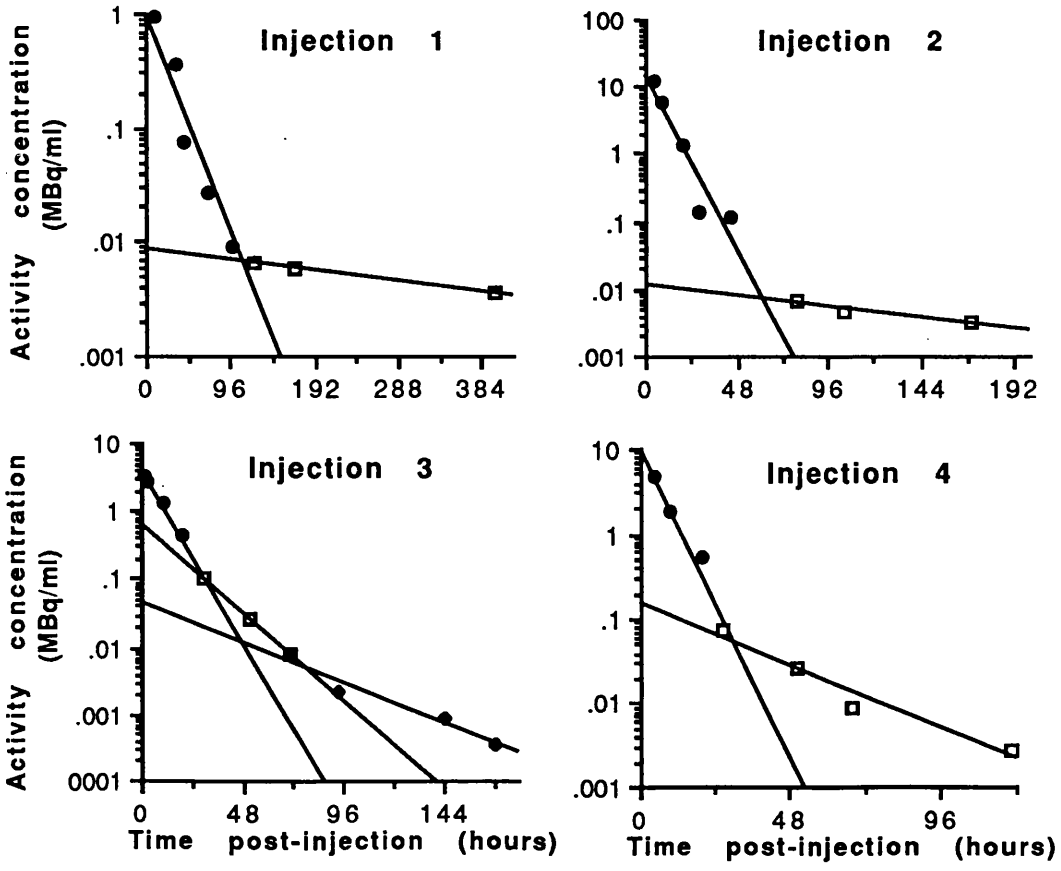

Table 11.12 Rate constants and half-times for biological elimination of ^{131}I from ventricular CSF in Patient 7.

Injection No.	Exponential Equation Fitted	R^2	Rate Constant (x 10^{-2} $hour^{-1}$)	Half-time (hours)
1a	$y = 0.998 \times 10^{-0.0197x}$	0.938	4.53	**15.28**
1b	$y = 0.00846 \times 10^{-0.0009x}$	0.997	0.21	**333.2**
2a	$y = 14.638 \times 10^{-0.0541x}$	0.889	12.46	**5.56**
2b	$y = 0.0117 \times 10^{-0.0033x}$	0.924	0.76	**91.57**
3a	$y = 4.161 \times 10^{-0.0534x}$	0.994	12.30	**5.64**
3b	$y = 0.656 \times 10^{-0.0272x}$	1.000	6.27	**11.05**
3c	$y = 0.04671 \times 10^{-0.0125x}$	0.953	2.88	**24.03**
4a	$y = 10.481 \times 10^{-0.0760x}$	0.969	17.51	**3.96**
4b	$y = 0.158 \times 10^{-0.156x}$	0.962	3.59	**19.30**

a = First clearance phase
b = Second clearance phase
c = Third clearance phase

Half-time values indicate a faster observed initial ventricular CSF clearance for injections 2 - 4, as compared with that for the first injection. Faster rates were also noted for subsequent clearance following injections 3 and 4 as compared with injection 2.

(d) Gamma camera imaging.

Scintigraphic imaging was undertaken following all ten therapeutic injections. The timing and number of acquisitions varied between patients, as governed by local radiation protection rules. The time of the first scan thus varied between 16 hours and seven days. As a result, meaningful analysis of CSF clearance by ROI analysis was not possible, but imaging was able to provide a general overview of the biodistribution of radioconjugate, as well as providing data for radiation dose estimates in two children who demonstrated renal uptake of radioisotope.

Complete distribution of radioisotope throughout the subarachnoid space was noted following all injections. Scans in both patients receiving conjugate by lumbar injection (patients 1 and 2) demonstrated marked lumbo-sacral activity (Figure 11.10), persisting for at least six days post injection. This was not observed in any other patient and almost certainly results from leakage of CSF into the subdural and extra-dural spaces, rather than subarachnoid pooling of radioisotope. In addition, cranial activity in patients 1 and 2 approached background levels by 84 hours and 40 hours respectively, whereas following intraventricular injections, cranial uptake was noted on all scans for at least four days and in all but one series (patient 6), at least seven days post therapy. These observations give further support to the choice of intraventricular injection as the preferred route of administration.

Uptake in both liver and spleen was noted following all injections, in common with that observed in previous studies [302] [303]. This was generally of low intensity and ROI analysis was not undertaken. Of more concern was the observation of renal uptake in two children. In patient 3, intense activity was noted on the first scan at 27 hours (Figure 11.11). This was still present on the final image taken 14 days post-therapy. In patient 4, maximal activity was demonstrated at 24 hours, with counts over the kidneys approaching background by seven days. Quantitative renal activity (MBq) was determined by the local Medical Physicist (patient 3, Dr L Hawkins, St. Bartholomew's Hospital, London; patient 4, Ms S Owens, Christie Hospital, Manchester) after gamma camera calibration and subtraction of background (Tables 11.13, 11.14). For patient 4, activity is given only for the left kidney, for which the margins were clearly distinguishable.

Figure 11.10

Spinal gamma camera scintigraphy following lumbar injection of radioimmunoconjugate.

Static acquisition in patient 1, 24 hours after injection of radioimmunoconjugate by lumbar puncture. Marked lumbo-sacral activity is noted.

Figure 11.11

Abdominal gamma camera scintigraphy in patient 3

Static acquisition in patient 3, 27 hours and six days after intraventricular injection of ^{131}I-WCMH. Marked uptake in both kidneys (K) is demonstrated.

A = 27 hours - Uptake of isotope is also noted in the head, liver (L), spleen (S) and bladder (B).

B = 6 days

Figure 11.10

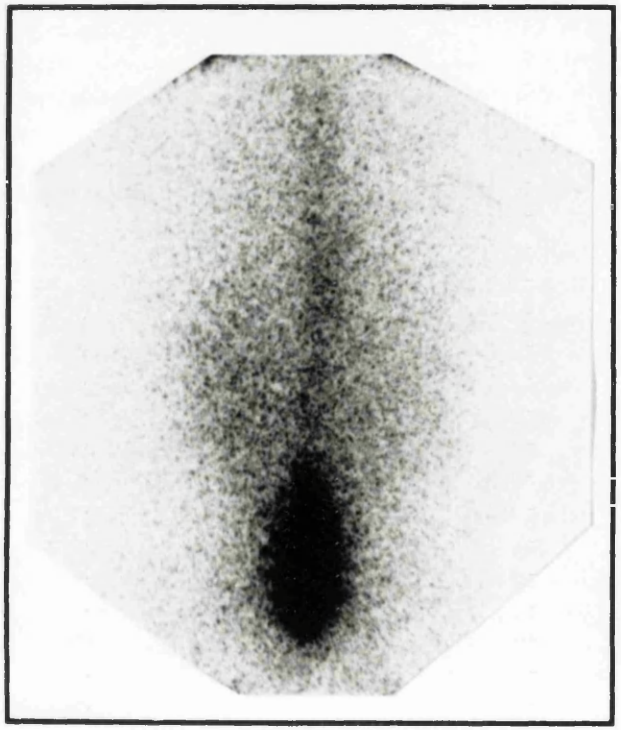

Figure 11.11

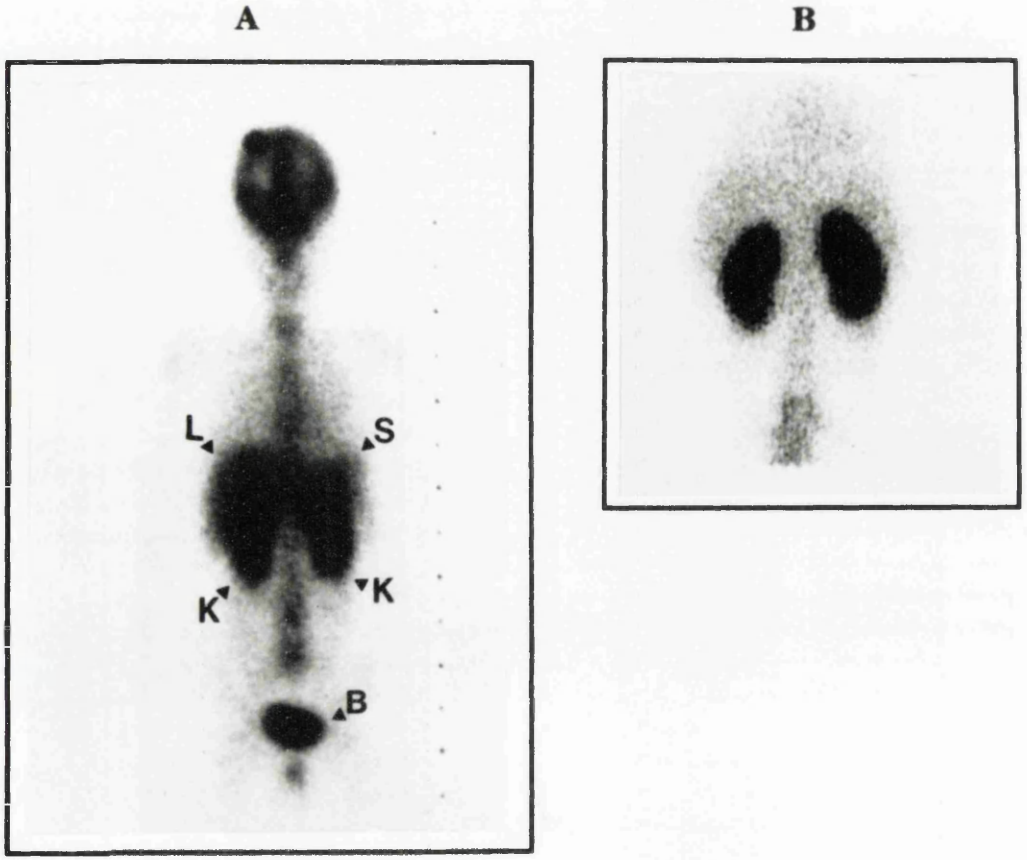

Table 11.13

Renal activity in patient 3 following intraventricular injection of ^{131}I-WCMH.

Time Post-Injection (hours)	Renal Activity (MBq)	
	Right Kidney	Left Kidney
27	97	96
70	61	61
144	20	23

Table 11.14

Activity in left kidney of patient 4 following intraventricular injection of ^{131}I-WCMH.

Time Post-Injection (hours)	Activity (MBq)
22	22.9
41	14.6
65	7.7
110	3.3
161	1.6
331	0.3
523	0.1

(e) External probe measurements in patient 7.

External probe measurements were performed in patient 7 following all four injections. Results as the mean of three 10 second counts for each CNS level are presented below, together with values corrected for physical decay (Table 11.15).

Table 11.15 Data from external probe measurements in patient 7.

Injection 1.

Time Post-Injection (hours)	Counts per 10 seconds					
	Effective			Biological		
	Vertex	C 7/8	L 4/5	Vertex	C 7/8	L 4/5
0.8	3075	1837	1288	3083	1842	1291
2.8	2544	1142	1643	2570	1154	1660
9.5	1549	1497	1341	1603	1549	1388
19.5	1164	1150	1120	1249	1233	1201
44.0	336	176	463	429	206	542
97.5	141	52	76	200	74	107
122.5	48	47	187	74	72	290
196.0	1.5	2.1	0.1	3.0	4.2	0.3

Injection 2.

Time Post-Injection (hours)	Counts per 10 seconds					
	Effective			Biological		
	Vertex	C 7/8	L 4/5	Vertex	C 7/8	L 4/5
0.2	4011	N/E	N/E	4013	N/E	N/E
3.58	3500	2549	1643	3545	2582	2033
8.8	1438	1228	1341	1484	1267	1045
20.0	145	145	1120	156	156	145
27.5	141	143	463	156	157	186
44.0	35	48	76	41	56	45
170	1.4	2.7	0.1	2.6	5.0	3.5

N/E = Not estimated

Injection 3.

Time Post-Injection (hours)	Counts per 10 seconds					
	Effective			Biological		
	Vertex	C 7/8	L 4/5	Vertex	C 7/8	L 4/5
0.08	1053	N/E	N/E	1053	N/E	N/E
0.2	1332	N/E	N/E	1333	N/E	N/E
0.3	1334	1332	1215	1335	1333	1216
1.6	1444	1664	1946	1452	1673	1957
4.6	1811	1785	1828	1841	1815	1858
7.3	1712	1673	1507	1758	1718	1547
9.8	1416	1358	1284	1467	1407	1330
19.7	316	281	242	339	302	260
28.8	73	84	87	81	93	96
50.8	48	23	21	58	28	25
70.8	6.8	10	14	8.8	13	19
93.3	8.35	6.4	9.0	12	9.0	13
144.5	1.7	2.5	2.7	2.8	4.1	4.5

N/E = Not estimated

Injection 4.

Time Post-Injection (hours)	Counts per 10 seconds					
	Effective			Biological		
	Vertex	C 7/8	L 4/5	Vertex	C 7/8	L 4/5
0.08	1753	N/E	N/E	1754	N/E	N/E
0.2	1652	1685	1512	1653	1686	1513
1.4	1443	1378	1312	1450	1385	1319
4.0	1129	1177	1243	1145	1194	1261
9.4	1082	998	935	1119	1032	967
19.7	105	61	64	113	66	69
26.8	24	27	27	26	30	30
50.4	12	25	12	14	30	14
69.3	7.7	8.1	6.9	9.9	10	8.8
118.0	5.8	6.1	5.5	8.8	9.3	8.4

N/E = Not estimated

Following the first injection, greater activity was recorded over the head as compared with the spine, at both 0.8 and 2.8 hours (Figure 11.12). Counts over the head and cervical spine were similar at 9.5 and 19.5 hours, with slightly lower activity over the lumbar spine. Thereafter, no differences was observed between measurements at each site. A similar pattern of distribution was observed after injection 2, with counts similar at each site from 20 hours. In contrast, rapid distribution of isotope was noted following the third injection, with identical counts over the head and cervical spine by 0.3 hours, with only slightly lower lumbar activity at this time. This may have resulted from using a larger volume of normal saline to flush the Ommaya reservoir. At 1.6 hours, counts were highest over the lower spine but thereafter activity was similar at all three sites. The pattern of distribution after the final injection was similar to that following the third, with equivalence in activity by 0.2 hours.

Because of differences in injected activity and the pattern of cerebrospinal distribution of isotope, it is not possible to accurately compare counts at each site between injections, especially at early time points. Nevertheless, a marked difference was noted in the rate of clearance of ^{131}I from the head and spine between the first injection and each of the administrations in the course of repeated therapy. Following injection 1, activity cleared from each site by apparent monoexponential kinetics (Figure 11.13). In contrast, clearance following subsequent injections was very similar, in which, after the initial distribution phase, activity cleared by biphasic kinetics, with a faster first phase and a slower second phase of clearance commencing at between 26 and 51 hours.

Elimination rate constants and half-times were calculated after curve-fitting data for biological clearance (Table 11.16).

Figure 11.12

External probe measurements in patient 7: time-activity curves by injection.

External probe measurements were undertaken using a single channel Scalar™ rate meter interfaced with a heavily collimated NaI detector. The mean of three measurements of the counts over 10 seconds was recorded for the probe placed on the cranial vertex and over the spine at levels $C_{7/8}$ and $L_{4/5}$. Counts were corrected for physical decay and plotted on a semi-log scale against time.

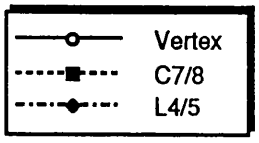

Figure 11.12

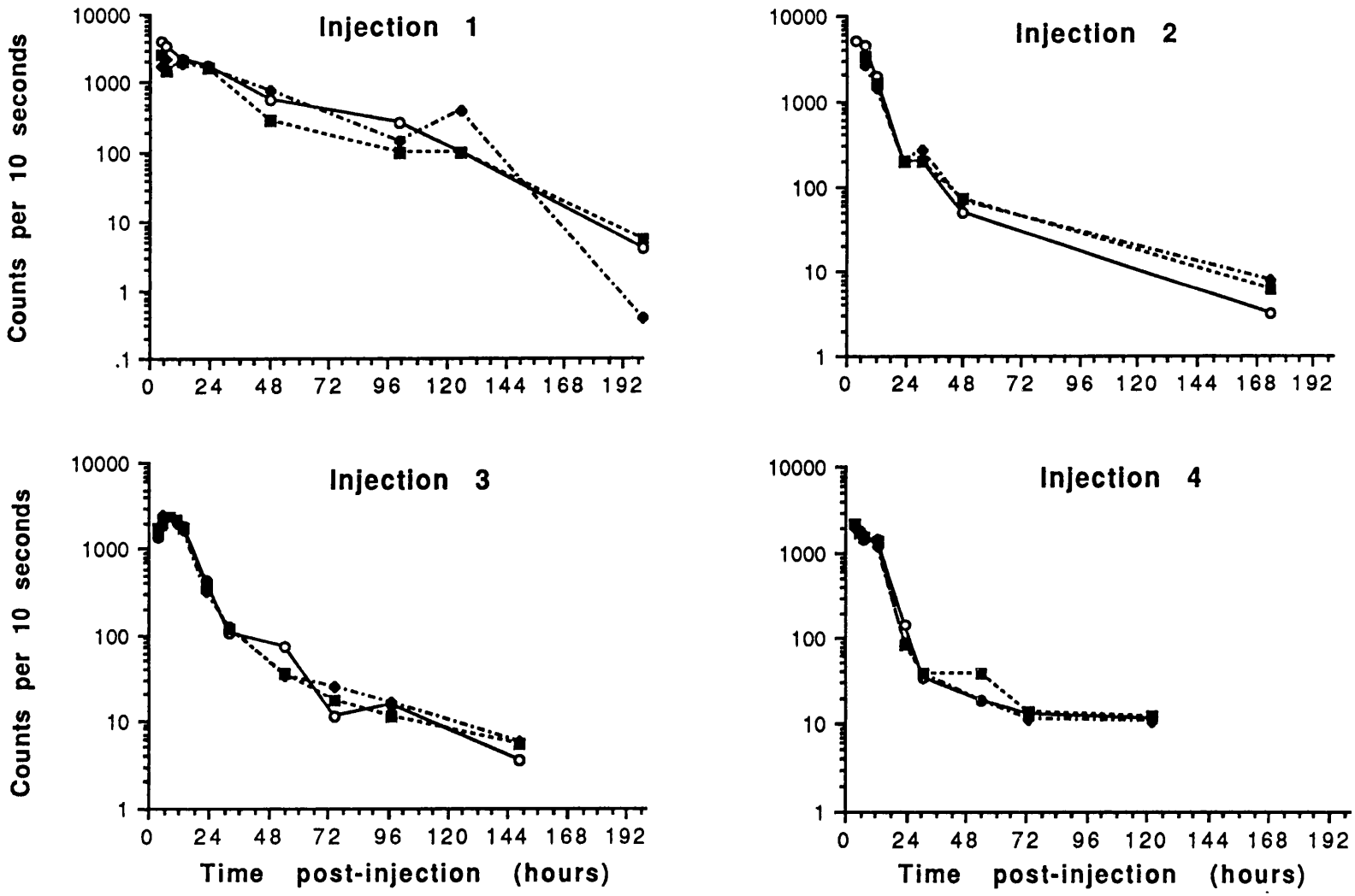
Injection 1
Injection 2
Injection 3
Injection 4
Counts per 10 seconds
Counts per 10 seconds
10000
1000
100
10
1
.1
0 24 48 72 96 120 144 168 192
Time post-injection (hours)
Time post-injection (hours)

Figure 11.13

External probe measurements in patient 7: time-activity curves by site.

Curves illustrate a comparison between injections of external probe measurements for each site (cranial vertex and spine at levels $C_{7/8}$ and $L_{4/5}$) (see Figure 11.12).

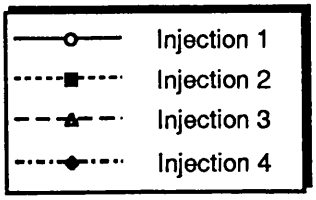

Figure 11.13

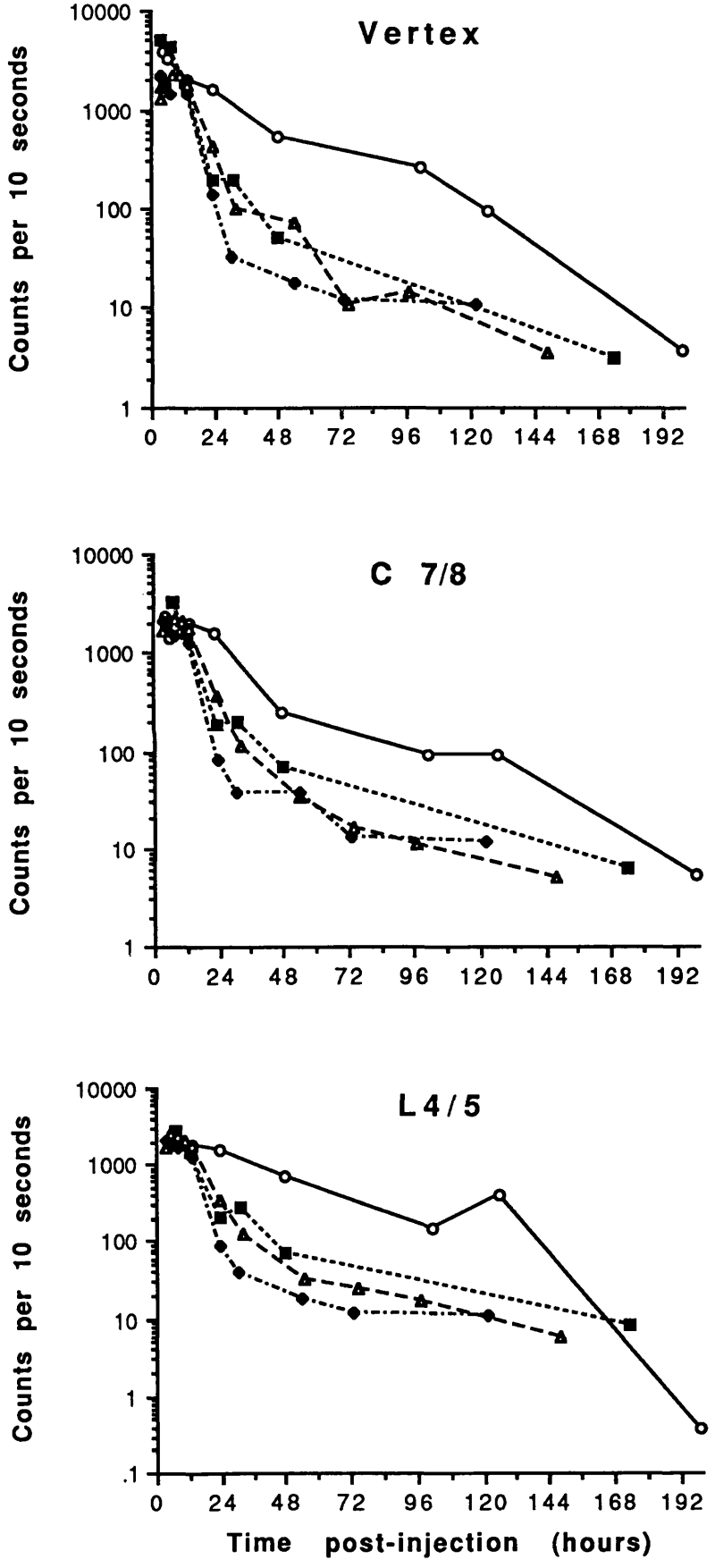
Vertex
C 7/8
L4/5
Counts per 10 seconds
10000
1000
100
10
1
.1
0
24
48
72
96
120
144
168
192
Time post-injection (hours)

Table 11.16

Rate constants and half-times for biological elimination of ^{131}I from the CNS in patient 7 - external probe data.

Probe Site	Injection No.	Rate Constant (x 10^{-2} $hour^{-1}$)	Half-time (hours)
Vertex	1	3.25	**21.3**
	2a	10.90	**6.4**
	2b	2.20	**31.5**
	3a	14.58	**4.8**
	3b	2.93	**23.6**
	4a	21.58	**3.2**
	4b	2.32	**29.9**
$C_{7/8}$	1	2.98	**23.2**
	2a	9.46	**7.3**
	2b	1.92	**36.1**
	3a	13.95	**5.0**
	3b	1.92	**36.1**
	4a	20.80	**3.3**
	4b	1.42	**48.7**
$L_{4/5}$	1	2.93	**23.7**
	2a	8.87	**7.8**
	2b	1.67	**41.5**
	3a	13.84	**5.0**
	3b	1.85	**37.5**
	4a	20.44	**3.4**
	4b	2.85	**24.3**

a = First elimination phase.

b = Second elimination phase.

These calculations confirm a much faster rate of ^{131}I clearance during the first elimination phase following injections 2 - 4 as compared to the overall rate of clearance following injection 1. In addition, values for $T_{1/2}$ for the first elimination phase became somewhat shorter with each injection in the course of repeated therapy.

(f) Demonstration of human anti-mouse antibody (HAMA) response in patient 7.

The faster clearance of ^{131}I from both blood and CSF following injections 2 - 4 almost certainly results from the development of a HAMA response. Evidence of immune complex formation was obtained by FPLC analysis of the CSF in patient 7. Two days after injection 1, 200 µl CSF was subjected to FPLC gel filtration on a Superose-12™ column (Chapter 2; 5e). The activity (cpm) in each 0.5 ml fraction was estimated and plotted against fraction number. A large peak (fractions 23 - 30), equivalent to IgG was noted (Figure 11.14). No higher molecular weight species were observed, although there was evidence of fragmentation (fractions 31 - 45) and free iodine (fractions 65 - 70). A similar procedure was undertaken at both six and 24 hours after injection 4. At six hours, a single Ig peak was observed, together with that representing free iodine (Figure 11.15). In contrast, at 24 hours, the majority of ^{131}I was associated with higher molecular weight species, indicative of immune complex formation. These observations are discussed in detail below.

Figure 11.14

FPLC gel filtration analysis of CSF following patient 7's first injection of radioconjugate.

Two days after injection, 200 µl CSF was subjected to FPLC gel filtration on a Superose-12™ column (Chapter 2; 5e). The activity (cpm) in each 0.5 ml fraction was estimated and plotted against fraction number (see text).

Figure 11.15

FPLC gel filtration analysis of CSF following patient 7's fourth injection of radioconjugate.

FPLC gel filtration of CSF (see Figure 11.14) was undertaken at both six and 24 hours after injection 4 . At six hours, a single Ig peak is noted, together with that representing free iodine. At 24 hours, the majority of ^{131}I was associated with higher molecular weight species, indicative of immune complex formation.

Figure 11.14

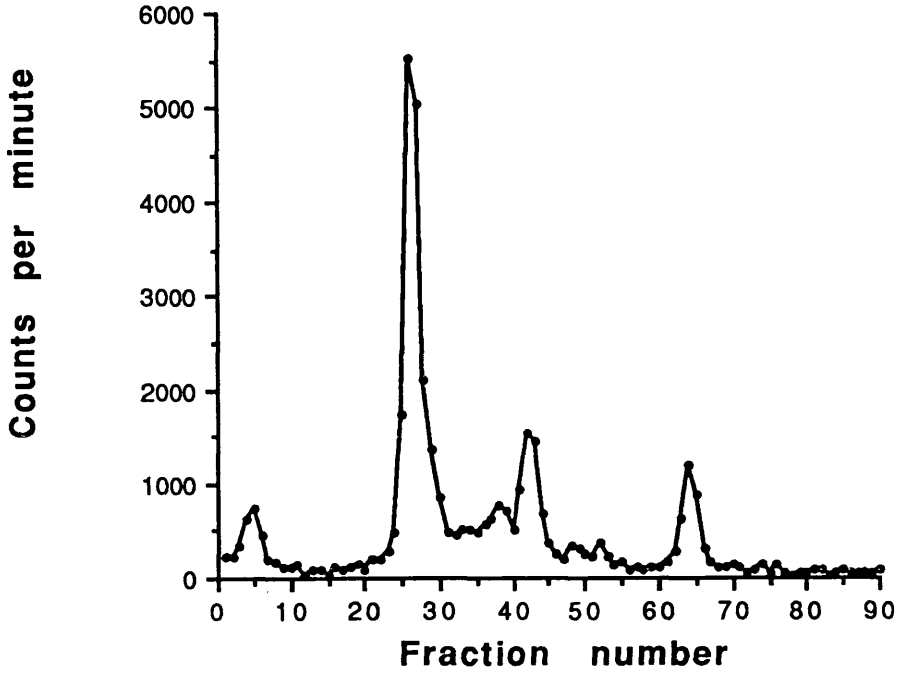

Figure 11.15

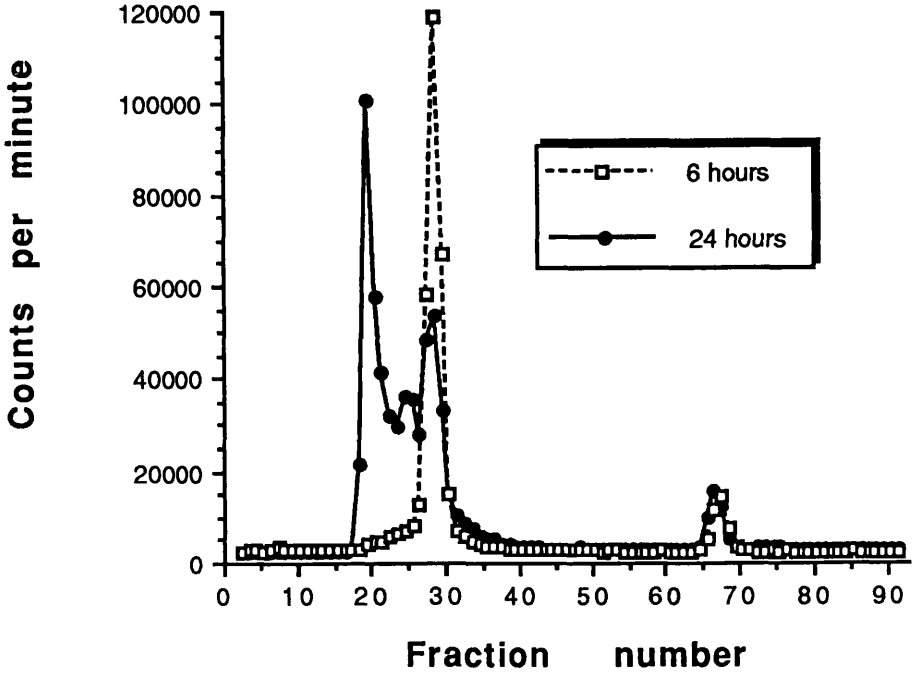

4. Discussion.

These studies were aimed to provide further data on the biodistribution of radioconjugates administered into the CSF, and thereby enable estimation of dosimetry for both normal tissues and CSF (Chapter 12). A drawback to this work has been the difficulty in examining fully the biodistribution of conjugate within the whole of the CSF pathways. Whilst CSF sampling from the Ommaya reservoir gives a direct measurement of ventricular activity, it is clear that this does not reflect the level of isotope present in the cerebral and spinal subarachnoid space.

Quantitative gamma camera scintigraphy could not reliably be undertaken to define the early biodistribution of radiolabel following injection of therapeutic amounts of ^{131}I. This is due to radiation protection considerations precluding imaging within 24 to 48 hours in the majority of institutions, and the energy spectrum of this isotope hindering precise ROI analysis of therapeutic activities. Direct sampling of lumbar CSF, either by intermittent puncture or by an indwelling spinal catheter/reservoir was considered too invasive. Another approach is to undertake pre-therapeutic tracer studies, as performed during our initial pilot study [302]. Again, these were considered unjustified for this study in terms of their relatively invasive nature, especially when undertaken in children. In addition, patients with CNS ALL often have rapidly progressive symptoms, precluding a lengthy interval between study entry and therapy. Finally, there is a risk of tracer amounts of injected antibody inducing a HAMA response, thereby altering the pharmacokinetics during therapy.

An alternative method of assessing CSF biokinetics was adopted for patient 7, namely external probe measurements. Problems with this approach include collimation of activity i.e. between CSF and blood, and precise and reproducible localisation of CSF pathways, especially within the

head. Nevertheless, external probe measurements were technically easy to perform, could be undertaken frequently, appeared reproducible for each time point and followed a consistent pattern between recording times. Consequently, the Physics Protocol for these studies now recommends external probe recordings in all patients. There remains, however, a problem with radiation exposure to staff performing such measurements, especially soon after injection.

Activity within the vascular compartment was measured directly. Blood profiles were unobtainable in two patients (patients 2 and 5) due to the well recognised difficulties with venous access in this study population. Whilst the recommended sampling times appear to give a good overview of the pattern of blood absorption and elimination, it is clear that the emphasis in future studies should be on increasing the frequency of sampling during the blood absorption phase. This is necessary to provide a more reliable estimation of the blood absorption rate constant, especially in the face of repeated therapy where absorption is more rapid (see below).

Assessment of the clearance pattern of isotope from the whole body was somewhat hindered by infrequent recordings (patients 6 and 7) and non-standardised techniques. This requires attention in future studies.

The first two patients received injection by LP. Although it is impossible accurately to compare CSF distribution patterns of ^{131}I following this with the intraventricular route, scintigraphic evidence suggested that the latter route provided both improved distribution to the cranial CSF pathways and, overall increased retention of isotope within the cranium.

Support for the use of intraventricular injection comes from a number of sources. In 1962, Rieselbach demonstrated that the pattern of subarachnoid distribution of agents injected by the lumbar route was highly volume dependent [112]. Using ^{198}Au colloid injected into monkeys, he demonstrated that a volume of at least 10% and 25% of the total CSF was required for

significant radioactivity to reach the basal cisterns and the cerebral ventricles respectively. Shapiro *et al.*, demonstrated that methotrexate concentrations in the cerebral ventricles are higher and less variable following intraventricular as compared with lumber injection [167]. In addition, studies of both radiocolloids and drugs have demonstrated a high incidence of leakage into the subdural and extradural spaces following lumbar injection, a phenomenon also observed in this study in both patients receiving immunoconjugate by this route.

The improved CSF distribution of intraventricularly injected agents was also confirmed in a recent study by Smith *et al.*, performed in collaboration with our group. In a paired-label experiment, the authors compared the pharmacokinetics of radiolabelled DTPA injected either intraventricularly or via a lumbar catheter [293]. Following lumbar administration, ventricular CSF activity only reached a maximum of 10% of the injected dose per gram of CSF, never achieving levels obtained in the lumbar subarachnoid space.

It is appreciated that determination of clearance kinetics from ventricular CSF may be subject to errors resulting from a relative infrequency of sampling, especially at early time points. A balance must be struck between the number of samples taken and radiation exposure to personnel. In addition, removing a large volume of CSF and may falsely alter CSF activity concentration in terms of accurate pharmacokinetics, dosimetry and possibly therapeutic efficacy. Nevertheless, the clearance pattern in all four patients for a single or first injection of radioimmunoconjugate followed biphasic exponential kinetics, consistent with data from our previous studies [67] [303], and from current data in five patients treated similarly for leptomeningeal medulloblastoma (Personal communication, Mr V Papanastassiou, Imperial Cancer Research Fund, Bristol). The first phase probably reflects ventricular CSF production. The rapid first phase clearance in patient 4 is difficult to explain, but may be due to excessive flushing of the reservoir. Similarly, the

reason for the somewhat slower clearance following patient 7's first injection is unclear.

Following initial clearance of radiolabel and distribution throughout the subarachnoid space, a state of equilibrium is probably reached between ventricular and subarachnoid isotope concentrations, as clearance reflecting CSF production is partially offset by retrograde flow back into the ventricles. This may account for the second phase of clearance, for which the rate constant was similar in patients 4, 5 and 6. Smith *et al.,* (see above) noted equivalence in ventricular and lumbar CSF activity concentration six hours after intraventricular injection [293]. After this time, activity at both sites cleared relatively slowly, with lumbar activity maintaining a level approximately twice that observed in the ventricles (20 v 10% of injected activity).

A fast early phase of ventricular clearance, between an assumed activity at time 0 and that of the first sample, was observed in all but one patient. This may reflect the CSF renewal rate with a lesser contribution from CSF backflow. Additional factors may be the volume of saline flush employed and positioning of the patient at, and shortly after, injection.

The method of residuals may be used to correct the rate constant for the first phase of CSF clearance using that for the second phase. Due to the large differences in observed rate constants between early and late phases, it is probable that the last phase has very little influence over the early phase/s. This is confirmed by a co-worker investigating similar kinetics in patients with medulloblastoma (see above).

Time-activity curves for the vascular compartment appeared similar between patients receiving a first conjugate injection. Both absorption and elimination phases approximated to a monoexponential pattern, confirming an apparent one compartment system. A peak blood activity of between 16.1 and 32.7% of injected activity is consistent with that noted in previous patients receiving IT targeted radiotherapy [67]. Similar peak blood levels were noted

following other compartmentalised injections. Stewart *et al.*, investigated the pharmacokinetics of intraperitoneal radioimmunotherapy in patients with ovarian carcinoma [304]. In this study, a mean peak of 26% injected activity was present in the blood at 40 hours. The later timing of the peak as compared with that observed in the present study (mean = 23.8 hours, SD = 7.6 hours) may be explained by a slower mechanism for conjugate absorption from the peritoneum eg. by lymphatic drainage. In Stewart's study, elimination of activity from the vascular compartment in patients without a HAMA response (as determined by enzyme linked immunosorbant assay (ELISA)) was also monoexponential.

Both blood and CSF pharmacokinetics were clearly altered in patient 7 for repeated injections of radioconjugate. Whilst not confirmed directly, this almost certainly results from the development of a HAMA response. The timing and magnitude of the blood peak following the first injection was consistent with those of previous patients. In contrast, a peak of between 4.1 and 7.5% of the injected activity was noted at the earlier time of between 6.2 and 9.9 hours. Elimination of activity from the blood following the second injection was more rapid, but again followed monoexponential kinetics over the period of sampling. In contrast, clearance was by biphasic kinetics after both the third and fourth injections.

These findings may be explained by HAMA, induced by the first injection of mouse Ig, resulting in immune complex formation between human anti-mouse Ig and the carrier antibody. This results in rapid clearance of radioconjugate from the bloodstream by mechanisms which include enhanced reticuloendothelial uptake, particularly by the liver [86]. In addition, *in-vivo* immune complex formation is associated with de-halogenation, either directly or following metabolism within the liver [304], which also contributes to faster clearance of the radiolabel. The second and third doses of mouse protein strengthens the HAMA response, leading to progressively faster

elimination of radioisotope. Under these circumstances, elimination of radioisotope conforms to a two compartment model as described by a biphasic elimination pattern. It is of note, that the second phase of elimination for injections two and three have a half-time (50.4 and 42.3 hours respectively) similar to that for elimination for the first injection (45.11 hours). A biphasic pattern of blood elimination was also observed by Stewart *et al.*, in HAMA-positive patients treated with repeated IP radioimmunotherapy [304], but in contrast to our observations, this occurred following a second IP injection.

The blood absorption half-time of 6.33 hours following the first injection in patient 7 was within the range of 3.63 - 12.41 hours (mean 8.36 hours) noted for patients 1, 3, 4 and 6. It is appreciated that the calculation of blood absorption rate may be subject to significant error, especially when the apparent absorption is rapid and the rate is calculated from the slope of a two point curve. This emphasises the need for more frequent sampling at earlier times. Nevertheless, following repeated therapy, radioconjugate was apparently absorbed more rapidly into the vascular compartment (faster elimination from the subarachnoid space), with half-times of 4.15, 2.22 and 3.22 hours for injections 2, 3 and 4 respectively.

Additional evidence for faster absorption is provided by data from external probe measurements, which clearly demonstrate faster elimination of ^{131}I from the CNS following injections 2 - 4. The mean of cervical and lumbar clearance half-times were 7.55, 5.0 and 3.55 hours for injections 2, 3 and 4 respectively, as compared with a mean value for the first injection of 23.5 hours. The difference between these values and those for half-times of blood absorption probably reflects on one side, the errors involved in these calculations and on the other, by the blood/background activity detected by the probe, in addition to that within the subarachnoid space. Half-times for the second phase of clearance for all sites varied between 23.6 and 48.7 hours

(mean = 34.4 hours), slightly longer than the half-time for injection 1 of between 21.3 and 23.7 hours. No overall difference was, however, observed between injections 2 to 4 in the rate of the second elimination phase.

These observations imply that immune complex formation occurs within the subarachnoid space itself, resulting from anti-mouse antibodies produced either within systemic lymphoid tissue and crossing into CSF, or from antibody produced within the CNS itself. Local IgG production in the CNS has been noted in inflammatory, demyelinating and infective disorders [305] [306], and has also been reported in carcinomatous meningitis [307].

The presence of immune complex formation within the CSF is supported by FPLC gel filtration profiles of CSF taken after patient 7's fourth injection. Higher molecular weight species, suggestive of immune complexes, were noted at 24 but not six hours post-administration. This would be unexpected if significant HAMA was present in the CSF at the time of injection, and suggests that either a CSF-derived HAMA response is initiated as a result of the injection of mouse protein or, more probably, that this response occurs systemically, with significant HAMA entering the CSF pathways. On the other hand, increased acute toxicity was noted during repeat therapy in patient 7, with moderately severe symptoms occurring as early as 1.5 hours after injection (Chapter 10; 3d). This may suggest the formation and meningeal deposition of immune complexes at this time, due to the presence of pre-existing HAMA in the CSF.

The observation of faster CSF clearance of higher molecular weight species is contrary to proposed mechanisms of absorption of macromolecules into the systemic circulation. It has been suggested that CSF exits from the subarachnoid space via subarachnoid villi or granulations by bulk flow, due to the CSF pressure of about 150 mm H_20 being almost twice that in the veins. The villi are reported to be valve-like, allowing particles as large as 2 - 7.5 μm to pass through passively [292] (Chapter 9; 6). Our study may

indicate that additional active processes are involved, as has been previously suggested [298]. An alternative explanation for increased CSF clearance during repeated therapy may be that the normal absorptive mechanisms are altered as a result of β-radiation damage from the initial targeted therapy. The blood-brain barrier at the level of the brain capillary endothelial membrane may also be subject to radiation or immune-complex damage, as may areas thought normally to contribute relatively little to the absorptive process, such as the choroid plexus. Experimental immune-complex disease in rabbits appears to be associated with a selective increase in the permeability of the blood-CSF barrier, leaving the blood-brain barrier intact [308]. Finally, these observations may be explained by increased de-halogenation associated with immune-complex formation, as has been noted previously [304]. Free iodine will be cleared rapidly from the CSF and, as such, it is difficult to assess clearly the rate of de-halogenation by conventional means, eg. TCA precipitation or gel filtration.

The faster clearance of radioisotope from the bloodstream following repeated therapy results in a smaller area under the blood time-activity curve, in turn resulting in a smaller radiation dose to the red bone marrow. Assuming bone marrow toxicity to be dose-limiting, the advantage of this phenomenon in terms of an increased therapeutic index, will depend upon the differential between the rate of blood and CSF elimination and the resultant areas under the respective time-activity curves. This concept is explored in the following chapter.

CHAPTER 12.

DOSIMETRIC STUDIES OF TARGETED RADIOTHERAPY FOR MENINGEAL ACUTE LYMPHOBLASTIC LEUKAEMIA.

Using pharmacokinetic data obtained during clinical studies of intrathecal targeted radiotherapy for CNS ALL, dosimetric models were established to estimate the absorbed radiation dose to both CSF and normal tissues.

1. Methods.

Dosimetric studies were based upon the Medical Internal Radiation Dosimetry (MIRD) scheme [91], where the mean absorbed dose, **D**, is defined as:

$$\mathbf{D} = \tilde{\mathbf{A}}_{\mathbf{S}} \cdot \Delta \cdot \Phi \qquad (1)$$

where,

$\tilde{\mathbf{A}}_{\mathbf{S}}$ is the number of nuclear transformations in the radiation source region during the time interval of interest. This is equivalent to the time-activity integral.

Δ is the mean energy emitted per nuclear transformation,

and Φ is the specific absorbed fraction, or the absorbed fraction per unit mass of the target tissue. This is the fraction of the particle energy emitted by the source element and imparted to the target organ, divided by the mass of the target organ.

Equation **(1)** can be simplified by use of the term $\mathbf{S}_{(\mathbf{t} \leftarrow \mathbf{s})}$, the mean dose per unit accumulated activity from a source (**s**) to a target organ (**t**).

Hence,

$$\mathbf{D} = \tilde{A}_S \cdot S_{(t \leftarrow s)}$$

where $S_{(t \leftarrow s)}$ is the sum of $\Delta\,\Phi$ values of ^{131}I for both penetrating (gamma) and non-penetrating (beta) radiation. The total dose to a particular organ is then the sum of all the source and self-dose contributions, i.e. using $S_{(t \leftarrow s)}$ and $S_{(t \leftarrow t)}$.

Values of **S** are listed by Kereiakis and Rosenstein for ages 0, 1, 5, and 15 years and above [300]. Values for other ages were obtained by interpolation. Where appropriate, values of **S** and $\Delta\Phi$ pertinent to this study were calculated by Mr F Zananiri, Department of Medical Physics, Frenchay Hospital, Bristol.

2. Results.

(a) Dose to the whole body.

The radiation dose to the whole body is derived from gamma and beta emissions from ^{131}I present in blood and, to a lesser extent, other tissues. In these calculations, the source element was assumed to be blood, distributed evenly throughout the whole body. The whole body dose, $\mathbf{D_{wb}}$ (Gray), was thus calculated from the formula:

$$\mathbf{D_{wb} = \tilde{A}_S \cdot S_{(wb \leftarrow wb)}}$$

where,

$\mathbf{\tilde{A}_S}$ is the time-activity integral in MBq hours

and $\mathbf{S_{(wb \leftarrow wb)}}$ the whole body to whole body S value in Gy MBq^{-1} $hour^{-1}$.

$\mathbf{\tilde{A}_S}$ was assumed to be equivalent to the cumulative blood activity, $\mathbf{\tilde{A}_{blood}}$, which is proportional to the area under a time-effective activity curve. This was calculated from the effective blood activity data (Tables 11.2, 11.6) using the linear trapezoidal method [288] (MathCAD™ software):

$$\mathbf{\tilde{A}_{blood}} = \sum_{1}^{n} \left[\frac{1}{2} \cdot \left[t_n - t_{(n-1)} \right] \cdot \left[a_{(n-1)} + a_n \right] \right] \qquad (2)$$

where, $\mathbf{t_n}$ is the time of the n^{th} sample,

$\mathbf{t_{(n-1)}}$ is the time of the $(n-1)^{th}$ sample,

$\mathbf{a_n}$ is the activity of the n^{th} sample,

and $\mathbf{a_{(n-1)}}$ is the activity of the $(n-1)^{th}$ sample

To approximate the time-activity integral to infinity, the terminal phase of effective blood clearance was plotted, and its exponential equation of best fit computed. This equation was integrated between the time of the last blood

sample to an arbitrary upper time limit of 10,000 hours, giving an extrapolated time-activity integral, $\tilde{A}_2$. $\tilde{A}_1 + \tilde{A}_2$ thus gives the total cumulative blood activity in per cent injected activity hours.

Results of whole body dose (Gy), together with values of dose per injected activity (IA) (mGy/MBq) are presented in Table 12.1.

Table 12.1 Whole body dose (D_{wb}).

Patients 1, 3, 4 and 6.

Patient Number	Time-Activity Integral-$\tilde{A}_{blood}$		$S_{(wb \leftarrow wb)}$ (Gy MBq^{-1} hour^{-1}) x 10^{-6}	D_{wb} (Gy)	D_{wb}/IA* (mGy/MBq)
	% Initial Activity hours	MBq hours x 10^4			
1	3097	1.948	7.00	**0.136**	**0.216**
3	1970	2.916	3.24	**0.093**	**0.063**
4	1009	1.307	3.24	**0.042**	**0.032**
6	1943	1.510	10.81	**0.153**	**0.197**

Patient 7.

Injection Number	Time-Activity Integral-$\tilde{A}_{blood}$		$S_{(wb \leftarrow wb)}$ (Gy MBq^{-1} hour^{-1}) x 10^{-6}	D_{wb} (Gy)	D_{wb}/IA* (mGy/MBq)
	% Initial Activity hours	MBq hours x 10^4			
1	1161	1.976	10.0	**0.198**	**0.116**
2	286	0.365		**0.037**	**0.029**
3	200	0.236		**0.024**	**0.020**
4	169	0.192		**0.019**	**0.017**

*IA = Injected activity (MBq).

In the single injection group, the whole body dose varied between 0.042 (0.032 mGy/MBq) in a 13 year old patient who received an injected

activity of 1295 MBq to 0.153 Gy (0.197 mGy/MBq) in the youngest, to whom 777 MBq was administered. Patient 1 received the highest dose/injected activity, of 0.216 mGy/MBq.

For patient 7, the whole body dose following the first injection of 1702 MBq was 0.198 (0.116 mGy/MBq). As a result of faster whole body/blood clearance, a lower total dose of 0.08 Gy (0.022 mGy/MBq) was received following injections 2 - 4, for a cumulative injected activity of 3592 MBq.

(b) Dose to the red bone marrow.

Dose to red bone marrow, $\mathbf{D_{rbm}}$, derives predominantly by beta irradiation from blood circulating within the marrow cavities themselves. This component can be calculated from:

$$\mathbf{D_{rbm} = \tilde{A}_{blood} \cdot S_{(rbm \leftarrow rbm)} \cdot F}$$

where: $\mathbf{\tilde{A}_{blood}}$ is the time-activity integral in MBq hours i.e. that used in the calculation of whole body dose.

$\mathbf{S_{(rbm \leftarrow rbm)}}$ the red bone marrow to red bone marrow S value in Gy MBq^{-1} $hour^{-1}$.

and **F** is the ratio of total red bone marrow weight to the total blood weight.

This calculation assumes no specific binding between antibody and bone marrow elements. Values of **F** were derived from standard tables listing red bone marrow and total blood weight for ages 1, 5, 10, and 15 years (adult) [300]. Values for other ages were obtained by interpolation. These ranged between 0.24 in patient 6 (aged 3 years) to 0.28 for ages 5 years and above.

An additional smaller component of marrow dose derives from gamma irradiation from the whole body and is calculated from:

$$D_{rbm} = \tilde{A}_{blood} \cdot S_{(rbm \leftarrow wb)}$$

In these calculations, the whole body source is assumed to be solely represented by activity within the vascular compartment. Adding these dose contributions gives the total red bone marrow dose (Table 12.2).

Table 12.2 Red bone marrow dose (D_{rbm}).

Patients 1, 3, 4 and 6.

Patient Number	S value (Gy MBq^{-1} hour^{-1})		D_{rbm} (Gy)	D_{rbm}/IA* (mGy/MBq)
	$S_{(rbm \leftarrow rbm)}$ x 10^{-4}	$S_{(rbm \leftarrow wb)}$ x 10^{-6}		
1	2.7	11.2	**1.69**	**2.69**
3	1.4	4.8	**1.28**	**0.87**
4	1.4	4.8	**0.58**	**0.44**
6	4.5	14.0	**1.84**	**2.37**

Patient 7.

Injection Number	S value (Gy MBq^{-1} hour^{-1})		D_{rbm} (Gy)	D_{rbm}/IA* (mGy/MBq)
	$S_{(rbm \leftarrow rbm)}$ x 10^{-4}	$S_{(rbm \leftarrow wb)}$ x 10^{-6}		
1	4.0	13.5	**2.24**	**1.32**
2			**0.41**	**0.32**
3			**0.27**	**0.23**
4			**0.22**	**0.19**

*IA = Injected activity (MBq)

For the single injection group, marrow dose varied markedly between 0.58 Gy (0.44 mGy/MBq) in patient 4, to 1.84 Gy (2.37 mGy/MBq) in patient 6 (aged 3), although the highest dose/injected activity (2.69 mGy/MBq) was noted in patient 1.

Again, as a result of more rapid clearance of radioisotope from the blood during the course of repeated therapy, the total marrow dose for injections 2 - 4 was 0.9 Gy (0.25 mGy/MBq) for a cumulative injected activity of 3592 MBq, less than half the dose of 2.24 Gy (1.32 mGy/MBq) for the first injection of 1702 MBq.

(c) Dose to CSF.

(i) Ventricular CSF.

Assuming the density of CSF to be 1.00 gm cm^{-3}, the dose to ventricular CSF, $\mathbf{D_{vcsf}}$, was calculated using the formula:

$$\mathbf{D_{vcsf} = \tilde{A}_{vcsf} \cdot \Delta\Phi}$$

where, $\mathbf{\tilde{A}_{vcsf}}$ is the accumulated total ventricular CSF activity in MBq ml^{-1} hours

and $\Delta\Phi$ the mean dose per unit accumulated activity, which for CSF, was calculated to be 0.1237 gm Gy MBq^{-1} $hour^{-1}$.

$\mathbf{\tilde{A}_{vcsf}}$ was calculated from effective ventricular activity concentration data (Tables 11.9, 11.10), again using the linear trapezoidal method (equation 2). This equation incorporated a value for activity concentration at time 0, assuming a ventricular volume of 25 ml (Chapter 11; 3c). As lack of early CSF sampling times may artificially increase the area under the time-activity curve between time 0 and the first sampling time, a value for activity concentration at an arbitrary time of four hours was predicted, where the first sample was taken after this. This was calculated by the substitution of four hours into the exponential equation of best fit of a plot of the first phase of observed effective ventricular CSF clearance. This predicted activity concentration was incorporated into the summation formula. It was also assumed that ventricular

activity present after the last sampling time made a negligible contribution to radiation dose. Values of $\tilde{A}_{vcsf}$ and D_{vcsf} are given in Table 12.3.

Table 12.3 Radiation dose to the ventricular CSF (D_{vcsf}).

Patients 4, 5 and 6.

Patient Number	Time-activity concentration Integral - $\tilde{A}_{vcsf}$ (MBq ml^{-1} hours)	D_{vcsf} (Gy)	D_{vcsf}/IA* (mGy/MBq)
4	143.73	**17.78**	**13.73**
5	108.28	**13.39**	**12.06**
6	84.94	**10.51**	**13.53**

Patient 7.

Injection Number	Time-activity concentration Integral - $\tilde{A}_{vcsf}$ (MBq ml^{-1} hours)	D_{vcsf} (Gy)	D_{vcsf}/IA* (mGy/MBq)
1	163.81	**20.26**	**11.90**
2	207.21	**25.63**	**19.78**
3	73.41	**9.08**	**7.71**
4	131.98	**16.33**	**14.35**

*IA = Injected activity (MBq)

*IA = Injected activity.

For patients 4, 5 and 6, values of $D_{vcsf/IA}$ was similar, at between 12.06 and 13.73 mGy/MBq. In patient 7, the highest value of D_{vcsf} (19.78 Gy) was observed following the second injection. In contrast with values of marrow dose, no relationship was noted between dose to ventricular CSF and injection number.

These results represent a maximum self dose to the ventricular CSF, and assume that each target point of CSF is completely surrounded by a sphere of source CSF of a radius at least as great as the maximum range of ^{131}I β-electrons. These calculations will not apply to CSF within the β-particle range of the surrounding tissues which will receive a progressively smaller dose as it approaches the edge of the CSF containing channels. At the CSF:ventricular lining interface, the CSF dose approximates to half of the maximum CSF dose, as the isotropic nature of β-emissions results in each point of CSF at this site being irradiated by a hemisphere of source CSF.

(ii) Subarachnoid CSF.

Dosimetry for subarachnoid CSF and hence, indirectly, dosimetry for the surface of the brain and spinal cord, presented difficulties due the lack of direct CSF sampling and inability to perform scintigraphic ROI analysis. An approximation to subarachnoid CSF dose was obtained where both blood and ventricular CSF was sampled (patients 4, 6 and 7), by assuming the subarachnoid space to represent a one compartment model with first order absorption and elimination kinetics (see Chapter 11; 3b).

Therefore:

$$C_{sacsf} = \frac{F \cdot A_0}{V} \cdot \frac{k_a}{(k_a - k_{el})} \cdot (e^{-k_{el}t} - e^{-k_a t}) \qquad (3)$$

where C_{sacsf} is the activity concentration in subarachnoid CSF,

F is the fraction of activity absorbed from ventricular into subarachnoid CSF (assumed to be 1.0),

A_0 is the administered activity,

V is the volume of subarachnoid CSF,

	$\mathbf{k_a}$	is the absorption rate constant into the subarachnoid CSF (equivalent to the ventricular elimination rate constant),
	$\mathbf{k_{el}}$	is the elimination rate constant from the subarachnoid CSF (equivalent to the blood absorption rate constant),
and	$\mathbf{t}$	is the time lapsed from injection.

For patients 6 and 7 (both aged 3 years), **V** was assumed to be 100 ml and for patient 4 (aged 13 years), 125 ml. As the majority of activity from the ventricles cleared before the first CSF sampling time, the calculation of $\mathbf{k_a}$ was based upon the slope of the curve between the predicted ventricular CSF activity at time 0 and the first sampling time or at the extrapolated value at four hours used in calculation for $\mathbf{D_{vcsf}}$ (see above).

Again, assuming the density of CSF to be 1.00 gm cm^{-3}, the maximum dose to subarachnoid CSF, $\mathbf{D_{sacsf}}$,was calculated from:

$$\mathbf{D_{sacsf} = \tilde{A}_{sacsf} \cdot \Delta\Phi}$$

where,	$\tilde{\mathbf{A}}_{\mathbf{sacsf}}$	is the accumulated total subarachnoid CSF activity in MBq ml^{-1} hours,
and	$\Delta\Phi$	the mean dose per unit accumulated activity for CSF (0.1237 gm Gy MBq^{-1} $hour^{-1}$).

Values for $\tilde{\mathbf{A}}_{\mathbf{sacsf}}$ were estimated by incorporating appropriate values for each patient into equation **(3)** and integrating between 0 and 400 hours using MathCAD™ software. These, together with corresponding values for $\mathbf{D_{sacsf}}$, are given in Table 12.4.

Table 12.4

Radiation dose to the subarachnoid CSF (D_{sacsf}).

Patients 4 and 6.

Patient Number	Time-activity concentration Integral - $\tilde{A}_{sacsf}$ (MBq ml^{-1} hours)	D_{sacsf} (Gy)	D_{sacsf}/IA* (mGy/MBq)
4	204.7	**25.33**	**19.56**
6	98.5	**12.19**	**15.69**

Patient 7

Injection Number	Time-activity concentration Integral - $\tilde{A}_{sacsf}$ (MBq ml^{-1} hours)	D_{sacsf} (Gy)	D_{sacsf}/IA* (mGy/MBq)
1	161.5	**20.57**	**12.09**
2	78.8	**10.04**	**7.87**
3	38.4	**4.89**	**4.15**
4	54.2	**6.91**	**6.07**

*IA = Injected activity (MBq).

In contrast to values of maximum dose to ventricular CSF, D_{sacsf} in patient 7 was smaller following injections 2 - 4 (overall dose per MBq injected activity = 6.05 mGy/MBq) than that following the injection 1 (12.09 mGy/MBq). This reflects the contribution of the respective absorption rate constants of blood in the calculation.

As above, the dose to subarachnoid CSF will become progressively lower towards the edge of the CSF pathways, and at the interface between subarachnoid CSF and the surface of the brain and spinal cord, will approximate to half of the maximum CSF dose.

(d) Dose to neural tissue.

The highest radiation dose to the CNS was predicted to be that to the spinal cord and brain surrounding the ventricular CSF channels. The gamma component to tissue dose was considered negligible and thus, assuming no penetration of radioisotope into neural tissues, a significant radiation dose will only be received by tissues within the maximum β-particle range.

A method for calculating total dose to the spinal cord was described by Harbart and McCullough in relation to ^{131}I-labelled human serum albumin cisternography [309]. This method necessitates extensive mathematical computation which reflect: (1) changes in source volume as the distance from the cord surface increases, (2) the difference in β-particle range between spinal cord and CSF, and (3) consideration of dose to each section of the spinal cord. A similarly detailed dosimetric model, with an emphasis on dose rate changes as a function of distance from the cord surface, was established by Millar and Barrett for antibody targeted radiotherapy [310].

In order to obtain an estimate of mean dose to peri-ventricular tissue and spinal cord, a simplified model was established in collaboration with Mr F Zananiri (Department of Medical Physics, Frenchay Hospital, Bristol).

(i) Dose to peri-ventricular neural tissue.

Radiation dose to tissues adjacent to the ventricular lining was calculated from direct measurements of ventricular CSF activity. This was undertaken assuming the ventricular compartment to be a sphere of radius, **r**, with a volume of 25 ml (see above). The dose, $\mathbf{D_{vent}}$, can then be calculated from:

$$\mathbf{D_{vent}} = \tilde{A}_S \cdot \Delta\Phi \qquad (4)$$

where,

$\tilde{A}_S$ is the accumulated activity (MBq hours) of the source element (CSF) contributing to dose,

and $\Delta\Phi$ the mean dose per unit accumulated activity, which for brain (and spinal cord) was calculated as 0.040668 gm Gy MBq^{-1} $hour^{-1}$, assuming a mean value for Φ of 0.4.

The source element, i.e. the proportion of CSF contributing to dose, is contained within a rim of ventricular CSF of a volume, **V**, defined as:

$$V = 4 \pi r^2 . R95 . 0.5 \qquad (5)$$

where,

r is the radius of the "ventricular sphere",

R95 the distance in which 95% of all the β–particles are absorbed in water, equal to 9.2×10^{-4} metres [91],

and **0.5** a factor introduced due to the isotropic nature of ^{131}I β–particle emissions i.e. only half of the activity in the source element will contribute to the absorbed dose.

The mass of irradiated tissue is given by: mass = density x volume.
If it is assumed that only a thickness of ventricular lining equivalent to the R_{95} is irradiated and that the target is at a mean radius, **r**, from the centre of the "ventricular sphere", equivalent to that of the source, then:

$$m = \frac{1.04}{4 \pi r^2 . R95} \qquad (6)$$

where,

1.04 gm cm^{-3} is the mean density of brain [311].

From **(5)** and **(6)**, equation **(4)** can thus be simplified to:

$$D_{vent} = 0.5 \cdot \frac{\tilde{A}_{vcsf}}{1.04} \cdot \Delta\Phi \qquad (7)$$

where,

$\tilde{A}_{vcsf}$ is the accumulated total ventricular CSF activity in MBq ml^{-1} hours.

Using equation **(7)**, dose to the ventricular lining was calculated for patients 4, 5, 6 and 7 (Table 12.5).

Table 12.5

Radiation dose to the ventricular lining (D_{vent}).

Patients 4, 5 and 6.

Patient Number	D_{vent} (Gy)	D_{vent}/IA* (mGy/MBq)
4	2.81	2.17
5	2.12	1.91
6	1.66	2.14

Patient 7.

Injection Number	D_{vent} (Gy)	D_{vent}/IA* (mGy/MBq)
1	3.20	1.88
2	4.05	3.18
3	1.44	1.22
4	2.58	2.27

*IA = Injected activity (MBq)

In patients 4 - 6, D_{vent} varied between 1.66 and 2.81 Gy. When expressed as dose/injected activity, a range of similar values, of 1.91 - 2.17 mGy/MBq, was observed. In patient 7, D_{vent} ranged between 1.44 and 4.05 Gy. The highest value was noted following the second injection, which reflects the relatively high activity in early ventricular CSF samples.

(ii) Dose to surface of the brain and spinal cord.

This was estimated using the calculated values of the time-activity integral of subarachnoid CSF activity. This was undertaken in a similar fashion to that for estimation of the dose to the ventricular lining, i.e. assuming the source element (CSF) and the target (brain/spinal cord) to have identical configurations, with the thickness of both the source and target to be equivalent to the R_{95} for ^{131}I. Again, the gamma component to radiation dose is considered to be negligible.

The dose, $\mathbf{D_{surface}}$, can thus be calculated from:

$$\mathbf{D_{surface}} = 0.5 \cdot \frac{\tilde{A}_{sacsf}}{1.04} \cdot \Delta\Phi$$

Values of $\mathbf{D_{surface}}$ are given in Table 12.6.

Table 12.6

Radiation dose to the surface of the brain and spinal cord ($D_{surface}$).

Patients 4 and 6.

Patient Number	$D_{surface}$ (Gy)	$D_{surface}$/IA* (mGy/MBq)
4	4.00	3.09
6	1.92	2.48

Patient 7

Injection Number	$D_{surface}$ (Gy)	$D_{surface}$/IA* (mGy/MBq)
1	3.16	1.85
2	1.54	1.21
3	0.75	0.64
4	1.06	0.93

*IA = Injected activity.

Reflecting values of $\tilde{A}_{sacsf}$, values of $\mathbf{D_{surface}}$ in patient 7 were again lower for repeat injections.

(iii) Dose to the whole brain.

The total radiation dose to the whole brain was estimated from both gamma and beta components. The gamma component derives from CSF activity within both the ventricular system and the cerebral subarachnoid space. In this study, only the gamma dose from ventricular CSF activity has been estimated. Calculation of S values for determination of the subarachnoid gamma component needs to be undertaken, but dose from activity within this space is predicted to be much less than that from within the ventricles. The beta component derives from blood circulating within the brain substance.

(iiia) Dose to whole brain from ventricular CSF activity.

This was calculated assuming the brain to be a homogeneous structure with a point source within it. S values for a brain point source to a brain target, $\mathbf{S_{(br \leftarrow br)}^{pt}}$, were calculated to be approximately 4.5×10^{-5} Gy MBq^{-1} $hour^{-1}$, across the age range 3 to 15 years. The whole brain dose, $\mathbf{D_{brain}}$, from this component is thus given by:

$$\mathbf{D_{brain} = \tilde{A}_{vcsf} \cdot S_{(br \leftarrow br)}^{pt} \cdot 25}$$

where, $\mathbf{\tilde{A}_{vcsf}}$ is the accumulated total ventricular CSF activity in MBq ml^{-1} hours (from Table 12.3),

and **25** the volume of the ventricles (ml).

Estimates of this component to radiation dose are given in Table 12.7.

Table 12.7

Radiation dose to the whole brain (D_{brain}) from ventricular CSF activity.

Patients 4, 5 and 6.

Patient Number	$\tilde{A}_{vcsf}$ (MBq ml^{-1} hours)	D_{brain} (Gy)	D_{brain}/IA* (mGy/MBq)
4	143.73	**0.163**	**0.13**
5	108.28	**0.123**	**0.11**
6	84.94	**0.120**	**0.15**

Patient 7.

Injection Number	$\tilde{A}_{vcsf}$ (MBq ml^{-1} hours)	D_{brain} (Gy)	D_{brain}/IA* (mGy/MBq)
1	163.81	**0.185**	**0.11**
2	207.21	**0.233**	**0.18**
3	73.41	**0.083**	**0.07**
4	131.98	**0.148**	**0.13**

*IA = Injected activity (MBq)

(iiib) Dose to whole brain from circulating blood (Table 12.8).

This assumes that beta activity within blood is evenly distributed throughout the whole brain, and is calculated from:

$$D_{brain} = \tilde{A}_{blood} \cdot S_{(br \leftarrow br)circ} \cdot F$$

where,

$\tilde{A}_{blood}$ is the time-activity integral of effective blood activity in MBq hours (Table 12.1),

$S_{(br \leftarrow br)circ}$ the whole brain to whole brain S value for circulating blood, in Gy MBq^{-1} hour^{-1},

and F the ratio of circulating blood in the brain to total whole blood mass [312].

Table 12.8 Radiation dose to the whole brain (D_{brain}) from circulating blood activity.

Patients 1, 3, 4 and 6.

Patient Number	$\tilde{A}_{blood}$ (MBq hours x 10^4)	F	$S_{(br \leftarrow br)circ}$ (x 10^{-4} - Gy MBq^{-1} $hour^{-1}$)	D_{brain} (Gy)	D_{brain}/IA^* (mGy/MBq)
1	1.948	0.018	1.1	**0.039**	**0.060**
3	2.916	0.009	1.0	**0.026**	**0.018**
4	1.307	0.009	1.0	**0.012**	**0.009**
6	1.510	0.022	1.3	**0.043**	**0.055**

Patient 7.

Injection Number	$\tilde{A}_{blood}$ (MBq hours x 10^4)	F	$S_{(br \leftarrow br)circ}$ (x 10^{-4} - Gy MBq^{-1} $hour^{-1}$)	D_{brain} (Gy)	D_{brain}/IA^* (mGy/MBq)
1	1.976	0.025	1.3	**0.064**	**0.038**
2	0.365			**0.012**	**0.009**
3	0.236			**0.008**	**0.007**
4	0.192			**0.006**	**0.005**

*IA = Injected activity.

Assuming a negligible dose from gamma activity within the subarachnoid space, whole brain dose, $D_{tot\text{-}brain}$, can be estimated in patients 4, 6 and 7 by adding the two contributions (Table 12.9):

Table 12.9

Total radiation dose ($D_{tot\text{-}brain}$) to the whole brain.

Patients 4 and 6.

Patient Number	$D_{tot\text{-}brain}$ (Gy)	$D_{tot\text{-}brain/IA^*}$ (mGy/MBq)
4	**0.175**	**0.135**
6	**0.163**	**0.210**

Patient 7.

Injection Number	$D_{tot\text{-}brain}$ (Gy)	$D_{tot\text{-}brain/IA^*}$ (mGy/MBq)
1	**0.249**	**0.146**
2	**0.245**	**0.189**
3	**0.091**	**0.077**
4	**0.154**	**0.135**

*IA = Injected activity (MBq)

(e) Dose to the kidneys.

This was undertaken in patients 3 and 4 using the MIRD scheme by the respective local Medical Physicist (Chapter 11; 3d). In patient 3, the dose to both kidneys was 7.0 Gy and for patient 4, the dose to the left kidney was calculated as 2.2 Gy.

3. Discussion.

The rationale behind targeted radiation therapy is the desire to increase the therapeutic index, i.e. the ratio of tumour radiation dose to that of critical normal tissues, as compared to conventional radiotherapy. Dosimetric estimations were thus considered a vital aspect of these studies. It was hoped to be able to correlate radiation dose with both clinical efficacy and toxicity. In addition, it was intended to broadly compare dosimetry of targeted radiation therapy with those doses conventionally delivered by external beam radiotherapy.

Bone marrow toxicity has been dose-limiting in the great majority of clinical studies of either systemically or regionally administered radioimmunotherapy (Chapter 1; 1d). Whilst the method used here for calculation of red bone marrow dose ($\mathbf{D_{rbm}}$) is that generally employed, considerable debate has focused on the accurate estimation of the value of **F**, the ratio of red bone marrow to blood weight. The values used here were derived from standard tables, **F** being equal to 0.28 for all subjects older than five years. More recent work has suggested **F** to be greater than this in adults. The Oak Ridge Laboratory Group have suggested a value of between 0.3 and 0.4, although no revised estimates have been made for children (Personal communication, Dr M Myers, Hammersmith Hospital, London). A recent study employing single photon emission computed tomography (SPECT) in adult patients receiving an ^{131}I-labelled antibody, showed the marrow:blood concentration ratio to vary widely between 0.19 and 0.52, with a mean value of 0.38 [313].

Calculation of $\mathbf{D_{rbm}}$ assumes no specific binding of the radioconjugate to marrow elements. The values here may thus represent an underestimate of the true dose, although antigens recognised by these antibodies are found on

less than 10% of bone marrow cells, with no evidence for their expression on haemopoetic stem cells (Chapter 3; 8).

In this study, marrow doses for patients receiving a single or first injection of radioconjugate ranged between 0.58 and 2.24 Gy, with dose per injected activity varying six-fold between 0.44 mGy/MBq (patient 1) and 2.69 mGy/MBq (patient 4). This variation partially reflects differences in biokinetics which can be considered in terms of the per cent injected activity hours time-activity integral, which varied three-fold between patients 1 and 4 (Table 12.1). Other variation may result from the accuracy of the parameter values used in respect to the age of the patient, eg. those of S-values and F factors.

The lack of significant myelotoxicity and the number of patients investigated makes it difficult to correlate clinical toxicity with $\mathbf{D_{rbm}}$. Despite doses as high as 2.24 Gy, WHO grade 3 - 4 was only noted in one child (patient 3). In this patient, toxicity was almost certainly compounded by the myelosuppressive effect of chemotherapy (Chapter 10; 3e). This is supported by the estimation of a relatively modest marrow dose of 1.28 Gy.

Altered blood kinetics in patient 7 following injections 2 - 4, are clearly reflected in the calculation of $\mathbf{D_{rbm}}$. Despite a cumulative injected activity of 3592 MBq, delivered over a 2 week period, a dose of only 0.9 Gy was received by the red bone marrow. This is equivalent to only 0.25 mGy/MBq, a value five times less than that noted for the first injection.

Values of $\mathbf{D_{rbm}}$ for patients in our original pilot study of IT targeted therapy have recently been calculated [314]. Of 10 adults investigated, marrow dose ranged widely between 0.10 and 2.10 Gy (0.07 - 1.01 mGy/MBq). Four developed significant myelosuppression (combined platelet and neutrophil WHO scores of 6 - 8) with bone marrow doses of between 1.25 and 2.10 Gy (0.56 - 0.95 mGy/MBq).

Stewart *et al.*, published data on toxicity in 15 patients with ovarian carcinoma treated with an intraperitoneal (IP) injection of between 3219 and 5846 MBq ^{131}I-labelled antibodies [304]. Marrow doses in nine evaluable patients ranged between 75 and 325 cGy (0.19 - 0.60, mean 0.39 mGy/MBq). There is no significant difference between the marrow doses/injected activity received by the adult patients in our original pilot study and those of Stewart's study, reflecting similar blood pharmacokinetics following either IT or IP injection.

Care should be taken in comparing values of $\mathbf{D_{rbm}}$ in these two reports with those of the present study, in which three patients received doses of greater than 1.5 Gy and yet failed to develop clinical toxicity with a combined score greater than 3. The differences may be due to an overestimate of bone marrow dose in young children due, for instance, to inappropriate listed values of $\mathbf{S_{(rbm\text{-}rbm)}}$ for this age group. Alternatively, the marrow in this group may be more resistant to radiation damage, although this would be surprising in heavily pre-treated leukaemic patients, who would be expected to have low marrow "reserve"

Assuming marrow dose to be activity-limiting, it is difficult to make accurate predictions as to the maximum injected activity. For patients 1 and 6 the marrow dose/injected activity was approximately 3.7 mGy/MBq. If a marrow dose of 3 Gy is assumed to be limiting, the maximum injected activity would be 810 MBq. In contrast, a mean of 0.53 mGy/MBq in the older patients (patients 3 and 4), would thoeretically allow 5660 MBq to be given.

Calculation of the dose to tumour cells in this clinical situation is extremely difficult due a number of factors. These include the small but variable size of tumour deposits, which range from single cells to small clumps or sheets of tumour. As such, conventional radioimmunolocalisation or resection studies are impossible and reliable dosimetric models are lacking. Tumour dosimetry is also hindered by lack of knowledge as to the extent and

distribution of leukaemic cells. It can be assumed, however, that a relationship exists between the dose to tumour and that to the surrounding CSF within the β-particle range. The dose to leukaemic cells in direct contact with CSF will presumably be higher than that to CSF as a result of the targeting effect, and will be determined by factors discussed in relation to the *in-vitro* and mathematical models (Chapters 6, 7). The majority of tumour cells will, however, lie on the surface of the leptomeninges and will thus receive a dose proportional to approximately half of the maximum CSF dose. This reduction in tumour dose as compared with that for free-floating cells may be partially offset by the crossfire effect as a result of cell aggregation on the meninges. Due to the complex anatomy and pathology involved in this disease, a proportion of cells may not be in contact with CSF. These may be either irradiated by CSF within the β-particle range, albeit with a lower dose, or escape irradiation altogether.

As a result of the relatively short clinical responses and the low number of patients studied, it is not possible to draw any correlation between clinical efficacy and either ventricular or subarachnoid CSF dose. Dose to the ventricular CSF was calculated from the ventricular CSF time-activity integral. For patients receiving a single or first injection, the maximum dose to ventricular CSF per injected activity was similar, at between 11.9 and 13.7 mGy/MBq, resulting in total doses of between 10.5 and 20.6 Gy. It is appreciated, however, that these doses are potentially subject to large errors, particularly with respect to the assumed activity concentrations at 0 and four hours, and the relative lack of early sampling times (Chapter 11; 4). As ventricular elimination is rapid, the dose predominantly reflects the measured or assumed activity within the first few hours.

No relationship was observed in patient 7 between dose to ventricular CSF and the injection number. This was expected, as pharmacokinetic data indicated that the presence of CSF or serum HAMA has no influence over the

rate of ventricular clearance (Chapter 11; 3c). Total ventricular CSF doses of greater than 20 Gy were only noted following two injections, and in only one instance was this greater than the 24 Gy conventionally delivered by external beam therapy for CNS relapse of ALL.

Dosimetry for subarachnoid CSF and adjacent neural tissue was more problematical than that for the bone marrow and ventricular CSF. Other studies, such as those investigating regional therapy of the peritoneal cavity, have utilised direct measurements of dose, by means of devices such as Lithium Fluoride thermoluminesscense dosimeters (TLDs) placed within the cavity itself. This was not considered feasible in this study. In addition, as discussed in Chapter 11, construction of accurate time-activity curves from scintigraphic data was not possible.

Estimation of the subarachnoid CSF time-activity integral was, therefore, obtained by integration of the standard equation for a one-compartment model. This incorporated the calculated rate constants for ventricular CSF elimination and blood absorption. Again, this method is considered subject to potentially large errors.

Using this method, dose to the subarachnoid CSF ranged between of between 12.2 and 25.3 Gy (12.1 and 19.6 mGy/MBq, mean = 15.8 mGy/MBq) for three patients receiving a first injection (patients 4, 6 and 7 [injection 1]). In two children (patients 4 and 6), these values were higher than those for the dose to the ventricular CSF. This is because the slower elimination of activity from the subarachnoid space more than offsets the reduction in dose due to the increased volume of distribution. As expected, due to faster blood absorption, lower doses to subarachnoid CSF were observed as a result of repeated therapy in patient 7, the overall dose/injected activity being half that noted for the first injection (6.1 v 12.1 mGy/MBq), and the cumulative dose being only 21.8 Gy.

An alternative method of calculating the subarachnoid CSF time-activity integral, using spinal external probe measurements, is currently being evaluated. A time-activity integral can be obtained in units of counts hours. This integral can then be converted to units of activity hours by measurement of ventricular CSF activity and assuming an equivalence in ventricular and subarachnoid CSF activity concentration at an arbitrary time point, eg. four to eight hours.

Areas of neural tissue most likely to receive a significant radiation dose are those within the ^{131}I β–particle range of CSF, in either the ventricular system or subarachnoid space. Clinical significance will also depend on the function and radiosensitivity of these structures. To define these tissues, multiple sections of normal CNS were examined under light microscopy and structures within 1 mm (~R_{95}) of the CSF pathways were delineated (Table 12.10).

Table 12.10 CNS structures located within 1mm of the CSF pathways.

Ventricular system:

Choroid plexus.

Ventricular ependymal and subependymal layers (0 - 0.3 mm).

Subependymal white matter.

Thalamus, Pineal gland (3rd ventricle),

Caudate nucleus (lateral and 3rd ventricles).

Optic chiasma (3rd ventricle).

Brain Stem - Superficial cranial nerve nuclei particularly VII, X, XII
(floor of 4th ventricle).

Subarachnoid system:

Cerebral Cortex -	layers 1 and 2.
Cerebellum -	Molecular and Perkinje layers +/- Granular layer.
Cranial nerves	All cranial nerves when crossing the subarachnoid space.
Brain stem -	Subpial white matter.
Spinal Cord -	White matter (not spinal cord grey matter)
	Spinal nerve roots.

Calculation of dose to either ventricular or subarachnoid CSF and to its respective adjacent neural tissue utilizes the same CSF time-activity integral. Differences in dose between CSF and tissue reflect the isotropic nature of ^{131}I β-particles, the differential density of neural tissue CSF, and differences in values of $\Delta\Phi$, all of which are constants. Thus, for both ventricular and subarachnoid systems, the maximum dose to the CSF is 6.3 times that of the mean dose to the surrounding neural tissue.

With regard to the ventricular lining, the dose, $\mathbf{D_{vent}}$, ranged two-fold between 1.66 and 3.20 Gy for patients receiving a first injection. However, the calculated doses/injected activity was consistent for this group at between 1.88 and 2.17 mGy/MBq. These are somewhat lower than those noted for seven patients in our original 15 patient pilot study, which varied between 3.3 and 4.0 mGy/MBq [314]. In these adult patients, the first phase of ventricular elimination was generally much slower (mean $T1_{1/2}$ = 13.1 hours) than that observed in the present study. This may reflect a true delay in ventricular elimination, a greater lack of early CSF samples and a method that did not include assumed values of CSF activity before the first CSF sample.

As expected, no difference was observed in calculation of dose to the ventricular lining in patient 7 in respect of repeated injections of radioconjugate. The highest value of $\mathbf{D_{vent}}$ of 4.05 Gy (3.17 mGy/MBq) was noted following the second injection. The reason for the relatively high early

CSF activities in this case remains unclear. Thus, while the radiation dose for single or first injections were all below 3.5 Gy, a cumulative dose of 8.1 Gy was delivered as a result of injections 2 - 4. This relatively modest dose nevertheless needs monitoring during further dose escalation studies. However, assuming no penetration of ^{131}I, a significant proportion of dose will be delivered to the neurone-free ependymal and subependymal layers, the thickness of which, by microscopic inspection of normal brain, may be up to 0.3 mm (Table 13.10). Of the neural structures adjacent to the ventricular system, areas most likely to receive a proportion of this dose include the subependymal white matter, thalamus, pineal gland, caudate nucleus and certain cranial nerve nuclei.

Dose to the surface of the brain and spinal cord, $\mathbf{D_{surface}}$, were identical, as it is assumed that activity is evenly distributed throughout the subarachnoid CSF. As with dose to the ventricular system, these calculations do not take into account the complex anatomy of these regions eg. the convolutions of brain and spinal cord. $\mathbf{D_{surface}}$ for single or first injections varied between 1.9 and 4.0 Gy (1.9 to 3.1 mGy/MBq), much lower than that conventionally delivered. Reflecting dose to the subarachnoid CSF, values of $\mathbf{D_{surface}}$ were lower for injections 2 - 4 in patient 7, with a cumulative dose of 3.35 Gy (0.93 mGy/MBq).

It is of note that these calculations assume the source (CSF) and target (neural tissues) to be of equal configuration and dimension. Whilst this assumption appears valid in respect of the range of ^{131}I β-particles and of the dimensions of the irradiated tissues, calculations for therapy employing isotopes with longer range emissions will need to incorporate different values of the volume of the source and the target. This is especially true for dosimetry for the ventricular system and spinal cord. In the latter case, the range of β-particle emissions from, for example, ^{90}Y or ^{32}P, may approach or

exceed the radius of the spinal cord, in which case a significant radiation dose will be delivered to most, if not all, of this structure.

It should be appreciated that the dose estimations to nervous tissue represent a mean value. As distance from the CSF:tissue interface increase a smaller volume of source CSF will contribute to dose and β-particle penetration progressively shortens, reducing the tissue dose. This fall off in dose will be rapid and non-linear. Millar calculated for spinal cord 0.1 mm from the cord:CSF interface a dose rate of 0.5 that of the interface itself and 0.27 that of the maximum dose rate in the CSF [310]. At 1 mm, these ratios were approximately 0.30 and 0.16 respectively, very similar to the respective ratios in the model used here, of 0.32 and 0.16 (1/6.3).

It is difficult to compare directly the results obtained here with the doses to the CNS delivered by external beam radiotherapy, in terms of the biological effect on both tumour and normal tissues. As previously discussed (Chapter 1; 1d), this will depend on a variety of radiobiological factors including dose-rate effects, the differential radiosensitivity of tissues to β-particles and X-rays and the heterogeneity of antibody distribution.

Other models for dosimetry to the CNS following intrathecally injected isotopes have been described. Richardson *et al.*, used different methodology to the determine dose delivered to the meninges in four patients with leptomeningeal disease treated as part of our initial pilot study [253]. Prior to therapy, each patient was administered tracer amounts of ^{131}I-labelled antibodies by lumbar puncture. The dose contribution to the meninges from CSF activity was calculated following direct sampling of subarachnoid CSF. A mean dose to the thoraco-lumbar spinal meninges of 2.6 mGy/MBq was lower than that of 7.89 mGy/MBq obtained here for patients receiving a first injection (0.5 x mean D_{sacsf}/IA). An additional component from isotope assumed to be bound to the meninges was calculated from external probe measurements. This gave a mean total dose per unit activity of 3.9 mGy/MBq.

Döge and Hlinscs undertook dosimetric studies during the evaluation of intrathecally injected ^{198}Au-colloid for the prevention of overt CNS leukaemia (Chapter 1; 1e) [315]. Dose to the cord surface, 0.1 mm from CSF, (i.e. thickness of pia mater) was calculated using the MIRD scheme from scintigraphic data. A mean dose of 45 mGy/MBq was delivered to the cerebral meninges. This is much higher than that noted here, and probably reflects the higher average β-particle energy of ^{198}Au (0.316 MeV) as compared to ^{131}I (0.183 MeV), the slower elimination of colloid as compared to antibody and differences in the target tissue examined (dose at 0.1 mm from CSF against mean dose over a thickness equivalent to the R_{95}). In that study, however, the mean dose to the spinal meninges was 189 mGy/MBq. The difference between dose to spinal and cerebral meninges is due to the relatively poor distribution of colloid following lumbar injection. Whilst this magnitude of dose will be delivered to tumour cells, the longer range of ^{198}Au emissions (R_{95} ^{198}Au = 1.88 mm, R_{95} ^{131}I = 0.992 mm) will result in a greater proportion of the cord being irradiated (Chapter 1; 1e).

The most important advantage of intrathecal ^{131}I targeted radiation therapy, as compared to external beam therapy, lies in the differential dose delivered to the whole brain and whole spinal cord. The calculated doses to brain exclude a gamma component from subarachnoid CSF (predicted to be relatively small) and again are based on a number of assumptions. Nevertheless, maximal dose following each injection did not exceed 0.25 Gy, a 100th of that delivered by a course of external beam radiotherapy. Thus, dose to the whole brain is unlikely to be clinically significant and influence the design of future studies.

Whilst caution should be taken in over-interpreting data from one patient, and accepting that errors involved in the calculations may be large, an advantage in terms of reduced bone marrow dose appears to be offered by the altered biokinetics observed in patient 7. This must be considered in

respect of concomitant changes in CSF dose. For the first injection, the ratio of ventricular CSF : blood dose/injected activity was 5.89 and for subarachnoid CSF : blood, 5.99. For injections 2, 3 and 4 the ratios of cumulative dose/total injected activity were 37.29 and 15.96 respectively. If confirmed, this raises the issue as to whether a HAMA response should be induced at the time of therapy, eg. by prior immunization or by the injection of anti-mouse antibodies (Chapter 13; 2a). This pattern of pharmacokinetic and dosimetric changes was also observed by a co-worker in a patient with leptomeningeal relapse of medulloblastoma, treated in a similar fashion.

A similar increase in the therapeutic index was suggested for HAMA positive patients treated with intraperitoneal radioimmunotherapy [304]. Whilst the dose to the peritoneal cavity was significantly greater in patients receiving a first therapy than those receiving a second therapy (mean 3.04 v 1.86 cGy/mCi, $p = 0.025$) an even greater difference was observed in terms of bone marrow dose for these respective groups (mean = 1.51 v 0.13 cGy/mCi, $p = 3.87 \times 10^{-7}$). The lower peritoneal dose for HAMA positive patients was attributed to rapid clearance of free ^{131}I, due to de-halogenation following immune complex formation.

Finally, a significant dose to the kidneys was estimated in two patients. In patient 2, this was as high as 7.0 Gy, and has probably resulted in clinical toxicity. As previously discussed (Chapters 3; 8) this may be due to the presence of CALLA on renal tissue, and clearly requires close attention in future studies. It is possible that kidney dose may be activity-limiting if future patients, receiving higher activities, demonstrate a similar degree of renal uptake.

CHAPTER 13.

GENERAL DISCUSSION.

1. Summary of Results and Potential of Current Clinical Program.

Despite the theoretical advantages of antibody-mediated cancer treatment, numerous limitations to the success of this mode of therapy have been identified. Some of these may be circumvented by the injection of antibody conjugates into a tumour-bearing body compartment, particularly in cases of low volume, diffuse disease.

The use of β-emitting radionuclides as a short range radiotherapy source within a confined space has the advantage of obtaining a high concentration of radioactivity within the tumour-bearing region. Cytotoxic effects are limited to tumour cells and normal tissues within the range of the principle emissions. A carrier molecule may be used to delay the elimination of radionuclide from the compartment. Providing that the distribution and retention of the carrier is satisfactory, a high tumour dose, which is essentially independent of the nature of the carrier molecule, may potentially be delivered.

A second consideration is that of antibody specificity. In diffuse leptomeningeal disease, conventional methods of determining the degree of specificity, radiolocalisation and resection, are impracticable. To address this issue, the use of either an *in-vitro* or an animal model was required. Data presented in Chapter 6 clearly demonstrates the advantage of using a specific antibody carrier to target ^{131}I to leukaemia cell lines in a single cell suspension. This was not predicted on the basis of previous geometric modelling studies [92] [93].

A shortcoming of the assay system used here, is that time-response relationships are not clearly defined, as surface bound radioisotope may irradiate cells within both the incubation and cloning phases. Further

experimentation with an alternative system is indicated to address this point. This work does, however, suggest that the increased cell kill associated with specific antibodies is as a direct result of targeting ^{131}I to the cell surface and, furthermore, that for a given cell line, cell survival is inversely proportional to the amount of radionuclide bound to the cell. These conclusions are supported by the modification of Humm's mathematical model, which incorporated parameter values relevant to the clinical scenario investigated here. These results are also applicable to other studies of targeted therapy for diffuse tumours, particularly those presenting within other body compartments.

As discussed in Chapter 1, there is a need to increase the overall rate of long-term remission following CNS relapse of ALL, and to reduce the toxicity associated with therapy, particularly neuroaxis external beam radiotherapy. Nevertheless, because conventional chemoradiotherapy in some patients is effective in producing a prolonged CNS remission (Chapter 1), the exploration of targeted therapy was restricted to patients with second or subsequent isolated CNS relapse (Chapter 10). This has inevitably resulted in a low rate of patient entry into these studies, reflecting the rarity of this situation.

It is anticipated that a radiation dose, proportional to the maximum CSF dose, will be delivered by this technique to free floating cells within the CSF, to enable cell sterilisation to at least as great a degree as that achieved by external beam therapy. The success of targeted radiation therapy will probably be limited by the ability to sterilize cells adjacent to the meningeal surfaces, particularly those within relatively inaccessible areas such as the neuro-capillary spaces (deep arachnoid) which may penetrate deep into the brain substance. In addition, the degree of dural infiltration will limit the therapeutic range, as the distance between the CSF and the dura mater precludes a significant radiation dose to this meningeal layer. An appreciation of the extent of tumour infiltration in meningeal leukaemia is thus required.

Azzarelli and Roessman examined the distribution of leukaemic infiltrates in the CNS of 31 cases of either ALL or AML, although the number of patients in whom CNS involvement was clinically diagnosed was not detailed [131]. Infiltrates were present in the dura mater in 29 patients (93%) and in the arachnoid in 22 (71%). Leukaemic extension into the deep arachnoid was observed in 15 patients (48%), with parenchymal infiltration associated with massive arachnoid involvement noted in five cases (16%).

Thomas examined the brains of 111 patients with ALL who died between 1953 and 1963, prior to the advent of CNS preventative therapies [130]. In two series of patients, he found dural involvement of "grade 1 - 2" in 38 to 51% of cases and of "grade 3 - 4" in 14 to 19%. Overall, arachnoid involvement was detected in 43 to 59% of brains.

Price and Johnson studied the brains of 126 patients who had previously received CNS directed therapy for either the prevention or treatment of CNS ALL [132]. Again, further clinical details were lacking in this report. In 44% of cases, there was no evidence of leukaemic infiltrate in the arachnoid, whilst 34% demonstrated a mild to moderate leukaemic infiltration of the superficial arachnoid and isolated deep arachnoid infiltration. In 8% of cases, the superficial arachnoid was extensively infiltrated, with consistent contamination of the deep arachnoid, but the disease was confined to this region by the pial-glial membrane. Finally, in 13.4% of cases, there was extensive superficial and deep arachnoid involvement, obliteration of the peri-vascular spaces, destruction of the pial-glial membrane, and parenchymal invasion with tumour cells. In this, and other reports [197], Price stresses that CNS leukaemia is essentially a disease of the leptomeninges and, as opposed to the hypothesis of Azzarelli and Roessman, asserts that leukaemic cells first enter the CNS via the walls of leptomeningeal vessels, rather than via the epidural veins (Chapter 1).

The distribution of radioconjugates to the deep arachnoid and parenchyma will be hindered by both the complex anatomy and by the tumour deposits themselves. These observations support the use of emitters of β-irradiation, particularly in frank relapse. Treatment with short range isotopes eg. alpha-emitters or emitters of Auger electrons, or with toxins (see below), may be more suited to the prevention of overt relapse.

The relative lack of clinical toxicity, and favourable estimates of radiation doses to critical organs, suggests that dose escalation should proceed in the present study. Nevertheless, due to the extent of disease present in advanced CNS ALL, it is questionable whether a single injection of radioconjugate will be able to sterilize sufficient tumour cells for a prolonged remission to be obtained. The investigation of multiple administrations of radioconjugate is therefore indicated (Chapter 10), which will probably be associated with an improved tumour : blood dose ratio as a result of the HAMA response (Chapter 12). This will enable higher activities to be administered during second and subsequent therapies, assuming that toxicity and dose estimates to the CNS remain acceptable.

If such modifications to the current treatment protocol produce extended CNS remissions, it may be justifiable to investigate targeted therapy in patients in first CNS relapse, although the precise criteria by which this may be undertaken have yet to be determined. The current range of dose estimates to both the whole brain, and particularly areas of the CNS adjacent to the CSF pathways, appear to be low enough not to compromise delivery of a second course of CNS external beam irradiation. However, these doses will have to be carefully evaluated in the light of dose escalation and repeated therapy, to ensure that this remained the case.

For patients in first CNS relapse, it is anticipated that targeted therapy would be administered following cytoreduction with IT chemotherapy, in a similar fashion to that employed for external beam therapy. A clinical trial

would be required to assess the relative efficacy of delivering radiation therapy in this way. In view of the histopathological findings discussed above, targeted therapy may be of most value as an adjunct to external beam radiotherapy, possibly permiting a reduction of standard doses. This will be most applicable for patients who have received previous CNS irradiation as first line therapy.

A further consideration may be the use of other treatment modalities, such as high dose IV chemotherapy for the treatment of CNS disease. Whilst the toxicity and efficacy of these regimens have not been fully determined, targeted therapies may need to be evaluated in comparison to such alternative treatments. It is possible that the reduction in whole brain irradiation with radionuclide therapy will allow moderate or high dose IV chemotherapy to be administered in conjunction with this technique, without a significant risk of complications such as white mater necrosis (Chapter 1).

Antibody-targeted approaches using ^{131}I or other agents (see below) are likely to be most effective where disease extent is minimal. Despite concerns with regard to the toxicity of currently used preventative therapies, they are of proven effectiveness. Whether targeted therapies will ever play a similar role to that of external beam radiotherapy in the prevention of overt CNS relapse must, at present, be considered questionable.

Our group is conducting similar studies into the development of targeted radiotherapy for other leptomeningeal tumours, particularly PNETs. This has enabled an exchange of information which has benefited the development of both studies.

PNETs such as medulloblastoma have a marked propensity to disseminate throughout the subarachnoid space, necessitating craniospinal irradiation as primary therapy. Two recent multi-centre trials have suggested that a dose to the neuroaxis of 35 Gy is superior to 25 Gy in preventing subsequent relapse of medulloblastoma [316] [317]. This dose is, however,

associated with a high incidence of significant neurological sequelae (Chapter 1). It is possible that in these malignancies, IT targeted radiotherapy may have a role in enabling reduction in the radiation dose to the neuraxis in primary therapy, as well as possibly facilitating control of disease for leptomeningeal relapse.

Furthermore, our group has not abandoned investigation of targeted therapy for other tumours involving the leptomeninges. Six of 15 patients in our previous pilot study had a complete response to therapy, of whom two had disseminated melanoma and one, breast carcinoma (Chapter 1).

In addition to extending the current clinical programs as described above, further work should consider other ways in which tumour dose may be increased, toxicity reduced, or both. Alternative targeting strategies should also be considered.

2. Suggestions for Further Studies.

(a) Reducing toxicity.

It is probable that using the present protocol, myelosuppression will prove dose-limiting for single injections of radioconjugate. Bone marrow toxicity may be reduced by increasing the elimination rate of radionuclide from the vascular compartment. Several approaches are suitable for further investigation.

The catabolism of IgG appears to be influenced by antibody isotope. In man, Morrel *et al.,* found little difference between clearance rates of IgG subclasses, except for IgG_3, which had a significantly shorter circulation time [318]. This phenomenon has been noted in other work examining the catabolism of different subclasses of myeloma proteins [319], and is thought to result from characteristics of both the Fc and Fab portions of the molecule [320]. IgG_3 antibodies may thus prove particularly useful in targeted therapy. A disadvantage of using IgG_3 MoAbs is the reported poor solubility and

instability of some antibodies of this subclass. Despite this, the IgG_3 anti-GD_2 MoAb, 3F8, has been successfully administered as a carrier molecule in the treatment of neuroblastoma [321].

An increased rate of systemic clearance of conjugated radionuclide may be achieved by the use of antibody fragments (Chapter 1). Before they can be considered for IT therapy, data from animal and human studies should be obtained to ensure that the rate of clearance from the subarachnoid space is not disproportionately greater than that from the vascular compartment. Evidence from animal studies, including primate models, suggest that the size of the drainage pathways of the arachnoid villi are sufficiently large to allow polystyrene microspheres as large as 2 μm in size and erythrocytes (7.5 μm) to exit freely from the CSF [292]. In addition, data from patients undergoing cisternography [322] and from a small pig animal model (personal communication, Mr P Brown, Department of Medical Physics, Frenchay Hospital, Bristol) suggest that the clearance pattern of ^{131}I-labelled human serum albumin (molecular weight 67000) is similar to that of ^{131}I-labelled whole IgG. These studies suggest that there should be no difference in the rate of overall CSF elimination between whole IgG and its fragments.

Data from patient 7 indicates the effect of a HAMA response in enhancing vascular clearance of radioisotope, with a consequent reduction in bone marrow radiation dose (Chapters 11, 12). This was proportionately greater than that observed for the reduction in dose to the CSF resulting from increased elimination of ^{131}I from the CNS.

The administration of a second antibody to enhance vascular clearance of the first, anti-tumour antibody, has been investigated in studies of both immunoscintigraphy and immunotherapy. In 1982, Begent *et al.*, reported five patients with colorectal carcinoma who received radiolabelled polyclonal goat anti-CEA for tumour localisation [323]. After 24 hours, liposomally entrapped horse anti-goat immunoglobulin was administered, producing an

accelerated clearance of the initial antibody from blood in four patients, with enhanced tumour imaging in three.

This group extended this approach by the use of a second antibody alone. The ability to improve tumour to blood ratios by this means was confirmed for the radiolocalisation of colonic carcinoma using ^{131}I-anti-CEA antibodies in a nude mouse xenograft model [324]. Accelerated clearance of ^{131}I and improved tumour imaging was also documented in a further five patients with colorectal cancer, treated with 50 mCi ^{131}I-anti-CEA followed by a second antibody. No significant toxicity was associated with infusions of the second antibody. A similar advantage for this approach has recently been reported by other workers [325] [326].

The use of a second antibody or the presence of HAMA, in increasing the therapeutic index of radiommunotherapy, appears particularly pertinent to compartmentalized therapy. In this case, dose to tumour is largely independent of clearance rate of radionuclide from the bloodstream. As discussed in Chapter 12, Stewart *et al.,* noted a greatly increased rate of vascular clearance of ^{131}I in patients receiving a second IP dose of ^{131}I-labelled MoAb for ovarian carcinoma, with a consequent reduction in bone marrow dose [304].

This group subsequently investigated the feasibility of administering exogenous HAMA to patients receiving a first therapeutic injection of radioconjugate [327]. HAMA was purified by affinity chromatography from the serum of patients previously treated in other studies, and who had developed high HAMA titres. Five patients were treated with an IP injection of between 113 and 130 mCi of ^{131}I-HMFG1. The first received an IV infusion of 30 mg HAMA, 17 hours after the injection of radioconjugate. The remaining four patients received two injections of 15 to 18 mg of HAMA, the first either before or at 18 hours following conjugate administration, and the second at between 36 and 41 hours. In three patients who received ^{131}I-HMFG1 prior to

HAMA, the initial blood pharmacokinetics were as expected from previous studies. However, after each injection of HAMA, there was a rapid decrease of circulating ^{131}I activity, with an associated increase in counts over the liver. This was followed by a marked increase in free ^{131}I in the serum, presumably released from the hepatic catabolism of antibody. This was reflected in the rate of urine excretion of ^{131}I, which was greater in patients receiving exogenous HAMA than in previously studied patients.

Patients receiving HAMA prior to ^{131}I-HMFG1 had altered pharmacokinetics from the beginning of the post-treatment period, with a second injection of HAMA producing a further pronounced increase in the blood elimination of radioisotope. The mean radiation dose to the marrow in the five patients receiving HAMA was 0.21 cGy/mCi (range 0.14 - 0.25 cGy/mCi), compared to a mean of 0.97 cGy/mCi (0.63 - 1.09) in patients receiving a first treatment. Despite the rapid hepatic uptake of immune complexes, the mean dose to the liver was significantly lower in patients receiving HAMA (0.11 cGy/mCi) than that in nine patients receiving ^{131}I-HMFG1 with no HAMA (0.44 cGy/mCi). This was attributed to rapid de-halogenation and release of free ^{131}I. Two patients experienced transient hot flushes and tachycardia following the injection of HAMA, and one patient developed a single episode of rigor which resolved spontaneously. The administration of exogenous HAMA provided insufficient passive immunization to prevent the production of an endogenous HAMA response in all five patients, indicating that this approach is mainly applicable to a first injection.

This approach would appear suitable for use with IT targeted radiotherapy. An alternative strategy would be to actively immunize patients with mouse protein, providing that a sufficient time delay was acceptable prior to therapy to allow an endogenous HAMA response to develop.

Myelosuppressive toxicity may be circumvented by the use of infusions of autologous bone marrow following injection of the radioconjugate. This strategy has been documented in the treatment of lymphoma [90], neuroblastoma [321] and Hodgkin's lymphoma [25]. Similarly, Wheldon *et al.*, presented a theoretical argument for the case of antibody-targeted radiotherapy to partially replace the external beam component of total body irradiation (TBI) as "megatherapy" for disseminated malignancies [328]. It is conceivable that radioconjugates may be administered both intrathecally and systemically during such a procedure for the treatment of relapsed leukaemia, with or without overt CNS involvement.

The use of cytokines such as granulocyte-macrophage colony-stimulating factor (GM-CSF), may allow higher activities of radioisotope to be administered before marrow aplasia ensues, as well as promoting more rapid re-engraftment in patients receiving bone marrow infusions.

Approaches to circumvent or greatly reduce myelosuppression will allow much higher activities of radioisotope to be administered. Under these circumstances, it is not clear which tissues will be dose-limiting, in terms of either clinical toxicity or calculated radiation dose. This most obviously applies to the CNS, but organs such as the liver and lung should also be considered in this respect.

A high radiation dose to the kidney was noted in two patients (Chapter 10 and 12), which probably relates to the expression of CALLA on renal tissue (Chapter 3). The use of CD10 antibodies may thus be abandoned following the development of antibodies recognising antigens with more limited expression on normal tissues.

(b) Improving efficacy.

The efficacy of a combination of two ^{131}I-labelled MoAbs, in terms of increased cell kill, has been demonstrated *in-vitro*. It would therefore seem

appropriate to undertake *in-vitro* investigation of cocktails of three or more antibodies. Provided criteria for human administration are met (Chapters 3, 4 and 10), there appears no logistic reason why such combinations should not be introduced into clinical studies. For B-lineage disease, antibodies recognising the CD20 and CD22 antigens appear most appropriate for further investigation.

CD20, a 35 - 37 kDa non-glycosylated phosphoprotein [329], is expressed on approximately 50% of blast cells in childhood pre-B ALL [225]. CD22 is a 135 kDa glycoprotein and expressed in the cytoplasm of greater than 90% of B-cells [330]. As such, the extent of surface expression of CD22 on ALL cells has been difficult to ascertain, although Borowitz reported that 74% of cases of childhood ALL had blast cells of which at least 20% were membrane positive for this antigen [223]. No normal cells, other than B-cells, with the possible exception of follicular dendritic reticulin cells, have been shown to react with either CD20 or CD22 antibodies [229] [230].

MoAbs recognising the CD5 antigen would be suitable for incorporation into a cocktail of reagents for targeting both T-cell ALL and NHL. This antigen is a 67 kDa monomeric glycoprotein, expressed on malignant cells in more than 75% of cases of T-ALL [40]. There appears to be a subset of B-lymphocytes which also express this antigen, although its presence on other normal tissues has not been demonstrated [331].

In-vitro experiments also suggested an advantage for antibodies recognising epitopes expressed with high density on the target cell, and for MoAbs radiolabelled to a high specific activity. The development of site-specific methods of radiolabelling may be useful to overcome the reduction in immunoreactivity associated with high specific activity radiolabelling. For the present clinical studies, it would seem appropriate to adopt a gradual

approach to the increase in specific activity, eg. by 100 - 200 MBq/mg increments.

The penetration of antibody conjugates into the inaccessible areas may be enhanced by the use of antibody fragments. Both $F(ab')_2$ and particularly Fab fragments have been shown to be superior to whole IgG in respect of penetration into human tumour xenografts in nude mice [49] and into multicellular tumour spheroids [79]. This, combined with faster whole body clearance, would encourage their further investigation.

The penetration of antibody species into neural tissue from the CSF should also be considered in the context of the radiation dose to deep-seated tumour cells and to the neural tissue itself (Chapter 12). Data on this point in humans comes from a post mortem study undertaken by our group. A 59 year old woman died 72 hours following an intraventricular injection of ^{131}I-labelled antibody for carcinomatous meningitis [332]. Autoradiography of brain slices revealed marked diffusion of isotope into the periventricular white matter, but with relative sparing of the grey matter. The presence of isotope was associated with marked oedema noted on histology, the cause of which remains uncertain. In contrast, very little penetration of isotope into the sub-pial tissues was observed. In overt CNS leukaemia, however, histological studies suggest that penetration will probably be enhanced as a result of destruction of the pial-glial membrane [132]. Additional information in this respect may be provided in future studies by use of techniques such as SPECT imaging.

In addition, several animal studies have examined penetration of macromolecules into the extracellular space of the brain substance. Klatzo *et al.*, examined the distribution of either fluorescein-labelled serum albumin or globulin injected into either the subarachnoid or ventricular CSF [333]. They observed that the ependymal surface was far more permeable than the pial membrane to albumin, which was seen to penetrate readily into the

subependymal grey matter. In contrast, there was no such penetration of globulin. Subsequent studies have confirmed the ready permeability of the ependymal lining, but there is conflicting data on the ability of macromolecules to penetrate through the pia under physiological conditions [298].

Bulk flow of fluid within the extracellular space of rat brain was demonstrated by Cserr and Ostrach, who showed that molecules of different molecular weight move at the same rate within this space, indicating that such movement is by convection rather than by diffusion [334].

(c) Alternative radionuclides.

Several workers have stressed the importance of selecting suitable radionuclides for use in antibody-mediated therapy on the basis of the characteristics, eg. morphology, of the particular tumour under consideration [92] [93]. Those emitting alpha-particles, with a range of 40 - 80 μm, would appear particularly suitable for targeting tumours consisting of single cells or clumps of a few cell diameters. Alpha-particles have the advantage of a very high LET. For example, Humm calculated that the alpha-emitter ^{211}Ast should be about 600 times as effective for cell sterilization as ^{131}I, in terms of the relative masses of radiolabelled antibodies [92].

The alpha-emitters usually considered for targeted therapy are ^{211}Ast and ^{212}Bi. The chemistry of ^{211}Ast conjugation with antibodies has been well described. Both Vaughan *et al.*, and Harrison *et al.*, used a method in which ^{211}Ast is incorporated in an intermediate compound, para-astatobenzoic acid, which is then coupled to protein amino groups by acylation with the mixed anhydride derivative of the acid [13] [96]. Both preservation of immuno-reactivity and stability of the MoAbs conjugates was demonstrated *in-vivo*. ^{212}Bi is produced from ^{212}Pb using a radionuclide generator, and may be

conjugated to antibodies using DTPA [97]. Specific and highly efficient cell kill effects have been demonstrated for conjugates of both ^{212}Bi and ^{211}Ast in tissue culture studies [97] [13], and for ^{211}Ast in tumour bearing animal models [13] [96]. Disadvantages of these alpha-emitters include their very short half-lives; 7.2 hours and 60.6 minutes for ^{211}Ast and ^{212}Bi respectively. These may be too short to permit adequate distribution of conjugate throughout the CSF pathways, particularly into the deep arachnoid. Because ^{212}Bi is a decay product of ^{212}Pb which has a half-life of 10.6 hours, it may be possible to conjugate ^{212}Pb to a MoAb and thus generate the alpha-source *in-situ*. However, the peak ^{212}Bi activity occurs at 3.8 hours, which again is probably to short a time to permit adequate tumour uptake. The limited crossfire effect from short-range alpha-emissions does not support their use against the dense deposits of leukaemic cells frequently noted in post mortem studies, unless marked penetration into these deposits was possible. In addition, the cost of these reagents may be prohibitive. In particular, ^{211}Ast, requires generation by cyclotron.

Alpha-particles may also be generated *in-situ* by the use of antibody-mediated boron neutron capture therapy [335]. A non-radioactive isotope such as ^{10}Boron may be conjugated to a specific MoAb and targeted to tumour. After an optimum period of time to allow maximal antibody uptake, the tumour site is irradiated with low-energy thermal neutrons. This results in ^{10}B undergoing nuclear fission with the release of high energy alpha-particles. Problems with this technique include the inability to focus the neutron beam accurately, and the poor tissue penetration of these particles.

As discussed in Chapter 8, Auger electrons are of even shorter range, and radionuclides emitting these high LET particles, eg. ^{77}Br and ^{125}I, require both internalisation within the cell and passage to the nucleus to exert a cytotoxic effect. Providing this is possible, these isotopes offer the scope for highly efficient and specific tumour cell kill. However, as no cross-fire effect is

possible, it is unlikely, especially in cases of overt CNS leukaemia, that antibodies will be able to deliver this group of radioisotopes to a critical number of tumour cells.

Shorter range β-emitters appear most promising for further study in the treatment of CNS leukaemia. ^{199}Au and ^{67}Cu have been proposed as the most suitable candidates, for which their β-emissions have a R_{90} value in water of 0.0276 and 0.0589 cm respectively (cf. ^{131}I, R_{90} = 0.0822 cm) [310]. In addition, a proportion of the decay energy is by emission of gamma-rays, of lower energy than those of ^{131}I. Gamma camera scintigraphy and external probe studies may thus be undertaken, but with reduced radiation exposure to personnel.

In a dosimetric model of intrathecal antibody targeted radiotherapy, Millar and Barrett examined the relative merits of four radionuclides; ^{90}Y, ^{131}I, ^{67}Cu and ^{199}Au [310]. For radionuclide uniformly distributed in CSF, he calculated the dose rate profiles for both CSF and surrounding neural tissues (spinal cord and nerve roots), and the dose rate ratio relative to that 100 μm from the surface of the cord. The ratio of average dose to the spinal cord to maximum dose to CSF was 0.34 and 0.037 for ^{90}Y and ^{131}I respectively, and 0.026 and 0.013 for ^{67}Cu and ^{199}Au respectively. The ratio of average dose to the lumbar spinal nerve roots to maximum CSF dose was 1.0, 0.35, 0.25 and 0.13 for ^{90}Y, ^{131}I, ^{67}Cu and ^{199}Au respectively. Millar extended this model to examine the dose rate profiles assuming radionuclide is distributed over the meningeal surfaces with finite thickness. The ratio of average dose to the spinal cord to maximum dose at 0.2 mm from the cord surface was 0.31 and 0.066 for ^{90}Y and ^{131}I respectively, and 0.051 and 0.030 for ^{67}Cu and ^{199}Au respectively. This work highlights the disadvantage of using long-range β-emitters such as ^{90}Y and ^{32}P to treat leptomeningeal tumours, for which an unacceptably high doses to normal tissues are predicted. In the context of the

simplified anatomical assumptions, this model also suggests an advantage for radionuclides emitting β-particles of shorter range than those of ^{131}I.

De Nardo and colleagues have prepared MoAb conjugates of ^{67}Cu using the macrocycle chelators, DOTA and TETA [336]. As with other radiometals such as ^{90}Y, conjugates using these reagents have proved more stable both *in-vitro* and *in-vivo* than either EDTA- or DTPA- chelates. To date, there are no similar reports for antibody conjugates of ^{199}Au. Other factors to be considered in respect of these isotopes include their degree of radiochemical purity and their high cost, which again may prohibit their investigation.

Finally, due to variability in the distribution and size of tumour deposits in CNS lymphoproliferative disease, it seems probable that the use of combinations of radionuclides, each with differing physical properties, may be effective.

(d) Other therapeutic approaches.

Enhanced delivery of radionuclide may be achieved by means of a two phase approach to targeting. An example is the avidin (or streptavidin)-biotin system. Biotin is a small water-soluble vitamin (molecular weight 244 Da). Streptavidin is a 60 kDa protein with four very high affinity ($K_a = 10^{15}\ M^{-1}$) binding sites for biotin. Its lack of glycosylation may confer an advantage over avidin in respect of non-specific binding.

Both biotin and streptavidin may be radiolabelled with halogens or conjugated with antibodies, with preservation of immunoreactivity [337]. Using a target of conjugated agarose beads in the peritoneum of mice, Hnatowich *et al.*, were able to demonstrate tumour localisation with either ^{111}In-labelled biotin or avidin following the administration of avidin or biotin conjugated MoAbs respectively [337]. Tumour localisation was also

demonstrated to be superior to that using ^{111}In-labelled MoAb in the same model system.

Paganelli *et al.*, have investigated a three step approach in the localization of CEA-expressing tumours in patients [338]. A biotinylated anti-CEA MoAb was initially administered. After three days, 4 - 6 mg of cold avidin was injected, followed 48 hours later by a biotin derivative labelled with 2 - 3 mCi ^{111}In. Known primary tumours and metastases were detected in 18 of 19 patients.

Both the two step methods described above may potentially be used to deliver an increased activity of radionuclide to the tumour cell surface by virtue of the interaction involving four high affinity binding sites. However, accessibility to tumour cells may be increased by exploiting the small size of a radionuclide-biotin conjugate administered following optimum distribution of streptavidin labelled MoAb. This method will also have the advantage of a lower dose to marrow and systemic organs by virtue of the extremely rapid elimination of radiolabelled biotin from blood, for which Paganelli *et al.*, calculated first and second phase half-times of five minutes and 2.4 hours respectively. On the other hand, for IT targeting, the rate of elimination from the subarachnoid space is also expected to be rapid, and would have to be carefully evaluated to ensure that it would not preclude adequate distribution of the radiolabelled biotin.

A number of plant (eg. ricin and abrin), bacterial (eg. diptheria toxin) and fungal (eg. alpha-sarcin) toxins have been shown to be highly toxic when internalised into cells, by virtue of inactivation of ribosomal protein synthesis. MoAb conjugates of these reagents have demonstrated to exert specific and highly efficient tumour cell killing effects in both *in-vitro* [229] and animal model systems [339].

With regard to clinical studies, a variable response to immunotoxin therapy was noted in half of 22 patients with metastatic melanoma given IV

infusions of a MoAb Ricin A-chain conjugate, with one patient showing a complete response to therapy [340]. Vitteta *et al.*, recently reported the results of a Phase 1 trial of a Fab fragment of a CD22 MoAb coupled to deglycosylated Ricin-A chain in patients with relapsed B-cell NHL [341]. 38% of 14 evaluable patients developed a partial response to therapy, sustained for up to four months.

In these, as in other studies of immunotoxin therapy [342], the majority of patients developed a vascular leak syndrome with weight gain, hypoalbuminaemia and oedema. Other toxicities included fever, myalgia, fatigue, aphasia, pulmonary oedema, rhabdomyolysis and decreased voltage on electrocardiography. A further major problem with immunotoxins is their short *in-vivo* half-life of approximately one to two hours [343].

The rationale for the use of intracavity administrations of immunotoxins is similar to that for conjugates of radionuclides. A WT1-ricin A chain immunotoxin has been subject to toxicity testing in 13 Rhesus monkeys as part of an evaluation for the treatment of meningeal T-cell leukaemia [228]. Peak CSF immunotoxin concentrations exceeded the ID_{50} for a T-ALL line *in-vitro* by more than 100-fold, and exceeded the ID_{50} for as long as 24 hours. Toxicity was mild, with no animal exhibiting evidence of gross behavioural change or neurotoxicity.

On the other hand, Urch *et al.*, noted the toxic deaths of all of guinea pigs injected intrathecally with a dose of saporin-anti-Id-I of 15 μg and above, and in half the animals given a dose of 10 μg in conjunction with systemic cyclophosphamide therapy. This was in contrast to doses of either 5 or 0.5 μg of immunotoxin, which were necessary to result in a prolonged survival of tumour-bearing animals.

The potential for serious toxicity suggests a cautious approach to the development of immunotoxins for the treatment of meningeal malignancy.

Extensive *in-vivo* toxicity testing and screening of normal tissues for cross-reactivity is required before clinical studies could commence.

The efficacy and specificity of IT therapy with either ricin A chain or saporin conjugates was demonstrated in two studies using the L_2C/guinea pig meningeal leukaemia models (Chapter 9). A major limitation of these studies is that immunotoxin was introduced only 24 hours after inoculation with the L_2C tumour cell line, before the tumour was fully established on the leptomeninges. Experiments in which the saporin-anti-Id-I was injected at least seven days after tumour inoculation failed to produce a significant therapeutic benefit (Personal communication, Dr M Glennie, Tenovus Research Laboratory, Southampton). This highlights the potential limitation to the therapeutic range of reagents which requiring both cell binding and internalization to be effective.

3. In Conclusion

The development of site-specific radiotherapy offers considerable promise for cancer treatment. The optimism resulting from pre-clinical studies has, however, been tempered by the results of clinical trials, which suggest that this potential is far from being fulfilled. Increasing awareness of the limitations of this approach has, however, resulted in sustained improvements in developing methods, such as the targeting of compartmentalised tumours, to overcome these obstacles, justifying continued interest and development.

REFERENCES.

1. Massin, J. P., Savoie, J. C., Garnier, H., Guiraudon, G., Leger, F. A. and Bacourt, F. Pulmonary metastases in differentiated thyroid carcinoma: Study of 58 cases with implications for primary tumour treatment. *Cancer,* (1984). 53: p. 982-992.

2. Smit, A. J., Van Essen, L. H., Hollema, H., Muskiet, F. A. and Piers, D. A. ^{131}I-*m*IBG uptake in non-secreting paraganglioma. *J. Nucl. Med.,* (1984). 25: p. 984-986.

3. Hoefnagel, C. A., Voute, P. A., de Kraker, J. and Marcuse, H. R. Total body scintigraphy with ^{131}I-*m*IBG for detection of neuroblastoma. *Diag. Imag. Clin. Med.,* (1985). 54: p. 21-27.

4. Muller-Gartman, H. W., Erttmann, R. and Helmke, K. *m*IBG scintigraphy in neuroblastoma: A comparison with conventional X-ray and ultrasound. *Ped. Hematol. Onc.,* (1986). 3: p. 97-107.

5. Voute, P. A., Hoefnagel, C. A., de Kraker, J., Valdes-Olmos, R., Baker, D. J. and van de Kleij, A. J. Results of treatment with ^{131}I-*m*IBG in patients with neuroblastoma: Future prospects of zetotherapy, In *Advances in Neuroblastoma Research 3,* A.E. Evans, G.J. D'Angio, A.G. Kundson and R.C. Seeger, (Eds). (1991), Wiley-Liss: New York. p. 439-446.

6. Lewis, I. J., Lashford, L. S. and Fielding, S. UKCCSG study of therapeutic use of ^{131}I-*m*IBG in chemoresistant neuroblastoma (Abstract). *Med. Paed. Oncol.,* (1990). 18: p. 379.

7. de Kraker, J., Voute, P. A. and Hoefnagel, C. A. Induction therapy with ^{131}I-*m*IBG in neuroblastoma advanced disease: Preliminary Results (Abstract). *Med. Paed. Oncol.,* (1990). 18: p. 380.

8. Poste, G., Kirsh, R. and Bugelski, P. Liposomes as a drug delivery system in cancer therapy. In *Novel Approaches to Cancer Chemotherapy,* P.S. Sunkura, (Ed). (1984), Academic Press: New York. p. 165-230.

9. Davis, S. S. and Illum, L. Colloidal delivery systems - Opportunities and challenges, In *Site Specific Drug Delivery,* E. Tomlinson and S.S. Davis, (Eds). (1986), J. Wiley and Sons: New York. p. 93-110.

10. Fidler, I. J. Immunodulation of macrophages for cancer and antiviral therapy, In *Site Specific Drug Delivery,* E. Tomlinson and S.S. Davis, (Eds). (1986), J. Wiley and Sons: New York. p. 111-134.

11. Ehrlich, P. Chemotherapy. *Himmelweit, The Collected Papers of Paul Ehrlich,* Vol. 3. (1913), Oxford: Pergamon Press.

12. Order, S. E., Klein, J. L., Ettinger, D., Alderson, P., Siegelman, S. and Leichner, P. Use of isotopic immunoglobulin in therapy. *Cancer Res.,* (1980). 40: p. 3001-3007.

13. Vaughan, A. T., Bateman, W. J. and Fisher, D. R. The *in-vivo* fate of a ^{211}At-labelled monoclonal antibody with a known specificity in a murine system. *Int. J. Rad. Oncol. Biol. Phys.,* (1982). 8: p. 1943-1946.

14. Woo, D. V., Derui, L., Brady, L. W., Emrich, J., Mattis, J. and Steplewski, Z. Auger electron damage induced by radioiodinated ^{125}I monoclonal antibodies, In *The Present and Future Role of Monoclonal Antibodies in the Management of Cancer Research. Front. Radiat. Therapy Oncol.,* J.M. Vaeth and J.L. Meyer. (Eds) Vol. 24. (1990), Basel: Krager. p. 47-63.

15. Baldwin, R. W. Monoclonal antibodies for targeting chemotherapeutic agents, In *Prog. Exp. Tumour Res.* (1985), Karger: Basel. p. 140-151.

16. Jansen, F. K., Blythman, H. E., Carriere, D., Casellas, P., Gros, O., Gros, P., Laurent, J. C., Paolucci, F., Pau, B., Poncelet, P., Richer, G., Vidal, H. and Voisin, G. A. Immunotoxins: Hybrid molecules combing high specificity and protein cytotoxicity. *Immunol. Rev.,* (1982). 62: p. 185-216.

17. Pressman, D. and Keighly, G. The zone of activity of antibodies as determined by the use of radioactive tracers: The zone of activity of nephrotoxic anti-kidney serum. *J. Immunol.,* (1948). 59: p. 141-146.

18. Pressman, D., Day, E. D. and Blau, M. The use of paired labelling in the determination of tumour localising antibodies. *Cancer Res.,* (1957). 17: p. 845-850.

19. Bale, W. F., Contreras, M. A. and Goody, E. D. Factors influencing localisation of labelled antibodies in tumours. *Cancer Res.,* (1980). 40: p. 2965-2972.

20. Goldenberg, D. M. and DeLand, F. H. History and status of tumour imaging with radiolabelled antibodies. *J Biological Response Modifiers,* (1982). 1: p. 121-136.

21. Primus, F. J., MacDonald, R., Goldenberg, D. M. and Hansen, H. J. Localisation of human GW-39 tumours in hamsters by radiolabelled heterospecific antibody to carcinoembryonic antigen. *Cancer Res.,* (1977). 37: p. 1544-1547.

22. Primus, F. J., Wang, R. H., Goldenberg, D. M. and Hansen, H. J. Tumour detection and localisation with purified antibodies to carcinoembryonic antigen. *Cancer Res.* (1973). 33: p. 2977-2982.

23. Ettinger, D. S., Order, S. E., Wharam, M., Parker, M. K., Klein, J. L. and Leichner, P. K. Phase I/II study of isotopic immunoglobulin therapy for primary liver cancer. *Cancer Treat. Rep.,* (1982). 66: p. 289-297.

24. Lenhard, R. E., Order, S. E., Spunberg, J. J., Asbell, S. O. and Leibel, S. A. Isotopic immunoglobulin: A new systemic therapy for advanced Hodgkins disease. *J. Clin. Oncol.,* (1985). 3: p. 1296-1300.

25. Vriesendorp, H. M., Herpst, J. M. Leichner, P. K., Klein, J. L. and Order, S. E. Polyclonal ^{90}Y labelled anti-ferritin for refractory Hodgkin's disease. *Int. J. Rad. Oncol., Biol. and Physics,* (1989). 17: p. 815-821.

26. Kohler, G. and Milstein, C. Continuous cultures of fused cells secreting antibody of a pre-defined specificity. *Nature,* (1975). 256: p. 495-497.

27. Kipps, T. J., Parham, P., Punt, J. and Herzenberg, L. A. Importance of immunoglobulin isotype in human antibody dependent cell mediated cytotoxicity directed by murine monoclonal antibodies. *J. Exp. Med.,* (1985). 161: p. 1-17.

28. Seto, M., Takahashi, T., Nakamura, S., Matsudaira, Y. and Nishizuka, Y. *In-vivo* anti-tumour effects of monoclonal antibodies with different immunoglobulin sub-classes. *Cancer Res.,* (1983). 43: p. 4768-4773.

29. Herlyn, D. and Koprowski, H. IgG_{2a} monoclonal antibodies inhibit human tumour growth through interaction with effector cells. *Proc. Natl. Acad. Sci,* (1982). 79: p. 4761-4765.

30. Saarinen, U. M., Coccia, P. F., Gerson, S., Pelley, R. and Cheung, N-K. I*n-vitro* eradication of neuroblastoma cells by monoclonal antibody and human complement. A method for purging autologus bone marrow. *Cancer Res.,* (1985). 45: p. 5969-5975.

31. Herlyn, D., Steplewski, Z., Herlyn, M. and Koprowski, H. Inhibition of growth of human colorectal carcinoma in nude mice by monoclonal antibody. *Cancer Res.,* (1980). 40: p. 717-721.

32. Bernstein, I. D., Tam, M. R. and Nowinski, R. C. Mouse leukaemia, therapy with monoclonal antibodies against a thymus differentiation antigen. *Science,* (1980). 207: p. 68-71.

33. Kirch, M.E. and Hammerling, U. Immunotherapy of murine leukaemias by monoclonal antibody. *J. Immunol.,* (1981). 127: p. 805-810.

34. Nadler, L. M., Stashenko, P., Hardy, R., Kaplan, W. D., Button, L. N., Kufe, D. W., Antman, K. H. and Schlossman, S. F. Serotherapy of a patient with a monoclonal antibody directed against a human lymphoma-associated antigen. *Cancer Res.,* (1980). 40: p. 3147-3154.

35. Miller, R. A., Maloney, D. G., Warnke, R. and Levy, R. Treatment of B-cell lymphoma with monoclonal anti-idiotype antibody. *New Eng. J. Med.,* (1982). 306: p. 517-522.

36. Miller, R. A., Maloney, D. G., McKillop, J. and Levy, R. *In-vivo* effects of a murine hybridoma monoclonal antibody in a patient with T-cell leukaemia. *Blood,* (1981). 58: p. 78-86.

37. Ritz, J., Pesando, J. M., Sallan, S. E., Clavell, L. A., Notis-McConarty, J., Rosenthal, P. and Schlossman, S. F. Serotherapy of acute lymphoblastic leukaemia with monoclonal antibody. *Blood,* (1981). 58: p. 141-152.

38. Ball, E. D., Bernier, G. M., Cornwell, G. G., McIntyre, O. R., O'Donnell, J. F. and Fanger, M. W. Monoclonal antibodies to myeloid differentiation antigens: *In-vivo* studies of three patients with acute myelogenous leukaemia. *Blood,* (1983). 62: p. 1203-1210.

39. Foon, K. A., Schroff, R. W. and Bunn Jnr, P. A. Clinical applications of monoclonal antibodies for patients with leukaemia and lymphoma. *Prog. Clin. Biol. Res.,* (1986a). 211: p. 265-284.

40. Foon, K. A. and Todd, R. F. Immunologic classification of leukaemia and lymphoma. *Blood,* (1986b). 68: p. 1-31.

41. Lowder, J. N.,Meeker, T. C., Maloney, D. G., Thielmans, K., Miller, R. A. and Levy, R. Anti-idiotype monoclonal antibody therapy of human B-lymphocytic malignancy. *Proc. Am. Soc. Clin. Oncol.,* (1983). 3: p. 250.

42. Dillman, R. O., Shawler, D. L. and Collines, H. A. Murine monoclonal antibody therapy in two patients with chronic lymphocytic leukaemia. *Blood,* (1982). 59: p. 1036-1045.

43. Boyse, E. A., Stockert, E. and Old, L. J. Modification of the antigenic structure of the cell membrane by thymus-leukaemia (TL) antibody. *Proc. Natl. Acad. Sci. USA,* (1967). 58: p. 954-958.

44. Ritz, J., Pesando, J.M., Notis-McConarty, J. and Schlossman, S. F. Modulation of human acute lymphoblastic leukaemia antigen induced by monoclonal antibody *in-vitro. J. Immunol.,* (1980). 125: p. 1506-1514.

45. Moshakis, V., McIlhiney, R. A. and Reghaven, D. Localisation of human tumour xenografts after IV administration of radiolabelled monoclonal antibodies. *Br. J. Cancer,* (1981). 44: p. 91-99.

46. Jones, D. H.,Goldman, A., Gordon, I., Pritchard, J., Gregory, B. and Kemshead, J. T. Therapeutic application of a radiolabelled monoclonal antibody in nude mice xenografted with human neuroblastoma: Tumoricidal effects and distribution studies. *Int. J. Cancer,* (1985). 35: p. 715-720.

47. Hedin, A., Wahren, B. and Hammarstrom, S. Tumour localisation of CEA containing tumours in nude mice by means of monoclonal anti-CEA antibodies. *Int. J. Cancer,* (1982). 30: p. 547-552.

48. Colcher, D., Keenan, A. M., Larson, S. M. and Schlom, J. Prolonged binding of radiolabelled monoclonal antibody (B72.3) used for the *in-situ* radioimmunodetection of human colon cancer xenografts. *Cancer Res.,* (1984). 44: p. 5744-5751.

49. Buchegger, F., Mach, J. P., Leonnard, P. and Carrel, S. Selective tumour localisation of radiolabelled anti-human melanoma monoclonal antibody fragment demonstrated in the nude mouse model. *Cancer,* (1986). 58: p. 655-662.

50. Weinstein, J. N., Eger, R. R., Covell, D. G., Black, C. D., Mulshine, J., Carrasquillo, J. A., Larson, S. M. and Keenan, A. M. The pharmacology of monoclonal antibodies. *Ann. N. Y. Acad. Sci.,* (1987). 507: p. 199-210.

51. Hagan, P. L., Halpern, S. E., Dillman, R. O.,Shawler, D. L., Johnson, D. E., Chen, A., Krishnan, L.,Frincke, J., Bartholomew, R. M., David, G. S. and Carlo, D. Tumour size: Effect on monoclonal antibody uptake in tumour models. *J. Nucl Med.,* (1986). 27: p. 422-427.

52. Rogers, G. T., Boden, J., Harwood, P. J., Pedley, R. B., Rawlins, G. A. and Bagshawe, K. D. Dose dependent localisation of a monoclonal Fab_2 fragment against CEA studied in a mouse model. *Eur. J. Cancer Clin. Oncol.,* (1986). 22: p. 709-710.

53. Zalutsky, M. R., Moseley, R. P., Coakham, H. B., Coleman, R. E. and Bigner, D. D. Pharmacokinetics and tumour localisation of ^{131}I labelled anti-tenascin monoclonal antibody 81C6 in patients with gliomas and other intracranial malignancies. *Cancer Res.*, (1989a). 49: p. 2807-2813.

54. Philben, V. J., Jakowatz, J. G., Beatty, B. G., Vlahos, W. G., Paxton, R. J., Williams, L. E., Shively, J. E. and Beatty, J. D. The effect of tumour CEA content on tissue uptake of indium-111 Labelled anti-CEA monoclonal antibody. *Cancer,* (1986). 57: p. 571-576.

55. Mach, J. P., Buchegger, F. and Forni, M. Use of radiolabelled antibodies for the detection of human carcinomas by external photoscanning. *Immunol. Today,* (1981). 2: p. 239-249.

56. Larson, S. M., Brown, J. P., Wright, P. W., Carrasquillo, J. A., Hellstrom, I. and Hellstrom, K. E. Imaging of melanoma with ^{131}I labelled monoclonal antibodies. *J. Nucl. Med.,* (1983a). 24: p. 123-129.

57. Epenetos, A. A., Snook, D., Durbin, H., Johnson, P. M. and Taylor-Papadimitriou, J. Limitations of radiolabelled monoclonal antibodies for localisation of human neoplasms. *Cancer Res.,* (1986). 46: p. 3183-3191.

58. Farrands, P. A., Perkins, A. C. and Pimm, M. V. Radioimmunodetection of human colorectal cancers by an anti-tumour monoclonal antibody. *Lancet,* (1982). ii: p. 397-400.

59. Buraggi, G. L., Callegaro, L., Mariani, G., Turrin, A., Cascinelli, N., Attili, A., Bombardieri, E., Terno, G., Piassio, G. and Douis, M. Imaging with ^{131}I labelled monoclonal antibodies to a high molecular weight melanoma associated antigen. *Cancer Res.,* (1985). 45: p. 3378-3387.

60. Esteban, J. M., Colcher, D., Carrasquillo, J. A., Sugarbaker, P., Reynolds, J. C., Bryant, G., Larson, S. M. and Schlom, J. Quantitative analyses of selective radiolabelled monoclonal antibody localisation in metastatic lesions of colorectal cancer patients. *Cancer Res.*, (1987). 47: 1185-1189.

61. Kemshead, J. T., Lashford, L. S., Jones, D. and Coakham, H. B. Diagnosis and therapy of neuroectodermally associated tumours using targeted radiation. *Dev. Neurosci.,* (1987). 9: p. 69-83.

62. Rosen, S. T., Zimmer, A. M., Goldman-Leikin, R., Goldman-Leikin, R., Gordon, L. I., Kazikiewicz, J. M., Kaplan, E. H., Variakojis, D., Marder, R. J., Dykewicz, M. S., Piergies, A., Silverstein, E. A., Roenigk, H. H. and Spies, S. M. Radioimmunodetection and radioimmunotherapy of cutaneous T-cell lymphomas using a ^{131}I-labelled monoclonal antibody: An Illinois Cancer council study. *J. Clin. Oncol.,* (1987). 5: p. 562-573.

63. Carrasquillo, J. A., Krohn, K. A., Beaumier, P., McGuffin, R. W., Brown, J. P., Hellstrom, K. E., Hellstrom, I. and Larson, S. M. Diagnosis of and therapy for solid tumours with radiolabelled antibodies and immune fragments. *Cancer Treat. Rep.,* (1984). 68: p. 317-328.

64. De Nardo, S. J., De Nardo, G. L., O'Grady, L. F., Levy, N. B., Mills, S. L., Macey, D. J.,McGahan, J. P., Miller, C. H. and Epstein, A. L. Pilot studies of radioimmunotherapy of B-cell lymphoma and leukaemia using ^{131}I Lym-1 monoclonal antibody. *Antibody, Immunoconj. Radiopharm.,* (1988). 1: p. 17-33.

65. Vaughan, A. T., Anderson, P., Dykes, P. W., Chapman, C. E. and Bradwell, A. R. Limitations to the killing of tumours using radiolabelled antibodies. *Br. J Radiol.,* (1987). 60: p. 567-578.

66. Lee, Y. S., Bullard, D. E., Wikstrand, C. J., Zalutsky, M. R., Mahlbaier, L. H. and Bigner, D. D. Comparison of monoclonal antibody delivery to intracranial glioma xenografts by intravenous and intracarotid administration. *Cancer Res.,* (1987). 47: p. 1941-1946.

67. Moseley, R. P. Aspects of monoclonal antibody technology in diagnosis and therapy of central nervous system neoplasia. *PhD Thesis, Bristol,* (1990).

68. Bloomer, W. D., Lipsztein, R. and Dalton, J. F. Antibody-mediated radiotherapy. *Cancer,* (1985). 55: p. 2229-2233.

69. Buchsbaum, D. J., Kaminski, M. S., Normolle, D. P. and Wahl, R. L. Improved MB-1 antibody delivery of lymphoma by pre-dosing, In *Monoclonal Antibodies: Applications in Clinical Oncology,* A. Epenetos, (Ed). (1991), Chapman and Hall: London. p. 115-121.

70. Gullino, P. M. Extracellular compartments of solid tumours, In *Becker, Cancer.* (1975), Plenum Press: New York. p. 327-354.

71. Folkman, J. Tumour angiogenesis. *Adv. Cancer Res.,* (1985). 43: p. 175-203.

72. Jain, R. K. Determinants of tumour blood flow. A review. *Cancer Res.,* (1988). 48: p. 2641-2658.

73. Jain, R. K. Tumour physiology and antibody delivery, In *The Present and Future Role of Monoclonal Antibodies in the Management of Cancer. Front. Radiat. Ther. Oncol.,* J.M. Vaeth and J.L. Meyer, (Eds). (1990), Karger: Basel. p. 32-46.

74. Herlyn, M., Steplewski, Z., Herlyn, D. and Koprowski, H. Colorectal carcinoma-specific antigen. Detection by means of monoclonal antibodies. *Somat. Cell. Genet.,* (1979). 5: p. 957-972.

75. Butler, T. P., Grantham, F. H. and Gullino, P. M. Bulk transfer of fluid in the interstitial compartment of mammary tumours. *Cancer Res.,* (1975). 35: p. 3084-3088.

76. Zalutsky, M. R., Noska, M. A., Golapinto, E. V., Garg, P. G. and Bigner, D. D. Enhanced tumour localisation and *in-vivo* stability of a monoclonal antibody radioiodinated using N-succinimidyl 3-(Tri-butylstannyl)benzoate. *Cancer Res.,* (1989b). 49: p. 5543-5549.

77. Swabb, E. A.,Wei, J. and Gullino, P. M. Diffusion and convection in normal and neoplastic tissues. *Cancer Res.,* (1974). 34: p. 2814-2822.

78. Jain, R. K. Transport of molecules across tumour vasculature. *Cancer Metastasis Rev.,* (1987). 6: p. 559-594.

79. Sutherland, R., Buchegger, F., Schreyer, M., Vacca, A. and Mach, J. P. Penetration and binding of radiolabelled anti-carcinoembryonic antigen monoclonal antibodies and their antigen binding fragments in human colon multicellular tumour spheroids. *Cancer Res.,* (1987). 47: p. 1627-1633.

80. Epenetos, A. A. and Kosmas, C. Monoclonal antibodies for imaging and therapy. *Br. J. Cancer,* (1989). 59: p. 152-155.

81. Britton, K. E. and Granowska, M. The role of radiolabelled antibodies in cancer diagnosis, In *Monoclonal Antibodies - Applications in Clinical Oncology,* A.A. Epenetos, (Ed). (1991), Chapman and Hall Medical: London. p. 223-236.

82. Pedley, R. B., Dale, R., Boden, J. A., Begent, R. H., Keep, P. A. and Green, A. J. The effect of a second antibody clearance on the distribution and dosimetry of radiolabelled anti-CEA antibody in a human colonic tumour xenograft model. *Int. J. Cancer,* (1989). 43: p. 713-718.

83. Begent, R. H., Ledermann, J. A., Green, A. J., Bagshawe, K. D., Riggs, S. J. Searle, F., Keep, P. A., Adam, T., Dale, R. G. and Glaser, M. G. Antibody distribution and dosimetry in patients receiving radiolabelled antibody therapy for colorectal cancer. *Br. J. Cancer,* (1989). 60: p. 406-412.

84. Schroff, R. W., Foon, K. A., Beatty, S. M., Oldham, R. K. and Morgan Jnr, A. C. Human anti-murine immunoglobulin responses in patients receiving monoclonal antibody therapy. *Cancer Res.,* (1985). 45: p. 879-885.

85. Shawler, D. L., Bartholomew, R. M., Smith, L. M. and Dillman, R. O. Human immune response to multiple injections of murine monoclonal antibody. *J. Immunol.,* (1985). 135: p. 1530-1535.

86. Courtenay-Luck, N. S., Epenetos, A. A., Moore, R., Larche, M., Pectasides, D., Dhokia, B. and Ritter, M. A. Development of primary and secondary immune responses to mouse monoclonal antibodies used in the diagnosis and therapy of malignant neoplasms. *Cancer Res.,* (1986). 46: p. 6489-6493.

87. Ledermann, J. A., Begent, R. H., Massof, C., Kelly, A. M., Adam, T. and Bagshawe, K. D. A phase I study of repeated therapy with radiolabelled antibody to carcinoembryonic antigen using intermittent or continuous administration of cyclosporin A to suppress the immune response. *Int. J. Cancer,* (1991). 47: p. 659-664.

88. Hale, G. Human monoclonal antibodies, in *Oncology Today.* (1991), Wellcome UK Ltd. p. 15-19.

89. Hale, G., Dyer, M. J. and Clark, M. R. Remission induction in non-Hodgkin's lymphoma with reshaped human monoclonal antibody CAMPATH-1H. *Lancet,* (1988). ii: p. 1394-1399.

90. Press, O. W., Eary, J. F., Badger, C. C., Martin, P. J., Appelbaum, F. R., Nelp, W. B., Krohn, K. A., Fisher, D., Porter, B., Thomas, E. D., Miller, R., Brown, S., Levy, R. and Bernstein, I. D. High-dose radio-immunotherapy of B-cell lymphomas, In *The Present and Future Role of Monoclonal Antibodies in the Management of Cancer. Front. Radiat. Ther. Oncol.,* J.M. Vaeth and J.L. Meyer, (Eds). (1990), Karger: Basel. p. 204-213.

91. MIRD, Medical Internal Radiation Dose Committee. *J. of Nucl. Med.,* (1971). 12: p. 1-32.

92. Humm, J. L. Dosimetric aspects of radiolabelled antibodies for tumour therapy. *J. Nucl. Med.,* (1986). 27: p. 490-497.

93. Wheldon, T. E. and O'Donoghue, J. A. The radiobiology of targeted radiotherapy. *Int. J. Radiat. Biol.,* (1990). 58: p. 1-21.

94. Wessels, B. W. and Rogus, R. D. Radionuclide selection and model absorbed dose calculations for radiolabelled tumour associated antibodies. *Med. Phys.*, (1984). 11: p. 638-645.

95. Brady, L. W., Markoe, A. M., Woo, D. V., Amendola, B. E., Karlsson, U. L., Rackover, M. A., Koprowski, H., Steplewski, Z. and Peyster, R. G. ^{125}I-labelled anti-epidermal growth factor receptor-425 in the treatment of glioblastoma multiforme, In *The Present and Future Role of Monoclonal Antibodies in the Managment of Cancer. Front. Radiat. Ther. Oncol.*, J.M. Vaeth and J.L. Meyer, (Eds). (1990), Karger: Basel. p. 151-160.

96. Harrison, A. and Royle, L. Efficacy of Astatine-211-labelled monoclonal antibody in treatment of murine T-cell lymphoma. *NCI Monogr,* (1987). 3: p. 157-158.

97. Kozak, R. W., Atcher, R. W., Gansow, O. A., Friedman, A. M., Hines, J. J. and Waldman. T. A. Bismuth-212-labelled anti-Tac monoclonal antibody: alpha-particle-emitting radionuclides as modalities for radioimmunotherapy. *Proc. Natl. Acad. Sci, USA,* (1986). 83: p. 474-478.

98. Leichner, P. K., Klein, J. L., Siegelman, S. S., Ettinger, D. S. and Order, S. E. Dosimetry of ^{131}I-labelled antiferritin in hepatoma: Specific activities in the tumour and liver. *Cancer Treat.*, (1983). 67: p. 647-658.

99. Humm, J. L., Gladstone, D. J., Bellerive, M. R. and Chin, L. M. Dosimetry of radiolabelled antibodies, In *Monoclonal Antibodies: Applications in Clinical Oncology,* A.A. Epeneos, (Ed). (1991), Chapman and Hall Medical: London. p. 79-86.

100. Gladstone, D. J., Chin, L. M. and Hanson, J. A radiation dosimetry system using miniature MOSFET probes, presented at the 38th annual meeting of the Radiation Society, New Orleans, Louisiana, April 7-12. (1990).

101. Dale, R. G. The application of the linear-quadratic dose-effect equation to fractionated and protracted radiotherapy. *Brit. J. Radiology,* (1985). 58: p. 515-528.

102. O'Donoghue, J. A. and Wheldon, T. E. Dose-rate effects in biologically targeted radiotherapy. *Int. J. Radiat. Biol.,* (1989). 56: p. 745-749.

103. Thames, H. D. An 'incomplete repair' model for survival after fractionated and continuous irradiations. *Int. J. Rad. Biol.,* (1985). 47: p. 319-339.

104. Wessels, B. W., Vessella, R. L., Palme, D. F., Berkopec, J. M., Smith, G. K. and Bradley, E. W. Radiobiological comparison of external beam irradiation and radioimmunotherapy in renal cell carcinoma xenografts. *Radiation Oncol. Biol. Phys.,* (1989). 17: p. 1257-1263.

105. Hilton, G., Halnan, K. E., Howard, N. and Godfrey, B. E. Effects of the injection of colloidal ^{198}gold in malignant effusions. *J. Faculty radiol.,* (1957). 8: p. 339-346.

106. Boye, Y. N., Lindegard, M. W., Paus, E., Skretting, A., Davy, M. and Jakobsen, E. Whole body distribution of radioactivity after intra-peritoneal administration of ^{32}P colloids. *Br. J. Radiol.,* (1984). 57: p. 395-402.

107. The Imperial Cancer Research Fund and the Hammersmith Oncology Group. Antibody-guided irradiation of malignant lesions: Three cases illustrating a new method of treatment. *The Lancet,* (1984). June: p. 1441-1443.

108. Epenetos, A. A., Munro, A. J., Stewart, S., Rampling, R., Lambert, C.G., McKenzie, C. G., Soutter, P., Rahemtulla, A., Hooker, G., Sivolapenko, G. B., Snook, D., Courtenay-Luck, N., Dhokia, B., Krausz, T., Taylor-Papadimitriou, J. and Bodmer, W. F. Antibody guided irradiation of advanced ovarian carcinoma with intra-peritoneally administered radiolabelled monoclonal antibodies. *J. Clin. Oncol.,* (1987). 12: p. 1890-1899.

109. Pectasides, D., Stewart, S., Courtenay-Luck, N., Rampling, R., Munro, A. J., Krausz, T., Dhokia, B., Snook, D., Hooker, G., Durbin, H., Taylor-Papadimitriou, J., Bodmer, W. F. and Epenetos, A. A. Antibody-guided irradiation of malignant pleural and pericardial effusions. *Brit. J. Cancer,* (1986). 53: p. 727-732.

110. Hird, V., Stewart, J. S., Snook, D., Dhokia, B., Coulter, C., Lambert, H. E., Mason, W. P., Soutter, W. P. and Epenetos, A. A. Intraperitoneally administered ^{90}Y-labelled monoclonal antibodies as a third line of treatment in ovarian cancer. A phase 1-2 trial: Problems encountered and possible solutions. *Br. J. Cancer,* (1990). 62: p. 48-51.

111. Moi, M. K., Meares, C. F. and De Nardo, S. J. The peptide way to macrocyclic bifunctional chelating agents: synthesis of 2-(p-nitro-benzyl)-1, 4, 7, 10-teraazacyclododecane-N, N', N'', N'''-tetraacetic acid and study of its yttrium (III) complex. *J. Amer. Chem. Soc.,* (1988). 110: p. 6266-6267.

112. Rieselbach, R. E., Di Chiro, G., Freireich, E. J. and Rall, D. P. Subarachnoid distribution of drugs after lumber injection, In *New Eng. J. Med.* (1962). p. 1273-1278.

113. D'Angio, G.J., French, L. A., Stadlan, E. M. and Kieffer, S. A. Intrathecal radioisotopes for the treatment of brain tumours. *Clin. J. Neuro.,* (1968). 15: p. 288-300.

114. Gold, L. H. A., Kieffer, S. A., D'Angio, G. J., Fallon, V. T. and Long, D. M. Current status of intrathecal radiogold in the treatment of medulloblastoma. *Acta. Radiol. Ther.,* (1972). 11: p. 329-340.

115. Fuller, L. G. A., Rogoff, E., Deck, M., Galicich, J., Ghavimi, F., Levitt, S., Smith, C. E. and D'Angio, G. J. Recent experience with intrathecal radiogold for medulloblastoma and ependymoblastoma: A progress report. *Am. J. Roentgenol.,* (1974). 22: p. 75-79.

116. Metz, O., Stoll, W. and Plenert, W. Meningosis prophylaxis with intrathecal ^{198}Au-colloid and methotrexate in childhood acute lymphocytic leukaemia. *Cancer,* (1982). 49: p. 224-228.

117. Sackmann-Muriel, F., Schere, D., Barengols, A., Eppinger-Helft, M., Braier, J. L., Pavlovsky, S., Macchi, G. H. and Guman, L. Remission maintenance therapy for meningeal leukaemia: Intrathecal methotrexate and dexamethasone versus intrathecal craniospinal irradiation with a radiocolloid. *Brit. J. Haemat.,* (1976). 33: p. 119-127.

118. Moseley, R. P.,Davies, A. G., Richardson, R. B., Zalutsky, M., Carrell, S., Fabre, J., Slack, N.,Bullimore, J., Pizer, B. L., Papanastassiou, V., Kemshead, J. T., Coakham, H. B. and Lashford, L. S. Intrathecal administration of ^{131}I radiolabelled monoclonal antibody as a treatment for neoplastic meningitis. *Brit. J. Canc.,* (1990b). 62: p. 637-642.

119. Faber, S. Temporary remissions in acute leukaemia in children produced by folic acid anatgonist, 4-aminopteroylglutamic acid (aminopterin). *New. Eng. J. Med.,* (1948). 238: p. 787-793.

120. Steinherz, P. G. Acute lymphoblastic leukaemia in childhood, In *Heamatology/Oncology Clinics of North America,* C. Pochedly, (Ed). (1987), W. B. Saunders Company: Philadelphia. p. 549-566.

121. Hustu, H. O., Aur, R. J. A., Verzosa, M. S., Simone, J. V. and Pinkel, D. Preventional of central nervous system leukaemia by irradiation. *Cancer,* (1973). 32: p. 585-597.

122. Evans, A., Gilbert, E. S. and Zaudstra, R. The increasing incidence of central nervous system leukaemia in children. *Cancer,* (1970). 26: p. 404-409.

123. West, R. J., Graham-Pole, J., Hardisty, R. M. and Pike, M. C. Factors in pathogenesis of central nervous system leuakema. *Br. Med. J.,* (1972). 3: p. 311-314.

124. Gribbon, M. A., Hardsty, R. M. and Chessels, J. M. Long term control of central nervous system leukaemia. *Arch. Dis. Child.,* (1977). 52: p. 673-678.

125. Eden, O. B. Extramedullary leukaemia, In *Butterworth's Modern Trends in Paediatric Haematology and Oncology,* M. Willoughby and S. Siegel, (Eds). (1982), p. 47-79.

126. Aur, R. J. A., Simone, J. V., Hustu, H. O., Walters, T., Borella, L., Pratt, C. and Pinkel, D. Central nervous system therapy and combination chemotherapy of childhood lymphocytic leuakema. *Blood,* (1971). 37: p. 272-281.

127. Bleyer, W. A. Central nervous system leukaemia in *Leukemia,* E.S. Henderson and T.A. Lister, (Eds), (1990), W. B. Saunders Company: Philadelphia. p. 733-768.

128. Pinkel, D. Patterns of failure in acute lymphocytic leukaemia. *Cancer Treat. Symp.,* (1983). 2: p. 259-266.

129. Zeulzer, W. W., Radivdranath, Y., Lusher, J. M., Sarniak, S. and Considine, B. IMGFRA (intermittent intrathecal methotrexate and fractional radiation) plus chemotherapy in childhood leukaemia. *Am. J. Haematol.,* (1976). 1: p. 191-199.

130. Thomas, L. B. Pathology of leukaemia in the brain and meninges: postmortem studies of patients with acute leukaemia and of mice given innoculations of L1210 leukaemia. *Cancer Res.,* (1965). 25: p. 1555-1571.

131. Azzarelli, B. and Roessmann, B. Pathogenesis of central nervous system infiltration in acute leukaemia. *Arch. Pathol. Lab. Med.,* (1977). 101: p. 203-205.

132. Price, R. A. and Johnson, W. W. The central nervous system in childhood leukaemia. I. The arachnoid. *Cancer,* (1973). 31: p. 530-533.

133. Schweinle, J. E. and Alperin, J. B. Central nervous system recurrence ten years after remission of acute lymphoblastic leukaemia. *Cancer,* (1980). 45: p. 16-18.

134. Kuo, A. H., Yataganas, X., Galicich, J. H., Freid, J. and Clarkson, B. D. Proliferative kinetics of central nervous system leukaemia. *Cancer,* (1975). 36: p. 232-239.

135. Tsuchiya, J., Moteki, M., Shimano, S., Shinonome, S., Suda, T., Omine, M. and Maekawa, T. Proliferative kinetics of the leukaemic cell in meningeal leukemia. *Cancer,* (1978). 42: p. 1255-1262.

136. Zovickian, J. and Youle, R. J. Efficacy of intrathecal immunotoxin therapy in an animal model of leptomeningeal neoplasia. *J. Neurosurg.,* (1988). 68: p. 767-774.

137. Thomas, L. B., Chirigos, M. A., Humphreys, S. R. and Goldin, A. Pathology of the spread of L1210 leukaemia in the central nervous system of mice and effect of treatment with Cytoxan. *J. Natl. Cancer Inst.,* (1962). 28: p. 1355-1389.

138. Hyman, C. D., Bogle, J. M., Brubaker, C. A., Williams, W. and Hammond, D. Central nervous system involvement by leukaemia in children. *Blood,* (1965). 25: p. 13-22.

139. Hardisty, R. M. and Norman, P. M. Meningeal leukaemia. *Arch. Dis. Childhood,* (1967). 42: p. 441-447.

140. Veerman, A. J. P., Huismans, L. D. R. and van Zantwijk, I. C. Diagnosis of meningeal leukaemia using immunoperoxidase methods to demonstrate common acute lymphoblastic leukaemia cells in cerebrospinal fluid. *Leuk. Res.,* (1985). 9: p. 1195-1200.

141. Seidenfeld, J. and Martin, L. J. Biochemical markers of central nervous system tumours measured in cerebrospinal fluid and their potential use in diagnosis and patient management: a review. *J. Natl. Cancer. Inst.,* (1979). 63: p. 919-931.

142. Tallman, R. D., Kimbrough, S. M., O'Brien, J. F., Goellner, J. R. and Yanagihara, T. Assay for *beta*-glucuronidase in cerebrospinal fluid: usefulness for the detection of neoplastic meningitis. *Mayo. Clin. Proc.,* (1985). 60: p. 293-298.

143. Coccia, P. F., Bleyer, W. A. and Siegel, S. E. Development and preliminary findings of Children's Cancer Study Group Protocols for low, average and high risk acute lymphoblastic leukaemia in children, In *Leukaemia Research - Advances in Cell Biology and Treatment,* S. Murphy and J.R. Gilbert, (Eds). (1983), Elsevier/North Holland: Amsterdam. p. 241-250.

144. Sullivan, M. P., Vietti, T. J., Fernbach, D. J., Griffith, K. M., Haddy, T. B. and Watkins, W. L. Clinical investigations in the treatment of meningeal leukaemia: Radiation therapy regimens vs. conventional intrathecal methotrexate. *Blood,* (1969). 34: p. 301-319.

145. Melhorn, D. K., Gross, S., Fisher, E. J. and Hewman, A. J. Studies on the use of "prophylactic" intrathecal amethopterin in childhood leukaemia. *Blood,* (1970). 36: p. 55-60.

146. Pavlovsky, S., Eppinger-Helft, M. and Sackmann-Muriel, F. Factors that influence the appearance of CNS leukaemia. *Blood,* (1973). 39: p. 935-938.

147. Bowman, W. P., Melvin, S. L., Aur, R. K. A. and Mauer, A. M. A clinical perspective on cell markers in acute lymphocytic leukaemia. *Cancer Res.,* (1981). 33: p. 4794-4801.

148. Dow, L. W., Borella, L., Sen, L., Aur, R. J., George, S. L., Mauer, A. M. and Simone, J. V. Initial prognostic factors and lymphoblast erythrocyte rosette formation in 109 children with acute lymphoblastic leukaema. *Blood,* (1977). 50: p. 671-682.

149. Kersey, J., Coccia, P., Siegel, S., Bleyer, A., Sather, H., Lukens, J., Gross, S. and Hammond, D. The presence of erythrocyte receptors on leukaemic lymphoblasts indicates extramedullary origin, lymphomatous presentation and relapse in extramedullary sites. *Blood,* (1981). 58: p. 161a.

150. Bleyer, W. A. Central nervous system leukaemia, In *Leukemia,* F. Gunz and E.S. Henderson, (Eds). (1982), Grune & Stratton: New York. p. 865-911.

151. Nesbit, M. E., Sather, H., Robison, L. L., Donaldson, M., Littman, P., Ortega, J. A. and Hammond, G. D. Sanctuary therapy: A randomised trial of 724 children with previously untreated acute lymphoblastic leukaemia. A report from the Children's Cancer Study Group. *Cancer Res.*, (1982). 42: p. 674-680.

152. Bleyer, W. A., Coccia, P. F., Sather, H. N., Level, C., Lukens, J., Niebrugge, D. J., Siegel, S., Littman, P. S. and Leiken, S. L. Reduction in central nervous system leukaemia with a pharmacokinetically derived intrathecal methotrexate dosage regimen. *J. Clin. Oncol.*, (1983). 1: p. 317-325.

153. Nesbit, M. E., Robinson, L. L., Littman, P. S., Sather, H. N., Ortega, J., D'Angio, G. J. and Hammond, G. D. Presymptomatic central nervous system therapy in previously untreated childhood acute lymphoblastic leukaemia: Comparison of 1800 rad and 2400 rad. *Lancet*, (1981). i: p. 461-467.

154. Freeman, A. I., Weinberg, V., Brecher, M. L., Jones, B., Glicksman, A. S., Sinks, L. F., Weil, M., Pleuss, H., Hananian, J., Burgert, E. U. Jnr, Glohrist, G. S., Necheles, T., Harris, M. and Kung, F. Comparison of intermediate-dose methotrexate with cranial irradiation for the post-induction treatment ofacute lymphocytic leukaemia in children. *N. Eng. J. Med.*, (1983). 308: p. 477-484.

155. Frankel, L. S., Wang, Y. M., Pullen, J., Patterson, R. B., Maurer, H., Leventhal, B., Chevalier, L., Forman, E. and Holland, J. F. High-dose intravenous methotrexate with an intrathecal methotrexate boost in the maintenance of ALL in children: A pilot study (Abstract). *Proc. Am. Assoc. Cancer Res.*, (1980). 21: p. 389.

156. Nesbit, M. E., D'Angio, G. J., Sather, H. N., Robinson, L. L., Ortega, J. A. and Hammond, D. Post-induction treatment of childhood acute lymphocytic leukaemia. *New. Eng. J. Med.*, (1984). 310: p. 262-263.

157. Sullivan, M. P., Chen, T., Dyment, P. K., Hvizdala, E. and Steuber, C. P. Equivalence of intrathecal chemotherapy and radiotherapy as central nervous system prophylaxis in children with acute lymphatic leukaemia: A paediatric oncology group study. *Blood,* (1982). 60: p. 948-958.

158. Moe, P. J., Wesenberg, F., Stokland, T. and Hapnes, C. Long term results of MTX infusions in childhood ALL (Abstract). *Med. Paed. Oncol.,* (1991). 19: p. 411.

159. Poplack, D., Reaman, G., Bleyer, A., Miser, J., Feusner, R. and Hammond, D. Central nervous system preventive therapy with high-dose methotrexate in acute lymphoblastic leukaemia: A preliminary report (Abstract). *Proc. Am. Soc. Clin. Oncol.,* (1984). 3: p. 204.

160. Brouwers, P., Moss, H. and Reaman, G. Central nervous system preventive therapy with systemic high-dose methotrexate versus cranial radiation and intrathecal methotrexate: Longitudinal comparison of effects of treatment on intellectual function of children with acute lymphoblsatic leukaemia (Abstract). *Proc. Am. Soc. Clin. Oncol.,* (1987). 6: p. 158.

161. Land, V. J., Thomas, P. R., Boyett, J. M., Glicksman, A. S., Culbert, S., Castleberry, R. P., Berry, B. H., Vats, T. and Humphrey, G. B. Comparison of maintenance treatment regimens for first central nervous system relapse in children with acute lymphoblastic leukaemia: A Paediatric Oncology Group study. *Cancer,* (1985). 56: p. 81-87.

162. Willoughby, M. L. N. Treatment of overt CNS leukaemia, In *Central Nervous System Leukaemia: Prevention and Treatment.* R. Mastrangelo, D.G. Poplack and R. Riccardi. (Eds). (1983), Boston: Martinus Nijuoff. 113-122.

163. Wells, R. J., Weetman, R. M. and Baehner, R. The impact of isolated central nervous system relapse following initial complete remission in childhood acute lymphocytic leukaemia. *J. Padiatr.,* (1980). 97: p. 429-432.

164. Sullivan, M. P., Vietti, T. J., Haggard, M. E., Donaldson, M. H., Krall, J. M. and Gehan, E. A. Remission maintenance therapy for meingeal leukaemia: Intrathecal methotrexate versus intravenous bis-nitrosourea. *Blood,* (1971). 38: p. 680-688.

165. Sullivan, M. P., Moon, T. E., Trueworthy, R., Vietti, T. J. and Humphrey, G. B. Combination intrathecal therapy for meningeal leukaemia: Two versus three drugs. *Blood,* (1977). 50: p. 471-479.

166. Humphrey, G. B., Krons, H. F., Filler, J., Maxwell, J. D. and VanHoutte, J. J. Treatment of overt CNS leukaemia. *Am. J. Paediatr. Haematol. Oncol.,* (1979). 1: p. 37-47.

167. Shapiro, W. R., Young, D. F. and Mehta, B. M. Methotrexate: Distribution in cerebrospinal fluid after intravenous, ventricular and lumbar injections. *New Eng. J. Med.,* (1975). 293: p. 161-166.

168. Bleyer, W. A. and Poplack, D. G. Intraventricular versus intralumbar methotrexate for central nerous system leukaemia. *Med. Paediatri. Oncol.,* (1979). 6: p. 207-213.

169. Shapiro, W., Posner, J. B., Ushio, T., Chemik, N. L. and Young, D. F. Treatment of meningeal neoplasms. *Cancer Treat. Rep.,* (1977). 61: p. 733-743.

170. Balis, F., Savitch, J., Bleyer, W. A., Reaman, G. and Poplack, D. G. Remission induction of meningeal leukaemia with high-dose intravenous methotrexate. *J. Clin. Oncol.,* (1985). 3: p. 485-489.

171. Frick, J., Ritch, P. S., Hansen, R. M. and Anderson, T. Successful treatment of meningeal leukaemia using systemic high-dose cytosine arabinoside. *J. Clin. Oncol.,* (1984). 2: p. 365-368.

172. Willoughby, M. L. N. Treatment of overt meningeal leukaemia in children: results of second MRC meningeal leukaemia trial. *Brit. Med. J.,* (1976). 1: p. 864-867.

173. Law, I. P. and Blom, J. Adult acute leukaemia. Frequency of central nervous system involvement in long term survivors. *Cancer,* (1977). 40: p. 1304-1306.

174. Omura, G. A., Moffit, S., Vogler, W. R. and Salter, M. M. Combination chemotherapy of adult acute lymphoblastic leukaemia with randomized central nervous system prophylaxis. *Blood,* (1980). 55: p. 199-204.

175. Bojson-Moeller, M. and Nielsen, J. L. CNS involvement in leukaemia. An autopsy study in 100 consecutive patients. *Acta. Path. Microbiol. Immunol. Scand. Sect. A,* (1983). 91: p. 209-216.

176. Choi, S. and Simone, V. J. Acute non-lymphocytic leukaemia in 171 children. *Med. Pediatr. Oncol.,* (1976). 2: p. 119-146.

177. Kay, H. E. M. Development of CNS leukaemia in acute myeloid leukaemia in childhood. *Arch. Dis. Child.,* (1976). 51: p. 73-74.

178. Bunn, P. A., Schein, P. S., Banks, P. M. and De Vita, V. T. J. Central nervous system complications in patients with diffuse histiocytic and undifferentiated lymphoma: Leukaemia revisited. *Blood,* (1976). 47: p. 3-10.

179. Skarin, A. T., Zuckerman, K. S., Pitman, S. W., Rosenthal, D. S., Moloney, W., Frie, E. I. and Canellos, G. P. High-dose methotrexate with folinic acid in the treatment of advanced non-Hodgkin lymphoma including CNS involvement. *Blood,* (1977). 50: p. 1039-1047.

180. Casteels-van Dael, M. and van de Casseye, W. Acute encephalopathy after initiation of cranial irradiation for meningeal leukaemia (Letter). *Lancet,* (1978). 2: p. 834.

181. Oliff, A., Bleyer, W. A. and Poplack, D. G. Acute encephalopathy after initiation of cranial irradiation for meningeal leukaemia (Letter). *Lancet,* (1978). 2: p. 13.

182. Freeman, J. E., Johnston, P. G. and Voke, J. M. Somnolence after prophylactic cranial irradiation in children with acute lymphoblastic leukaemia. *Br. Med. J.,* (1973). 4: p. 523-525.

183. Sheline, G. E. Irradiation injury of the human brain: A review of clinical experience, In *Radiation Damage to the Nervous System,* H.A. Gilbert and A.R. Kragan, (Eds). (1980), Raven Press: New York. p. 155-174.

184. Choux, M. Prognosis and long-term follow-up in patients with medulloblastoma in clinical neurosurgery, In *Proceedings of the Congress of Neurological Surgeons.* (1982), Williams and Wilkins: London.

185. Le Baron, S. Neuropsychological sequelae in survivors of medulloblastoma, In *Medulloblastomas in Children,* P.M. Zeltzer and C. Pochedly, (Eds). (1986), p. 237-249.

186. Hirsch, J. F., Renier, D., Czernichow, P., Benveniste, L. and Pierre-Kahn, A. Medulloblastoma in childhood - Survival and functional results. *Acta. Neurochir.,* (1979). 48: p. 1-15.

187. Deutsch, M. Late effects of craniospinal radiotherapy for medulloblastoma, in *Medulloblastomas in Children,* P.M. Zeltzer and C. Pochedly, (Eds). (1986), p. 213-237.

188. Bleyer, W. A. Neurologic sequelae of methotrexate and ionizing radiation: a new classification. *Cancer Treat. Rep.,* (1981). 65: p. 89-98.

189. Lansky, S. B., Cairns, G. T.. Lanksy, L. L., Cairns, N. U., Stephenson, L. and Garin, G. Central nervous system prophylaxis. Studies showing impairment in verbal skills and academic achievement. *Am. J. Pediatr. Hematol. Oncol.,* (1984). 6: p. 183-190.

190. Moss, H. A., Nannis, E. D. and Poplack, D. G. The effects of prophylactic treatment of the central nervous system on the intellectual functioning of children with acute lymphocytic leukaemia. *Am. J. Med.,* (1981). 71: p. 47-52.

191. Price, R. A. Therapy related central nervous system diseases in children with acute lymphoblastic leukaemia, In *Central Nervous System Leukaemia: Prevention and Treatment,* R. Mastrangelo, D.G. Poplack and R. Riccardi, (Eds). (1983), Martinus Nijhoff Publishers: Boston. p. 71-82.

192. Rubinstein, L. J., Herman, M.M., Long, T. F. and Wilbur, J. R. Disseminated necrotizing leukoencephalogpathy: A complication of treated central nervous system leukaemia and lymphoma. *Cancer,* (1975). 35: p. 291-305.

193. Clayton, P. E., Shalet, S. M., Morris-Jones, P. H. and Price, D. A. Growth in children treated for acute lymphoblastic leukaemia. *Lancet,* (1988). i: p. 460-462.

194. Kirk, J. A., Raghupathy, P. and Stevens, M. M. Growth failure and growth hormone deficiency after treatment for acute lymphoblastic leukaemia. *Lancet,* (1987). i: p. 190-193.

195. Shalet, S. M. Endocrine consequences of treatment of malignant disease. *Arch. Dis. Childhood,* (1989). 64: p. 1635-1641.

196. Leiper, A., Stanhope, R., Kitching, P. and Chessells, J. M. Precocious and premature puberty associated with treatment of ALL. *Arch. Dis. Child.,* (1987). 62: p. 1107-1112.

197. Price, R. A. The pathology of central nervous system leukaemia, In *Central Nervous System Leukaemia - Prevention and Treatment,* R. Mastrangelo, D.G. Poplack and R. Riccardi, (Eds). (1983b), Martinus Nijhoff Publishers: Boston. p. 1-11.

198. Schneider, U., Schwenk, H. U. and Bornkamm, G. Characterisation of EBV-genome negative "null" and "T" cell lines derived from children with acute lymphoblastic leukaemia and leukaemic transformed non-Hodgkin lymphoma. *Int. J. Cancer,* (1977). 19: p. 621-626.

199. Hurwitz, R., Hozier, J., LeBien, T.,Minowada, J., Gajl-Peczalska, K., Kubonishi, I. and Kersey, K. Characterisation of a leukaemic cell line of the pre-B phenotype. *Int. J. Cancer,* (1979). 23: p. 174-180.

200. Minowada, J., Dnuma, T. and Moore, G. E. Brief communication: Rosette forming human lymphoid cell lines. I. Establishment and evidence for origin of thymus-derived lymphocytes. *J. Natl. Cancer Inst.,* (1972). 49: p. 891-895.

201. Rosenfeld, C., Goutner, A. and Choquet, C. Phenotypic characterisation of a unique non-T, non-B acute lymphoblastic leukaemia cell line. *Nature,* (1977). 267: p. 841-843.

202. Klein, E., Klein, G., Nadkarni, J. S., Nadkarni, J. N., Wigzell, H. and Clifford, P. Surface IgM-kappa specificity on a Burkitt lymphoma cell *in-vivo* and in derived cultured lines. *Cancer Res.,* (1968). 28: p. 1300-1310.

203. Minowada, J., Koshiba, H., Sagawa, K., Kubonishi, I., Lok, M. S., Tatsumi, E., Han, T., Srivastava, B. I. S. and Ohnuma, T. Marker profiles of human leukaemia and lymphoma cell lines. *J. Cancer Res. & Clin. Oncol.,* (1981). 101: p. 91-100.

204. Green, I., Forni, G., Konen, T., Hu, C. P., Schwartz, B. D., Kask, A. and Shevach, E. M. Immunological studies of the guinea pig L_2C leukaemia. *Federation Proceedings,* (1977). 36: p. 2264-2267.

205. Hurrell, J. G. R. *Monoclonal hybridoma antibodies: Techniques and Applications,* J.G.R. Hurrell, (Ed). (1982), CRC Press: Boston.

206. Ey, P. L., Prowse, S. J. and Jenkin, C. R. Isolation of pure IgG_1, IgG_{2a} and IgG_{2b} immunoglobulins from mouse serum using protein A Sepharose. *Immunochemistry,* (1978). 15: p. 429-436.

207. Laemmeli, U. K. Cleavage of structural proteins during the assembly of the head of bacteriophage T4. *Nature,* (1970). 227: p. 680-685.

208. Weber, K. and Osborn, M. The reliability of molecular weight determinations by sodium dodecyl sulphate polyacrylamide gel electrophoresis. *J. Biol. Chem.,* (1969). 244: p. 4406-4412.

209. Hudson, L. and Hay, F. C. *Practical Immunology.* (1976), Oxford: Blackwell Scientific Publications. 298.

210. Fraker, P. J. and Speck, J. C. Protein and cell membrane iodinations with a sparingly soluble chloroamide, 1,3,4,6-Tetra-chloro-3a,6a-diphenylglycoluril. *Biochem. and Biophys. Res. Comms.,* (1978). 80: p. 849-857.

211. Hunter, W. M. and Greenwood, F. C. Preparation of ^{131}I labelled growth hormone of high specific activity. *Nature,* (1962). 194: p. 495-496.

212. Lindmo, T., Boven, E., Cuttitta, F., Fedorko, J. and Bunn, P. A. Determination of the immunoreactive fraction of radiolabelled monoclonal antibodies by linear extrapolation of binding at infinite antigen excess. *J. Immuno. Meths.,* (1984). 72: p. 77-89.

213. Lindmo, T. and Bunn, P. A. Determination of the true immunoreactive fraction of monoclonal antibodies after radiolabelling. *Mets. Enzymology,* (1986). 121: p. 678-691.

214. Dorken, B., Moller, P., Pezzutto, A., Schwartz-Albiez, R. and Moldenhauer, G. B-cell antigens: Section report, In *Leucocyte Typing IV: White Cell Differentiation Antigens,* W. Knapp, B. Dorken, W.R. Gilks, E.P. Rieber, R.E. Schmidt, H. Stein and A.E.G. Kr von dem Borne, (Eds). (1989), Oxford University Press: Oxford. p. 15-31.

215. Dorken, B., Schwarz, E., Feller, A. C., Hammerling, G. and Hunstein, W. Production of monoclonal antibodies for the diagnosis of minimal infiltration of leukaemic cells into the bone marrow. B-cell specific antibodies. *Verh. Desch. Ges. Path.,* (1983). 67: p. 65-69.

216. Tax, W. J., Tidman, N., Janossy, G., Trejdosiewicz, L., Willems, R., Leeuwenberg, J., De Witte, T. J. M., Capel, P. J. A. and Koene, R. A. P. Monoclonal antibody (WT1) directed against a T-cell surface glycoprotein: Characteristics and immunosuppressive activity. *Clin. Exp. Immunol.*, (1984). 55: p. 425-436.

217. Van Keuren, M. L., Goldman, D. and Merril, C. R. Detection of radioactively labeled proteins is quenched by silver staining methods: quenching is minimal for 14C and partially reversible for 3H with a photochemical stain. *Anal. Biochem.*, (1981). 116: p. 248-255.

218. Weary, M. E. Understanding and setting endotoxin limits. *J. Parenteral. Science and Technology,* (1990). 44: p. 16-18.

219. Scatchard, G. The attraction of proteins for small molecules and ions. *Ann NY Acad Sci,* (1949). 15: p. 660.

220. Trucco, M. and Petris, S. Determination of equilibrium binding parameters of monoclonal antibodies specific for cell surface antigens. *Immunol. Methods.*, (1981). p. 1-26.

221. Greaves, M. F., Brown, G., Rapson, N. T. and Lister, T. H. Antisera to acute lymphoblastic leumemia cells. *Clin. Immunol. Immuno-pathol.*, (1975). 4: p. 67-84.

222. Letarte, M., Vera, S., Tran, R., Addis, J. B. L., Onizuka, R. J., Quackenbush, E. J., Jongeneel, C. V. and McInnes, R. R. Common acute lymphcytic leukemia antigen is identical to neutral endopeptidase. *J. Exp. Med.*, (1988). 168: p. 1247-1253.

223. Borowitz, M. J. Immunologic markers in childhood acute lymphoblastic leukaemia, in *Hematology/Oncology Clinics of North America.* (1990), p. 743-765.

224. Ling, N. R., Maclennan, I. C. and Mason, D. B-cell and plasma cell antigens: New and previously defind cluster, In *Leucocyte Typing III: White Cell Differentiation Antigens,* A.J. McMichael, Editor. (1987), p. 302-335.

225. Nadler, L. M. B-cell/leukaemia panel workshop: Summary and Comments, In *Leukocyte Typing II,* E.L. Reinherz, B.F. Haynes, L.M. Nadler and I.D. Bernstein, (Eds). (1986), Springer-Verlag: New York. p. 3-43.

226. Foon, K. A., Schroff, R. W. and Bunn Jnr, P. A. Clinical applications of monoclonal antibodies for patients with leukaemia and lymphoma. *Prog. Clin. Biol. Res.,* (1986). 211: p. 265-284.

227. Myers, C. D., Thorpe, P. E., Ross, W. C. J., Cumber, A. J., Katz, F. E., Tax, W. and Greaves, M. F. An immunotoxin with therapeutic potential in T-cell leukaemia: WT1-Ricin A. *Blood,* (1984). 63: p. 1178-1185.

228. Hertler, A. A., Schlossman, D. M., Borowitz, M. J., Poplack, D. G. and Frankel, A. E. An immunotoxin for the treatment of T-acute lymphoblastic leukaemic meningitis: Studies in rhesus monkeys. *Cancer Immunol. Immunother.,* (1989). 28: p. 59-66.

229. Ghetie, M. A., May, R. D., Till, M., Uhr, J. M., Ghetie, V., Knowles, P. P. Relf, M., Brown, A., Wallace, P. M., Janossy, G., Amlot, P., Vitetta, E. S. and Thorpe, P. E. Evaluation of Ricin A chain-containing immunotoxins directed against CD19 and CD22 antigens on normal and malignant human B-cells as potential reagents for *in-vivo* therapy. *Cancer Res.,* (1988). 48: p. 2610-2617.

230. Mechtersheimer, G. and Moller, P. Expression of the common acute lymphoblastic leukemia antigen (CD10) in mesenchymal tumours. *Am. J. Path.,* (1989). 134: p. 961-965.

231. Bourne, S., Pemberton, L., Moseley, R., Lashford, L. S., Coakham, H. B. and J.T. Kemshead, Monoclonal antibodies M340 and UJ181.4 recognise antigens associated with primitive neuroectodermal tumours/tissues. *Hybridoma,* (1989). 8: p. 415-425.

232. Ritz, J., Pesando, J. M., Notis-McConarty, J. and Schlossman, S. F. Modulation of human acute lymphoblastic leukaemia antigen induced by monoclonal antibody *in-vitro. J. Immunology,* (1980). 125: p. 1506-1514.

233. Matzku, S., Kirchgessner, H., Moldenhauer, G., Dorken, B. and Bihl, H. Antibodies against CD19 and CD22 differentiation antigens for B lymphoma targeting (Abstract). *8th International Hammersmith Meeting, Advances in the Application of Monoclonal Antibodies in Clinical Oncology,* (1991). p. 52.

234. Lazarovits, A. L., Colvin, R. B., Camerini, D.,Karsh, J. and Kurnick, J. T. Modulation of CD7 is associated with T-lymphocyte function, In *Leucocyte Typing III: White Cell Differentiation Antigens,* A.J. McMichael, (Ed). (1987), Oxford University Press: Oxford. p. 219-225.

235. Ritz, J., Pesando, J. M., Sallan, S. E., Clavell, L. A., Notis-McConarty, J., Rosenthal, P. and Schlossman, S. F. Serotherapy of acute lymphoblastic leukaemia with monoclonal antibody. *Blood,* (1981). 58: p. 141-152.

236. Salacinski, P. R. Iodination of proteins, glycoproteins and peptides using a solid phase oxidizing agent 1,3,4,6-tetrachloro-3a,6a-diphenylglycoluril. *An. Biochem.,* (1981). 177: p. 136-146.

237. Ferguson, K. M., Hayes, M. M. and Jeffcoate, S. L. Preparation of tracer LH and FSH for multicentre use, In *Immunoassays for Clinical Chemistry,* W.M. Hunter and J.E. Corrie, (Eds). (1983), Churchill Livingstone: Edinburgh. p. 289-294.

238. Bolton, A. E. and Hunter, W. M. The labelling of proteins to high specific radioactivities by conjugation to a ^{125}I-containing acylating agent. *Biochem. J.,* (1973). 133: p. 529-538.

239. Bolton, A. E., *Radioiodination Techniques.* (1985), Amersham International plc.

240. Marchalonis, J. J. An enzymic method for the tracer iodination of immunoglobulins and other proteins. *Biochem. J.,* (1969). 113: p. 299-305.

241. Miller, L. and Watkins, B. F. Scope and mechanism of aromatic iodination with eletrochemically generated iodine (I). *J. Am. Chem. Soc.,* (1976). 98: p. 1515-1519.

242. Matzku, S., Kirchgessner, H., Dippold, W. G. and Bruggen, J. Immunoreactivity of monoclonal anti-melanoma antibodies in relation to the amount of radioactive idoine substituted to the antibody molecule. *Eur. J. Nucl. Med.,* (1985). 11: p. 260-264.

243. Eary, J., Krohn, K. A., Kishore, R. and Nelp, W. Radiochemistry of halogenated antibodies, In *Antibodies in Radiodiagnosis and Therapy,* M.R. Zalutsky, (Ed). (1989), CRC Press: Boca Raton, Fla. p. 83-102.

244. Zalutsky, M. R. and Narula, A. S. Radiohalogenation of a monoclonal antibody using an N-succinimidyl 3-(tri-n-butylstannyl) benzoate interdediate. *Cancer Res.,* (1988). 48: p. 1446-1450.

245. Courtenay, V. D. and Mills, J. An *in-vitro* colony assay for human tumours grown in immune-suppressed mice and treated *in-vivo* with cytotoxic agents. *Brit. J. Cancer,* (1978). 37: p. 261-268.

246. Hall, E. J. *Radiobiology for the Radiologist.* Third ed. (1988), Philadelphia: J. B. Lippincott Company. p. 535.

247. Roper, P. R. and Drewinko, B. Comparison of *in-vitro* methods to determine drug-induced cell lathality. *Cancer Res.,* (1976). 36: p. 2182-2188.

248. Rupniak, H. T., Dennis, L. Y. and Hill, B. T. An intercomparison of *in-vitro* assays for assessing cytotoxicity after a 24 hour exposure to anti-cancer drugs. *Tumori,* (1983). 69: p. 37-42.

249. Hamburger, A. W. and Salmon, S. E. Primary Bio-assay of human tumour stem cells. *Science,* (1977). 197: p. 461-436.

250. Hill, B. T. and Whelan, R. D. Attempts to optimise colony-forming efficiencies using three different survival assays and a range of human tumour continuous cell lines. *Cell Biology International Reports,* (1983). 7: p. 617-624.

251. Fleiss, J. L. *Statistical Methods of Rates and Proportions.* (1981), New York: J. Wiley & Sons Inc.

252. Patel, K., Rossell, R. J., Bourne, S., Moore, S. E., Walsh, F. S. and Kemshead, J. T. Monoclonal antibody UJ13A recognises the neural cell adhesion molecule (NCAM). *Int. J. Cancer,* (1989). 44: p. 1062-1068.

253. Richardson, R. B., Kemshead, J. T. and Davies, A. G. Dosimetry of intrathecal ^{131}I labelled monoclonal antibody in cases of neoplastic meningitis. *Eur. J. Nucl. Med.,* (1990). 17: p. 42-48.

254. Vistica, D. T., Skehan, P., Scudiero, D., Monks, A., Pittman, A. and Boyd, M. R. Tetrazolium-based assays for cellular viability: A critical examination of selected parameters affecting formazan production. *Cancer Res.,* (1991). 51: p. 2515-2520.

255. Pimm, M. V., Clegg, J. A., Garnett, M. C. and Baldwin, R. W. Biodistribution and tumour localisation of methotrexate monoclonal antibody 791T/36 conjugate in nude mice with human tumour xenografts. *Int. J. Cancer,* (1988). 41: p. 886-891.

256. Chatel, J. F., Saccavini, J. C. and Fumoleau, P. Immunoscintigraphy of colon carcinoma. *J. Nucl. Med.,* (1984). 25: p. 307-314.

257. White, S., Taetle, R., Seligman, P. A., Rutherford, M. and Trowbridge, I. S. Combinations of anti-transferrin receptor monoclonal antibodies inhibit human tumour cell growth *in-vitro* and *in-vivo*: Evidence for synergistic antiproliferative effects. *Cancer Res.,* (1990). 50: p. 6295-6301.

258. Le Bien, T. W., Ash, R. C., Zanjani, E. D. and Kersey, J. H. *In-vitro* cytodestruction of leukaemic cells in human bone marrow using a cocktail of MoAbs. *Haematol. Bluttransfus.,* (1983). 28: p. 112-116.

259. Vallera, D. A., Ash, R.C., Zanjani, E. D., Kersey, J. H., LeBien, T. W., Beverley, P. C., Neville, D. M. and Youle, R. J. Anti-T-cell reagents for human bone marrow transplantation: Ricin linked to three monoclonal antibodies. *Science,* (1983). 222: p. 512-515.

260. Tsai, L. C., Lin, J. K., Han, S. H. and Chen, H. M. Suppression of the growth of human colorectal carcinoma cells (LS174T) by radiolabelled monoclonal antibody (^{131}I-Mab C27) in tissue culture and nude mice. *Dis. Colon. Rectum.,* (1988). 31: p. 781-785.

261. Capala, J., Prahl, M., Scott-Robson, S., Ponten, J., Westermark, B. and Carlsson, J. Effects of ^{131}I-EGF on cultured human glioma cells. *J. Neuro-Oncology,* (1990). 9: p. 201-210.

262. Kwok, C. S., Crivici, A., MacGregor, W. D. and Unger, M. W. Optimization of radioimmunotherapy using human malignant melanoma multicell spheroids as a model. *Cancer Res.,* (1989). 49: p. 3276-3281.

263. Langmuir, V. K., McGann, J. K., Buchegger, F. and Sutherland, R. M. ^{131}I-anticarcinoembryonic antigen therapy of LS174T human colon adenocarcinoma spheroids. *Cancer Res.,* (1989). 49: p. 3401-3406.

264. Walker, K. A., Murray, T., Hildich, T. E., Wheldon, T. E., Gregor, A. and Hann, I. M. A tumour spheroid model for antibody targeted therapy of micrometastases. *Brit. J. Cancer,* (1988). 58: p. 13-16.

265. McDonald, G. A., Doods, T. C. and Cuickshank, B. *Atlas of Haematology.* 3rd ed. (1970), Edinburgh and London: Churchill Livingstone.

266. Hofer, K. G. and Hughes, W. L. Radiotoxicity of intranuclear tritium, ^{125}I and ^{131}I. *Radiat. Res,* (1971). 47: p. 94-109.

267. Bradley, E. W., Chan, P. C. and Adelstein, S. J. The radiotoxicity of ^{125}I in mamalian cells. I. Effects on the survival curve of radioiodine incorporated into DNA. *Radiat. Research,* (1975). 64: p. 555-563.

268. Chan, P. C., Lisco, E., Lisco, H. and Adelstein, S. J. The radiotoxicity of ^{125}I in mammalian cells. II. A comparitive study on cell survival and cytogenetic responses to ^{125}IUdR, ^{131}IUdR and 3HtdR. *Radiat. Res.,* (1976). 67: p. 332-343.

269. Martin, R. F. and Haseltine, W. A. Range of radiochemical damage to DNA with decay of ^{125}I. *Science,* (1981). 213: p. 896-898.

270. Kassis, A. I., Adelstein, S. J. and Bloomer, W. D. Therapeutic implications of Auger-emitting radionuclides, In *Radionuclides in therapy,* Spencer, Seevers and Friedman, (Ed). (1988), CRC Press: Boca Raton. p. 119-134.

271. Bloomer, W. D. and Adelstein, S. J. 5-(^{125}I)-iododeoxyuridine and the Auger effect. Biological consequences and implications for therapy. *Pathobiol. Annu,* (1978). 8: p. 407.

272. Boven, E., Lindmo, T., Mitchell, J. B. and Bunn, P. A. Selective cytotoxicity of ^{125}I-labelled monoclonal antibody T101 in human malignant cell lines. *Blood,* (1986). 67: p. 429-435.

273. Brady, L. W. The adjuvant use of ^{125}I radiolabelled EGF-425 in the treatment of high grade astrocytomas, In *Second International Neuro-Oncology Conference.* (1991). The Royal Marsden Hospital, London.

274. Sugiyama, Y., Chen, F. A., Takita, H. and Bankert, R. B. Selective growth inhibition of human lung cancer cell lines bearing a surface glycoprotein gp160 by ^{125}I-labelled anti-gp160 monoclonal antibody. *Cancer Res.,* (1988). 48: p. 2768-2773.

275. Elliott, T. J., Glennie, M. J., McBride, H. M. and Stevenson, G. T. Analysis of the interaction of antibodies with immunoglobulin idiotypes on neoplastic B-lymphocytes: implications for immunotherapy. *J. Immunology,* (1987). 138: p. 981-988.

276. Congdon, C. C. and Lorenz, E. Leukaemia in guinea pigs. *Am. J. Pathol.,* (1953). 30: p. 337-359.

277. Perk, K., Pearson, J. W., Torgersen, J. A. and Chirigos, M. A. An animal model for meningeal leukaemia. *Int. J. Cancer,* (1974). 13: p. 863-866.

278. Hoogerbrugge, P. M. and Hagenbeek, A. Leptomeningeal infiltration in rat models for human acute myelocytic and lymphocytic leukemia. *Leuk. Res.,* (1985). 9: p. 1397-1404.

279. Fiebig, H. H., Zeller, W. J. and Schmahl, D. An experimental model for meningeal leukemia in rats (L5222). Effect of treatment with BCNU and cyclophosphamide. *Int. J. Cancer,* (1976). 18: p. 710-716.

280. Greenberger, J. S., Muse, M. B., Bocaccino, C. A. and Moloney, W. C. Brief communication: Central nervous system relapse following chemotherapy of WF rat acute myelogenous leukemia: A model for human CNS leukemia., (1977). 4: p. 1139-1143.

281. Urch, C. E., George, A. J. T., Stevenson, G. T., Bolognesi, A., Stirpe, F., Weller, R. and Glennie, M. J. Intrathecal treatment of leptomeningeal lyphoma with immunotoxin. *Int. J. Cancer,* (1991). 47: p. 909-915.

282. Pearson, J. W., Perk, K., Chirigos, M. A. and Torgersen, J. A. Drug therapy against a transplantable guniea pig leukemia. *Cancer Res.,* (1975). 35: p. 1093-1098.

283. Gregg, E. O., Bridges, S. H. and Toule, J. R. Whole ricin and recombinant ricin A chain idiotype-specific immunotoxins for therapy of guniea pig L_2C B-cell leukaemia. *J. Immunol.,* (1987). 138: p. 4502-4508.

284. Hamblin, T. J., Cattan, A. R., Glennie, M. J., MacKenzie, M. R., Stevenson, F. K., Watts, H. F. and Stevenson, G. T. Initial experience in treating human lymphoma with a chimeric univalent derivative of monoclonal anti-idiotype antibody. *Blood,* (1987). 69: p. 790-797.

285. Dedrick, R. L. Interspecies scaling of regional drug delivery. *J. Pharmacol. Sci,* (1986). 75: p. 1047-1052.

286. Campana, D. and Jannosy, G. Leukaemia diagnosis and testing of complement-fixing antibodies for bone marrow purging in acute lymphoid leukaemia. *Blood,* (1986). 68: p. 1264-1271.

287. Sisk, D. B.,Physiology,In *The Biology of the Guinea Pig,* J.E. Wagner and P.J. Manning, (Ed). (1977), Academic Press: New York. p. 63-98.

288. Gibaldi, M. and Perrier, D. *Pharmacokinetics.* 2nd ed. (1982), New York: Marcel Dekker.

289. Lynch, R. G., Medoff, G. and Valeriote, F. A murine model for central nervous system leukemia and its possible relevance to human leukemia. *J. Nat. Cancer Inst.,* (1975). 55: p. 611-616.

290. Stevenson, F. K., Glennie, M. J. and Johnston, D. M. Consumption of monoclonal anti-idiotypic antibody by neoplastic B-lymphocytes: A guide for immunotherapy. *Br. J. Cancer,* (1984). 50: p. 407-413.

291. Bradbury, M. Breakdown of the blood-brain barrier. In *The Concept of the Blood-Brain Barrier.* (1979), Wiley: New York. p. 354-382.

292. Welch, K. and Pollay, M. Perfusion of particles through arachnoid villi of the monkey. *Am. J. Physiol,* (1961). 201: p. 651-654.

293. Smith, D. B., Moseley, R. P., Begent, R. H., Coakham, H. B., Glaser, M., Dewhurst, S., Kelly, A. and Bagshawe, K. D. Quantitative distribution of ^{131}I-labelled monoclonal antibodies administered by intraventricular route. *Euro. J. Cancer,* (1990). 26: p. 129-136.

294. Dichiro, G. Cisternography: from early tribulations to a useful diagnostic procedure. *Hopkins Med. J.,* (1973). 133: p. 1-15.

295. Pinkerton, C. R. and Chessells, J. M. Failed central nervous system prophylaxis in children with acute lymphoblastic leukaemia: Treatment and outcome. *Br. J. Haematol.,* (1984). 57: p. 553-561.

296. Maren, T. H. Bicarbonate formation in cerebrospinal fluid: Role in sodium transport and pH regulation. *Am. J. Physiol.,* (1972). 222: p. 885-899.

297. Rubin, R. C., Henderson, E. S. and Ommaya, A. K. The production of cerebrospinal fluid in man and its modification by acetazolamide. *J. Neurosurg.,* (1966). 25: p. 430-436.

298. McComb, J. G. Recent research into the nature of cerebrospinal fluid formation and absorbtion. *J. Neurosurg.,* (1983). 59: p. 369-383.

299. Ganong, W. F. *Review of Medical Physiology.* (1969), Los Altos: Lange Medical Publications.

300. Kereiakes, J. and Rosenstein, M. *Handbook of Radiation Doses in Nuclear Medicine and Diagnostic X-ray.* (1980), New York: CRC Press.

301. Renwick, A. G. Pharmacokinetics in toxicology, In *Principles and Methods of Toxicology,* A. Wallace-Hayes, (Ed). (1989), Raven Press Ltd: New York. p. 835-878.

302. Lashford, L. S., Davies, A. G., Richardson, R. B., Bourne, S. P., Bullimore, J. A., Eckert, H., Kemshead, J. T. and Coakham, H. B. A pilot study of ^{131}I monoclonal antibodies in the therapy of leptomeningeal tumours. *Cancer,* (1988). 61: p. 857-868.

303. Lashford, L. S. Studies in targeted radiotherapy. *PhD Thesis, London,* (1988).

304. Stewart, J. S., Hird, V., Snook, D., Sullivan, M., Hooker, G., Courtenay-Luck, M., Sivolapenko, G., Griffiths, M., Myers, M. J., Lambert, H. E., Munro, A. J. and Eppenetos, A. A. Intraperitoneal radioimmuno-therapy for ovarian cancer: Pharmacokinetics, toxicity and efficacy of ^{131}I labelled monoclonal antibodies. *Int. J. Radiation Oncology, Biology and Physics,* (1989). 16: p. 405-413.

305. Hershey, L. A. and Trotter, J. L. The use and abuse of the cerebrospinal fluid IgG profile in the adult: A practical evaluation. *Ann. Neurol.,* (1980). 8: p. 426-434.

306. Tourtelotte, W. On cerebrospinal IgG quotients in multiple sclerosis and other diseases: A review and a new formula to estimate the amount of IgG synthesized per day by the central nervous system. *J. Neurol. Sci.*, (1970). 10: p. 279-304.

307. Schipper, H. I., Bardosi, A., Jacobi, C. and Felgenhauer, K. Meningeal carcinomatosis: Origin of local IgG production in the CSF. *Neurology,* 1988. 38: p. 413-416.

308. Hoffman, S. A., Arbogast, D. N. and Day, T. T. Permeability of the blood-cerebrospinal fluid barrier during acute immune complex disease. *J. Immunol.*, (1983). 130: p. 1695-1698.

309. Harbart, J. and McCullough, D. Spinal cord dosimetry in ^{131}I-IHSA cisternography. *J. Nucl. Med.*, (1970). 11: p. 534-540.

310. Millar, W. T. and Barret, A. Dosimetric model for antibody targeted radionuclide therapy of tumour cells in cerebrospinal fluid. *Cancer Res).*, (1990). 50: p. 1043s-1048s.

311. *CRC Handbook of Radiation Measurement and Protection: Biological and Mathematical Information.* Vol. II. (1980), Boca Raton: CRC Press. p. 110.

312. White, D. R. Tissue Composition, attenuation and substitutes, In *Health Physics*. (1977). Vol. 33. Pergammon Press. p. 73-81.

313. Lee, R. E., Siegel, J. A., Harowitch, J., Steimle, V., Khalvati, S., Front, D., Murthy, S. and Goldenberg, D. M. The use of SPECT in monoclonal antibody imaging to determine marrow to blood activity ratio (Abstract). *Antibody Immunoconjugates and Radiopharmaceuticals,* (1991). 4: p. 53.

314. Moseley, R. P., Zalutsky, M. R., Evans, S., Papanastassiou, V. and Kemshead, J. T. Immunoreactivity, pharmacokinetics and bone marrow dosimetry of intrathecal radioimmunoconjugates. *Br. J. Cancer,* (1992). (Submitted).

315. Doge, H. and Hliscs, R. Intrathecal therapy with ^{198}Au-colloid for meningosis prophylaxis. *Euro. J. Nucl. Med.,* (1984). 9: p. 125-128.

316. Finlay, J. An update on the brain tumour trials of the children's cancer study group. *The Ninth International Conference on Brain Tumour Research and Therapy (Abstract),* (1991) p. Asilomar Conference Centre.

317. Gnekow, A. K., Bailey, C., Michaelis, J., Wellek, S. and Kleihues, P. SIOP/GPO medulloblastoma trial II - Med 84: Annual status report (Abstract). *Medical and Paediatric Oncology,* (1991). 19: p. 435.

318. Morrel, A., Terry, W. D. and Waldmann, T. A. Metabolic properties of IgG sub-classes in man. *J. Clin. Invest.,* (1970). 49: p. 673-680.

319. Speigelberg, H. L. and Fishkin, B. G. The catabolism of human gamma-G immunoglobulins of different heavy chain sub-classes. *Clin. Exp. Immunol.,* (1972). 10: p. 599-607.

320. Gergely, E., Medgyesi, G. A. and Stanworth, D. R. Structural studies of immunoglobulins II. The varying susceptibility to papain digestion of a group of human myeloma gamma globulins. *Immunochemistry,* (1967). 4: p. 369-374.

321. Cheung, N. K. V., Yeh, S. D. H., Kushner, B. H., Burch, L., Gulati, S. and Larson, S. Radioimmunotherapy using ^{131}I-3F8 in neuroblastoma (NB): A phase I clinical trial. *Medical and Paediatric Oncology,* (1990). 18: p. 380 (Abstract).

322. Morin, R. L. and Brookeman, V. A. ^{169}Yb-DTPA distribution and dosimetry in cisternography. *J. Nucl. Med. Technology,* (1974). 2: p. 786-796.

323. Begent, R. H. J., Green, A. J. and Bagshawe, K. D. Liposomally entrapped second antibody improves tumour imaging with radiolabelled first anti-tumour antibody. *Lancet,* (1982). i: p. 739-742.

324. Begent, R. H. J., Bagshawe, K. D., Pedley, R. B., Searle, F., Ledermann, A. J.,Green, A. J., Keep, P. A., Chester, K. A., Glaser, M. G. and Dale, R. G. Use of second antibody in radiotherapy. *NCI Monographs,* (1987). 3: p. 59-61.

325. Klein, J. L., Leichner, P. K. and Callahan, K. M. Effects of anti-antibodies on radiolabelled antibody therapy. *Antibody, Immunoconjugates and Radio-Pharmaceuticals,* (1988). 1: p. 55-64.

326. Goldenberg, D. M., Sharkey, R. M. and Ford, E. Anti-antibodies enhacement of ^{131}I anti-CEA radioimmunodetection in experimental and clinical studies. *J. Nucl. Med.,* (1987). 28: p. 1604-1610.

327. Stewart, J. S. W., Sivolapenko, G. B., Hird, V., Davies, K. A. A., Walport, M., Ritter, M. A. and Epenetos, A. A. Clearance of ^{131}I-labelled murine monoclonal antibody from patients' blood by intravenous human anti-murine immunoglobulin antibody. *Cancer Res.,* (1990). 50: p. 563-567.

328. Wheldon, T. E., O'Donaghue, J. A., Hilditch, T. E. and Barrett, A. Strategies for systemic radiotherapy of micrometastases using antibody-targeted radiotherapy. *Radiation and Oncology,* (1988). 11: p. 133-142.

329. Dorken, B., Moller, P., Pezzutto, A., Schwartz-Albiez, R. and Moldenhauer, G. B-cell antigens: CD20, In *Leucocyte Typing IV: White Cell Differentiation Antigens,* W. Knapp, (Ed). (1989), Oxford University Press: Oxford. p. 46-62.

330. Dorken, B., Moller, P., Pezutto, A., Schwartz-Albiez, R. and Moldenhauer, G. B-cell antigens: *CD22,* In *Leucocyte Typing IV: White Cell Differentiation Antigens,* W. Knapp, (Ed). (1989), Oxford University Press: Oxford. p. 63-74.

331. Reiter, C. T5 Cluster report: CD5, In *Leucocyte Typing IV: White Cell Differentiation Antigens,* W. Knapp, (Ed). (1989), Oxford University Press: Oxford. p. 331-332.

332. Benjamin, J. C., Moss, T., Moseley, R. P., Maxwell, R. and Coakham, H. B. Cerebral distribution of immunoconjugate after treatment for neoplastic meningitis using an intrathecal radiolabelled monoclonal antibody. *Neursurg.,* (1989). 24: p. 253-258.

333. Klatzo, I., Miquel, J., Ferris, P. J., Prokop, J. D. and Smith, D. E. Observations on the passage of the fluorescein labeled serum proteins (FLSP) from the cerebrospinal fluid. *J. Neuropath. Exp. Neurol.,* (1964). 23: p. 18-35.

334. Cserr, H. F. and Ostrach, L. H. Bulk flow of interstitial fluid after intracranial injection of blue dextran 2000. *Exp. Neurol.,* (1974). 45: p. 50-60.

335. Barth, R. F., Johnson, C. W., Wei, W., Carey, W. H., Soloway, A. H. and McGuire, J. Neutron capture therapy using boronated monoclonal antibodies against tumour associated antigens. *Cancer Detect. Prevent.,* (1982). 5: p. 315.

336. De Nardo, S. J., Deshpande, S. V., Moi, M. K., Adamas, G. P., McCall, M. K., De Nardo, G. L. and Meares, C. F. Today and tomorrow: Radiochemistry for radioimmunotherapy of breast cancer, In *The Present and Future Role of Monoclonal Antibodies in the Management of Cancer. Front. Radiat. Ther. Oncol.,* J.M. Vaeth and J.L. Meyer, (Eds). (1990), Karger: Basel. p. 142-150.

337. Hnatowich, D. J., Virzi, F. and Rusckowski, M. Investigations of avidin and biotin for imaging applications. *J. Nucl. Med,* (1987). 28: p. 1294-1302.

338. Paganelli, G., Magnani, P., Zito, F., Villa, E., Sudati, F., Lopalco, L., Rossetti, C., Malcovati, M., Chiolerio, F., Seccamani, E., Siccardi, A. G. and Fazio, F. Three-step monoclonal antibody tumour targeting in carcinoembryonic antigen-positive patients. *Cancer Res.,* (1991). 51: p. 5960-5966.

339. Krolick, K. W., Uhr, J. W., Slavin, S. and Vitetta, E. S. *In-vivo* therapy of a murine B-cell tumour (BCL) using antibody-ricin A chain immunotoxins. *J. Exp. Med.,* (1982). 155: p. 1797-1809.

340. Spitler, L. E., del Rio, M., Khentigan, A., Wedel, N. I., Brophy, N. A., Miller, L. L., Harkonen, W. S., Rasendorf, L. L., Lee, H. M., Mischak, R. P. Kawahata, R. T., Stoudemire, J. B., Fradkin, L. B., Bautista, E. E. and Scannon, P. J. Therapy of patients with malignant melanoma using a monoclonal anti-melanoma antibody-ricin A chain immunotoxin. *Cancer Res.,* (1987). 47: p. 1717-1723.

341. Vitetta, E. S., Stone, M., Amlot, P., Fay, J., May, R., Till, M., Newman, J., Clark, P., Collins, R., Cunningham, D., Ghetie, V., Uhr, J. W. and Thorpe, P. E. Phase I immunotoxin trial in patients with B-cell lymphoma. *Cancer Res.,* (1991). 51: p. 4052-4058.

342. Byers, V. S., Rodvien, R., Grant, K., Durrant, L. G., Hudson, K. H., Baldwin, R. W. and Scannon, P. J. Phase I study of monoclonal antibody ricin A chain immunotoxin XOMAZYME-791 in patients with metastatic colon cancer. *Cancer Res.,* (1989). 49: p. 6153-6160.

343. Hertler, A. A. and Frankel, A. E. Immunotoxins: A clinical review of their use in the treatment of malignacies.*J. Clin. Oncol.,* (1989). 7: p. 1932-1942.